Universidad de Valladolid

FACULTAD DE CIENCIAS

DEPARTAMENTO DE FÍSICA APLICADA

TESIS DOCTORAL:

Phase-segregated copoly(ether-imide)s, Optimization of structure and composition for gas separation applications

Presentada por Alberto Tena Matías para optar al grado de doctor por la Universidad de Valladolid

Dirigida por:
Ángel Marcos Fernández
Pedro Prádanos del Pico

TABLE OF CONTENTS

SECTION I. INTRODUCTION AND GENERAL METHODOLOGY 1

Chapter 1. Introduction.....1

1.1 Climate change 3
1.2 Capture technologies and challenges.....9
1.3 Separation membrane process 10
1.4 Gas separation membranes 12
1.5 Transport in gas separation membranes.....15
1.6 PEO-Based membranes 17
1.7 Aims and Outline of the thesis.....19
1.8 References 21

Chapter 2. General methodology: synthesis and characterization.....25

2.1 Introduction 27
2.2 Synthesis of the copolyimides 27
2.3 Films preparation and thermal treatments 30
2.4 Polymer characterization 31
2.4.1 ATR-FTIR 31
2.4.2 SAXS.....32
2.4.3 TGA.....33
2.4.4 DSC 35
2.4.5 TMA 37
2.4.6 Density.....38
2.4.7 Solubility 39
2.4.8 Mechanical properties.....40
2.4.9 SEM/TEM 42
2.4.10 AFM 42
2.5 Gas transport in membranes 43
2.6 References 48

SECTION II. STUDY OF THE INFLUENCE OF THE COMPOSITION ON THE COPOLYMER PROPERTIES.....51

Chapter 3. Thermally treated copoly(ether-imide)s made from BPDA and aliphatic plus aromatic diamines. Dependence of gas separation properties on the aromatic diamine 53

Abstract 55
3.1 Introduction 56
3.2 Experimental.....58
3.2.1 Chemicals 58
3.2.2 Synthesis of copoly(ether-imide)s 59
3.2.3 Characterization Methods.....60
3.2.4 Gas permeation and selectivity.....61

3.3 Results and discussion 62
3.3.1 Copoly(ether-imide)s imidization 62
3.3.2 Thermal stability 64
3.3.3 Calorimetric studies 65
3.3.4 Thermomechanical analysis 66
3.3.5 Small Angle X-ray Scattering 67
3.3.6 Mechanical properties 70
3.3.7 Gas permeation and selectivity 71
3.4 Conclusions 77
3.5 Acknowledgements 78
3.6 References 78

Chapter 4. Phase Segregation and Gas Separation Properties of Thermally Treated Copoly(ether-imide) from an Aromatic Dianhydride, an Aromatic Diamine and Various Aliphatic Diamines 85

Abstract 87
4.1 Introduction 88
4.2 Experimental section 90
4.2.1 Chemicals 90
4.2.2 Synthesis of copoly(ether-imide)s 90
4.2.3 Preparation of dense films of copolyimide 91
4.2.4 Characterization methods 92
4.3 Results and discussion 93
4.3.1 Copoly(ether-imide)s imidization 93
4.3.2 Thermal stability 94
4.3.3 Calorimetric studies 96
4.3.4 Thermomechanical analysis 97
4.3.5 Small Angle X-ray Scattering 99
4.3.6 Mechanical properties 101
4.3.7 Gas permeation and selectivity 101
4.4 Conclusions 108
4.5 Acknowledgements 109
4.6 References 110

Chapter 5. Advances in the design of co-poly(ether-imide) membranes for CO_2 separations. Influence of aromatic rigidity on crystallinity, segregation and gas transport 115

Abstract 117
5.1 Introduction 118
5.2 Experimental 119
5.2.1 Chemicals 119
5.2.2 Synthesis of copoly(ether-imide)s 120
5.2.3 Preparation of dense films of copolyimide 121
5.2.4 Characterization methods 121
5.3 Results and discussion 122
5.3.1 Copoly(ether-imide)s imidization 122
5.3.2 Thermal stability 123
5.3.3 Calorimetric studies 124

5.3.4 Thermomechanical analysis 126
5.3.5 Small Angle X-ray Scattering 127
5.3.6 Gas transport properties 128
5.4 Conclusions 131
5.5 Acknowledgements 132
5.6 References 132

SECTION III. STUDY OF THE INFLUENCE OF THE STRUCTURE ON THE COPOLYMER PROPERTIES 137

Chapter 6. Influence of the PEO length in gas separation properties of segregating aromatic-aliphatic copoly(ether-imide)s 141

Abstract 143
6.1 Introduction 144
6.2 Experimental 146
6.2.1 Chemicals 146
6.2.2 Synthesis of copoly(ether-imide)s 147
6.2.3 Preparation of the dense films 147
6.2.4 Characterization Methods 148
6.2.5 Gas permeation and selectivity 149
6.3 Results and discussion 149
6.3.1 Copoly(ether-imide)s imidization 149
6.3.2 Thermal stability 150
6.3.3 Calorimetric studies 152
6.3.4 Thermomechanical analysis 155
6.2.5 Density 156
6.3.6 Small Angle X-ray Scattering 157
6.3.7 Gas permeation and selectivity 160
6.4 Conclusions 168
6.5 Acknowledgements 170
6.6 References 171

Chapter 7. Physical properties of films made of copoly(ether-imide)s with long poly(ethylene oxide) segments 175

Abstract 177
7.1 Introduction 178
7.2 Experimental 179
7.2.1 Chemicals 179
7.2.2 Synthesis of copoly(ether-imide)s 180
7.2.3 Experimental methods 181
7.3 Results and discussion 183
7.3.1 Copoly(ether-imide)s imidization 183
7.3.2 Thermal stability 184
7.3.3 Calorimetric studies 187
7.3.4 Small Angle X-ray Scattering 190
7.3.5 Thermomechanical analysis 197

7.3.6 Mechanical properties 199
7.4 Conclusions 201
7.5 Acknowledgements 202
7.6 References 203

Chapter 8. On the influence of the proportion of PEO in thermally controlled phase segregation of copoly(ether-imide)s for gas separation 207

Abstract 209
8.1 Introduction 210
8.2 Experimental 212
8.2.1 Chemicals 212
8.2.2 Synthesis of copoly(ether-imide)s 212
8.2.3 Preparation of the dense films 213
8.2.4 Characterization Methods 213
8.3 Results and discussion 215
8.3.1 Copoly(ether-imide)s imidization 215
8.3.2 Thermal stability 216
8.3.3 Calorimetric studies 218
8.3.4 Thermomechanical analysis 219
8.2.5 Small Angle X-ray Scattering 220
8.3.6 Density 221
8.3.7 Gas transport properties 222
8.3.8 Permeability modeling 226
8.4 Conclusions 227
8.5 Acknowledgements 228
8.6 References 229
8.7 Supporting Information 233

Chapter 9. On the influence of the proportion of PEO in thermally controlled phase segregation of copoly(ether-imide)s for gas separation 237

Abstract 239
9.1 Introduction 240
9.2 Experimental 241
9.2.1 Chemicals 241
9.2.2 Synthesis of copoly(ether-imide)s 242
9.2.3 Preparation of the copolyimide dense films 243
9.2.4 Physical characterization 244
9.2.5 Gas permeation 245
9.3 Results and discussion 245
9.3.1 Thermal stability 245
9.3.2 Calorimetric analysis 247
9.3.3 Gas transport properties 249
9.4 Conclusions 258
9.5 Acknowledgements 259
9.6 References 260

Chapter 10. Thermally Segregated Copolymers with PPO Blocks for Nitrogen Removal from Natural Gas 265

Abstract 267
10.1 Introduction 268
10.2 Experimental 270
10.2.1 Chemicals 270
10.2.2 Synthesis of copoly(ether-imide)s 271
10.2.3 Experimental methods 271
10.3 Results and discussion 274
10.3.1 Copoly(ether-imide)s imidization 274
10.3.2 Thermal stability 275
10.3.3 Calorimetric studies 277
10.3.4 Density 278
10.3.5 Small Angle X-ray Scattering 278
10.3.6 Thermomechanical analysis 282
10.3.7 Mechanical properties 283
10.3.8 Gas transport properties 283
10.4 Conclusions 289
10.5 Acknowledgements 290
10.6 References 290
10.7 Supporting Information 294

SECTION IV. PREDICTION OF THE PERMEABILITY PROPERTIES 297

Chapter 6. Prediction of Gas Permeability of Block-Segregated Polymeric Membranes by an Effective Medium Model 299

Abstract 301
11.1 Introduction 302
11.2 Experimental 303
11.2.1 Chemicals 304
11.2.2 Synthesis of copoly(ether-imide)s 304
11.2.3 Preparation of the dense films 305
11.2.4 Characterization of the membranes 305
11.3 Theory 306
11.3.1 Maxwell-Garnet models 306
11.3.2 Effective medium theory 309
11.3.3 Modifications of the Maxwell models 310
11.3.4 Percolation models 312
11.2.5 Volume fractions 314
11.4 Results and discussion 314
11.5 Conclusions 321
11.6 Acknowledgements 321
11.7 References 322

Conclusions *327*
Future directions *333*
Summary *337*

CHAPTER 1

Introduction

1.1 Climate change

The consciousness of occurrence of a global climate change, usually referred to as *global warming*, has increased due to, for instance, the media attention surrounding the Kyoto protocol in 1997 [1] and by other actions [2]. These climate changes mainly manifest themselves as a worldwide increase in the average temperature as shown in the Figure (Figure 1) published in the fourth assessment report on climate change (2007) by the Intergovernmental Panel on Climate Change (IPCC) [3].

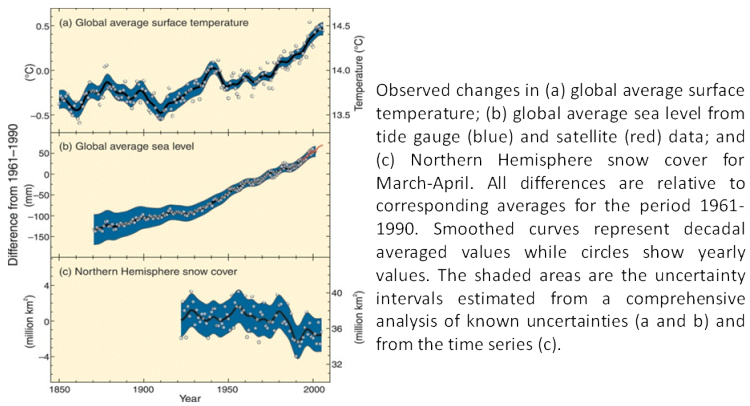

Figure 1. Effects of the climate change on different natural indicators.

The warmest years in the instrumental record of global surface temperature (since 1850) are corresponding for the last 15 years. These climate changes are not limited to the raise in global temperature, but also other phenomena are believed to be related to global warming, such as the augment in sea level and temperature, the retreat of glaciers, and the increased frequency of more extreme weather conditions. In general, the reason for the current climate change is thought to be caused by an increase in the atmospheric concentration of greenhouse gases (GHG), such as carbon dioxide (CO_2), methane (CH_4), nitrous oxide (N_2O), hydrofluorocarbons (HFCs), perfluorocarbons (PFCs) and sulfur hexafluoride (SF_6). Figure 1.2 shows the concentration and main origin of CO_2 and other major greenhouse gases (CH_4, N_2O and fluorinated gases) from 1970 to 2004.

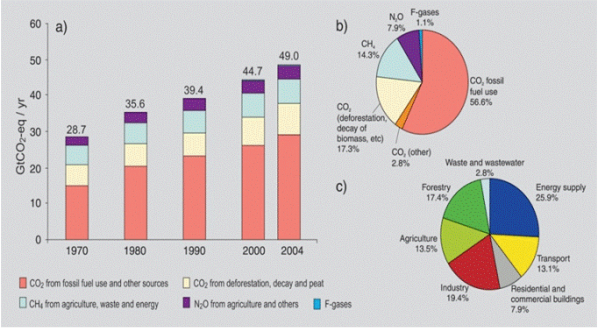

(a) Global annual emissions of anthropogenic GHGs from 1970 to 2004.* (b) Share of different anthropogenic GHGs in total emissions in 2004 in terms of CO_2-eq. (c) Share of different sectors in total anthropogenic GHG emissions in 2004 in terms of CO_2-eq. (Forestry includes deforestation.).

Includes only carbon dioxide (CO_2), methane (CH_4), nitrous oxide (N_2O), hydrofluorocarbons (HFCs), perfluorocarbons (PFCs) and sulphurhexafluoride (SF_6), whose emissions are covered by the United Nations Framework Convention on Climate Change UNFCCC. These GHGs are weighted by their 100-year Global Warming Potentials (GWPs), using values consistent with reporting under the UNFCCC.

Figure 2. Main source and kind of gases emitted to the atmosphere

An exponential increase in the atmospheric concentration of all three gases is observed and the start of this increase (~1900) coincides with the start of the increase in temperature as shown in Figure 1. The global consensus is that this rapid increase is not a natural phenomenon, but is related to the recent human activity on the planet. Since the Industrial Revolution, humans started to use large quantities of carbon containing fossil fuels (Figure 2). From the early 1900's, which coincide with the trends observed in Figure 1 and Figure 2, the use of fossil fuels has increased tremendously. These fossil fuels are mainly burned to generate electricity or facilitate transportation, thereby emitting large amounts of CO_2 to the atmosphere, contributing to global warming. To mitigate the climate changes it is important to stabilize or even decrease the atmospheric concentration of greenhouse gases and in particular the concentration of CO_2 as it has the highest Global Warming Potential (GWP). This is a challenging task as the worldwide CO_2 emissions reached a value of 23.5 $GtCO_2$/yr in the year 2000 [4]. Approximately 60% of these emissions come from large stationary sources (> 0.1 $MtCO_2$/yr). The main part of these large stationary sources are fossil fuel based power plants, while the other contribution is mainly from emitting sources related to the cement production, refineries, petrochemical and steel industry (see Table 1). The power sector is therefore (> 60%) the main contributor to the worldwide emissions of CO_2 and poses a significant potential for the worldwide reduction of CO_2 emissions.

Table 1. Profile by process or industrial activity of worldwide large stationary CO_2 sources with emissions of more than 0.1 million tonnes of CO_2 ($MtCO_2$) per year.

Process	*Number of sources*	*Emisions ($MtCO_2$/year)*
Fossil Fuels		
Power	4.942	10.539
Cement Production	1.175	932
Refineries	638	798
Iron and Steel industry	269	646
Petrochemical industry	470	379
Oil and gas processing	Not available	50
Other sources	90	33
Biomass		
Bioethanol and bioenergy	303	91
Total	7.887	13.466

Therefore it is necessary to search for ways that allow us severely reduce the emission of greenhouse gases into the atmosphere. One of the most promising alternatives for recovery of carbon dioxide (CO_2) is the carbon capture and storage (CCS). CCS is a process consisting of the separation of CO_2 from industrial and energy-related sources, transport to a storage location and long-term isolation from the atmosphere; a general scheme of the process can be observe in Figure 3 Other mitigation options include energy efficiency improvements, the switch to less carbon-intensive fuels, nuclear power, renewable energy sources, enhancement of biological sinks, and reduction of non-CO_2 greenhouse gas emissions. CCS has the potential to reduce overall mitigation costs and increase flexibility in achieving greenhouse gas emission reductions.

Capture of CO_2 can be applied to large point sources. The CO_2 would then be compressed and transported for storage in geological formations, in the ocean, in mineral carbonates, or for use in industrial processes. Potential technical storage methods are: geological storage, ocean storage and industrial fixation of CO_2 into inorganic carbonates. Another kind of employ this gas is the industrial uses of CO_2, but this is not expected to contribute much to the reduction of CO_2 [4].

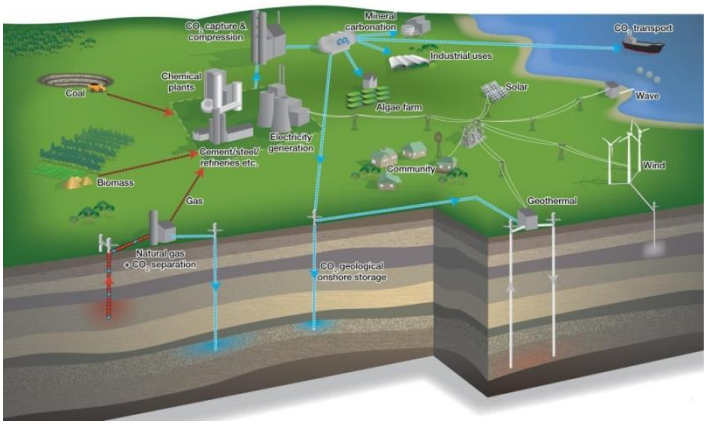

Figure 3. Schematic diagram of possible CCS systems showing the sources for which CCS might be relevant, transport of CO_2 and storage options (Courtesy of Cooperative Research Centre for Greenhouse Gas Technologies CO2CRC[5]).

There are three pathways that can be pursued for CO_2 capture from a fossil fuel based power plant, known as post-combustion capture, pre-combustion capture, and oxy-combustion capture (Figure 4).

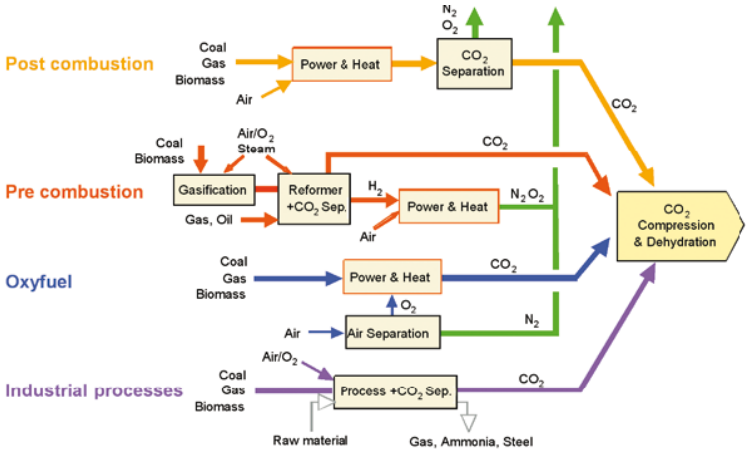

Figure 4. Overview of CO_2 capture processes and systems [4].

In post-combustion capture, CO_2 capture occurs after the combustion process. The CO_2 is separated from other flue gas constituents either originally present in the air or produced by combustion and it mainly involves the separation of CO_2 from N_2. In pre-combustion capture, the CO_2 is removed from the fuel before the actual combustion process takes place. The principle of this process is first to convert the fossil fuel into CO_2 and hydrogen gas (H_2) via gasification. Then, the CO_2 and H_2 are separated and this results in a hydrogen-rich gas, which can be combusted to yield electricity.

Table 2. Advantages and disadvantages of different CO_2 capture pathways [6].

	Advantages	Barriers to implementation
Post-combustion	●Applicable to the majority of existing coal-fired power plants ●Retrofit technology option	Flue gas is… ●Dilute in CO_2 ●At ambient pressure … resulting in … ●Low CO_2 partial pressure -Significantly higher performance or circulation volume required for high capture level -CO_2 produced at low pressure compared to sequestration requirements
Pre-combustion	Synthesis gas is… ●Concentrated in CO_2 ●High pressure … resulting in … ●High CO_2 partial pressure -Increased driving force for separation -More technologies available for separation ●Potential for reduction in compression costs/loads	●Applicable mainly to new plants, as few gasification plants are currently in operation ●Barriers to commercial application of gasification are common to pre-combustion capture -Availability -Cost of the equipment -Extensive supporting systems requirements
Oxy-combustion	●Very high CO_2 concentration in flue gas ●Retrofit and repowering technology option	●Large cryogenic O_2 production requirement may be cost prohibitive ●Cooled CO_2 recycle required to maintain temperatures within limits of combustor materials -Decreased process efficiency -Added auxiliary load

In oxy-combustion capture, the fossil fuel is burned with an oxygen enriched stream that contains little or no nitrogen (N_2). The exhaust gas from this system is therefore highly concentrated in CO_2 and after the removal of water vapor; the CO_2 is ready for subsequent transport and storage. All three pathways have their advantages and disadvantages. These are summarized in Table 2 [6].

Different technologies are currently considered to effectively capture of the CO_2 following either one of these three pathways (or a combination of them). Although this thesis focuses on the CO_2 capture the storage options of carbon dioxide are briefly discussed before going into detail regarding these pathways and associated technologies.

Considering the way the carry out the storage of the CO_2, two main options exist, which are: geological storage and ocean storage [4]. Other options that are considered are (1) mineral carbonation, which involves the conversion of CO_2 into solid inorganic carbonates via chemical reactions and (2) the industrial usage of CO_2, for instance for the production of various carbon containing chemicals [4]. However, the capacity of these two last options is limited and would not match with the vast amounts of CO_2 that need to be captured from power plants. The research and industrial focus is therefore on the first two options and these will be shortly discussed hereafter.

- Geological storage: the CO_2 is injected into underground reservoirs. The CO_2 is expected to be isolated from the atmosphere for several hundreds of years [4]. An overview of geological storage options is presented in Figure 5. Geological storage of CO_2 can performed in a variety of geological formations. CO_2 can be stored in empty oil and gas reservoirs (1) or deep saline formations (3). It is also possible to take advantage of the CO_2 and use it for enhanced oil recovery (EOR) (2), enhanced gas recovery (EGR) (2) or enhanced coal bed methane recovery (ECBM) (4).

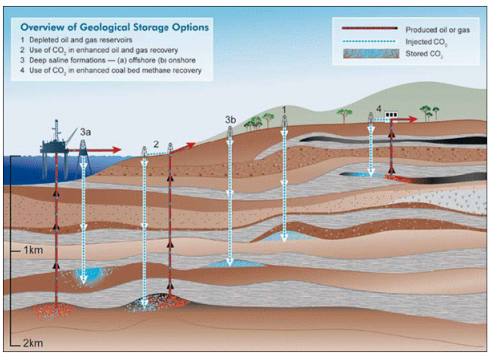

Methods for storing CO_2 in deep underground geological formations. Three methods may be combined with the recovery of hydrocarbons: EOR (2), EGR (2) and ECBM (4)

Figure 5. Geological methods for CO_2 storage [4].

- Ocean storage: The Earth's oceans cover almost 70% of the Earth's surface with an average depth of 3,800 meters and these are the world's largest buffer to store CO_2. There have been small-scale field experiments and 25 years of theoretical, laboratory, and modeling studies of intentional ocean storage of CO_2, but ocean storage has not yet been deployed or thoroughly tested [4]. Various technologies have been envisioned to enable and increase ocean CO_2 storage (Figure 6) [4]. One class of options involves storing a relatively pure stream of carbon dioxide that has been captured and compressed. This CO_2 can be placed on a ship, injected directly into the ocean, or deposited on the bottom of the sea. CO_2 loaded on ships could either be dispersed from a towed pipe or transported to fixed platforms feeding a CO_2 lake on the sea floor. Such CO_2 lakes must be deeper than 3 km where CO_2 is denser than sea water. Any of these approaches could in principle be used in conjunction with neutralization of CO_2 with carbonate minerals.

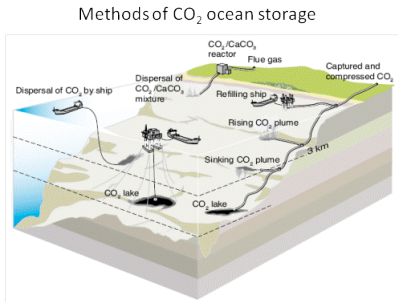

Figure 6. Ocean methods for CO_2 storage [4].

1.2 CO_2 Capture technologies and challenges

Currently, two promising technologies for CO_2 capture from these large point sources are solvent based absorption processes and membrane-based separation processes [4]. An absorption based process can also rely on chemical solvents (envisioned for post-combustion), such as monoethanolamine (MEA) and methyldiethylamine (MDEA) or physical solvents (envisioned for pre-combustion), such as dimethylethers of poly(ethylene glycol) and methanol (trade names are respectively Selexol and Rectisol). However, such solvent-based absorption processes have several disadvantages that limit their applicability. The inherent disadvantage of absorption based processes is the very energy intensive solvent regeneration step [4, 7]. This regeneration step needs either a change in pressure or a change in temperature requiring a large amount of energy. Furthermore, in its design, a system that captures CO_2 from power plants should be very simple. Not only would lead an absorption based process to large installations and operating costs, also the presence of vast amounts of fluids that needs to be pumped around is likely to result in permanent maintenance issues.

In contrast, polymer-based membranes, in comparison to absorption, are less energy intensive, require no phase change in the process, and due to their inherent simplicity membranes have typically low-maintenance. This gives a membrane-based system considerable advantage with respect to engineering and economics and thus has the potential to compete with an absorption based process [8].

Comparing to other well-developed gas separation processes, such as cryogenic distillation, pressure swing adsorption and liquid absorption, membrane gas separation has the following features:

- Membrane gas separation does not involve phase change.

- Membrane gas separation is efficient for bulk separation.
- Membranes can be easily integrated with other separation techniques.
- Membrane gas separation is environmentally friendly.
- Membranes are compact and light, easy to operate and maintain.

However, although membranes play a significant role in the removal of CO_2 from methane, commercial membrane systems for the removal of CO_2 from flue gas in either pre- or postcombustion are not yet available. Nowadays, numerous design and scale-up challenges remain, but membrane-based systems are moving forward [9]. The membrane process will be further explained in the next paragraph.

1.3 Separation membrane process

A membrane behaves as a selective barrier that allows the passage of certain components and retains in the mixture others [10]. In essence, a membrane is nothing more than a discrete, thin interface that moderates the permeation of chemical species in contact with it. Since it has not a definite meaning, we could consider it as "any region that acts as a barrier between two fluids, restricting or allowing the flow of one or more components, or both fluids through it" [11].

There are different criteria to make a broad classification of membranes according to different viewpoints, covering most of their characteristics [10]. The first clearest distinction which could be used for a possible classification is their nature, i.e. biological or synthetic membranes. Along this work we will focus only on synthetic membranes (those which are synthetically created and intended for separation purposes in laboratory or in industry). Moreover, there are sub-classifications for synthetic membranes based on surface chemistry, bulk structure, morphology (form, structure and specific structural features) production method or other parameters [12]. Separations using membranes of different components are generally based on differences in size and electrostatic charge of the substances to be separated, and cover a wide range of sizes, as shown in Figure 7.

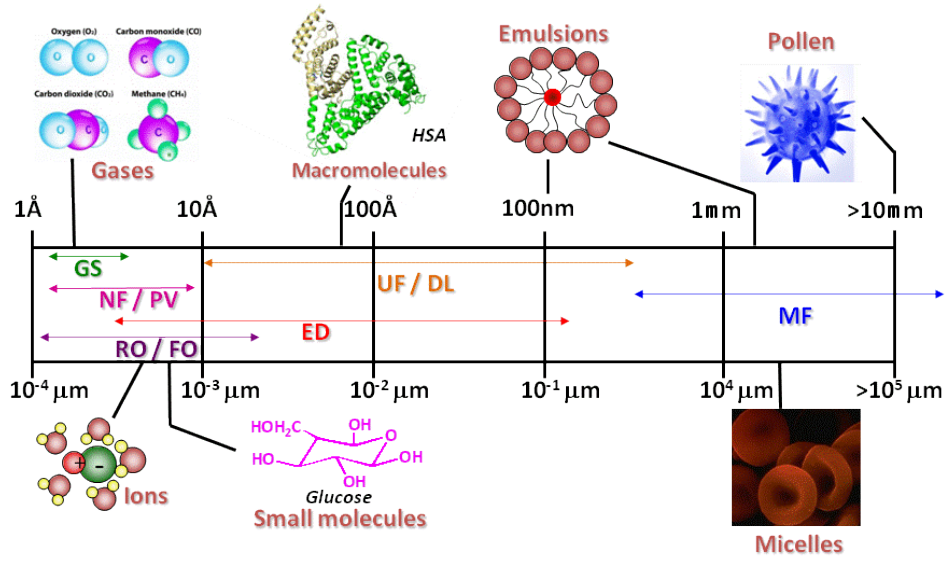

Figure 7. Porous size chart [13].

Important technological advances in past decades have been in the industrial development of membrane separation processes such as reverse osmosis (RO), forward osmosis (FO), nanofiltration (NF), ultrafiltration (UF), microfiltration (MF), dialysis (DL), electrodialysis (ED), pervaporation (PV) and gas separation (GS) [10, 14-16]. In this way, a membrane for separation process is applicable to a broad range of highly specialized end user markets. The total world sales for membrane modules are given as current year estimates and forecast for the period from 2006 to 2011 in Table 3. The development of membrane reactors in Gas Separation (GS) is opening a number of new gas applications, from smaller applications ranging from dehydration of air and natural gas to organic vapor removal from air and nitrogen streams. In this case, GS processes are growing rapidly from a small base, with a rate higher than 15% per year. This technology is expanding rapidly and further growth is likely to continue for the next 10 years [17]. Originally, the market for GS processes was 6.2% of the global membrane market, but having by far the highest growth rates of the membrane process segment.

Table 3 The world market for membrane modules (US$ Million).

Membrane Process	2006	2007	2008	2009	2010	2011
RO/NF	2222	2391	2571	2764	2936	3102
UF	1927	2090	2265	2443	2616	2779
MF	2928	3208	3517	3720	3939	4106
GS	679	758	846	935	1024	1102
Other Separations	2605	2887	3200	3405	3598	3775
Total	10361	11334	12399	13267	14113	14864

These advances have been associated with the discovery of new materials of different kind: ceramic, metallic, polymeric, so, by the moment, only the polymers have been settled favorably price-performance relationships-durability to be met in any industrial development. In the context of this thesis, the research will be focus in the design, preparation and characterization of new polymeric membranes to be evaluated as alternative materials in gas separation processes.

1.4 Gas separation membranes

The evolution of the gas separation processes has been fairly recent and fast. Graham was the first to demonstrate the potential of membrane gas separation by showing that air can be enriched in O_2 through a natural rubber film in 1866. However, the gas separation membranes in the early days did not lead to commercial applications, primarily due to the low permeation flux obtained with relatively thick polymer films. A significant breakthrough in this area was the formation of a high flux asymmetric membrane made of cellulose acetate for reverse osmosis by Loeb and Sourirajan (1963) in the 1960s. Unfortunately, when the membrane was dried for gas separation, pinholes developed on the membrane surface. Then Henis and Tripodi (1980) developed a defect-free composite membrane based on the “resistance model” concept using asymmetric polysulfone membrane with surface defects being sealed by silicone rubber. Based on this approach, Monsanto developed the first commercial hollow fiber membrane for hydrogen separation. Since then, the separation of gas mixtures of industrial interest by membranes has become economically

competitive. Figure 8 shows a timeline with the most relevant milestones in the history of membrane-based gas separation technology.

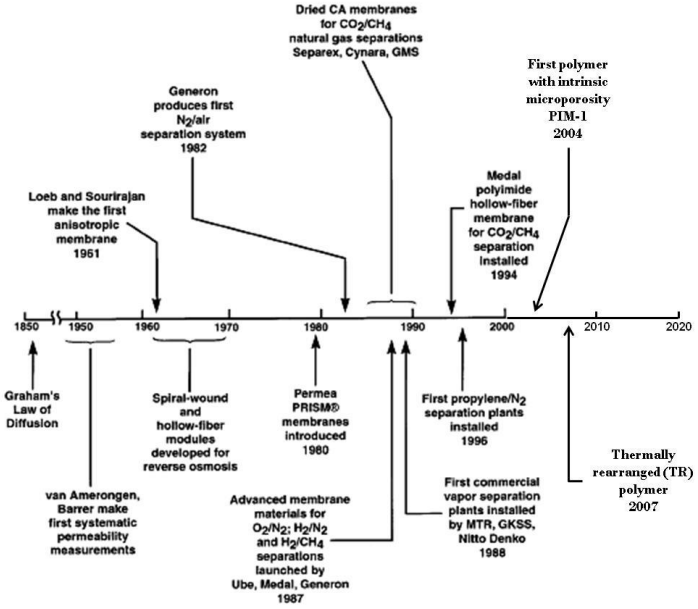

Figure 8. Milestones in the development of membrane gas separations [18].

Extensive work has been done in the literature that relates to the development of membranes and membrane processes for gas separation. Several books have been published on membrane science and technology, where the process principles, membrane materials, membrane formation, membrane modules, process design and applications for various major membrane processes are presented [10, 19-21]. Kesting (1985) discussed the preparation of polymeric membranes by the phase inversion technique [22].The book edited by Freeman and Yampol'skii (2011) devotes entirely to gas separation membranes [23]. The most recent advances in the field of gas separation are based on the use of new systems with a very high fractional free volume (FFV). Despite that there were materials with similar properties, such as carbon molecular sieve (CMS) or zeolites (usually with good separation properties but the way to obtain is complex and expensive), the discovery of materials with high microporosity is a great advance and its mechanical properties are much better than CMS. This kind of compound is probably the most extreme example of how to influence the permeability (P) by changing the packing of the polymer chains and how rigidity determines the selectivity (α). This is accomplished by very rigid polymers and high conformational restrictions [24-30]. These materials are called polymers with an intrinsic microporosity (PIM) by

the authors, and they are obtained by a synthesis pathway theoretically very efficient, but nowadays, the method is not simple and also the cost is high [31-33].

In 2007, Lee et al. presented a paper that caused a quantum leap in the field of separation of gases [34]. The authors proposed structures of poly (o-hydroxyimides) which, by a heat treatment at high temperature (close to 400 °C), are transposed to polybenzoxazoles, by a restructuring with severe conformational changes in the structure, with the loss of one molecule of CO_2. This poly (1,3-benzoazole)s materials called thermally rearranged materials (TR), which have shown excellent properties in the separation of certain gases pairs, whereas, in contrast to carbon molecular sieves, have good mechanical properties. The authors associate these good separation properties to the formation of structures in which the FFV is very high and with a very narrow distribution, and to the high interconnection volume between the open channels, with very well defined dimensions, although currently there are numerous studies that attempt to better understand of the phenomenon [35-40].

All these recent developments represent a revaluation of the gas separation technology presenting new materials with promising properties and characteristics. Table 4 shows the Baker's prediction for gas separation market evolution that was made in 2000 [18]. It can be observed by comparison with Table 1.3 that increased membrane market is much higher than predicted. This is possibly due to the incursion of new materials and applications for membrane processes such as the incorporation of membranes in pre- and post-combustion processes [41]. Table 5 shows some of the suppliers of these technologies along with the type of polymeric material used in each case for the formation of membranes.

Table 4. Future Membrane Market predicted by Baker in 2000 [18].

Separation	*Membrane market ($ million, 2000 dollars)*		
	2000	2010	2020
Nitrogen from air	75	100	125
Oxygen from air	<1	10	30 (?)
Hydrogen	25	60	100
Natural gas	30	90	220
Vapor/nitrogen	10	30	60
Vapor/vapor	0	30	125 (?)
Other	10	30 (?)	100 (?)
Total	150	350	760

Table 5. Principal polymers, markets and producers for membrane systems [18].

Membrane material	Market	Company
Polysulfone		Permea (Air Products)
Polyimide / polyaramide	Nitrogen / air	MEDAL (Air Liquide)
Tetrabromo polycarbonate	H_2 separation	Generon (MG)
Polyimide		Ube / IMS (Praxair)
		GMS (Kvaerner)
Cellulose acetate	Natural gas	Separex (UOP)
	CO_2/CH_4	Cynara (Natco)
		Aquilo
Polyphenylene oxide	Vapor/gas	Parker-Hannifin
Polyimide	Air dehydratation	Ube
Silicone rubber	Other	GKSS
		MTR

Despite the large number of polymeric materials investigated for gas separation, the number of polymers used commercially is quite small mainly due to cost, durability and performance balance. Therefore it is still necessary to develop more effective new materials and to improve existing materials to be able to carry out new applications and to replace materials currently used by others with higher effectiveness. Obviously one of the requirements necessary for applicability in a gas separation membrane is to have good transport properties, and a short description of the transport criteria will be made in the next paragraph.

1.5 Transport in gas separation membranes

The fundamental parameters to evaluate the transport properties in a gas separation membrane are: permeability coefficient (P), defined as the gas flow that passes through a membrane, and the selectivity (α), that is the ratio of the permeabilities for a pair of gases. The permeability is directly proportional to the gas diffusivity of a certain gas through the membrane, and to the solubility (based on the affinity between gas and the matrix) [20]. A detailed explanation of these terms can be found in Annex I of this work.

Experimentally it has been observed that due to the separation mechanism, there is an inverse relationship between the membrane permeability to different gases and its ability to separate these gases (selectivity). Robeson, by using a series of semi-empirical relationships, worked out a set of upper bounds for different couples, that allows a fairly easy way to analyze the quality of the membranes [42-43].

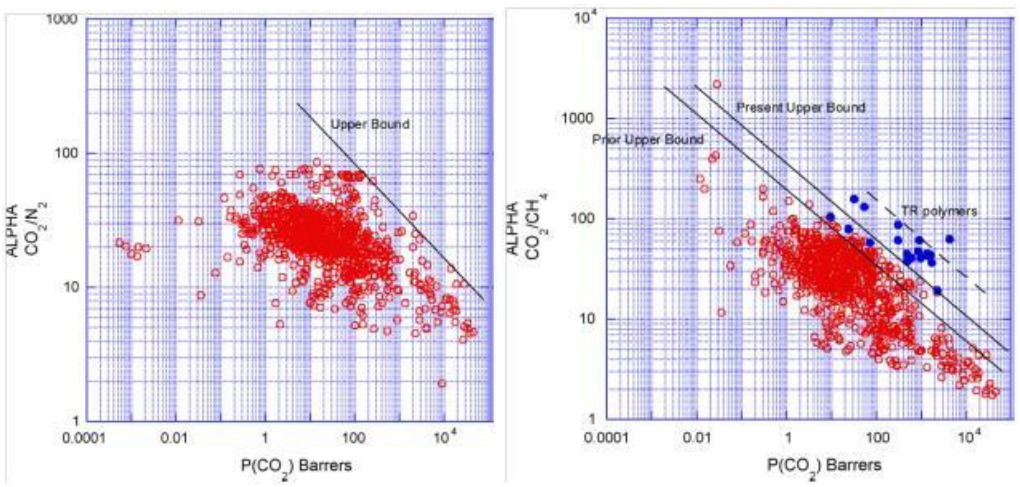

Figure 9. Robeson's upper bound for the couples CO_2/N_2 and CO_2/CH_4 [43].

Furthermore, the main drawback of the membranes against other gas purification processes is achieved when a permeability increase occurs simultaneously the selectivity decrease and vice versa. It is therefore crucial to understand the transport mechanism that occurs in the membranes to successfully design new materials to meet the needs in the gas separation process. Besides a good permselectivity property, two key considerations must be addressed: membrane productivity and membrane stability. Membrane productivity is concerned with the permeation rate, determined by the intrinsic permeability of the polymer, the effective membrane thickness, and the membrane packing density, (i.e., the amount of membrane area per unit module volume). High permeation flux can be achieved by using asymmetric or thin film composite membranes with thin permselective layers, and using hollow fibers for a large membrane area. Membrane stability is the ability to

maintain membrane permeability and selectivity for a long period of time. For the applications of condensable gas separation, membranes with good chemical resistance, and thermal and mechanical stabilities are required. So once known the process and criteria of evaluation, this thesis will attend the objective, considering that the membrane process is more effective to apply to the pre- and post-combustion processes.

1.6 PEO-Based membranes

The variation between pre- and post-combustion CO_2 capture process is significant. Besides the fundamental difference of the separation (CO_2/H_2 vs. CO_2/N_2), also the feed pressure, CO_2 partial pressure, total volume and temperature are considerably different. Post-combustion flue gas streams usually have a temperature around 50-60 ºC and are in general high in volume due to the presence of a 79 % of nitrogen in air. Furthermore, they are at low pressure (atmospheric) and the CO_2 concentration is usually low 10-15 vol. % [9]. In contrast, pre-combustion flue gas streams, as found in integrated gasification combined cycle (IGCC) power plants, are available at high temperature (300 ºC), are typically smaller in volume (as they use nearly pure oxygen for the coal gasification) and the concentration of CO_2 is 40-50 % corresponding to a CO_2 partial pressure of 26-38 bar [9]. Especially the large difference in the partial pressure of CO_2 between pre- and post-combustion has a profound influence on the membrane (process) design as the pressure difference across the membrane provides the driving force in any membrane-based gas separation. In this respect pre-combustion capture seems the most promising technique as it has a high partial pressure CO_2 stream providing such a system with inherent design advantages over a post-combustion capture system. However, the problem of a large volume, low pressure and very dilute stream makes post-combustion CO_2 capture an enormous engineering challenge. As a result of the low driving force a prerequisite for any membrane material to be considered for this separation is the necessity of an extremely high permeability for CO_2 [9, 44]. Some commercially available materials exists that have sufficiently high CO_2/N_2 selectivity (40-50) for this separation, like PEBAX® [45-46] and Polyactive® [47], but their relative low permeability remains a problem.

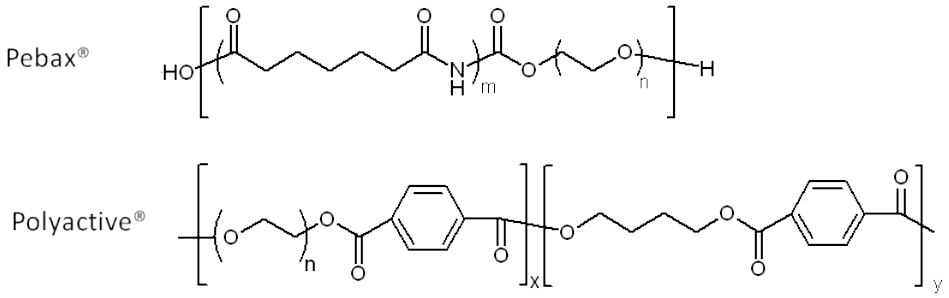

Figure 10. PEBAX® or Polyactive® structures.

Therefore, it is necessary to search for new systems with improved properties, which provide similar selectivities but that improve the permeabilities. The motivation for the current research is to study and understand systems similar to those in Figure 10. In this case, this work is based on the study of polyimides-PEO copolymers.

Glassy polymers and in particular polyimides are well known for their excellent thermal oxidative stability, good organic solvent resistance, exceptional mechanical properties, and tunable free cavities, along with an extraordinary ability to separate complex mixtures of gases in diverse applications [48-50]. Typically these materials have a high selectivity but they sometimes do not exhibit sufficiently high permeability [51-52]. In order to increase the selectivity to CO_2, it is convenient to increase the affinity of the material for this gas. One of the most common approaches to meet these requirements is the use of block-copolymers having moieties able to interact with a certain gas.

Block-copolymers can combine hard and soft blocks. The hard block consists of a polymer with well-packed rigid structures; while the soft segments usually contain more flexible chains. The hard segments are glassy while the soft segments behave as rubbery polymers with relatively high free volume fractions. In this way the glassy polymer segments will provide the mechanical resistance. The rubbery segments generally form continuous microdomains with high gas permeability [53-54].

It is widely known that CO_2 is highly soluble in polyethylene oxide (PEO) and thus it has been used to separate carbon dioxide from other light gases [55-56]. Poly(ethylene oxide) is known to possess a high affinity towards CO_2 and consists of polar ether groups, which could produce quadrupolar interactions with CO_2. Hence, membranes fabricated from PEO would be of much interest in the processes like production from syngas, sweetening of low-quality natural gas and cleaning of flue gases. Based on this, the use of block-copolymers combining aromatic diamines with aliphatic ones based on PEO (Jeffamines), appears to be a promising route [57-59]. These compounds have good

permselectivity for the couple CO_2/N_2 [58, 60], which was attributed mainly to the high solubility-selectivity due to the existence of strong interactions between the oxyethylene groups in PEO and CO_2. The role of the interaction between CO_2 and ethylene oxide (EO) groups in CO_2 selectivity has been discussed and used for the development of new membranes [61-62]. Then, aromatic-aliphatic copolymers based on PEO are presented as a very promising choice.

1.7 Aims and Outline of the thesis

The main objective of this PhD thesis is the study of copoly(ether imide)s as gas separation membranes aim of using them for the CO_2 separation. The work includes 4 different sections, all them focusing on the same fundamental polymeric structure built form an aromatic dianhydride, plus an aromatic diamine ad an aliphatic one. The system most used along the thesis, that could taken as reference copolymer, is formed by the BPDA dianhydride plus the aromatic diamine ODA and the aliphatic one PEO2000. The so synthetized copolyimide is BPDA-PEO2000-ODA with a diamine ratio of 2:1 w/w. The corresponding structure can be seen in Figure 11.

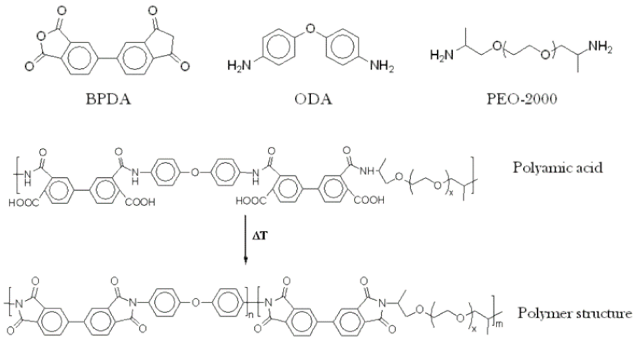

Figure 11. Synthesis and general structure for the reference copolymer of this work.

Section I is centered on the general aspects of methodology and the details of the processes carried out. The section is divided into 2 chapters. Chapter 1 introduces the present problems in gas separation and present the different alternative approaches to solve these problems. Chapter 2 compiles general methodology, used techniques and important theoretical points that appear along the rest of the manuscript.

Section II was focused on the study of the consequences of structure on the physicochemical properties of the copolymers. Their influence on the gas separation properties of the resulting films is also studied in this section. In chapter 3 entitled "*Thermally treated copoly(ether-imide)s made from BPDA and aliphatic plus aromatic diamines. Dependence of gas separation properties on the aromatic diamine*" the synthesis of new systems with different aromatic diamines is shown. Chapter

4 entitled "*Phase Segregation and Gas Separation Properties of Thermally Treated Copoly(ether-imide) from an Aromatic Dianhydride, an Aromatic Diamine and Various Aliphatic Diamines*" presents the development of new systems with several aliphatic diamines of different nature. In both cases the effect of these different structures on the properties of the final copoly(ether imide)s is studied. In Chapter 5 entitled "*Advances in the design of co-poly(ether-imide) membranes for CO_2 separations. Influence of aromatic rigidity on crystallinity, segregation and gas transport*" new aromatic-aliphatic systems are shown where the aromatic dianhydride has been changed. In this way new structures with different rigidity are studied for different proportions of the aliphatic diamine.

Section III is deepens on the study of the effect of the composition of the copolymers. Therefore, Chapter 6 entitled "*Influence of the PEO length in gas separation properties of segregating aromatic-aliphatic copoly(ether-imide)s*" brings into focus the effect of changing the length of the aliphatic diamine. There, the effect on permselectivity and physicochemical properties of the length of the diamine is investigated. Chapter 7 entitled "*Physical properties of films made of copoly(ether-imide)s with long poly(ethylene oxide) segments*" examines in depth the influence of the amount of polyether in the copolymer. In this case starting from the same aliphatic diamine, PEO6000, with the same aromatic diamine, ODA, and two aromatic dianhydrides, BPDA and BKDA, a complete physicochemical characterization of the obtained copolymers has been achieved. On the basis of this chapter, the next two chapters have been developed. In Chapter 8 named "*On the influence of the proportion of PEO in thermally controlled phase segregation of copoly(ether-imide)s for gas separation*" the proportion between diamines has been changed for the same fundamental structure, that we named reference structure, BPDA-PEO-ODA. The resulting coply(ether-imide)s were characterized and their gas separation properties tested. Chapter 9, "*On the influence of the proportion of PEO in thermally controlled phase segregation of copoly(ether-imide)s for gas separation*" continues the lines of Chapter 7 the gas separation properties of these systems have been investigated. Finally, in Chapter 10 "*Thermally Segregated Copolymers with PPO Blocks for Nitrogen Removal from Natural Gas*" is rooted on Chapter 4, where the influence of the different polyether diamines was analyzed. Now, poliproilene oxides, PPG, that showed a quite good permselective behavior for the separation of the CH_4/N_2 gas couple, are thoroughly considered. This couple of gases is especially relevant when facing natural gas treatment and transport. Different lengths and proportions of the PPO diamine have been studied and the influence of these parameters on permselectivity has been analyzed.

With the results obtained along the preceding chapters, it appeared as highly advantageous to be able to predict the behavior of these copolymers in gas separation. This predictive scheme would be very interesting in order to guide in designing new copolymeric systems from a theoretical approach by keeping the number of parameters to be known as low as possible. Section IV is centered on this equation. Chapter 11 entitled "*Prediction of Gas Permeability of Block-Segregated Polymeric Membranes by an Effective Medium Model*" presents the different models existing to predict the properties of composite polymeric systems from the properties of the phases entering in their composition. In this chapter a predictive model is proposed on the basis on the so called effective medium approximation that is capable of performing predictions on the permeability of segregated copolymers on the basis of their separate permeability. The model should be applicable to many new systems.

Finally Section V brings together the conclusions of this PhD thesis with a recapitulation of the gas separation properties of all the copoly(ether-imide)s studied in order to get a general perspective of the information gathered and the results obtained. A critical prospective on the future ways to gain deeper knowledge on these polymeric systems and their applications is also presented.

1.8 References

1. C. Breidenich;, D. Magraw;, A. Rowley;, J.W. Rubin;, The Kyoto Protocol to the United Nations Framework Convention on Climate Change, The American Journal of International Law, 92 (1998) 315-331.
2. A. Gore, An inconvenient truth: the crisis of global warming, Viking, 2007.
3. M.L. Parry;, O.F. Canziani;, J.P. Palutikof;, P.J.v.d. Linden;, C.E. Hanson, Climate Change 2007: Impacts, Adaptation and Vulnerability. Contribution of Working Group II to the Fourth Assessment Report of the Intergovernmental Panel on Climate Change, Cambridge University Press, Cambridge, UK, 2007.
4. B. Metz, O. Davidson, H.d. Coninck, M. Loos, L. Meyer, IPCC special report on carbon dioxide capture and storage, 2005.
5. CO2CRC, Clean energy facilities, in.
6. J.D. Figueroa, T. Fout, S. Plasynski, H. McIlvried, R.D. Srivastava, Advances in CO_2 capture technology—The U.S. Department of Energy's Carbon Sequestration Program, International Journal of Greenhouse Gas Control, 2 (2008) 9-20.
7. H.H. Khoo, R.B.H. Tan, Life Cycle Investigation of CO2 Recovery and Sequestration, Environmental Science & Technology, 40 (2006) 4016-4024.
8. E. Favre, Carbon dioxide recovery from post-combustion processes: Can gas permeation membranes compete with absorption?, Journal of Membrane Science, 294 (2007) 50-59.

9. S. Shelley, Capturing CO_2: Membrane-based systems move forward, Chemical Engineering Progress, 105 (2009).
10. M. Mulder, Basic Principles of Membrane Technology Second Edition, Kluwer, 1996.
11. N. Lakshminarayanaiah, Equations of membrane biophysics, Academic Press, NY, USA, 1984.
12. V. Silva, Theoretical Foundations and Modelling in NanoFiltration Membrane Systems, in: Applied Physics (SMAP), University of Valladolid, Valladolid, 2010.
13. M. Cheryan, Ultrafiltration and microfiltration: handbook, Technomic, 1998.
14. K. Ghosal, B.D. Freeman, Gas separation using polymer membranes: an overview, Polymers for Advanced Technologies, 5 (1994) 673-697.
15. S.P. Nunes, K.V. Peinemann, Membrane technology in the chemical industry, Wiley-VCH, 2001.
16. K. Scott, Handbook of industrial membranes, Elsevier Science & Technology Books, 1995.
17. H. Strathmann, L. Giorno, E. Drioli, Introduction to membrane science and technology, Wiley-VCH Verlag & Company, 2011.
18. R.W. Baker, Future directions of membrane gas separation technology, Industrial & Engineering Chemistry Research, 41 (2002) 1393-1411.
19. R. Baker, Membrane Technology and Applications, Wiley, 2004.
20. W.S.W. Ho, K.K. Sirkar, Membrance handbook, Chapman & Hall, 1992.
21. T. Matsuura, Synthetic Membranes and Membranes Separation Processes, CRC PressINC, 1994.
22. R.E. Kesting, Synthetic polymeric membranes: a structural perspective, Wiley, 1985.
23. B. Freeman, Y. Yampolskii, Membrane Gas Separation, Wiley, 2011.
24. P.M. Budd, S.M. Makhseed, B.S. Ghanem, K.J. Msayib, C.E. Tattershall, N.B. McKeown, Microporous polymeric materials, Materials Today, 7 (2004) 40-46.
25. P.M. Budd, N.B. McKeown, B.S. Ghanem, K.J. Msayib, D. Fritsch, L. Starannikova, N. Belov, O. Sanfirova, Y. Yampolskii, V. Shantarovich, Gas permeation parameters and other physicochemical properties of a polymer of intrinsic microporosity: Polybenzodioxane PIM-1, Journal of Membrane Science, 325 (2008) 851-860.
26. P.M. Budd, K.J. Msayib, C.E. Tattershall, B.S. Ghanem, K.J. Reynolds, N.B. McKeown, D. Fritsch, Gas separation membranes from polymers of intrinsic microporosity, Journal of Membrane Science, 251 (2005) 263-269.
27. M. Heuchel, D. Fritsch, P.M. Budd, N.B. McKeown, D. Hofmann, Atomistic packing model and free volume distribution of a polymer with intrinsic microporosity (PIM-1), Journal of Membrane Science, 318 (2008) 84-99.
28. S. Thomas, I. Pinnau, N. Du, M.D. Guiver, Hydrocarbon/hydrogen mixed-gas permeation properties of PIM-1, an amorphous microporous spirobisindane polymer, Journal of Membrane Science, 338 (2009) 1-4.
29. S. Thomas, I. Pinnau, N. Du, M.D. Guiver, Pure-and mixed-gas permeation properties of a microporous spirobisindane-based ladder polymer (PIM-1), Journal of Membrane Science, 333 (2009) 125-131.
30. J. Weber, N. Du, M.D. Guiver, Influence of Intermolecular Interactions on the Observable Porosity in Intrinsically Microporous Polymers, Macromolecules, 44 (2011) 1763-1767.
31. C.G. Bezzu, M. Carta, A. Tonkins, J.C. Jansen, P. Bernardo, F. Bazzarelli, N.B. McKeown, A Spirobifluorene-Based Polymer of Intrinsic Microporosity with Improved Performance for Gas Separation, Advanced Materials, 24 (2012) 5930-5933.
32. P.M. Budd, N.B. McKeown, Highly permeable polymers for gas separation membranes, Polym. Chem., 1 (2010) 63-68.

33. N.B. McKeown, P.M. Budd, Exploitation of intrinsic microporosity in polymer-based materials, Macromolecules, 43 (2010) 5163-5176.
34. H.B. Park, C.H. Jung, Y.M. Lee, A.J. Hill, S.J. Pas, S.T. Mudie, E. Van Wagner, B.D. Freeman, D.J. Cookson, Polymers with cavities tuned for fast selective transport of small molecules and ions, Science, 318 (2007) 254-258.
35. M. Calle, A. Lozano, Y.M. Lee, Formation of Thermally Rearranged (TR) Polybenzoxazoles; Effect of Synthesis Routes and Polymer Form, European Polymer Journal, (2012).
36. J.I. Choi, C.H. Jung, S.H. Han, H.B. Park, Y.M. Lee, Thermally rearranged (TR) poly (benzoxazole-< i> co</i>-pyrrolone) membranes tuned for high gas permeability and selectivity, Journal of Membrane Science, 349 (2010) 358-368.
37. S.H. Han, H.J. Kwon, K.Y. Kim, J.G. Seong, C.H. Park, S. Kim, C.M. Doherty, A.W. Thornton, A.J. Hill, Á. Lozano, Tuning microcavities in thermally rearranged polymer membranes for CO_2 capture, Physical Chemistry Chemical Physics, 14 (2012) 4365-4373.
38. J.H. Hodgkin, M.S. Liu, B.N. Dao, J. Mardel, A.J. Hill, Reaction mechanism and products of the thermal conversion of hydroxy-containing polyimides, European Polymer Journal, 47 (2011) 394-400.
39. C.H. Jung, J.E. Lee, S.H. Han, H.B. Park, Y.M. Lee, Highly permeable and selective poly (benzoxazole-co-imide) membranes for gas separation, Journal of Membrane Science, 350 (2010) 301-309.
40. C.H. Park, E. Tocci, Y.M. Lee, E. Drioli, Thermal Treatment Effect on the Structure and Property Change between Hydroxy-Containing Polyimides (HPIs) and Thermally Rearranged Polybenzoxazole (TR-PBO), The Journal of Physical Chemistry B, 116 (2012) 12864-12877.
41. Y. Yampolskii, Polymeric gas separation membranes, Macromolecules, 45 (2012) 3298-3311.
42. L.M. Robeson, Correlation of separation factor versus permeability for polymeric membranes, Journal of Membrane Science, 62 (1991) 165-185.
43. L.M. Robeson, The upper bound revisited, Journal of Membrane Science, 320 (2008) 390-400.
44. T.C. Merkel, H. Lin, X. Wei, R. Baker, Power plant post-combustion carbon dioxide capture: An opportunity for membranes, Journal of Membrane Science, 359 (2010) 126-139.
45. V. Bondar, B. Freeman, I. Pinnau, Gas sorption and characterization of poly (ether-b-amide) segmented block copolymers, Journal of Polymer Science Part B: Polymer Physics, 37 (1999) 2463-2475.
46. V. Bondar, B. Freeman, I. Pinnau, Gas transport properties of poly (ether-b-amide) segmented block copolymers, Journal of Polymer Science Part B: Polymer Physics, 38 (2000) 2051-2062.
47. S. Metz, M. Mulder, M. Wessling, Gas-permeation properties of poly (ethylene oxide) poly (butylene terephthalate) block copolymers, Macromolecules, 37 (2004) 4590-4597.
48. I. Bessonov, W.W. Wright, Polyimides--thermally stable polymers, Consultants Bureau, 1987.
49. M.K. Ghosh, K.L. Mittal, Polyimides: Fundamentals and Applications, Marcel Dekker Incorporated, 1996.
50. H.R. Kricheldorf, J. De Abajo, Progress in Polyimide Chemistry: I, Springer-Verlag, 1999.
51. D. Ayala, A. Lozano, J. De Abajo, C. Garcıa-Perez, J. De la Campa, K.-V. Peinemann, B. Freeman, R. Prabhakar, Gas separation properties of aromatic polyimides, Journal of Membrane Science, 215 (2003) 61-73.

52. K. Tanaka, H. Kita, K. Okamoto, A. Nakamura, Y. Kusuki, Gas permeability and permselectivity in polyimides based on 3, 3', 4, 4'-biphenyltetracarboxylic dianhydride, Journal of Membrane Science, 47 (1989) 203-215.
53. T. Barbari, W. Koros, D. Paul, Gas transport in polymers based on bisphenol-A, Journal of Polymer Science Part B: Polymer Physics, 26 (1988) 709-727.
54. Y. Li, M. Ding, J. Xu, Gas separation properties of aromatic polyetherimides from 1, 4-bis (3, 4-dicarboxyphenoxy) benzene dianhydride and 3, 5-diaminobenzic acid or its esters, Journal of applied polymer science, 63 (1997) 1-7.
55. Y. Hirayama, Y. Kase, N. Tanihara, Y. Sumiyama, Y. Kusuki, K. Haraya, Permeation properties to CO_2/N_2 of poly (ethylene oxide)-containing and crosslinked polymer films, Journal of Membrane Science, 160 (1999) 87-99.
56. M. Kawakami, H. Iwanaga, Y. Hara, M. Iwamoto, S. Kagawa, Gas permeabilities of cellulose nitrate/poly (ethylene glycol) blend membranes, Journal of applied polymer science, 27 (1982) 2387-2393.
57. K.-i. Okamoto, M. Fuji, S. Okamyo, H. Suzuki, K. Tanaka, H. Kita, Gas permeation properties of poly (ether imide) segmented copolymers, Macromolecules, 28 (1995) 6950-6956.
58. K.-i. Okamoto, N. Umeo, S. Okamyo, K. Tanaka, H. Kita, Selective permeation of carbon dioxide over nitrogen through polyethyleneoxide-containing polyimide membranes, Chemistry Letters, 22 (1993) 225-228.
59. H. Suzuki, K. Tanaka, H. Kita, K. Okamoto, H. Hoshino, T. Yoshinaga, Y. Kusuki, Preparation of composite hollow fiber membranes of poly (ethylene oxide)-containing polyimide and their CO_2/N_2 separation properties, Journal of Membrane Science, 146 (1998) 31-37.
60. A. Car, C. Stropnik, W. Yave, K.-V. Peinemann, Pebax®/polyethylene glycol blend thin film composite membranes for CO_2 separation: Performance with mixed gases, Separation and Purification Technology, 62 (2008) 110-117.
61. H. Lin, B.D. Freeman, Gas solubility, diffusivity and permeability in poly (ethylene oxide), Journal of Membrane Science, 239 (2004) 105-117.
62. S.R. Reijerkerk, M.H. Knoef, K. Nijmeijer, M. Wessling, Poly(ethylene glycol) and poly(dimethyl siloxane): Combining their advantages into efficient CO_2 gas separation membranes, Journal of Membrane Science, 352 (2010) 126-135.

CHAPTER 2

General methodology: synthesis and characterization

2.1 Introduction

As discussed in the first chapter, this report presents the synthesis and characterization of several aliphatic-aromatic copolyimides and their evaluation as gas separation membranes, with the ultimate goal of establishing relationships between the chemical structure of the monomers and the membrane performance of the corresponding polymers. This chapter collects the methodology and concepts that are common to all families regarding synthesis, characterization and properties, in order to facilitate the reading of the work carried out. Moreover, standard techniques that are employed to characterize the polymers are described, as well as the preparation protocol of the polymer films. Finally, the equations, experimental device and method for determining the transport coefficients of the membranes are presented.

This part analyzes the characterization in a generic way; more specific details for each type of polymer are shown in the corresponding chapter.

2.2 Synthesis of the copolyimides

It is desirable to achieve polymers with a high molecular weight, indispensable to obtain films with good mechanical properties and sufficiently robust membranes that can be evaluated as gas separation membranes. Carothers's equation is used to determine the degree of polymerization in polycondensation polymers:

$$DP = \frac{\mathrm{r+1}}{\mathrm{r+1-2pr}} \tag{1}$$

where p is the progress of the reaction (conversion), DP is the degree of polymerization and r is the stoichiometric disproportion defined as $r = \frac{\mathrm{Eq_a}}{\mathrm{Eq_b}}$ ($1 \geq r > 0$), being Eq_a and Eq_b the amount in equivalents of reactive groups of the monomers present in the medium. The maximum theoretical degree of polymerization will be infinite only when r = 1 (equivalent stoichiometric functional groups) and the reaction conversion is complete.

The presence of impurities in the monomers decreases de degree of polymerization and the optimum conditions for the formation of a polymer are not achieved. Therefore, the purity of the monomers must be very high as a necessary condition to obtain high molecular weight polymers. Moreover, the water present in the solvent may react with the dianhydride, resulting in non-reactive acid compounds leading to a stoichiometric disproportion. In addition, the partial oxidation of the

diamines also results in monofunctional monomers or non reactive molecules, which together with the hydrolysis products of the amide solvents compete with the diamines, producing lower molecular weight polymers. Therefore, the use of inert atmosphere and pure and anhydrous solvents is critical in this type of polymerizations.

In this work, aliphatic-aromatic polyimides synthesis was performed using the classical polycondensation reaction [1] between an aromatic dianhydride and two different diamines, aliphatic and aromatic. The formation of the copolyimide by this method involves two individual stages, as shown in Figure 1:

a) Formation of polyamic acid or poly (amide acid). This reaction takes place by nucleophilic attack of the amino group onto one of the carbonyl carbons of the cyclic dianhydride leading to ring opening with consequent formation of an amide and a carboxylic acid group. Diamines reactivity is controlled by the electronic density on the nitrogen, so that the presence of electron-donating groups in the ring of the aromatic diamine increases its reactivity.
b) Cyclodehydration of the polyamic acid to the corresponding polyimide. It is produced by the loss of one H_2O molecule, and subsequent closure of the cycle, thus forming the corresponding copolyimide

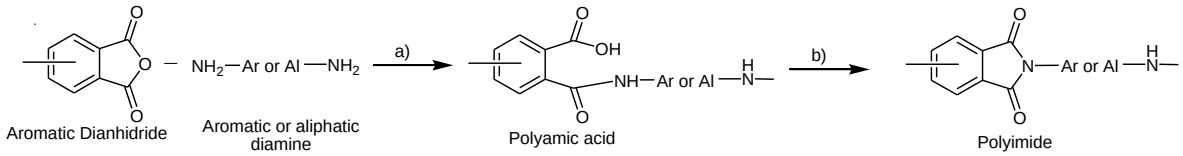

Figure 1. Polyimide synthesis en two steps.

Depending on the type of method used to carry out the cyclodehydration, we can distinguish between:

- Chemical cyclization: the imidation is performed by treating the polyamic acid with a mixture containing aliphatic anhydride (the most commons are acetic anhydride and triflic anhydride $(CF_3SO_2)_2O$) and a base, usually a tertiary amine such as pyridine, triethylamine or quinoline among others, at moderate temperature [2-3]. This treatment transforms the carboxylic acid to a mixed anhydride which favors the nucleophilic attack of the amide nitrogen with removal of acetate group and imide ring formation. The percentage of imidization that can be achieved will depend on the solubility of the polyimide in the

medium of imidization. If the objective is obtaining films, this method cannot be employed in the case of obtaining insoluble polyimides, as it is in this case.

- Thermal cyclization: involves high temperature treatment of the polyamic acid solution, producing at the same time the removal of the solvent and the cyclodehydration. This procedure is generally used when the final product is obtained as a film or coating. However, this method often produces insoluble polyimides due to crosslinking reactions which occur at the temperatures required for cyclization. In this method, the solution is first casted onto a substrate (in this case a glass plate) to obtain the polyimide film. Then the film is subjected to a heat treatment generally consisting of a gradual heating to temperatures ranging from 80 ° C to 350 ° C or even higher temperatures, depending on the glass transition temperature of the polymer. Formation of the film (removal of the solvent) at a temperature which depends on the boiling point of the solvent used. The solvents commonly used are polar aprotic amides, that give a favorable conformation for the poliamic acid cyclization [4]. Moreover, the plasticizing effect of these solvents increases the mobility of the reactive functional groups and their basicity allows them to accept protons easily [4]. It is also necessary to note that cyclization speed is fast in the initial stages, due to the presence of solvent, which allows the chains to more easily adopt conformations suited to the cyclodehydration and polyimide formation [5].

The imidization can also be carried out in one step. This procedure is based on the use of solvents with high boiling point (cresols, nitrobenzenes, xylenes, α-chloronaphthalene, etc.) [6]. The dianhydride and diamine are dissolved in the appropriate solvent and heated in the temperature range between 180-220 °C. At these temperatures chain growth and cycloimidization processes are simultaneous. Sometimes catalysts are used, including: quinoline, tertiary amines, alkali metals and zinc salts of carboxylic acids. A critical aspect to be considered in this type of process is that the formed polyimide must be soluble in the reaction medium at the end of conversion. The imidization process in one step is commonly used in polymerizations which involve generally nucleophilic monomers with low solubility in common solvents, or if one presumes the existence of significant steric effects on the reaction process.

2.3 Films preparation and thermal treatments

The method chosen to make the cyclodehydration is this work was the thermal cyclization. The resultant viscous copolyamic acid solution from the synthesis was diluted with NMP or DMAc to the appropriate viscosity for casting, filtered through a nominal #1 fritted glass funnel, degassed, and cast onto a leveled a glass plate. The resulting film was covered with a funnel to avoid fast evaporation of the solvent, dried at 80 ºC overnight, and finally thermally treated under inert atmosphere at different temperatures (see Figure 2).

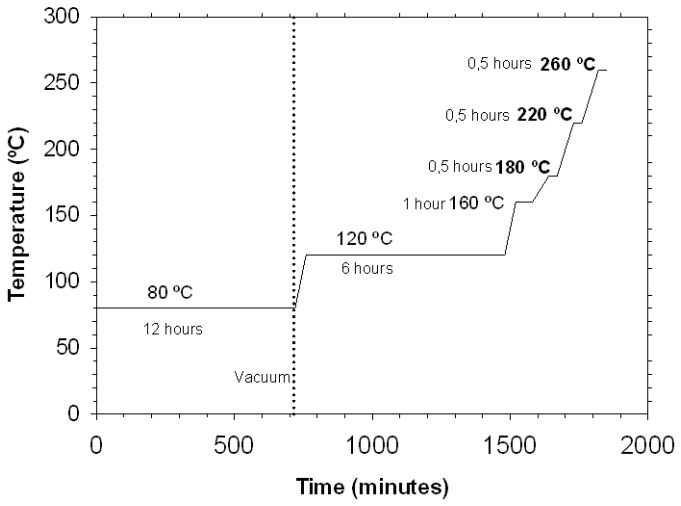

Figure 2. Graph of the thermal treatment protocol.

Figure 2 represents an example of a thermal treatment, but in the different chapters the corresponding thermal treatments have been specified for each series of polymers. Heat treatment had three objectives: first, to ensure complete imidization of the macromolecules; second, to achieve complete removal of the remaining solvent occluded after casting; and third to improve the phase segregation on the copolymers. Therefore, the film was heated above its aromatic glass transition temperature, Tg, so that the movements of the chains enabled the diffusion of molecules of the solvent to the outside and, moreover, the chains could adopt optimal conformation for the imide formation [7]. Subsequently, the film was allowed to cool slowly in the oven to room temperature.

Once the films were obtained, the next step was the characterization of the polymer properties.

2.4 Polymer characterization

Structural and morphological characterization of the copoly(ether-imide)s was done by Attenuated total internal reflectance-Fourier transform infrared analysis (ATR-FTIR), transmission electron microscopy (TEM) and Small Angle X-ray Scattering (SAXS); thermal characterization by thermogravimetric analysis (TGA) , differential scanning calorimetry (DSC), and thermomechanical analysis (TMA); polymer films properties by density measurements, solubility tests and tensile measurements; and surface characteristics by atomic force microscopy (AFM) and scanning electron microscopy (SEM).

In the following, the details for each technique and test are described:

2.4.1 Attenuated total internal reflectance-Fourier transform infrared analysis (ATR-FTIR)

ATR-FTIR has been used to verify the evalution of the imidization process, verifying that all the treated samples were completely imidized. Infrared analyses were performed at room temperature using a PerkinElmer Spectrum One infrared spectrometer equipped with an ATR accessory. Spectra taken directly from the films were the average of 16 scans at a resolution of 4 cm^{-1}.

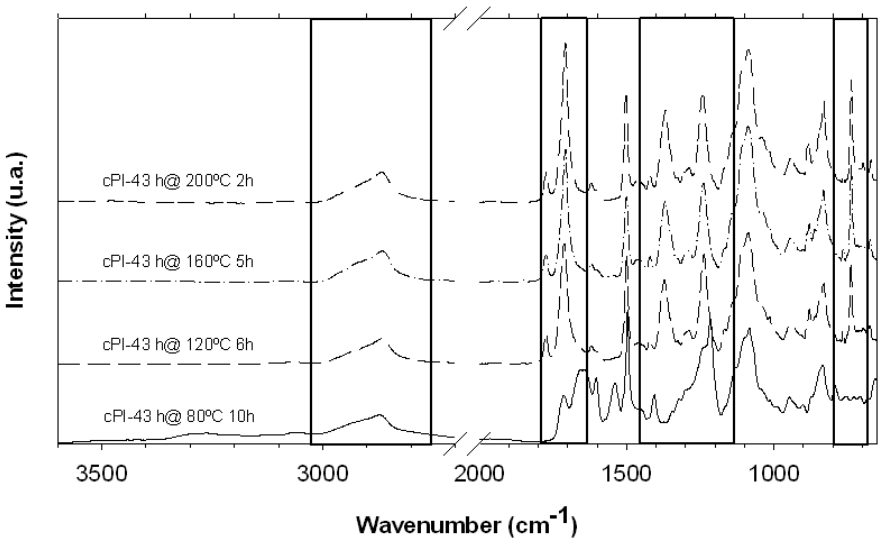

Figure 3. FTIR spectra of the sample BPDA-PEO2000-ODA 2:1 (cPI-43) before imidization (80 ºC) and after the thermal treatment at different temperatures (120, 160 and 200 ºC).

In general, for the copolymers presented in this memory, the bands centered around 3260 (O-H stretching from the polyamic acid), 1603 (amide I band from the polyamic acid) and 1538 (amide II band from the polyamic acid) cm-1 strongly decreased or disappeared, and the bands at approximately 1774 (symmetric stretching of C=O imide groups), 1712 (asymmetric stretching of C=O imide groups), 1370 (C-N stretching of imide groups) and 738 (imide ring deformation) cm^{-1} increased or appeared with imidization. The band at approximately 2880 cm^{-1}, related to aliphatic C-H stretching, did not change during imidization and it could be used as reference. The spectra (see Figure 3) for cPI-43 show the differences between the samples with and without imidization, and the lack of differentiation for the samples treated at 120 ºC, 160 ºC and 200 °C. This confirmed that at a temperature of 120 °C imidization was completed for this copolymer. The full imidization temperature needed for the copolymers with high polyether content was remarkably lower than that needed for fully aromatic polyimides [8-9].

2.4.2 Small Angle X-ray Scattering (SAXS)

SAXS measurements were performed at the beamline BM16 at the European Synchrotron Radiation Facility (Grenoble, France). Wavelength of the X-ray beam was 0.980 Å. Detector calibration was done with silver behenate ($AgC_{22}H_{43}O_2$), and the characteristic distance L was calculated from the maximum in the scattering vector ($q=4\pi(\sin\theta)/\lambda$, λ=wave length, 2θ=scattering angle). Disc samples cut from films were placed in a Linkam hot stage and heated at 10 ºC/min while the SAXS spectra were recorded. Calibration of temperature gave a difference of approximately 7 ºC between the temperature reading at the hot stage display and the real temperature at the sample.

X-ray scattering experiments were performed at a synchrotron radiation source in order to follow, in real-time conditions, the development of the phase-separated structure in these copolymers.

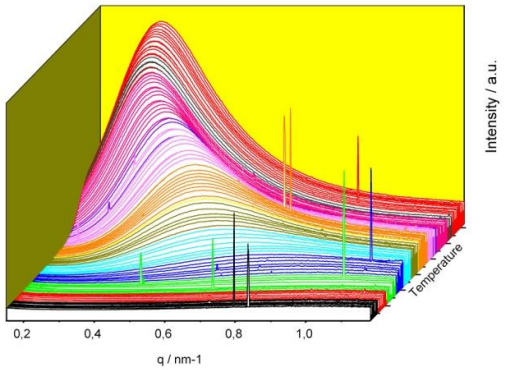

Figure 4. Typical evolution of the Iq^2–q curves with temperature for the PEO copolymers prepared in this work [10].

In Figure 4, the evolution of the scattering (Iq^2 vs. q) with increasing temperature is shown as an example. A single broad peak was obtained when the sample showed scattering. Two parameters were calculated over the scattering curve: the relative invariant, Q_0, as the integral below the curve Iq^2 vs. q in between the detector limits, related to the extent of the phase separation; and the maximum on the scattering curve, q_{max}, related to the size scale of the separated phases, calculated also from the curve Iq^2 vs. q. It is known that for lamellar systems the length scale (L) of the phase separation can be calculated directly from the curve Iq^2 vs. q, while for other morphologies a calculation of L from the I vs. q curve gives more realistic results [11].

Regardless of the organization of the phases, we are more interested on the changes with temperature than on the absolute values, and the representation Iq^2 vs. q highlights the maximum and makes it easier to detect, especially when using automated macros for the processing of the huge amount of data generated in a synchrotron experiment. Therefore this will be the criterion used here to get information on the L values. More details about the data analysis will be giving on the next chapters, especially in *Chapter 7*.

2.4.3 Thermogravimetric analysis (TGA)

Thermogravimetric analysis was based on the weight loss of a sample when subjected to a heat treatment as a result of degradation processes that lead to the release of volatiles. Thermogravimetry is a technique widely used in the thermal characterization of polymer materials [12], both in dynamic conditions, which measures the weight loss experienced by a sample subjected to a controlled heating program, as in isothermal conditions in which the weight loss is measured versus time at a given temperature. With the later it is possible to calculate the activation energies of the degradation processes. These experiments can be performed under nitrogen or air atmosphere in order to give information on the thermal stability in inert or oxidizing media. The instrument used in this work was a Thermal Analysis Q500 instrument. Disc samples cut from films with weights between 5 and 15 mg were tested. When running dynamic scans, it was done in Hi-Resolution mode, where the heating rate from 40 to 800 ºC is automatically adjusted in response to changes in the rate of weight loss, which results in improved resolution, with an initial heating rate of 10 ºC/min under a flux of nitrogen.

Heating the sample in an inert atmosphere first causes the loss of volatiles such as solvents and water absorbed [13], followed by the loss of low molecular weight components. These aromatic-aliphatic copolymers presented two more loss stages, after correcting for the first loss. The second

loss agreed well with the theoretical contribution of aliphatic diamine entering the copolymer composition, and it was therefore assigned to the loss of polyether block sequences. The third and final stage of weight loss was due to the thermal decomposition of the remaining aromatic polyimide segments.

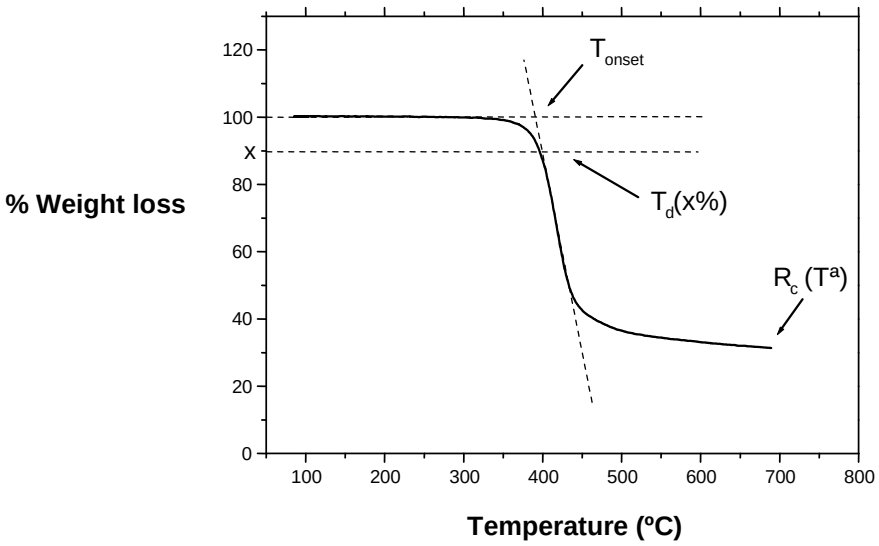

Figure 5. Typical TGA analysis

When a thermogravimetric curve is analyzed, two characteristic parameters are usually defined (Figure 5):

-T_{onset}: temperature at which it is considered that begins the process of weight loss (T_d). This value is calculated by taking the tangent to the curve and determining the cross point with the prolongation of the flat line before decomposition begins.

-R_c: carbonaceous residue is the weight (%) of the sample remaining after degradation to a certain temperature.

Sometimes, data for the temperatures at which partial decompositions have taken place (5, 10, 50% weight loss) are given.

The energy of the bonds present in the chemical structure of the polymer is the parameter that determines a priori the polymer heat resistance. Table 1 shows the energy of the bonds that exist in typical polyimides [14]. The presence of high-energy bonds provides high heat resistance to the

polymer, as is the case of sp^2 bonds C = C in conjugated aromatic rings. By contrast, the presence of labile bonds may trigger the rapid decomposition of the polymer and reduce its thermal resistance.

Table 1. Energy for the bonds presented in this work.

Bond	C-H	C-N	C-C	C=C	C-O	C=O
Energy (KJ/mol)	413	305	347	614	358	799

Keeping in mind that there are certain structural parameters that significantly influence the thermal stability of a polymer, it is required that certain conditions are met for high stability. Some of the most important are [15]:

a) Structures that do not easily transpose.

b) Structures stabilized by resonance.

c) Bond angles not stressed in the ring structures.

d) Intermolecular Interaction forces.

e) High molecular symmetry (structural regularity).

2.4.4 Differential Scanning Calorimetry (DSC)

The polymers can be divided into two groups, amorphous and semi-crystalline. In the first group, there is only one thermal transition associated with the onset of long range cooperative movements of the molecular chain, and the temperature at which it takes place is called the glass transition temperature, Tg. At this temperature there is a significant increase in large scale movements of the macromolecular chains and as a consequence of this, the chain mobility is increased, the polymer undergoes a significant decrease in its mechanical properties, which means that Tg is the maximum temperature of use as a structural material. The second group are the semi-crystalline polymers, and they have an amorphous part, characterized by its glass transition temperature and a crystalline part (as shown in Figure 6). As a result, a new thermal transition associated with the melting of the crystalline part of the material is detected and determined as the melting temperature Tm, which coincides with the classical concept of melting in conventional materials. Usually, both transition temperatures can be accurately determined by calorimetric methods.

Tg is strongly influenced by the chemical structure of the polymer, in particular molecular rigidity and the intensity of the intra-and intermolecular interactions and will depend on, among others, the following factors:

a) Structural rigidity. A more flexible chain produces a lower Tg.

b) Molecular weight. The increased mobility of the chain ends makes low molecular weight polymers have lower Tg. As molecular weight increases, the relative influence of the ends decreases and Tg increases up to a certain value at which the influence of the molecular weight is negligible. Therefore, it is convenient to overpass this critical molecular weight.

c) Bulky groups. The presence of bulky groups produces a double effect: decrease in Tg due to separation of the chains, caused by the volume of the groups, thereby hindering the formation of hydrogen bonds or other interactions between them; and, the presence of these groups increases intramolecular interactions, resulting in increased structural rigidity and, therefore, an increase in Tg.

d) Polar groups. The presence of polar groups favors the interaction between chains due to dipole interactions, charge transfer complexes and in some cases the existence of hydrogen bonding, resulting in an increase in Tg.

e) Low molecular weight fragments. May act as plasticizers, lowering the thermal (and mechanical) properties of the material being evaluated.

For the copolymers synthesized in this work, with soft and hard segments present in the structure, several possibilities can be found. Husken et al. and Reijerkerk et al., have described these possibilities for similar copolymers [16-17], as it is shown in Figure 6, but the morphology could vary greatly depending on the structure and composition of the copolymer.

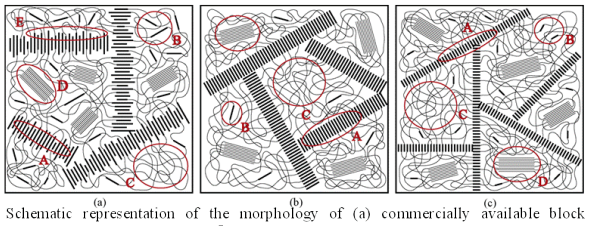

Schematic representation of the morphology of (a) commercially available block copolymers (e.g. the PEBAX© family), (b) PEO based block copolymers with monodisperse long T6T6T hard segments and (c) polyether based block copolymers with monodisperse short TΦT hard segments. The circled areas are representative for (A) crystalline hard segments, (B) non-crystallized rigid hard segments, (C) continuous amorphous soft phase, (D) crystalline soft phase and (E) intermediate region with mixed crystalline hard segments and non-crystalline soft segments.

Figure 6. Example of different conformation that could be find in a copolymer [16-17].

Differential scanning calorimetry (DSC) analyses were carried out in a Mettler Toledo (DSC 822e) calorimeter equipped with a liquid nitrogen accessory. Disc samples cut from films weighting 5–15 mg were sealed in aluminium pans. Samples were heated with the following cyclic method in order to monitor the changes in thermal properties with thermal treatment: from 25 ºC, the sample was heated at 10 ºC/min to a target temperature; once reached, the sample was cooled at the maximum cooling rate accessible for the instrument to -90 ºC, held at this temperature for 15 min and reheated at 10ºC/min to the next target temperature. The procedure was followed until the last treatment temperature was reached and a final run from -90 ºC to 80 ºC was performed. The Tg was determined as the value of the temperature at the midpoint in (1/2 Δ Cp) [18] of the interval where heat capacity changes. The melting temperature and the crystallization temperature of the crystalline part of the copolymers were determined from the maximum and the minimum of the exothermic and endothermic peak respectively, and the enthalpy of the melting/crystallization from the area below the peak. In this way, in each heating run, the thermal properties for the copolymers after treatment to the previously reached temperature were obtained, and a plot of thermal properties versus "instantaneous" thermal treatment could be built. The Tg of the aromatic segments in these copolymers was undetectable by this method.

2.4.5 Thermomechanical Analysis (TMA)

Thermomechanical analysis was carried out in order to detect the glass transition temperature of the aromatic polyimide hard segments, which was not detected by DSC. Several criteria can be chosen to determine the transition temperature. For example, it could be taken as the minimum in the first derivative of the strain vs. temperature curve, or the zero value in the second derivative. With the former criterion, the values were not clearly resolved, so that in this work it was decided to choose a different criterion, the temperature when strain is 10 times that of the sample at 100 ºC (see Figure 7), which gives lower transition values than the other two mentioned criteria. This criterion can be accepted at least for comparative purposes.

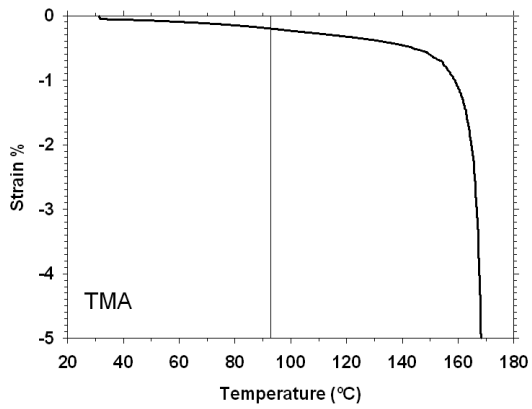

Figure 7. Example of TMA curve for the determination of the aromatic Tg.

Thermomechanical (TMA) tests were performed in a Rheometric Scientific instrument model DMTA V. Rectangular test pieces of 3 mm width and 20 mm length were cut from films. A distance of 10 mm was set between fixation clamps. Runs were carried out from ambient temperature at 2 ºC/min with a static stress of 3 MPa unless otherwise stated.

2.4.6 Density

Density, ρ, is an important property to characterize a membrane, to determine the degree of packing of the chains by estimating the fraction of the free volume (fractional free volume, FFV), which should help to predict the behavior of the membranes against the passage of gas, because FFV is the inner space of a solid or a liquid which is not occupied by molecules, as a result of imperfect packing.The densities (ρ) of the dense membrane films were determined using a CP225D Sartorius balance, provided with an immersion density kit, by measuring the weight difference of the sample in air and in a liquid of known density:

$$\rho_{sample} = \rho_{liq}\left[\frac{W_{air} - W_{liq}}{W_{air}}\right] \quad (2)$$

where ρ is the density of the sample, ρ_{liquid} is the density of the liquid used, W_{air} is the sample weight in air and W_{liq} is the sample weight when submerged in the liquid. Isooctane was used (ACS grade, purity ≥ 99%, Sigma-Aldrich) as the liquid for the measurements, and 10 measures were taken for each film. Figure 8 describes the volume change of an amorphous polymer with temperature:

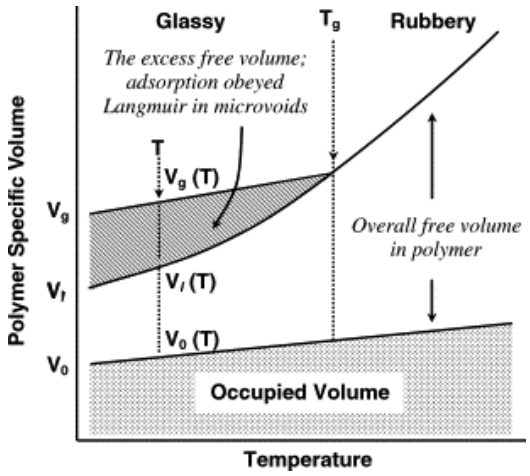

Figure 8. Schematic representation of the relationship between the polymer specific volume and temperature in amorphous polymers [19].

where V_0 is the volume occupied by the molecular chains being fully packaged and V is the specific volume of the material. When the temperature is gradually decreased, when Tg is reached, a sudden change in specific volume takes place due to the low mobility of the chains associated with the glass transition temperature; from this point, the volume decreases at slower rate than above Tg. Because of this kinetic component, the free volume in the amorphous glass state (T <Tg) depends on the cooling rate, a quick cooling will cause a sudden increase in viscosity which will lead to less efficient packing of the chains (V_g-V_0) and, therefore, an excess of free volume relative to the volume that would be reached by slow cooling (V_f-V_0).

For the copolymers presented in this work, there were two different Tg, one for the aromatic segments (usually close to or above 200 ºC); and another for the aliphatic segments (usually lower than 0 ºC). Then, at the characterization temperature, we will be always above the aliphatic Tg ($T_{experimental}$ >Tg) and below of the aromatic Tg ($T_{experimental}$<Tg).

2.4.7 Solubility

It is a usual problem for aromatic polyimides their very low solubility in most conventional organic solvents [20], and their processing has to be done in solvents such as N, N-dimethylformamide (DMF), N, N-dimethylacetamide (DMAc) or N-methylpyrrolidone (NMP). From these solutions, film forming, solvent removal and cyclodehydration reaction by a heat treatment is carried out simultaneously.

High chain stiffness, high cohesive energy values between chains as a result of charge transfer interactions, and the possibility that the heat treatment produces crosslinking reactions or induces crystallinity, are the three factors that are mentioned in the literature to explain the poor solubility values for aromatic polyimides [7]. The improvement of the solubility for these polymers may be addressed in several ways not mutually exclusive:

a) Introduction of monomers with relatively bulky lateral substituents, which increase the interchain distance.

b) Rupture of the symmetry of the polymer chains with meta-substituted aromatic rings.

c) Introduction of monomers with hindered rotation (structures with a spiro carbon, or with steric impediments) on certain links.

These factors produce a decrease in the cohesive energy density, while increasing the structural irregularity which inhibits the formation of crystalline regions.

Experimentally, solubility tests were carried out by weighing 10 mg of polymer in a test tube to which 1 ml of solvent was added. The system was magnetically stirred at room temperature until complete solubilization. If the polymer was not dissolved within 24 h, the solution was heated.

The films of the copolymers presented in this work resulted to be insoluble in DMAc (dimethylacetamide), NMP, Hexane, Toluene, THF (tetrahydrofuran) and CH_2Cl_2 (dichloromethane).

2.4.8 Mechanical Properties

In the great majority of applications involving polyimides, the polymer is subjected to high pressures, shear forces or pulling, so one of the important properties to be considered in choosing the polymer is its mechanical strength. The mechanical properties of an elastic solid can be described with Hooke's Law, which states that the resulting deformation of applying a stress is proportional to the same and independent of the strain rate. The viscous behavior of liquids, however, follows the Newton's law, according to which the deformation is independent of the stress. Both laws apply only to extreme cases or when the stress or strain rates are small. The mechanical properties are influenced by different external conditions (temperature, humidity, wind speed), and by the polymer itself (molecular weight, type of interaction between chains, etc). The

polymers, compared to conventional solids (e.g. metals), show a great dependence of its mechanical properties over time. This is due to its viscoelastic nature, which involves an intermediate behavior between viscous liquids and elastic solids. There are many types of mechanical tests to evaluate a material [21]. In this work tensile testing is chosen, since this is the most demanding test and easier to perform in films.

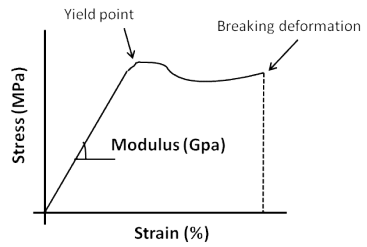

Figure 9. Stress-strain curve for a generic case of mechanical traction

A the typical stress-strain curve for a polymer (Figure 9) shows a first linear zone in which the material conforms to Hooke's law, behaving as an elastic solid, so that if the effort ceases, the material recovers its initial shape without any dissipation of energy. Therefore, Young's modulus or elastic modulus of a polymeric material is calculated from the slope in the initial stages of the test. The module measures the initial resistance that the material offers to deformation when subjected to an external force. After the initial linear zone, there is a second part where the deformation is no longer directly proportional to stress. For materials with plastic behavior, the stress can pass a maximum referred as yielding point where the material suffers plastic deformation, and from this point, the material does not recover its initial shape when stress is removed. One the yielding point is passed, the stress does not increase or slightly with the increase in strain until relatively large strains are reached and stress start to grow considerably with the increase in stress. Finally the material breaks, and at this point, the tensile strength and ultimate strain of the material are measured.

In this work, the assays were performed in a vertical extension dynamometer MTS Synergie 200 Universal Testing Machine. Rectangular test pieces of 5 mm width and 25 mm length were cut from films. A crosshead speed of 5 mm/min was used. Strain was measured from crosshead separation and referred to 10 mm initial length. At least six samples were tested for each polymer. Tests were conducted at room temperature and in some cases, when PEO was crystalline at ambient temperature, also at 50 ºC, as noted in the corresponding chapters. The samples were heated in situ by blowing hot air transversally to the cross-section side of the specimen in order to avoid stress on the sample. In this case, temperature was measured with a thermometer close to the specimen.

2.4.9 Scanning Electronic Microscopy (SEM) and Transmission Electronic Microscopy (TEM)

This group of techniques allows the imaging of the topography of the membrane at the surface surface and in cross-sections along the thickness (SEM) and the visualization of the morphology in phase-separated systems (TEM). The first uses the secondary electrons resulting from interactions with the sample beam (energy is between 0.2 and 30 kV), while the second uses an electron beam between 80 and 200 kV, resulting in the difference image of the scattering, both elastic and inelastic electron beam. A third technique, field effect scanning electron microscopy (FESEM or ESEM), similar to SEM, enables better decisions without the coating of the sample with conductive films. This kind of characterization is usually used, for example, to observe the pore size in porous membranes [22], as well the morphology in segmented copolymers.

In the case of the copolymers studied in this work, TEM was used in order to get information about the morphology of the samples as a function of the polymer composition. The system used in this case were FEI Quanta 200FEG (ESEM), and JEOL JEM-FS2200 HRP (TEM). Unfortunately, for the copolymers synthesized in this work, the morphology could not be directly visualized by TEM.

2.4.10 Atomic Force Microscopy (AFM)

This technique allows the study of materials, in a conductive and non-conductive way, reaching a nanometer scale. There are three characteristics that distinguish this microscopy: high resolution, three-dimensional imaging and the ability to operate in different environments (vacuum, liquid, air or other gases). The technique consists of a small tip attached to a flexible cantilever which runs along the surface while moving vertically according to its interaction with the sample. Typical distances between the probe (tip) and the sample are in the range of 0.1 to 100 nm. In this range there are different types of forces which defines the resulting interaction, attractive or repulsive. The type of force, the distance that exists between the tip and the sample, and the type of recorded signal defines the AFM operation mode [22].

For the determination of the surface topography there are three modes: contact mode which works in the repulsive forces, so no contact working in the attractive forces (in both cases what is measured is the deflection cantilever) and intermittent mode (tapping mode) in which the arm is oscillating at its natural frequency. The latter is related to the topography the amplitude of oscillation of the cantilever, but there is another signal related to the change in the swing phase

which is related to the change in the viscoelastic properties of the surface. This signal is useful for the analysis of surfaces formed by different materials or the same material at different stages of crystallization, hardness, adhesion, etc. Nevertheless phase changes also occur by abrupt topographical changes which reduce the usefulness of the method. The most effective way to detect changes in properties of the surface is modulated force microscopy (MFM Modulation Force Microscopy). The tip for a first sweep, generally in tapping mode, the natural frequency of oscillation of the cantilever, and a second scan following the topography of the sample oscillating at a lower frequency (of the bimorph crystal port tip). The interaction of the tip with the sample in this second scan only depends on the hardness of the sample. There are many other related modes (adhesion forces, electrical forces, magnetic forces, etc.), that are not dealt with because they are not used in this work.

AFM analysis was performed in a Digital Instruments Nanoscope IIIa. This technique was used to determine the surface topography. The instrument operated in tapping mode in order to obtain the morphology of both sides of the sample. In other cases the objective of the analysis was to determine topographic roughness inherent to the sample as a result of the manufacturing process and the thermal treatments [23].

2.5 Gas transport in membranes

The gas transport mechanism in membranes depends on whether the membrane is porous or nonporous. In general, nonporous or dense polymeric membranes are used as selective gas permeation barriers while porous membranes are used as substrates for mechanical support. Figure 10 illustrates the mechanisms of gas permeation. Gas permeation in dense membranes can be described by the solution-diffusion mechanism, while in porous membrane the gas transport follows viscous flow (convective flow), Knudsen flow, molecular sieving or a combination of them [24-26], depending on the relative size of the permeant molecules and the pores of the membrane.

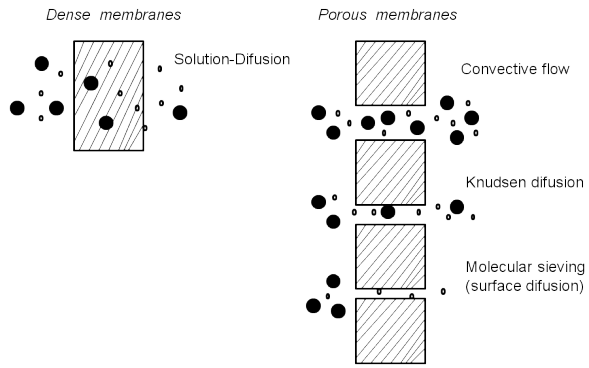

Figure 10. Mechanisms of gas permeation through dense and porous membranes [27].

The solution-diffusion mechanism is widely accepted by the majority of researchers for gas transport in nonporous membranes [28]. According to this mechanism, gas permeation through a membrane includes three consecutive steps (shown in Figure 11): (1) Gas dissolves into the membrane at the high pressure side; (2) Penetrant gas molecules diffuse through the membrane driven by the concentration difference across the membrane; (3) Gas molecules desorbs at the low pressure side of the membrane. Gas permeation is controlled by the diffusion of the penetrant gas molecules in the membrane matrix, while sorption/desorption equilibrium is assumed to be established at the two interfaces between the gas and the membrane. A gas mixture is separated because of the differences in the solubility and mobility of the gas components in the membrane matrix.

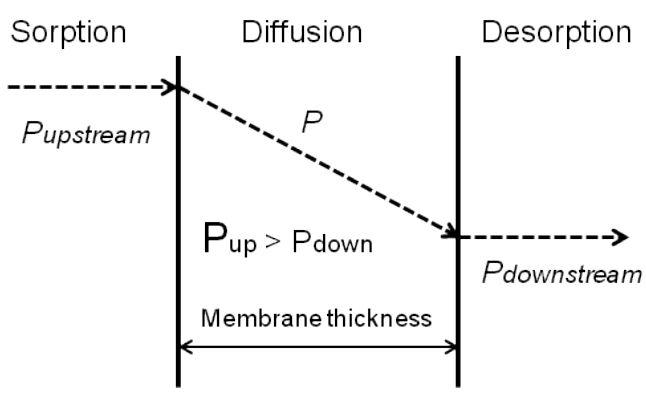

Figure 11. Schematic diagram of the solution-diffusion mechanism

Gas diffusion through a nonporous homogenous membrane at steady state can be described by the Fick's first law [29]. For one-dimensional diffusion, the permeation flux through the membrane can be written as

$$J^0 = -D(c)\frac{dc}{dZ} \tag{3}$$

where J^0 is the permeation flux, c the concentration of the permeating species dissolved in the membrane, and D(c) diffusion coefficient. For permanent gases (e.g., O_2, N_2, and H_2), D can normally be regarded as a constant that is independent of concentration. When condensable gases or vapors permeate through the membrane, D is usually concentration dependent due to the plasticization or swelling of the polymer by the permeant. The concentration dependence of the diffusion coefficient can be expressed by an exponential or a linear expression [30-31]. The equilibrium concentration c is related to the gas pressure, p, by

$$C = S(c) \cdot p \tag{4}$$

where *S(c)* is a solubility coefficient.

When the concentration of the penetrant in the polymer is very low, Eq. (4) can be represented by the Henry's law and S becomes a constant. When D is also a constant, substituting Eq. (4) into Eq. (3) and integrating, yields

$$J^0 = DS\frac{p_{up}-p_{down}}{l} = \left(\frac{P}{l}\right)\Delta p = J \cdot \Delta p \tag{5}$$

where P (P=DS) is the permeability, p_{up} and p_{down} are the pressures of upstream and downstream, respectively, l is the effective membrane thickness, and J the permeance for gas permeation.

The permeability (or permeance) ratio of two gas species (i and j) is often defined as the ideal selectivity (or ideal separation factor) α, shown in Eq. (6).

$$\alpha_{i/j} = \frac{P_i}{P_j} = \frac{J_i}{J_j} = \frac{D_i}{D_j} \cdot \frac{S_i}{S_j} \tag{6}$$

where the ratios D_i/D_j and S_i/S_j represent, respectively, the "diffusivity (or mobility) selectivity", reflecting the difference in the molecular sizes of the two permeants, and the "solubility selectivity", reflecting the relative condensabilities of the two gases. These ratios represent the contributions of the sorption and diffusion steps to the overall selectivity due to the differences in the diffusivities and solubilities of the two gases in the membrane.

For an ideal system where both the gas diffusivity and permeability coefficients are constant, the diffusivity coefficient is commonly determined by the gas permeation method, i.e., the time-lag

method, which has been described extensively by Barrer (1939) [32]. From the Fick's second law, under different assumptions: (i) the membrane is free of the penetrant molecules at the start of the permeation, (ii) the feed gas pressure (p_{up}) is kept constant, and (iii) the feed pressure is much larger than the permeate pressure; when t→∞, a steady state is approached and the Q_t (the amount of penetrant per unit membrane area) vs. t (time) plot becomes linear:

$$Q_t = \frac{Dc_{up}}{l}\left(t - \frac{l^2}{6D}\right) = \frac{DS}{l} \cdot p_{up}\left(t - \frac{l^2}{6D}\right) = \frac{P}{l} \cdot p_{up}\left(t - \frac{l^2}{6D}\right) \quad (7)$$

By extrapolating the steady state permeation curve, the intercept (θ) on the t-axis can be obtained, which is referred to as the time lag:

$$\theta = \frac{l^2}{6D} \quad (8)$$

Therefore, the gas permeability (P) and diffusivity coefficient (D) can be obtained from the slope ($\frac{P}{l} \cdot p_{up}$) and the intercept (θ) of the steady state permeation curve, and the gas solubility coefficient (S) can thus be determined from the relation P=DS.

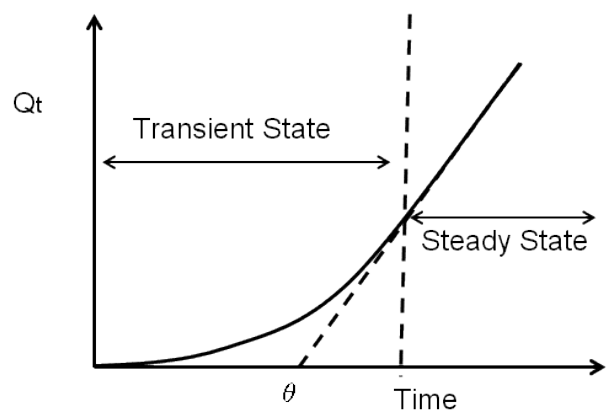

Figure 12. Time-lag measurement of gas permeation.

The diffusivity coefficient can also be determined from gas sorption kinetics [29]. When D is constant, two methods may be used, the short time and the long time methods. At short times (early stage of sorption), the plot of (M_t/M_∞) (normalized mass uptake, i.e., the ratio of sorption amount at time t over equilibrium sorption amount) vs. $(t/l^2)^{1/2}$ is a straight line, and the diffusion coefficient can be estimated from the slope $[4(D/\pi)^{1/2}]$ of the sorption uptake curve. When D is a function of concentration, the value so obtained is the apparent diffusivity coefficient. The short time method can be applied up to 50% (M_t/M_∞) with negligible deviations from the exact solution of the Fick's

second law. Normally the diffusivity coefficients obtained using the two methods are very close to each other [33].

Gas solubility in membranes can be determined by equilibrium sorption based on Eq. (4). There are two main techniques to measure the equilibrium sorption uptake: gravimetric sorption and barometric (pressure-delay) techniques. Generally, gravimetric technique is suitable for the sorption of carbon dioxide, organic vapor and water vapor, which have relatively high sorption capacity and low saturated pressures (lower than atmospheric) [34-35]. For gases with a low sorption capacity or when the sorption experiments need to be carried out at a relatively high pressure, the pressure-delay technique (also called the barometric technique) is often used [36-37]. The system consists of two chambers with known volumes, a sample chamber and a reference chamber. The penetrant from the reference chamber is introduced into the sample chamber, and the pressure gradually decreases due to the sorption and then becomes constant when the sorption reaches equilibrium. By measuring the pressures at the start of sorption and at sorption equilibrium, the sorption capacity can be determined.

Both techniques are affected by experimental errors caused by system leaking and wall adsorption as well as the accuracy of mass, pressure and volume measurements, especially when the sorption capacity is small. For permanent gases with a quite small sorption capacity, even barometric technique hardly renders accurate results.

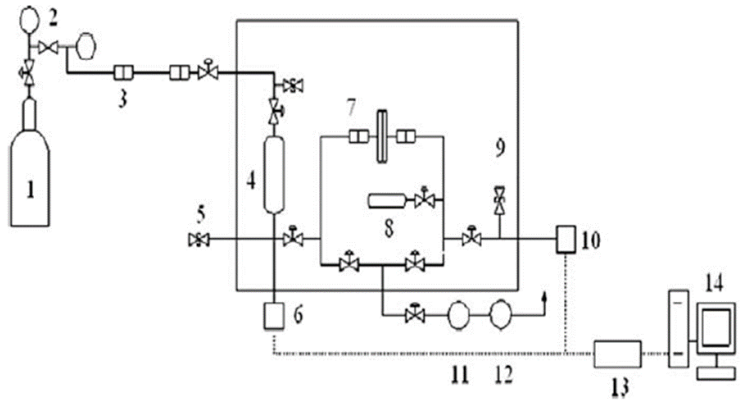

Figure 13. Diagram of the permeation device: (1) Gas supply, (2) Pressure regulator, (3) Quick connection, (4) Gas reservoir, (5) Relief valve, (6) High pressure transducer, (7) Permeation cell, (8) Expansion cylinder, (9) Relief valve, (10) Low pressure transducer, (11) Turbo-molecular pump, (12) Rotary pump, (13) Power source and (14) Data acquisition.

In this work, the conditions for each experiment will be described in the corresponding Chapters.

2.6 References

1. D.S. Wilson, H.D.; Hergenrother, P.M., Polyimides, in, Blackie, Glasgow, 1990.
2. A.L. Endrey, Aromatic polyimide particles from polycyclic diamines, in, US Patents 3179631, 1965.
3. R.W. Hendrix, Process for preparing polyimides by treating polyamide-acids with aromatic monocarboxylic acid anhydrides, in, US Patent 3179632, 1965.
4. M. Tsapovetskii, L. Laius, T. Zhukova, L. Shibayev, N. Stepanov, M. Bessonov, M. Koton, Study of the breakdown and resynthesis of polyamic acids in solid phase, Polymer Science USSR, 30 (1988) 295-301.
5. J.A. Kreuz, A. Endrey, F. Gay, C. Sroog, Studies of thermal cyclizations of polyamic acids and tertiary amine salts, Journal of Polymer Science Part A-1: Polymer Chemistry, 4 (1966) 2607-2616.
6. S.V. Vinogradova, V. Korshak, Advances in the Polycondensation Methods for the Synthesis of Thermostable Polymers, Russian Chemical Reviews, 39 (1970) 308.
7. K.L. Mittal, Polyimides and other high temperature polymers: synthesis, characterization and applications, CRC PressI Llc, 2005.
8. K.-i. Okamoto, N. Umeo, S. Okamyo, K. Tanaka, H. Kita, Selective permeation of carbon dioxide over nitrogen through polyethyleneoxide-containing polyimide membranes, Chemistry Letters, 22 (1993) 225-228.
9. K.-i. Okamoto, M. Fuji, S. Okamyo, H. Suzuki, K. Tanaka, H. Kita, Gas permeation properties of poly (ether imide) segmented copolymers, Macromolecules, 28 (1995) 6950-6956.
10. A. Marcos-Fernández, A. Tena, A.E. Lozano, J.G. de la Campa, J. de Abajo, L. Palacio, P. Prádanos, A. Hernández, Physical properties of films made of copoly(ether-imide)s with long poly(ethylene oxide) segments, European Polymer Journal, 46 (2010) 2352-2364.
11. F.J. Baltá-Calleja, C.G. Vonk, X-ray scattering of synthetic polymers, Elsevier, 1989.
12. J.R. McCallum, Thermogravimetric Analysis in Comprehensive Polymer Science, Pergamon Press Ltd., Oxford, 1989.
13. J.L. Hedrick, K.R. Carter, H.J. Cha, C.J. Hawker, R.A. DiPietro, J.W. Labadie, R.D. Miller, T.P. Russell, M.I. Sanchez, W. Volksen, D.Y. Yoon, D. Mecerreyes, R. Jerome, J.E. McGrath, High-temperature polyimide nanofoams for microelectronic applications, Reactive and Functional Polymers, 30 (1996) 43-53.

14. D.W. van Krevelen, K. te Nijenhuis, Properties of Polymers: Their Correlation with Chemical Structure; their Numerical Estimation and Prediction from Additive Group Contributions, Elsevier Science, 2009.
15. K.L. Mittal, S.o.P.E.M.-H. Section, Polyimides: synthesis, characterization, and applications, Plenum, 1984.
16. D. Husken, J. Feijen, R.J. Gaymans, Hydrophilic segmented block copolymers based on poly(ethylene oxide) and monodisperse amide segments, Journal of Polymer Science Part A: Polymer Chemistry, 45 (2007) 4522-4535.
17. S.R. Reijerkerk, A. Arun, R.J. Gaymans, K. Nijmeijer, M. Wessling, Tuning of mass transport properties of multi-block copolymers for CO_2 capture applications, Journal of Membrane Science, 359 (2010) 54-63.
18. K.-R. Lee, D.-J. Liaw, B.-Y. Liaw, J.-Y. Lai, Sorption and transport properties of gases in fluoro-containing aromatic polyamide membranes, European polymer journal, 34 (1998) 665-670.
19. S. Kanehashi, K. Nagai, Analysis of dual-mode model parameters for gas sorption in glassy polymers, Journal of Membrane Science, 253 (2005) 117-138.
20. F.W. Harris, R.B. Seymour, Structure-solubility relationships in polymers, Academic Press, 1977.
21. L.E. Nielsen, R.F. Landel, Mechanical Properties of Polymers and Composites, Second Edition, Marcel Dekker Incorporated, 1994.
22. L. Palacio, Caracterización estructural y superficial de membranas microporosas, in: Applied Physic, Valladolid, Valladolid, 1998.
23. K.C. Khulbe, C.Y. Feng, T. Matsuura, Synthetic Polymeric Membranes: Characterization by Atomic Force Microscopy, Springer London, Limited, 2008.
24. W.S.W. Ho, K.K. Sirkar, Membrane Handbook, Springer US, 1992.
25. M. Mulder, Basic Principles of Membrane Technology, Springer, 1996.
26. R. Baker, Membrane Technology and Applications, Wiley, 2012.
27. W. Koros, G. Fleming, Membrane-based gas separation, Journal of Membrane Science, 83 (1993) 1-80.
28. J. Wijmans, R. Baker, The solution-diffusion model: a review, Journal of Membrane Science, 107 (1995) 1-21.
29. J. Crank, G.S. Park, Diffusion in Polymers, Academic Press, 1968.

30. F. Greenlaw, R. Shelden, E. Thompson, Dependence of diffusive permeation rates on upstream and downstream pressures: II. Two component permeant, Journal of Membrane Science, 2 (1977) 333-348.
31. H.L. Frisch, Sorption and Transport in Glassy Polymers - A Review, Defense Technical Information Center, 1979.
32. R. Barrer, E.K. Rideal, Permeation, diffusion and solution of gases in organic polymers, Transactions of the Faraday Society, 35 (1939) 628-643.
33. M.E. Rezac, T. John, Correlation of penetrant transport with polymer free volume: additional evidence from block copolymers, Polymer, 39 (1998) 599-603.
34. M. Suwandi, S. Stern, Transport of heavy organic vapors through silicone rubber, Journal of Polymer Science: Polymer Physics Edition, 11 (1973) 663-681.
35. E. Favre, P. Schaetzel, Q. Nguygen, R. Clement, J. Neel, Sorption, diffusion and vapor permeation of various penetrants through dense poly (dimethylsiloxane) membranes: a transport analysis, Journal of Membrane Science, 92 (1994) 169-184.
36. V. Shah, B. Hardy, S. Stern, Solubility of carbon dioxide, methane, and propane in silicone polymers: effect of polymer side chains, Journal of Polymer Science Part B: Polymer Physics, 24 (1986) 2033-2047.
37. V. Bondar, B. Freeman, I. Pinnau, Gas sorption and characterization of poly (ether-b-amide) segmented block copolymers, Journal of Polymer Science Part B: Polymer Physics, 37 (1999) 2463-2475.

SECTION II. Study of the influence of the composition on the copolymer properties.

Within this section, the results to the study of the influence of the composition on the properties of different copolymers will be discussed. This work focuses on the systematic study of the properties of a series of copoly (ether-imide)s based on an aromatic diamine, an aliphatic diamine and an aromatic dianhydride. The reference structure throughout this section is composed of: BPDA (aromatic dianhydride) PEO2000 (aliphatic diamine) and ODA (aromatic diamine), with a weight ratio between the aromatic and aliphatic diamine of 2:1 (w / w). The structure can be seen in Figure 11 of the introduction. From this reference copolymer, the structure of the aromatic diamine, the structure of the aromatic dianhydride and the structure of the aliphatic diamine, was varied.

Chapter 3 investigates the effect of the type of aromatic diamine (ODA, BNZ and PPD) on the gas transport properties in polyether based block copolymers with BPDA as aromatic dianhydride and PEO2000 as aliphatic diamine. A complete characterization of the copolymers was carried out. The results were discussed in relation to the segregation ability, thermal properties and the gas separation properties.

Chapter 4 describes the synthesis, thermo-mechanical properties, segregation and gas separation properties of novel polyether based block copolymers using different soft segment structure (PEO, PPO, PEO-PPO copolymer and pTHF) and the same aromatic hard segment structure (BPDA and ODA).

Chapter 5 presents a study of the copolymers based on different aromatic dianhydrides, BPDA, BKDA and PMDA. In addition to the aromatic dianhydride, the PEO content was also varied. The influence of both parameters on the phase segregation ability, the thermal properties and the gas separation behavior was evaluated.

CHAPTER 3

Thermally treated copoly(ether-imide)s made from BPDA and aliphatic plus aromatic diamines. Dependence of gas separation properties on the aromatic diamine.

Alberto Tena[1,3], Ángel Marcos-Fernández[1,3], Ángel E. Lozano[1,3], José G. de la Campa[1,3], Javier de Abajo[1,3], Laura Palacio[1,2], Pedro Prádanos[1,2], Antonio Hernández[1,2]

[1]*Smap UA-UVA-CSIC, Parque Científico Universidad de Valladolid, Paseo de Belén, s/n, 47011 Valladolid, Spain.*

[2]*Dept. Física Aplicada, Facultad de Ciencias, Universidad de Valladolid, Paseo de Belén, 7, 47011 Valladolid, Spain*

[3]*Instituto de Ciencia y Tecnología de Polímeros, CSIC, Juan de la Cierva 3, 28006 Madrid, Spain.*

This chapter has been published in:

Journal of Membrane Science, 387 (**2012**) 54-65.

DOI: http://dx.doi.org/10.1016/j.memsci.2011.10.008

Abstract

A set of copoly(ether-imide)s, formed by the reaction between an aromatic dianhydride (BPDA), a polyoxyalkyleneamine (poly(ethylene oxide) diamino terminated) (PEO-2000) and various aromatic diamines (PPD, BNZ, and ODA) under different thermal treatments, has been obtained and characterized. The existence of phase segregation in these copolymers has been confirmed by SAXS. It has also been proved that aromatic diamines having a hinge group, such as ODA, produce bigger segregated domains while short and rigid aromatic diamines give higher percentages of phase segregation.

A direct relationship between gas permeability and percentage, and size of the domains, of the segregated phase has been obtained. Also, higher or similar selectivities have been observed as a function of the thermal treatment. In such way, the use of high temperatures during the thermal treatment, responsible of the improvement of the phase segregation, enhances the gas properties, producing materials with permeability/selectivity values close to the Robeson limit. In the case of the CH_4/N_2 pair an interesting reverse selectivity has been observed probably due both to a specific interaction of the gas with the polymer and to an increase in the solubility of CH_4 in the soft segregated portions of the copolymer.

The use of PPD as comonomer provides more phase segregation while the use of ODA gives bigger segregated domains. In terms of permselectivity the performances, for all the pairs of gases studied, follow the PPD>BNZ>ODA sequence when relatively low treatment temperatures are used whilst quite similar results for BNZ and ODA were observed when higher treatment temperatures are employed. This seems to indicate that the domains size is a key factor in the gas separation properties with a certain influence of the percentage of segregation. An adequate balance of short length with limited rigidity of the aromatic part should improve the properties of this kind of materials.

Graphical Abstract

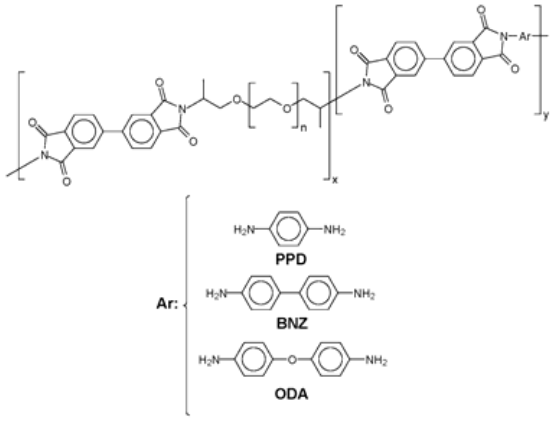

3.1 Introduction

Due to environmental concerns and economic interests, there is an imperative need for new materials with improved properties for gas separation applications [1-4]. In particular, the separation of CO_2 from its sources in power plants, steel, cement production plants and the chemical industry, among other industries, has attracted worldwide attention and an enormous amount of research due to that the greenhouse effect, generated mainly by the burning of fossil fuels in the last two centuries, is not being controlled. This greenhouse effect, which is accepted to be the reason of the climate change, is caused by the emission of various gases, most notably carbon dioxide. In the last years, it is mandatory and widely accepted to take account of it in order to stave off or at least to minimize the adverse effects that are expected for the next decades [5-9]. Thus, there is an imperative need of improving the efficiency in old energy sources as coal plants, and in new ones as in the derived from the so-known hydrogen economy, where a fossil fuel (mainly natural gas or coal) is reconverted into hydrogen along with the formation of carbon dioxide. This improvement of efficiency, combined with the position supported by many governments of taxing the emission of greenhouse gases, is forcing both to the academy and the industry to make research in the sequestration of CO_2. Therefore, new technologies must be found in order to separate such gases from diverse mixtures of gases in an efficient way. In this context, the technology of gas separation by membranes is considered a viable option. Gas separation membranes are very competitive attending to economical reasons, with good mechanical properties and excellent gas productivity (flux and ability to separate complex mixtures of gases), they are very easy to install and maintain and because of its efficiency, membranes show small carbon footprint [10,11].

Consequently, all separations where CO_2 is involved have a high social and economical interest because this gas is present as a contaminant or by-product in many industrial processes. Even though many systems have been tested, some of them presenting outstanding properties when compared with other ones developed 20 or 30 years ago, it is crucial, in order to accomplish the challenges need to fit the requirements of the industry, to study more thoroughly the chemical and physical properties of the materials used to make gas separation membranes, and to shed light on the effect of these properties in the separation of gases.

Glassy polymers and in particular polyimides are well known for their excellent thermal oxidative stability and exceptional mechanical properties, along with an extraordinary ability of separating complex mixtures of gases in diverse applications [12-14]. Thus, among all the polymeric membranes, it has been widely demonstrated that the use of aromatic polyimides is one of the best

alternatives [15-19]. However, the manufacture of new polymeric materials tailored for more specific applications is needed today. With regards to the separation of CO_2, aromatic polyimides are close to the trade-off of gas permeability versus gas selectivity obtained by Robeson in 1991 [19] but far away from the new one established in 2008 [20]. It should be commented at this point that not many materials have been capable to overpass and even to reach the cited 2008 Robeson limit [22,23] and hence, in order to achieve more serious enhancements in this fields, additional studies should be started.

There are a number of possible itineraries addressed to improve the permeability and selectivity of gas separation membranes. One of them consists of optimizing the structure of the polymer chains in solid sate to give high fractional free volume fractions with a well tailored distribution of sizes and with restrictive or selective channels communicating the voids in order to increase the diffusivity. Other possible approach consists of attempting to increase the solubility introducing a certain chemical affinity for a gas to make it to adsorb on certain moieties of the polymer [17,24]. The introduction of polar groups that can interact favourably with CO_2, such as amine [18] or carboxyl [19] groups has proved to be a very efficient approach to increase the CO_2/N_2 or CO_2/CH_4 selectivity. In this regard, poly(ethylene oxide) (PEO) is a very attractive polymer due to the strong affinity of CO_2 towards the oxygen of the oxyethylenic segments [25-29]. Thus, recently, there have been some studies devoted to the application of polymeric membranes containing PEO or similar polar ether segments in carbon dioxide separations as a result of the enhanced CO_2 solubility of the PEO moieties [30-32].

The use of PEO, which as a very low Tg and a strong ability to crystallize, forces to design materials where physical or chemical crossslinking appears in the polymer material in order to improve the mechanical strength and the membrane stability along the time. Okamoto et al, designed long ago a new generation of block aliphatic aromatic copolymers with PEO units where the aromatic parts are linked in solid state through charge transfer complex, CTC, interactions (as in whole aromatic polyimides) what produced materials with excellent mechanical properties and admirable ability to separate carbon dioxide from other gases [33-37].

Under these assumptions, this paper studies a series of aromatic-aliphatic copolyimides, in particular poly(ether imide)-segmented co-polymers consisting of micro-domains of rubbery PEO segments and of glassy polyimide segments in such a way that permeation occurs preferentially through rubbery PEO domains [33,34,38].

In previous papers, it has been demonstrated that, for copoly(ether-imide)s with long poly(ethylene oxide) chains of 6000 g/mol, the phase separation morphology of these copolymers can be largely improved by the use of thermal treatments [39-41]. This thermal conditioning leads to an improvement on the gas permeation properties [40]. However, when these long PEO sequences segregate, PEO is able to crystallize which is a serious drawback because permeability decreases. The crystallization process was studied and a dependence of the amount of crystallized PEO with the temperature used in the treatment was determined. In the work presented here, we have used a shorter diamine terminated PEO, 2000 g/mol, as the soft segment, in order to avoid PEO crystallinity. To build the hard segments, PEO-2000 and the rigid aromatic dianhydride has been combined with three different aromatic diamines of different rigidity to study the effect of the aromatic part on the phase separation and the resulting properties. The PEO/aromatic amine ratio was fixed in 2/1 by weight, resulting in a PEO weight percent from around 35 to 44% in the final copolymer, proportion that has been considered high enough to produce good permeation properties without compromising the superb mechanical properties of the resulting copolyimides.

These aromatic-aliphatic copolymers behave as multi-block polymers that segregate in two phases [38-41]. An exhaustive study of the properties of the synthesized copolyimides (as films obtained by the deposition-evaporation method) containing different aromatic diamines, has been carried out by ATR-FTIR, DSC, TGA, TMA, and SAXS after thermal treatment at different temperatures. The corresponding permeability, solubility, diffusivity and selectivity for different gases have also been studied. This work is part of an intensive study of this kind of materials which will permit to design materials with improved capability to separate condensable gases and in particular CO_2.

3.2 Experimental

3.2.1 Chemicals

p-Phenylenediamine (PPD), 4,4'-diaminobiphenyl (BNZ), 4,4'-oxydianiline (ODA) and 3,3′,4,4′-biphenyltetracarboxylic dianhydride (BPDA) were purchased from Aldrich. These products were purified by sublimation at high vacuum just before being used. Bis(2-aminopropyl) poly(ethylene oxide) 2000 (Jeffamine ED 2003) with nominal molecular weight of 2000 g/mol was kindly donated by Huntsman (Holland). This polyether was dried at 70ºC in vacuum for 5 hours and stored in a desiccator under vacuum until use. Anhydrous N-methylpyrrolidinone (NMP), to be used as

polymerization solvent, was purchased from Aldrich. Figure 1 shows the chemical structure of the monomers.

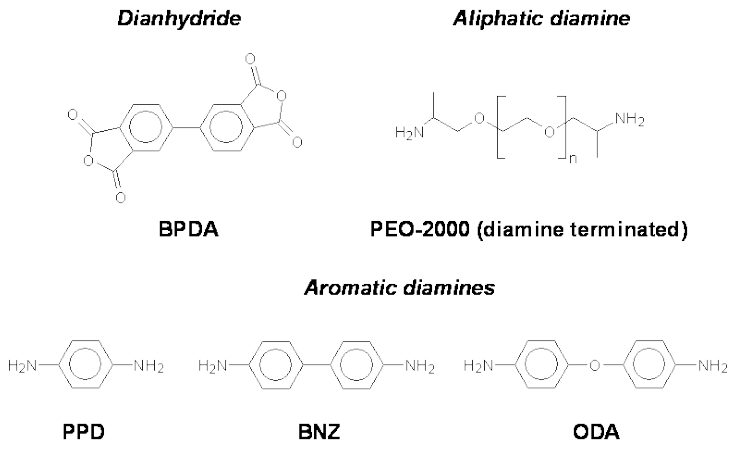

Figure 1. Chemical structure of the monomers.

3.2.2 Synthesis of copoly(ether-imide)s

The polymer samples were synthesized by combination of the dianhydride BPDA with the aliphatic diamine, PEO-2000, and the aromatic diamine (PPD, BNZ and ODA). The procedure for the synthesis of all the polymers in this study was as follows:

a) A mixture of Bis(2-aminopropyl) poly(ethylene oxide) 2000 (*x* mmol), PEO-2000, and the aromatic diamine (PPD, BNZ or ODA) (*y* mmol) in a weight ratio 2:1, was dissolved in anhydrous NMP ((x+y)=5 mmol in 10 mL of NMP) in a three-necked flask blanketed with nitrogen (see Table I).

Table I. Synthesis details of aromatic-aliphatic copolyimides

Copolymer	Reactants *			Aromatic amine/aliphatic amine	% PEO	*
	BPDA	Aromatic amine	PEO-2000**	Molar ratio	by weight	
cPI-PPD	1.3026	0.4308	0.8614	8.98 : 1	34.6	
cPI-BNZ	0.9445	0.4969	0.9968	5.25 : 1	42.9	
cPI-ODA	0.9441	0.5336	1.0565	4.90 : 1	43.7	

Grams of reactants added in the synthesis for a 10 ml NMP solution. Molar ratio dianhydride : total diamines = 1 : 1. Weight ratio PEO-2000 : aromatic diamine = 2 : 1

** Mn = 1942 (by titration, given by the supplier)

b) The reaction mixture was cooled down to 0 ºC, and under mechanical stirring, a stoichiometric amount of BPDA dianhydride (5 mmol) was added all at once and the mixture was stirred overnight at room temperature. During this time the dianhydride completely dissolved and the solution reached high viscosity.

c) The resultant viscous copolyamic acid solution was diluted with NMP to the appropriate viscosity for casting, filtered through a nominal number 1 fritted glass funnel, degassed, and cast onto levelled glass plates. The resulting films were covered with a conical funnel to avoid a fast evaporation of the solvent, dried at 80ºC overnight, and finally treated at 120ºC for 6 hours in a oven under vacuum.

d) Films were obtained of the copolymers with thickness in the range from 60 to 160 μm. Afterwards, thermal treatments under an inert atmosphere of nitrogen were carried out at different temperatures.

The broad distribution of the thickness of the resulting membranes is a consequence of the membrane preparation procedure that needs similar adequate viscosities reached by using different concentrations of the casting solution of each polymer. This variability in thicknesses is not uncommon in literature, and even if we look only at the papers published on copoly(ether-imide)s we can find this broadness frequently as for example in the early paper of Okamoto et al. [33], where the authors made films of 50-170 microns, to more recent papers [38] where Hangzheng et al made films of 50-150 microns. It should be commented that the thickness of the cast films has not any significant effect on permeation.

The resulting copolymers can be named with the acronym cPI before the starting aromatic diamine: PPD, BNZ and ODA (cPI-PPD, cPI-BNZ, cPI-ODA). Aliphatic PEO content in the final copolymer is 42.9, 43.7 and 34.6% by weight respectively.

3.2.3 Characterization Methods

Attenuated total internal reflectance-Fourier transform infrared analyses (ATR-FTIR) were performed at room temperature using a PerkinElmer Spectrum One infrared spectrometer equipped with an ATR accessory.

A Thermal Analysis Q500 instrument was used for thermogravimetric analysis (TGA). Disc samples cut from films with weights between 5 and 15 mg were tested. When running dynamic scans, it was done in High Resolution (HiRes) mode, where the heating rate is automatically

adjusted in response to changes in the rate of weight loss, which results in improved resolution [42], with an initial heating rate of 10ºC/min under a flux of nitrogen.

Differential scanning calorimetry (DSC) analyses were carried out in a Mettler Toledo (DSC 822e) calorimeter equipped with a liquid nitrogen accessory. Disc samples cut from films weighting 5–15mg were sealed in aluminium pans. Samples were heated with the following cyclic method in order to monitor the changes in thermal properties with thermal treatment: from 25 ºC, the sample was heated at 10 ºC/min to a target temperature; once reached, the sample was cooled at the maximum cooling rate accessible for the instrument to -90 ºC, held at this temperature for 15 min and reheated at 10 ºC/min to the next target temperature. The procedure was followed until the last treatment temperature was reached and a final run from -90 ºC to 80 ºC was performed. In this way, in each heating run, the thermal properties for the copolymers, after treatment to the previously reached temperature, were obtained.

Thermomechanical (TMA) tests were performed in a Rheometric Scientific instrument model DMTA V. Rectangular test pieces of 3 mm width and 20 mm length were cut from films. A distance of 10 mm was set between fixation clamps. Runs were carried out from ambient temperature at 2 ºC/min with a static stress of 3 MPa.

SAXS measurements were performed at the beamline BM16 at the European Synchrotron Radiation Facility (Grenoble, France). Wave length of the X-ray beam was 0.980 Å. Detector calibration was done with silver behenate ($AgC_{22}H_{43}O_2$). Disc samples cut from films were placed in a Linkam ® hot stage and heated at 10 ºC/min while the SAXS spectra were recorded. Calibration of temperature gave a difference of approximately 7 ºC between the temperature reading at the hot stage display and the real temperature at the sample.

Tensile properties were measured in a MTS Synergie 200 testing machine equipped with a 100 N load cell. Rectangular test pieces of 3.5 mm width and 25 mm length were cut from films. A crosshead speed of 5 mm/min was used. Strain was measured from crosshead separation and referred to 10 mm initial length. At least six samples were tested for each copolymer at room temperature.

3.2.4 Gas Permeation and Selectivity

The permeability, P, for O_2, N_2, CO_2 and CH_4 were determined by using a permeation device with constant volume and variable pressure which uses the *time-lag* operation method. The

measurements were carried out at 3 bar and 30 ºC. A sketch of the device used has been shown elsewhere [43].

The strategy known as ‘‘time-lag’’ method is attributed to Daynes et al. [44] and it is especially appropriate to determine permeability and diffusivity of a sample by a simple, rapid and accurate method working under transitory regime. The method has been successfully applied to polymer permeation by many authors [45,46]. Its theoretical framework, as well as the practical possibilities and limits of the time-lag technique have been abundantly documented, [47]. It is nowadays an accepted method to assess the permeability and diffusion coefficients of a gas through a polymer film. To sum up, the classical treatment postulates, among other hypothesis, the Fick’s law to hold with a constant diffusion coefficient for a constant thickness membrane thus assuming no swelling of the membrane by the permeant. When these conditions hold, the transitory response at the downstream part of a membrane to a pressure step at the upstream part enables the time-lag, t_0, to be easily computed. This parameter is linked to the diffusion coefficient, D, of the permeant through the simple expression [46]:

$$t_0 = \frac{\Delta x^2}{6D} \tag{1}$$

Δx being the thickness of the membrane.

The amount of gas transmitted at time t through the membrane is calculated from the permeate pressure, p_2, readings in the low-pressure side. The inherent leak rate in the downstream side determined after evacuating the system has been measured for each experimental run. The permeability coefficient can be obtained directly from the flow rate into the downstream volume upon reaching the steady state. Finally, solubility, S, can be obtained from directly measured permeabilities and diffusivities as follows

$$S = \frac{P}{D} \tag{2}$$

3.3 Results and Discussion

3.3.1 Copoly(ether-imide)s imidization

Poly(ethylene oxide) chains are prone to oxidation [48], and therefore, a great care was taken to carry out the imidization process. After casting the polymer solution, films were dried overnight, and subsequently they were additionally dried on heating at 120 ºC for 6 h. It is very important to

note that after the 6 h heating at 120 ºC the solvent was almost completely removed as proved by thermogravimetric analysis. Moreover, all the copolymers resulted to be insoluble in DMF (N,N-dimethylformamide), DMAc (N,N-dimethylacetamide), NMP (N-methyl-2-pyrrolidinone), hexane, toluene, THF (tetrahydrofuran), CH_2Cl_2 (dichloromethane) after this drying process.

Infrared spectra were recorded to check for the progress of imidization as shown for example in Figure 2 for the copolymer from ODA (cPI-ODA). In this figure, the IR bands centred around 3257, 2500, 1657, 1603 and 1538 cm^{-1} strongly decrease or disappear, and the bands at 1774, 1713, 1372 and 738 cm^{-1} increase or appear after imidization. It can be seen that imidization has been practically completed for these copolymers after treatment at 120 ºC. An additional treatment at 160 ºC for short time produced the whole imidization of the polyamic acid to polyimide as it could be clearly observed in the FTIR spectra. No differences appear in the FTIR spectra of samples cured at 160 ºC and temperatures up to 265 ºC.

This full imidization at relatively low temperatures is quite remarkable and has already been found for copoly(ether-imide)s based on 6000 g/mol PEO segments [40]. For fully aromatic polyimides, very high temperatures, generally above 300 ºC are necessary for complete imidization. Two works, studying similar copoly(ether-imide)s to the ones presented here, state that a thermal treatment at 170 ºC completely imidize the precursor poly(amic acid)s to polyimides[33,37]. However authors did not show any FTIR characterization to demonstrate the declared whole conversion. In other more recent research, authors affirm, by using AFT-FTIR, that all synthesized poly(amic acid)s are converted to PEO polyimides after a thermal treatment at 200 ºC [38].

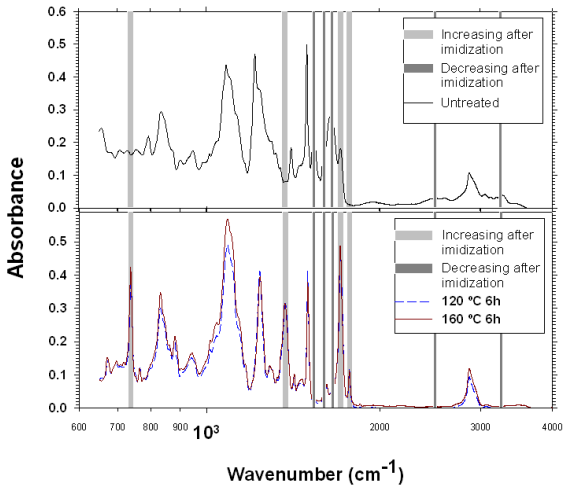

Figure 2. Typical FTIR spectra showing the difference between imidized and not imidized cPI-ODA.

3.3.2 Thermal Stability

Thermogravimetric analysis was performed to evaluate the thermal stability of the synthesized copolymers. Dynamic runs in Hi-Res mode, in a nitrogen atmosphere, showed a weight loss pattern in several steps for all the samples after being treated at 160 ºC for 2 hours (Figure 3).

The behaviour was similar for the different samples. The initial small loss (below a 2% in weight, from ambient temperature to approximately 300 ºC) can be attributed to the absorbed water and residual solvent in the sample. This initial loss was higher for the samples treated at 120ºC, where a significant amount of solvent is still retained. Other authors have found the same results in similar copoly(ether-imide)s. In these works it was shown, by TGA-FTIR, that residual solvent plus absorbed water were released after curing at 200 ºC and vacuum [49], and 300ºC were necessary to completely eliminate the residual solvent [50]. The second step is thought to be due to the degradation of bis(2-aminopropyl) poly(ethylene oxide) 2000, PEO-2000, included in the copolymer composition, and it is therefore assigned to the loss of the polyether block sequences.

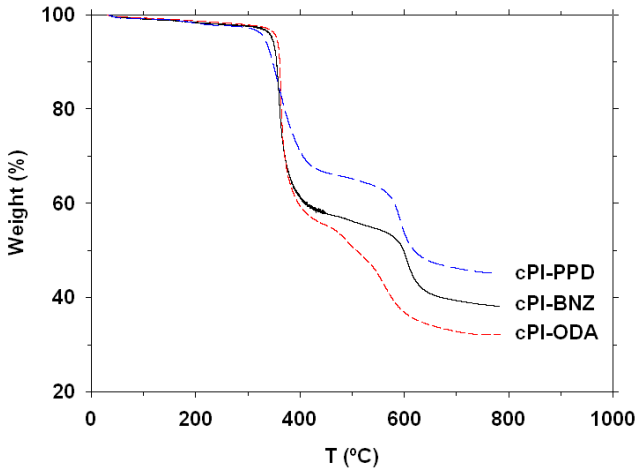

Figure 3. TGA curves in dynamic conditions for copolymers from different aromatic diamines treated at 160 ºC for 2 hours.

The differences between the weight losses should be due to the different mass percentages of PEO in the copolymers. In effect, there was a good agreement between the experimental weight loss (35, 41 and 44% losses for PPD, BNZ and ODA respectively) and what should be expected according to the mass balances (34.6, 42.9 and 43.7% for PPD, BNZ and ODA, respectively). In similar copolymers with the same poly(ethylene oxide) diamino terminated [41], and with longer PEO chains [40], the selective degradation of the polyether chains has been clearly demonstrated. The

final stage of weight loss is due to the thermal decomposition of the remaining aromatic polyimide segments, leaving a relatively high amount of carbonaceous residue.

3.3.3 Calorimetric Studies

The samples treated at 120ºC for 6 hours were heated in a DSC instrument with a cyclic method in order to monitor the changes in thermal properties after a thermal treatment [40]. The changes in the T_g and T_m for PEO chains are shown in Figures 4 and 5 (respectively) as a function of the treatment temperature (the temperature instantaneously reached by the DSC) for the three copolymers studied. No transition related to aromatic polyimide hard segments was detected by DSC.

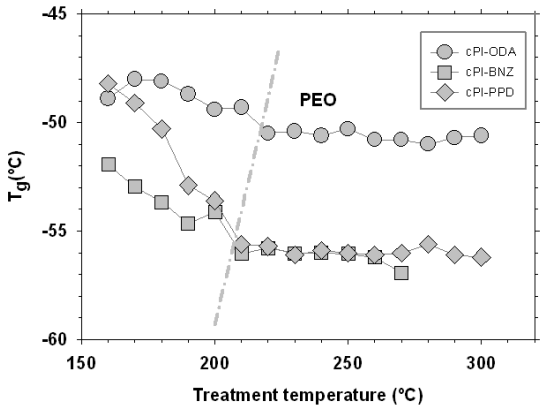

Figure 4. Glass transition temperatures as a function of the treatment temperature.

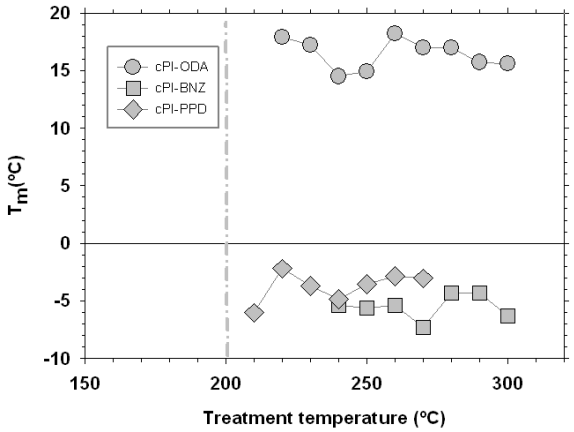

Figure 5. Melting temperatures as a function of the treatment temperature.

From figure 4 was clear that T_g changed when the sample was heated up to approximately 200ºC and it remained constant after higher T treatments. These changes were ascribed to an improvement

in the phase separation of the copolymers when simultaneously all the remaining solvent was released as found by TGA, which led to purer PEO domains with lower T_g. The final T_g was similar for copolymers BNZ and PPD, with values in the range of pure amorphous PEO, whereas for copolymer ODA, the final T_g value was clearly higher. The T_g of amorphous PEO is reportedly in the range -55 to -70 ºC depending on molecular weight [51]. The higher rigidity of BNZ and PPD diamines seems to produce, in principle, a better phase separated system and therefore a purer PEO phase than the more flexible ODA diamine.

When samples were treated above 200 ºC, some PEO crystallinity appeared (see figure 5). This means that PEO domains were very pure, because only pure PEO was able to crystallize. Melting temperature for PEO crystals is similar and very low for BNZ (cPI-BNZ) and PPD (cPI-PPD) copolymers (approximately -5 ºC) whereas for ODA copolymer (cPI-ODA) it is much higher (approximately 16 ºC) although still far from the melting point of high molecular weight PEO homopolymer [52]. It seems surprising that ODA copolymer, with less pure PEO domains according to the T_g data, had a higher T_m for PEO crystals than BNZ and PPD. However, melting point was strongly influenced by the size of the crystals, thus, higher melting point for ODA copolymer seemed to mean that the size of the PEO domains was bigger than those for BNZ and PPD copolymers, as it will be confirmed later by SAXS measurements.

If a value of 8.67 kJ/mol is taken for the melting enthalpy of PEO [52], the amount of crystallized PEO, in the samples studied in this paper, appeared as almost negligible, less than 1.5 % of the PEO contained in the copolymers. When we compare the ODA copolymer with the copolymer of the same structure and virtually the same PEO content in the copolymer, but having longer PEO chains (BPDA 2/1 in reference 40), crystallinity has been reduced after he thermal treatment at 300 ºC from 32 % to 0.9 % by lowering the length of the PEO sequences. In addition, it is worth noting out that at the temperature of measurement of permeabilities and selectivities, the PEO will be melted and hence it will be in a completely amorphous state.

3.3.4 Thermomechanical Analysis

Thermomechanical analysis was also carried out in order to detect the glass transition temperature of the aromatic polyimide hard segments, which were not detected by DSC. The criterion to determine the T_g of the polyimide segments was the temperature when strain was 10 times that of the sample at 100 ºC [40].

The corresponding results for T_g and some temperatures of treatment are shown in Table II. As seen for the PEO segments by DSC, the treatment at higher temperatures raised the T_g of the polyimide segments, what means that phase separation also improved within the hard domains when the remaining solvent in the copolymer is released. It was also evident that the use of the more flexible aromatic diamine, ODA, gave the copolymer with the lowest T_g of this series, and that the bigger length of BNZ seemed to increase the T_g over that of PPD for the rigid aromatic amines. For all the copolymers, the T_g of the aromatic polyimide was well above ambient temperature, although lower than the corresponding T_g for the pure aromatic homopolymer, due to the lower number of structural units (polymerization degree) and, consequently, lower length of the aromatic polyimide segments in the copolymer when compared with the corresponding homopolymer, and also due to the possible inclusion of some PEO segments in the polyimide domains [40].

Table 2. Hard segment T_g as obtained by TMA for some temperatures of treatment.

Copolymer	**Treatment T / ºC**	**Tg / ºC**
cPI-PPD	160	208
cPI-ODA	120	140
	160	180
cPI-BNZ	120	150
	160	242

3.3.5 Small Angle X-ray Scattering

A single broad peak was obtained in the scattering curves ($I(q)q^2$ vs. q). Two parameters can be calculated from the scattering curves: the relative invariant, Q', as the integral below the curve Iq^2 vs. q, which is related to the extent of the phase separation; and the maximum on the scattering curve, q_{max}.

Q' can be correlated with the electron density of the phases (assuming there are two of them) as:

$$Q' = k\left(\Delta\rho\right)^2 \phi(1-\phi) \tag{3}$$

where ϕ is the fraction of one of the phases, $\Delta\rho$ is the difference in the electron densities of both phases and K is a constant related to the experimental geometry and the Thomson scattering factor. Changes in Q' may arise from changes in the extent of phase segregation or from changes in the density difference between the phases.

q_{max} is related to the separation of domains or heterogeneities in the material or length scale L. In the simplest analysis for lamellar phases, the scattering may be treated according to Bragg's Law and hence:

$$L = \frac{2\pi}{q_{\max}} \tag{4}$$

For not truly lamellar morphologies a calculation from the curve I vs. q should be preferred [53]. In our case we were not interested in the absolute value for this length scale of the segregated phase but rather on the change of this scale with temperature. Thus, this procedure will be followed attending to its higher accuracy on determining the maximum of the scattering curve.

The obtained results for Q' and L, are represented in Figure 6 for the copoly(ether-imide) containing ODA. In the curves shown in Figures 6-a and 6-b for the sample treated at 120 ºC, there is a change (steep increase in both the relative invariant and the characteristic length in the segregated phases) that appears in a range from 180 to 220 °C, which approximately coincides with the decrease in T_g of the PEO phase as seen in Figure 4, and is related to the release of most of the remaining solvent trapped in the copolymers.

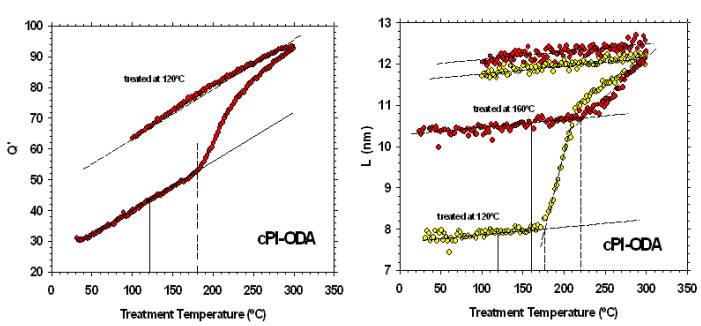

Figure 6. Q' and L as a function of the treatment temperature for the copolymer containing ODA. In graph (b), L differences for membranes treated at 120 and 160 ºC are compared.

The evolution of both parameters stood until the end of the test temperature range, 300 ºC. During cooling, this change in slope did not appear, demonstrating that the phase separation was

irreversible. The difference between heating and cooling curves for each temperature should correspond to the net change occurred. For the sample heated at 160 ºC for 2 hours, the change in Q' (not shown) was very small, meaning that this treatment was enough to almost fully develop the phase separated structure in this copolymer. The change in L for this sample, Figure 6-b, took place above 220 ºC, after T_g of the rigid polyimide segments was surpassed, and it was much lower than the change exhibited by the sample treated at 120 ºC. This slower change above 220 ºC took place after practically all the residual solvent had been released.

The same behavior was found for copolymers having BNZ and PPD treated at 120 ºC, as seen for example in Figures 7-a and 7-b. Q' and L increased from approximately 180 ºC until the highest temperature of the test was reached. In the same graphs (crosses), experimental data for samples treated in an oven at 120 ºC (6h), 160 ºC (2h), 180 ºC (2h), 200 ºC (2h), 220 ºC (2h), 250 ºC (1h) and 265 ºC (1h) and measured at ambient temperature are included. For these samples, the same trends in Q' and L were found for the samples heated in-situ at the Linkam hot stage.

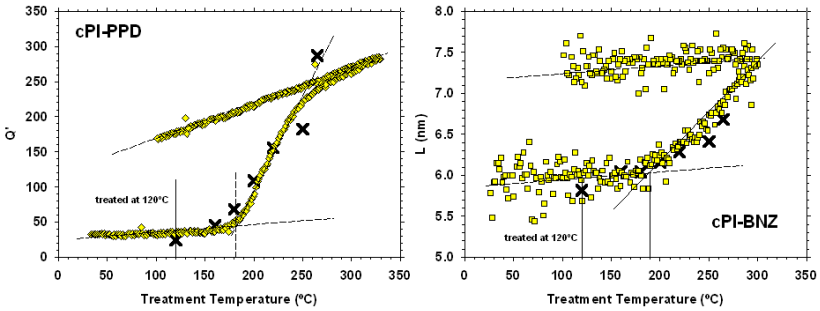

Figure 7. Examples of Q' (cPI-PPD) (a) and L (cPI-BNZ) (b) as a function of the treatment temperature. Crosses correspond to samples treated in an oven at the temperatures depicted in the graph (samples were measured at ambient temperature).

Figures 8-a and 8-b show the evolution of Q' and L with temperature for all the copolymers. The samples were obtained in situ (SAXS cell) from polymer films previously heated to 120 ºC during 6 h. Note that, to eliminate the influence of the different film thicknesses and electronic density, the relative Q'_r = Q'(T)/ Q'(baseline at T), is shown in Figure 8-a. Moreover, the influence of the different background and of the differences in the corresponding base lines was also removed by this procedure.

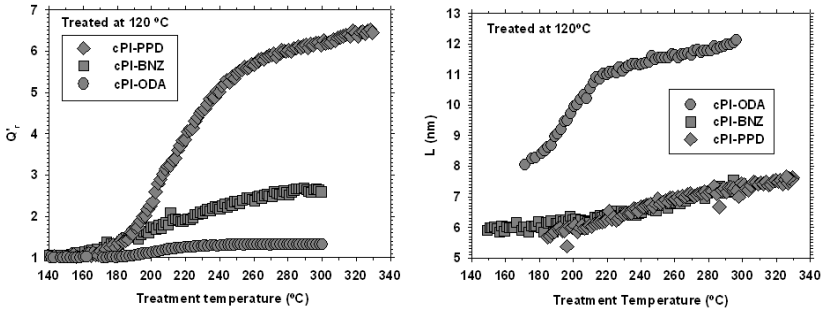

Figure 8. Evolution of Q'_r and L as a function of temperature of treatment.

It is seen that PPD containing copolymers gave higher proportion of separated phase while those containing ODA gave bigger phase separated domains. The sequence of the copolymers with increasing Q'_r coincided with the decrease in length of the aromatic diamine.

For the copolymers from BNZ and PPD, the spacing was very similar, and much lower than for copolymer from ODA as shown in Figure 8-b. For these samples treated at 120 ºC, when heated up to more than 300 ºC, L increased about a 25 % when the diamines are BNZ and PPD, whereas it increased about a 50 % for the copolymer having ODA. In summary, the size of the domains decreased with the rigidity of the aromatic diamine used.

A comparison of Figure 5 with the evolution of L as shown in Figure 8-b shows that the melting point increases with the size of the domains, L. This is in accordance with the predictions of the Gibbs-Thomson law which states that the melting-point of a substance decreases when the curvature radius of cavities decreases (with a proportionality constant depending only on the confined substance in question).

The spacing for copolymer from ODA after the thermal treatment until 300 ºC, was about 10 nm when measured at ambient temperature. This value was much lower than the spacing for the same copolymer built from a PEO having Mw= 6000 (L = 18.9 nm) [35], showing that there is a dependence of L with molecular weight of the PEO for this type of copolymers; the longer the polyether the larger the spacing.

3.3.6 *Mechanical Properties*

SAXS, DSC and thermomechanical studies have shown the changes produced in the morphology of the copolymers during thermal treatment and the changes in their thermal properties. To complete the study on the physical properties of these copoly(ether imide)s, mechanical properties were

measured in tensile mode for the copolymers treated at 160 ºC for 2 hours. The so obtained results are shown in Table 3.

Table 3. Mechanical properties at ambient temperature for the films treated at 160ºC for 2h.

Copolymer	**cPI-PPD**	**cPI-BNZ**	**cPI-ODA**
Maximum stress / MPa	61.5 ± 2.5	6.2 ± 1.9	22.1 ± 1.7
Strain / %	26 ± 10	1.1 ± 0.3	115 ± 53
Modulus / GPa	1.25 ± 0.09	0.65 ± 0.16	0.38 ± 0.04

For copolymers from ODA and PPD, yielding of the samples took place at approximately 10 % strain. At this point, strain increases with tensile strength almost unchanged until rupture. For copolymer from BNZ, rupture occurred very early, probably because it is the thinnest film (60 µm) and the occurrence of defects is more critical, triggering the rupture. The value of the modulus for ODA containing copolymers was smaller than for the other ones, as expected, because from thermal data it was confirmed a higher degree of mixing between the segments, and therefore, the polyimide hard domains, responsible for the mechanical resistance at the early stages of the test, were softer for ODA copolymer. If we compare the values for ultimate properties for ODA and PPD copolymers, it is seen that the shorter the diamine (PPD), the higher the tensile strength and the lower the ultimate strain. It is worth noting that in all cases the mechanical properties of the material were reasonably good.

3.3.7 Gas Permeation and Selectivity

Gas permeation measurements showed an improvement in the permeation properties, depending on the thermal treatment used, so that there is a direct relationship between: treatment temperature, phase segregation and permeation properties. An example, showing the increase in permeability of CO_2 with the treatment temperature, is presented in Figure 9 for the BNZ containing copolymer. The permeability versus treatment temperature trend was quite similar for all the copolymers and tested gases. In all cases the increase in permeability was gradual for treatment temperatures up to approximately 160 ºC, according to the increasing release of the remaining solvent and to the improvement in the phase segregation.

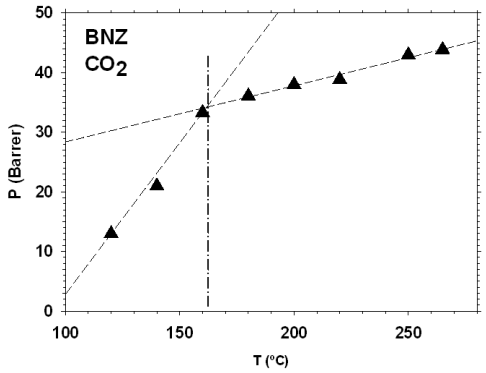

Figure 9. CO_2 permeability versus treatment temperature for the BNZ copolymer.

For all the copolymers, the selectivity versus diffusivity and the solubility-selectivity term versus the diffusivity-selectivity term for the different pairs of gases and the temperature treatments are shown in Figures 10 to 13. Also the PEO gas separation properties, both for semicrystalline and amorphous PEO, [27] are shown for each gas in these Figures. Note that semicrystalline and amorphous PEO showed the same selectivity and the same kind of selectivity with the same balance of solubility and diffusivity contributions, with a little more relevant contribution of the solubility-selectivity term for both forms of PEO. This seems to indicate that gas separation is fundamentally determined by the properties of the amorphous phase of PEO. Then, the crystalline part of semicrystalline PEO should act as mere inert obstacles to the flux that only reduce permeability [27]. In all cases, the observed tendency was to reach the PEO balance of selectivity (both the solubility and diffusivity terms), as the temperature of treatment increases; i.e. when the phase segregation proceeds. The thermal treatment also approaches the gas permeability value of these copolymers to that of the amorphous PEO.

The Robeson plots are shown in Figures 10-a to 13-a, for O_2/N_2, CO_2/CH_4, CO_2/N_2 and CH_4/N_2. Depicted arrows refer to the direction of increasing treatment temperatures. The Robeson's upper bounds are shown in these plots including both the old limit [20] and the new one [21] when both exist. Nevertheless, note that no Robeson limit has been determined for the CH_4/N_2 gas pair because this selectivity is the opposite of that determined by Robeson. This means that usually N_2 is more permeable than CH_4 while our copolymers showed the opposed trend.

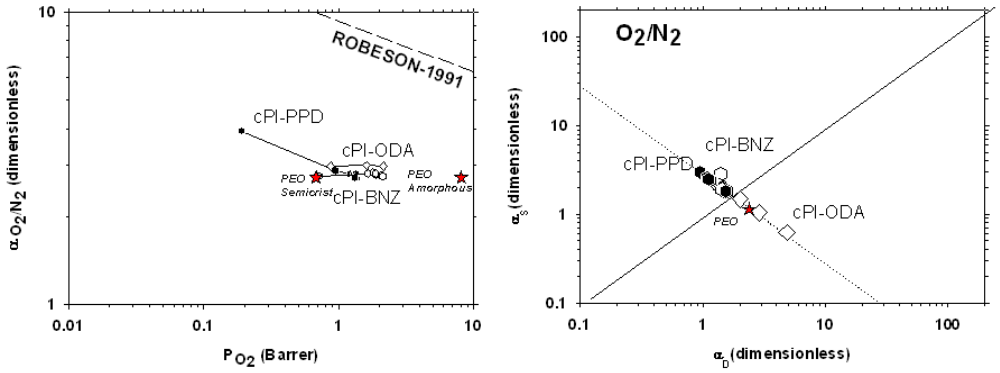

Figure 10. (a) Robeson's plot for the O_2/N_2 gas pair, (b) selectivity by solubility as a function of the selectivity by diffusivity. Stars correspond to the PEO values.

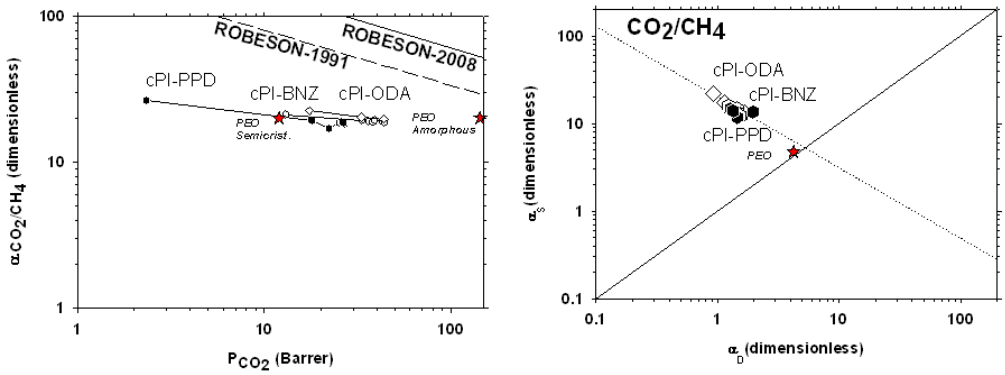

Figure 11. (a) Robeson's plot for the CO_2/CH_4 gas pair, (b) selectivity by solubility as a function of the selectivity by diffusivity. Stars correspond to pure PEO values.

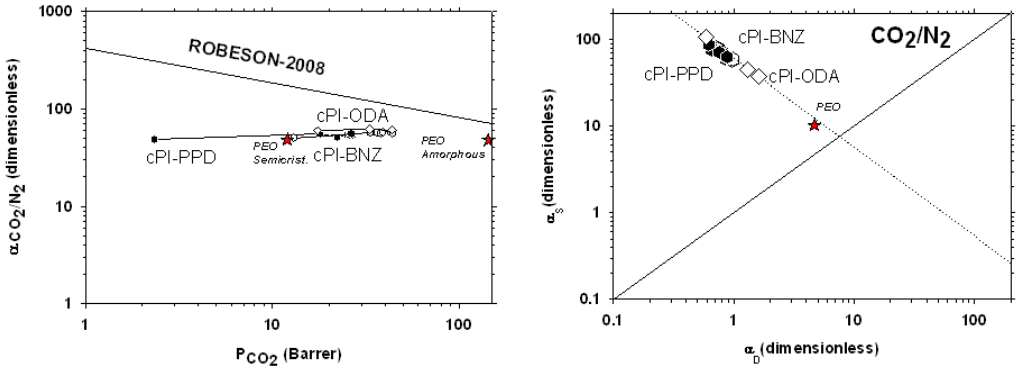

Figure 12. (a) Robeson's plot for the CO_2/N_2 gas pair, (b) selectivity by solubility as a function of the selectivity by diffusivity. Stars correspond to the PEO values

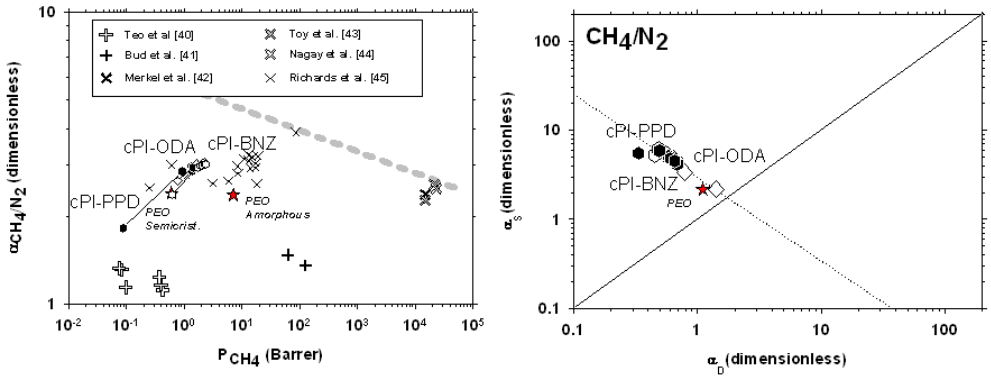

Figure 13. (a) Robeson's plot for the CH_4/N_2 gas pair, (b) selectivity by solubility as a function of the selectivity by diffusivity. Stars correspond to pure PEO values.

For the CH_4/N_2 Robeson plot, some data taken from the literature [54-59] have been shown in the graphic and a pseudo bond has been drawn based on these data only to give an idea on the best selectivity versus permeability trade-off achieved so far.

The permeability of the gases as a function of the aromatic diamine always followed the order: PPD, BNZ and ODA. Copolyimides from BNZ and ODA gave similar permeabilities when the treatment temperatures were high. When only one of the gases was a condensable one (CO_2/N_2 and CH_4/N_2 gas pairs), the selectivity increased with the temperature of treatment while for the rest of gas pairs (O_2/N_2 and CO_2/CH_4), selectivity decreased slightly with the temperature of treatment. In all cases the tendency went towards the selectivity versus permeability characteristics of amorphous PEO. An exception was observed for the CH_4/N_2 pair where an increase in the phase separation of PEO gives selectivity values over the characteristic gas selectivities of both semicrystalline and amorphous PEO.

When permeabilities and selectivities for the copolymer from ODA were compared with the same copolymer having longer PEO chains (6000 g/mole, PI-43 in reference 39) after a thermal treatment at 250 ºC (when phase segregation has been well developed) (see Table IV), it was found that permeability values decreased between 30 and 45 %, whereas selectivity values increased between 10 and 19 %. These differences can be related to the better phase separation achieved for the copolymer with longer PEO lengths, where, in addition, also the aromatic polyimide segments were longer. Thus, the PEO domains seem to be the main responsible for the permeability, and therefore a less perfect phase separation in the ODA copolymer leads to a reduction in permeability. On the other hand, it could be presumed that polyimide segments influenced the selectivity, and because a

higher mixing of polyimide segments in the PEO domains was expected for the copolymer from ODA, a small increase in selectivity was to be expected.

Additional information for the behaviour of these copolymers as gas membranes could be obtained from the analysis of the diffusivity and solubility parameters. It is well established that the diffusivity should decrease with the kinetic diameter of the gas while the solubility can be directly correlated with its critical temperature, [60,61].

Table 4. Permeabilities and selectivities for copolymers with different PEO length treated at 250ºC*

P_{O2}		P_{N2}		P_{CO2}		P_{CH4}		$\alpha\ O_2/N_2$		$\alpha\ CO_2/N_2$		$\alpha\ CO_2/CH_4$	
PI43	cPI-ODA	PI43	cPI-ODA	PI43	cPI-ODA	PI43	cPI-ODA	PI43	cPI-ODA	PI43	cPI-ODA	PI43	cPI-ODA
3.06	2.15	1.21	0.72	67	43.7	4.02	2.21	2.50	2.98	55	60.7	17	19.7

* PI43 results taken from reference [39]

These data are shown in Table V, [62,63]. The so-obtained diffusivities and solubilities followed these general trends with the exception of CO_2 that showed a much lower diffusivity than that expected according to its kinetic diameter.

Table 5. Kinetic diameter and boiling temperature of tested gases.

	Gas kinetic diameter (Å)	Critical temperature (K)
Carbon dioxide	3.30	304.2
Oxygen	3.46	154.6
Nitrogen	3.64	126.2
Methane	3.80	191.1

The solubility-selectivity term has been confronted versus the diffusivity-selectivity one for all the membranes and gas pairs studied in Figures 10-b to 13-b. These selectivities terms are defined according to:

$$\alpha_{ij} = \frac{P_i}{P_j} = \frac{D_i S_i}{D_j S_j} = (\alpha_D)_{ij} (\alpha_S)_{ij} \tag{5}$$

These Figures show that the ideal selectivity, α_{ij}, is mostly determined by the solubility term, $(\alpha_D)_{ij}$, for almost all the copolymers and gas pairs.

It is interesting to observe how the effect of the diffusivity term increased in the ideal selectivity except for the O_2/N_2 pair in the ODA copolymer, which showed a lessening of this term and an increment of the solubility term (as opposed to the other copolymers from PPD and BNZ), when it was increased the treatment temperature. In all cases the solubility and diffusivity contributions to the ideal selectivity approached those of the amorphous PEO. However, the solubility-selectivity factor had a higher effect on the ideal selectivity when there was at least a condensable gas in the studied gas pair. It is curious to note that a tendency to reach the solubility and diffusivity terms of PEO was shown also for the CH_4/N_2 pair, which presents, in the Robeson's plot, higher selectivity values than PEO when higher temperature treatments are employed.

The reverse selectivity of the CH_4/N_2, seen in Figure 13-a, was probably caused by an especially high enhancement of the CH_4 permeability when high temperature treatments were used. This fact could be due to a specific affinity of CH_4 for the segregated domains or their interfaces. In effect, the solubility parameter followed the same sequence than the degree of segregation (PPD ≥ BNZ > ODA), Figure 14-a, while diffusivity followed the tendency observed for the size of the domains, L, Figure 14-b.

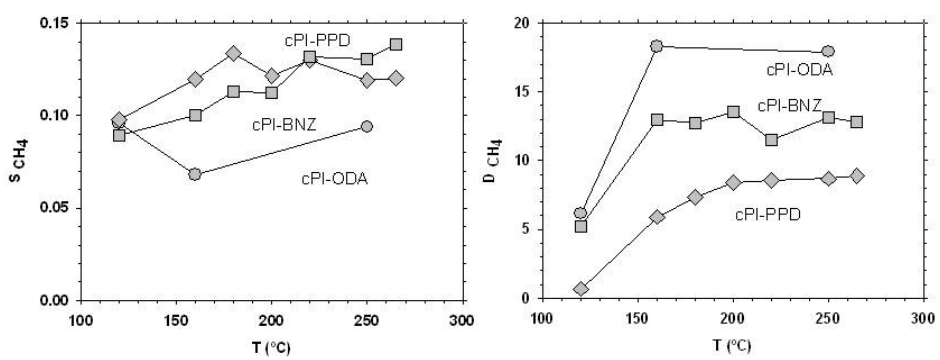

Figure 14. Solubility and diffusivity of methane as a function of the temperature of treatment.

3.4 Conclusions

A new series of copoly(ether-imide)s presenting good gas separation properties have been prepared. These copolymers have been synthesized by the reaction between an aromatic dianhydride (BPDA), a diamine terminated poly(ethylene oxide) having a molecular weight of 2000 g/mole (PEO-2000) and various aromatic diamines (PPD, BNZ and ODA).

FTIR showed that almost complete imidization was achieved at temperatures as low as 120ºC, and that this process was wholly achieved after treatment at 160 ºC, which is well below the temperature needed to imidize fully aromatic polyimides. Based on TGA data, these copolymers are stable in inert atmosphere up to 300 ºC, with a selective degradation of the polyether segments at higher temperatures. DSC, TMA and SAXS experiments proved the existence of a phase separated morphology in these copolymers, with an amorphous PEO phase at ambient temperature and an aromatic polyimide phase with a T_g well above room temperature. The degree of segregation of the phases followed the trend PPD ≥ BNZ > ODA, whereas the size scale of the morphology followed the reverse ODA > BZN ≈ PPD tendency, showing that less rigid aromatic diamines gave bigger segregated domains while more rigid aromatic diamines gave better phase segregation.

Thermal treatment of the copolymers affects the morphology and, in consequence, the physical properties. Initially, at intermediate treatment temperatures, the release of practically all the remaining solvent in the imidized copolymers produces a fast improvement in the phase separation, while treatments at higher temperatures (up to the degradation temperature) produce a further improvement. The possible variations of monomers, monomer percentages and treatment temperature open a wide range of potential for the optimization of these copoly(ether imide)s and other analogous to tailor materials with excellent functionality in different gas separation applications.

After complete imidization, all the samples show increasing selectivity for the studied pairs of gases. This improvement is due to the high percentage and size of the domains of the segregated phases that determine the extra permeability and selectivity shown at higher treatment temperatures. For the case of CH_4/N_2 an interesting reverse selectivity appears probably due to a higher selectivity of CH_4 in the soft segregated portions of the copolymer.

The use of PEO-2000 in these aromatic-aliphatic copolyimides produced a significant reduction in permeability and a slight increase in selectivity for all gases studied when they are compared with

the analogous copolymers having 6000 g/mol molecular weight PEO, due to a less perfect phase segregation.

In terms of permselectivity, the gas performances, followed the aromatic diamine; PPD>BNZ>ODA sequence when relatively low temperatures of treatment are employed whereas quite similar results for the copolymers from BNZ and ODA were obtained when high temperature treatments were used. This indicated that the segregated domains size seems to be the key factor along with a certain influence of the percentage of segregation. An adequate balance of short length with limited rigidity of the diamine responsible of the aromatic part should improve the gas separation results.

Finally, on comparing the permeability, solubility and diffusivity data with the data referred in the literature for pure PEO, it was concluded that the tendency of these parameters after the improvement of segregation is to approach the data exhibited by pure amorphous PEO (an exception was seen for the CH_4/N_2 gas pair that showed a much larger improvement).

3.5 Acknowledgements

We are indebted to the Spanish Junta de Castilla León for financing this work through the GR-18 Excellence Group Action and to the Ministry of Science and Innovation in Spain for their economic support of this work (MAT2008-00619/MAT, CIT-420000-2009-32 and MAT2010-20668/MAT). We also acknowledge financial support from the programme Consolider Ingenio 2010 (project CSD-0050-MULTICAT).

Authors thank the access to the beamline BM16 at the European Synchrotron Radiation Facility (ESRF) in Grenoble (France). We are grateful to Dr. Ana Labrador and Dr. François Fauth for their help at BM16 station at the ESRF. The help provided by Sara Rodriguez in measuring gas permeability and selectivity is greatly appreciated. A. Tena thanks CSIC for a predoctoral JAE fellowship.

3.6 References

1. W.J. Koros, Gas separation membranes: Need for combined materials science and processing approaches, Macromol. Symp. 188, 13–22 (2002)
2. P. Pandey, R.S. Chauhan, Membranes for gas separation, Prog. Polym. Sci., 26 (2001) 853-893
3. M. Ulbricht, Advanced functional polymer membranes, Polymer 47 (2006) 2217–2262

4. L.M. Robeson, Polymer membranes for gas separation, Curr. Opin. Solid State Mater. Sci. 4 (1999) 549–552
5. R. Steeneveldt, B. Berger, T.A. Torp, CO_2 capture and storage. Closing the knowing–doing gap, Chem. Eng. Res. Des. 84 (2006) 739–763
6. A. Meisen, X. Shuai, Research and development issues in CO_2 capture, Energy Convers. Manage., 38, (1997) 37-42
7. D. C. Victor, Strategies for cutting carbon, Nature 395 (1998) 8837-38.
8. J. D. Figueroa, T. Fout, S. Plasynnski, H. McIlvried, R.D. Srivastava, Advances in CO_2 capture technology—The U.S. Department of Energy's Carbon Sequestration Program, Int. J. Greenhouse Gas Control, 2 (2008) 9-20
9. H. J. Herzog, What future for carbon capture and sequestration? Environ. Sci. Technol. 35 (2001) 148-153
10. H. Lin, B.D. Freeman, Materials selection guidelines for membranes that remove CO_2 from gas mixtures, J. Mol. Struct. 739 (2005) 57–74
11. R.W. Baker, Future directions of membrane gas separation technology, Ind. Eng. Chem. Res. 41 (2002) 1393–1411
12. M.T. Bessonov, M.M. Koton, V.V. Kudryavtsev, L.A. Laius, Polyimides: Thermally Stable Polymers, Consultants Bureau, New York, 1987.
13. D. Wilson, H.D. Stenzenberger, P.M. Hergenrother, Polyimides, Blackie, Glasgow, 1990.
14. M.K. Ghosh, K.L. Mittal, Polyimides: Fundamentals and Applications, Marcel Dekker, New York, 1996.
15. L.S. White, T.A. Blinka, H.A. Kloczewski, I.-F Wang, Properties of a polyimide gas separation membrane in natural gas treams, J. Membr. Sci. 103 (1995) 73–82.
16. A. Bos, I.G.M. Punt, M. Wessling, H. Strathmann, Plasticization resistant glassy polyimide membranes for CO_2/CH_4 Separations, Sep. Purif. Technol. 14 (1998) 27–39.
17. A. Tena, L. Fernández, M. Sánchez, L. Palacio, A.E. Lozano, A. Hernández, P. Prádanos, Mixed matrix membranes of 6FDA-6FpDA with surface functionalized gamma-alumina particles. An analysis of the improvement of permselectivity for several gas pairs, Chem. Eng. Sci. 65 (6) (2010) 2227–2235.
18. K. Okamoto, N. Yasugi, T. Kawabata, K. Tanaka, H. Kita, Selective permeation of carbon dioxide through amine-modified polyimide membranes, Chem. Lett. 8 (1996) 613–614.
19. C. Staudt-Bickel, W.J. Koros, Improvement of CO_2/CH_4 separation characteristics of polyimides by chemical crosslinking, J. Membr. Sci. 155 (1999) 145–154.

20. L.M. Robeson, Correlation of separation factor versus permeability for polymeric membranes, J. Membr. Sci. 62 (1991) 165-185.
21. L.M. Robeson, The upper bound revisited, J. Membr. Sci. 320 (2008) 390–400
22. H.B. Park, C.H. Jung, Y.M. Lee, A.J. Hill, S.J. Pas, S.T. Mudie, E.V. Wagner, B.D. Freeman, D.J. Cookson, Polymers with cavities tuned for fast selective transport of small molecules and ions, Science 318 (2007) 254–258.
23. P.M. Budda, K.J. Msayib, C.E. Tattershall, B.S. Ghanema,K.J. Reynolds, N.B. McKeownb, D. Fritsch, Gas separation membranes from polymers of intrinsic microporosity, J.Membrane Sci. 251 (2005) 263–269
24. K. Ghosal, R.T. Chen, B.D. Freeman, W.H. Daly, I.I. Negulescu, Effects of basic substituents on gas sorption and permeation in polysulfone, Macromolecules 29 (1996) 4360–4369.
25. M. Kawakami , H. Iwanaga, Y. Hara, M. Iwamoto, S. J. Kagawa, Gas permeabilities of cellulose nitrate/poly(ethylene glycol) blend membranes, J. Appl. Polym. Sci. 27 (1982) 2387-2393.
26. J. Li, K. Nagai, T. Nakagawa, S. Wang, Preparation of Polyethyleneglycol (PEG) and Cellulose Acetate (CA) Blend Membranes and Their Gas Permeabilities, J. Appl. Polym. Sci. 58 (1995) 1455-1463.
27. H. Lin, B.D. Freeman, Gas solubility, diffusivity and permeability in poly(ethylene oxide), J. Membr. Sci. 239 (2004) 105-117.
28. H. Lin, E. van Wagner, J.S. Swinnea, B.D. Freeman, S.J. Pas, A.J. Hill, S. Kalakkunnath, D.S. Kalika, Transport and structural characteristics of crosslinked poly(ethylene oxide) rubbers, J. Membr. Sci. 276(1-2) (2006) 145-161.
29. Y. Hirayama, Y. Kase, N. Tanihara, Y. Sumiyama, Y. Kusuki, K. Haraya, Permeation properties to CO_2 and N_2 of poly(ethylene oxide)-containing and crosslinked polymer films, J. Membr. Sci. 160 (1999) 87-99.
30. J.J. Richards, M.K. Danquah, S. Kalakkunnath, D.S. Kalika, V.A. Kusuma, S.T. Matteucci, B.D. Freeman, Relation between structure and gas transport properties of polyethylene oxide networks based on crosslinked bisphenol A ethoxylate diacrylate, Chem. Eng. Sci. 64 (2009) 4707-4718
31. V.I. Bondar, B.D. Freeman, I. Pinnau, Gas sorption and characterization of poly(ether-b-amide) segmented block copolymers, J. Polym. Sci. Part B: Polym. Phys. 37 (1999) 2463-2475.
32. V.I. Bondar, B.D. Freeman, I. Pinnau, Gas transport properties of poly(ether-b-amide) segmented block copolymers, J. Polym. Sci. Part B: Polym. Phys. 38 (15) (2000) 2051-2062.

33. K. Okamoto, M. Fujii, S. Okamyo, H. Suzuki, K. Tanaka, H. Kita, Gas permeation properties of poly(ether imide) segmented copolymers, Macromolecules 28 (1995) 6950-6956.
34. Y. Hirayama, Y. Kase, N. Tanihara, Y. Sumiyama, Y. Kusuki, K. Haraya, Permeation properties to CO_2 and N_2 of poly(ethylene oxide)-containing and crosslinked polymer films, J. Membr. Sci. 160 (1999) 87-99.
35. M. Yoshino, K. Ito, H. Kita, K. Okamoto, Effects of hard-segment polymers on CO_2/N_2 gas separation properties of poly(ethylene oxide)-segmented copolymers, J. Polym. Sci. Part B: Polym. Phys. 38 (2000) 1707-1715.
36. H. Suzuki, K. Tanaka, H. Kita, K. Okamoto, H. Hoshino, T. Yoshinaga, Y. Kusuki, Preparation of composite hollow fiber membranes of poly(ethylene oxide)-containing polyimide and their CO_2/N_2 separation properties, J. Membr. Sci. 146 (1998) 31-37.
37. K. Okamoto, N. Umeo, S. Okamyo, K. Tanaka, H. Kita, Selective permeation of carbon dioxide over nitrogen through polyethyleneoxide-containing polyimide membranes, Chem. Lett. 5 (1993) 225-228.
38. C. Hangzheng, X. Youchang, C. Tai-Shung, Synthesis and characterization of poly (ethylene oxide) containing copolyimides for hydrogen purification, Polymer 51 (2010) 4077-4086
39. D.M. Muñoz, E.M. Maya, J. de Abajo, J.G. de la Campa, A.E. Lozano, Thermal treatment of poly(ethylene oxide)-segmented copolyimide based membranes: An effective way to improve the gas separation properties, J. Memb. Sci. 323 (2008) 53–59
40. A. Marcos-Fernandez, A. Tena, A.E. Lozano, J.G. de la Campa, J. de Abajo, L. Palacio, P. Prádanos, A. Hernández, Physical properties of films made of copy(ether-imide) with long poly(ethylene oxide) segments, Eur. Polym. J. 46 (2010) 2352-2374.
41. E.M. Maya, D.M. Muñoz, A.E. Lozano, J. de Abajo, J.G. de La Campa. Fluorenyl cardo copolyimides containing poly(ethylene oxide) segments: synthesis, characterization, and evaluation of properties. J. Polym. Sci. Part A: Polym. Chem. 46, (2008) 8170–8178
42. P.J. Haines, Thermal Methods of Analysis Principles, Applications and Problems, Chapman & Hall, New York, USA, 1995.
43. J. Marchese, M. Anson, N.A. Ochoa, P. Prádanos, L. Palacio, A. Hernández, Morphology and structure of ABS membranes filled with two different activated carbons, Chem. Eng. Sci. 61 (2006) 5448–5454.
44. H.A. Daynes, The process of diffusion through a rubber membrane, Proc. R. Soc. London 97 (1920) 286–307.
45. D. Paul, A.T. DiBenedetto, Gas and vapor solubility in crosslinked poly(ethylene glycol diacrylate), diffusion in amorphous polymers,. J. Polym. Sci. C 10 (1) (1965) 17–44.

46. J. Crank, The Mathematics of Diffusion, second ed Clarendon Press, Oxford, 1975
47. S.W. Rutherford, D.D. Do, Review of time-lag permeation technique as a method for characterization of porous media and membranes, Adsorpt. 3 (1997) 283–312.
48. J. Scheirs, S.W. Bigger, O. Delatycki, Characterizing the solid-state thermal oxidation of poly(ethylene oxide) powder, Polymer 32 (1991) 2014–2019.
49. M.A.B. Meador, V.A. Cubon, D.A. Scheiman, W.R. Bennett, Effect of branching on rod−coil block polyimides as membrane materials for lithium polymer batteries, Chem. Mater. 15 (15) (2003) 3018-3025
50. J.L. Hedrick, T. P. Russell, J. Labadie, M. Lucas, S. Swanson, High temperature nanofoams derived from rigid and semi-rigid polyimides. Polymer 36 (1995) 2685-2697
51. Y. Hu, M. Rogunova, V. Topolkaraev, A. Hiltner, E. Baer, Aging of poly(lactide)/poly(ethylene glycol) blends. Part 1. Poly(lactide) with low stereoregularity, Polymer 44 (2003) 5701–5710.
52. D.W.Van Krevelen, Properties of polymers, 3rd Ed. Amsterdam, Elsevier, p. 120 1990.
53. F.S. Baltá-Calleja, C.G.Vonk, X-ray scattering of synthetic polymers, Amsterdam, Elsevier, 1989.
54. L.S. Teo, C.Y. Chen, J.F. Kuo, The gas transport properties of amine-containing polyurethane and poly(urethane-urea) membranes, J. Membr. Sci. 141 (1998) 91-99.
55. P.M. Budd, K.J. Msayib, C.E. Tattershall, B.S. Ghanem, K.J. Reynolds, N.B. McKeown, D. Fritsch, Gas separation membranes from polymers of intrinsic microporosity, J. Membr. Sci. 251 (2005) 263.
56. T.C. Merkel, V. Bondar, K. Nagai, B.D. Freeman, Sorption and transport of hydrocarbon and perfluorocarbon gases in poly(1-trimethylsilyl-1-propyne), J. Polym. Sci. Part B: Polym. Phys. 38 (2000) 273-296.
57. L.G. Toy, K. Nagai, B.D. Freeman, I. Pinnau, Z. He, T. Masuda, M. Teraguchi, Y.P. Yampolskii, Pure-gas and vapor permeation and sorption properties of poly[1-phenyl-2-[p-(trimethylsilyl)phenyl]acetylene] (PTMSDPA), Macromolecules 33 (2000) 2516-2524.
58. K. Nagai, A. Higuchi, T. Nakagawa, Gas permeability and stability of poly(1- trimethylsilyl-1-propyne-co-1-phenyl-1-propyne) membranes, J. Polym. Sci. Part B: Polym. Phys. 33 (1995) 289-298.
59. J.J. Richards, M.K. Danquah, S. Kalakkunnath, D.S. Kalika, V.A. Kusuma, S.T. Matteucci, B.D. Freeman, Relation between structure and gas transport properties of

polyethylene oxide networks based on crosslinked bisphenol A ethoxylate diacrylate, Chem. Eng. Sci. 64(22) (2009) 4707-4718

60. R. Recio, , A.E. Lozano, P. Pradanos, A. Marcos, F. Tejerina, A. Hernandez, Effect of fractional free volume and Tg on gas separation through membranes made with different glassy polymers. J. Appl. Polym. Sci. 107 (2008) 1039–1046.
61. M. Sadeghi, M.A. Semsarzadeh, H. Moadel, Enhancement of the gas separation properties of polybenzimidazole (PBI) membrane by incorporation of silica nano particles, J. Membr. Sci. 331 (2009) 21–30.
62. H. Lin, B.D. Freeman, gas and vapor solubility in crosslinked Poly(ethylene glycol diacrylate), Macromolecules, 38 (2005) 8394-8407.
63. D.W. Breck, Zeolite Molecular Sieves: Structure, Chemistry and Use. Wiley, New York, NY. 1974.

CHAPTER 4

Phase Segregation and Gas Separation Properties of Thermally Treated Copoly(ether-imide) from an Aromatic Dianhydride, an Aromatic Diamine and Various Aliphatic Diamines

Alberto Tena[1,3], Ángel Marcos-Fernández[1,3], Laura Palacio[1,2], Purificación Cuadrado[1], Pedro Prádanos[1,2], Javier De Abajo[1,3], Ángel E. Lozano[1,3], A. Hernández[1,2]

[1]*Smap UA-UVA-CSIC, Parque Científico Universidad de Valladolid, Paseo de Belén, s/n, 47011 Valladolid, Spain.*

[2]*Dept. Física Aplicada, Facultad de Ciencias, Universidad de Valladolid, Paseo de Belén, 7, 47011 Valladolid, Spain*

[3]*Instituto de Ciencia y Tecnología de Polímeros, CSIC, Juan de la Cierva 3, 28006 Madrid, Spain.*

This chapter has been published in:

Industrial & Engineering Chemistry Research, 51, (**2012**), 3766−3775

DOI: dx.doi.org/10.1021/ie2028443

Abstract

Copoly(ether-imide)s formed by the reaction of an aromatic dianhydride (BPDA), an aromatic diamine (ODA), and various aliphatic diamines (PEO-2000, PPO-2000, RT-1000, pTHF-1700, and pTHF-350) have been obtained. These copolymers underwent phase segregation processes, as confirmed by small-angle X-ray scattering (SAXS), when they were thermally treated. Gas permeabilities of these materials depended on the phase separation. Thus, a linear relationship between gas permeability and increasing percentage and size of the domains of the segregated phase has been obtained. The differences in the degree of segregation have been examined for the different aliphatic diamines used in the synthesis of the copolymers. The effect of polarity, length, and structure of the chain were examined in terms of permeability for the gases O_2, N_2, CO_2, and CH_4. It has been shown those long aliphatic chains with adequate polarity and the ability to interact with and enhance the condensation of a certain gas give better materials. Improved selectivities, approaching the Robeson limit, were seen as a consequence of the thermal treatment. Also, an interesting reverse selectivity has been observed for the mixture CH_4/N_2, probably due to a combined effect of a specific interaction and an increase in solubility of CH_4 in the soft segregated portions of the copolymer.

4.1Introduction

Because of environmental concerns and economic interests, there is an imperative need for new materials and technologies with better efficiencies in gas separation applications [1-4]. New technologies must be found quickly in order to separate gases from diverse mixtures of gases with high selectivity and productivity. In this context, the technology of gas separation by membranes is considered a viable option. Gas separation membranes are very competitive for technological and economic reasons; they have good mechanical properties, they show excellent gas productivity (flux and ability to separate complex mixtures of gases), and they are very easy to install and maintain [5-6]. Glassy polymers show good properties as membrane materials for gas separations. In particular, aromatic polyimides are well-known for their excellent thermal oxidative stability, exceptional mechanical properties, along with an extraordinary ability to separate complex mixtures of gases in diverse applications [7-9]. These polymers are close to the trade-off of gas permeability versus gas selectivity obtained by Robeson in 1991 [10] for several gases. Nevertheless, they are below the new bound established in 2008 [11]. In this context, the manufacture of new polymeric materials tailored for more specific applications, with improved properties, is needed today.

A very promising way to develop new materials with improved properties consists of optimizing the structure of the polymer chains to attain high fractional free volume domains with a tailored distribution of sizes in order to increase the diffusivity and also with restrictive or selective channels communicating the interchain voids to increase the permselectivity. Another possible approach consists in increasing the solubility by introducing moieties in the polymer with a certain chemical affinity for a gas [12-13]. The introduction of polar groups that can interact favorably with CO_2 is a very attractive idea that has brought about new materials with enhanced properties. In this regard, polymers having poly(ethylene oxide) (PEO) chains are being extensively tested because of the strong affinity of CO_2 for the oxygen of the oxyethylenic moieties [14−17] and the resulting very high solubility of CO_2. For instance, Okamoto et al. designed a new generation of block aliphaticaromatic copolymers with PEO units that produced materials with good mechanical properties and excellent ability to separate carbon dioxide from other gases [18−20]. In previous papers, it was demonstrated that copoly(etherimide) s with long poly(ethylene oxide) chains of 6000 g/mol showed phase separation morphology, which can be largely improved by the use of thermal treatments [21−23]. Additionally, this thermal conditioning led to an important improvement in gas permeation properties [22]. Not many studies, to our knowledge, have analyzed the influence of the nature of the polyether segment in the gas separation properties in aliphatic-aromatic copolyimides.

Hence, we have carried out a complete study of the effect of using different types of aliphatic diamines on final properties. In a previous paper, a commercial Jeffamine having a molecular weight of 2000 (PEO-2000) was combined with three aromatic diamines: p-phenylenediamine (PPD), 4,4′-diaminobiphenyl (BNZ), and 4,4′-oxidianiline (ODA). These diamines were reacted with 3,3′,4,4′-biphenyltetracarboxylic dianhydride (BPDA) to form aliphatic-aromatic copolyimides. It was shown that ODA copolymers gave larger segregated domains due to their limited rigidity without compromising the mechanical properties of the resulting copolyimides. Thus, ODA will be used in this work as the aromatic diamine, BPDA as the dianhydride, and various aliphatic diamines (PEO-2000, PPO-2000, RT-1000, pTHF-1700, and pTHF-350 were employed) (see Figure 1).

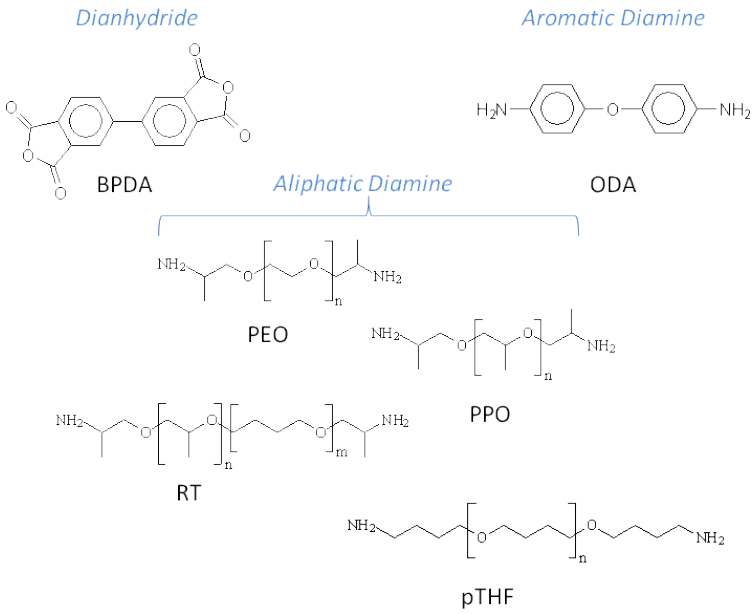

Figure 1. Chemical structure of the monomers used in this work.

An exhaustive study of the properties of the copolyimides (as films obtained by the deposition-evaporation method) containing different aliphatic diamines has been carried out by attenuated total internal reflectance-Fourier transform infrared (ATR-FTIR), differential scanning calorimetry (DSC), thermogravimetric analysis (TGA), Thermomechanical analysis (TMA), and small-angle X-ray scattering (SAXS) after the use of different thermal treatments. The corresponding permeability, solubility, diffusivity, and selectivity for different gases have also been studied.

4.2 Experimental section

4.2.1 Chemicals

3,3′,4,4′-Biphenyltetracarboxylic dianhydride (BPDA) and 4,4′-oxidianiline (ODA) were purchased from Sigma-Aldrich Co. These products were purified by sublimation at high vacuum just before being used. Bis(2-aminopropyl) poly(ethylene oxide), PEO-2000 (Jeffamine ED-2003), with nominal molecular weight of 2000 g/mol, bis(2-aminopropyl) poly(propylene oxide), PPO-2000 (Jeffamine D- 2000), with nominal molecular weight of 2000 g/mol, and bis(2-aminopropyl) poly(tetramethylene oxide-propylene oxide) (80 % / 20 % w/w) copolymer, RT-1000, with nominal molecular weight of 1000 g/mol (where n + m = 13−15), were kindly donated by Huntsman (Holland). Bis(amine) poly-(tetramethylene oxide), pTHF-350 (n = 2.2) and pTHF-1700 (n = 13.5), with two different nominal molecular weights of 350 and 1700 g/mol, respectively, were a kind gift from BASF The Chemical Company (Germany). All amino-terminated polyethers were dried at 70 °C under vacuum for 5 h and stored in a desiccator at vacuum until use. Anhydrous N-methylpyrrolidinone (NMP), used as the polymerization solvent, was purchased from Sigma-Aldrich. Figure 1 shows the chemical structure of the monomers.

4.2.2 Synthesis of Copoly(ether-imide)s

The polymer samples were synthesized by combination of the dianhydride BPDA with an aromatic amine, ODA, and an aliphatic amine (PEO-2000, PPO-2000, RT-1000, pTHF-350, or pTHF-1700). The corresponding copoly(ether-imide) will be designated by adding cPI before the acronym for the aliphatic portion. Thus, as an example, cPI-PEO-2000 means the copolymer of BPDA, ODA, and PEO-2000.

Actually, the synthesis of all the polymers shown here consisted of making a mixture of 4,4′-oxidianiline (ODA) (x mmol), and the aliphatic diamine (PEO-2000, PPO-2000, RT- 1000, pTHF-350, or pTHF-1700) (y mmol) in a weight ratio of 1:2. This mixture was dissolved in anhydrous NMP (5 mmol (x + y)/10 mL) in a 100 mL three-necked flask blanketed with nitrogen. Next, the reaction mixture was cooled to 0 °C, and under mechanical stirring, a stoichiometric amount of BPDA dianhydride (x + y mmol) was added and stirred overnight at room temperature (see final resulting amounts in Table 1). During this time the dianhydride completely dissolved and the solution reached high viscosity.

Table 1. Aliphatic and aromatic content of copoly(ether-imide)s.

Polymer	ODA (mmol)	Aliphatic Diamine (mmol)	BPDA (mmol)	Polyether content (%w/w)
cPI-PEO-2000	4.99	1.03	6.02	43.7 %
cPI-PPO-2000	5.04	1.04	6.08	43.8 %
cPI-RT-1000	3.94	1.58	5.52	41.7 %
cPI-pTHF-350	2.70	3.09	5.79	34.7 %
cPI-pTHF-1700	4.54	1.06	5.61	43.6 %

In the case of pTHF polyethers, the material has not only primary amines but also contains some secondary amines and a minimum amount of tertiary amines. The supplier gives content for the different amines of 80.1, 18.8, and 1.1 % for pTHF-350 and 72.1, 26.5, and 1.3 % for pTHF-1700 corresponding to primary, secondary, and tertiary amines, respectively. In the synthesis calculation, the y mmol for pTHF polyethers was calculated with respect to primary amines only, in order to avoid the reaction of the secondary amines that would lead to chemical cross-linking. Nevertheless, the species with tertiary amines are trifunctional with primary amines in the chain ends, and some chemical cross-linking is unavoidable. For this reason, in the cases of pTHF-350 and pTHF-1700, a certain amount of gelled material was obtained after completion of the reaction. This gel was separated from the soluble fraction by filtration. The soluble part of the reaction was considered as the final linear copolymer.

4.2.3 Preparation of Dense Films of Copolyimide

The resultant viscous copolyamic acid solutions were diluted with NMP to attain an appropriate viscosity for casting, filtered through a nominal no. 1 fritted glass funnel, degassed, and cast onto leveled glass plates. The resulting films were covered with a conical funnel to avoid fast evaporation of the solvent, dried at 80 °C overnight, treated at 120 °C for 8 h, and finally treated at 160 °C for 6 h in a vacuum oven. Copolymer films of 40−60 μm thickness were obtained. Additional thermal treatments, mentioned in the Gas Permeation and Selectivity section, were carried out on those films under inert atmosphere.

4.2.4 Characterization Methods

ATR-FTIR analyses of the films were performed at room temperature using a PerkinElmer Spectrum One. A Thermal Analysis Q500 instrument was used for TGA of the samples. Disc sections with weights between 5 and 15 mg were cut from the fabricated films and tested. When running dynamic scans, this was done in high-resolution mode, where the heating rate is automatically adjusted in response to changes in the rate of weight loss, which results in improved resolution, with an initial heating rate of 10 °C/min under a flux of nitrogen.

Differential scanning calorimetry (DSC) analyses were carried out in a Mettler Toledo (DSC 822e) calorimeter equipped with a liquid nitrogen cooler. Disc samples weighting 5−15 mg were cut from the films and sealed in aluminum pans. In order to monitor the changes in their thermal properties with thermal treatment, the samples were heated with the following cyclic method: from 25 °C, the sample was heated at 10 °C/min to a target temperature; once reached, the sample was cooled at the maximum cooling rate accessible for the instrument to −90 °C, held at this temperature for 15 min to equilibrate and reheated at 10ºC/min to the next target temperature. The procedure was followed until the last treatment temperature was reached. In this way, in each heating run, the thermal properties for the copolymers after treatment to the previously reached temperature were obtained.

Small-Angle X-ray Scattering (*SAXS*) measurements were performed at the beamline BM16 at the European Synchrotron Radiation Facility (Grenoble, France). The wave length of the X-ray beam was 0.980 Å. The detector was calibrated with silver behenate ($AgC_{22}H_{43}O_2$), and distance L was calculated from the scattering vector ($q=4\pi(\sin\theta)/\lambda$, λ=wave length, 2θ=scattering angle) as

$$L = \frac{2\pi}{q} \tag{1}$$

according to Bragg's Law. Disc samples cut from films were placed in a Linkam hot stage and heated at 10ºC/min while the SAXS spectra were recorded.

Thermomechanical (*TMA*) tests were performed in a Rheometric Scientific instrument model DMTA V. Rectangular test pieces of 3 mm width and 20 mm length were cut from films. A distance of 10 mm was set between fixation clamps. Runs were carried out from ambient temperature at 10 ºC/min with a static stress of 3 MPa.

The densities (ρ) of the dense membrane films were determined using a CP225D Sartorius balance, provided with an immersion density kit, according to

$$\rho = \rho_0 \frac{W_{air}}{W_{air} - W_{liq}} \tag{2}$$

where ρ is the density of the film, W_{air} and W_{liq} are the weights of the film in the air and an auxiliary liquid [24]) and ρ_o is the density of the auxiliary liquid (isooctane).

4.2.5 Gas permeation and selectivity

The permeability, P, has been determined for several gases (O_2, N_2, CO_2 and CH_4) by using a permeator with constant volume and variable pressure which uses the *time-lag* operation method. The measurements were carried out at 3 bar and 30 ºC. The equations used and the mode of operation of equipment, as well as an outline of it has been explained in previous studies [12].

4.3 Results and discussion

4.3.1 Copoly(ether-imide)s Imidization

Poly(ethylene oxide), poly(propylene oxide), and poly(tetramethylene oxide) chains are prone to oxidation, 25 and therefore, a great care was taken to carry out the imidization process. The films were heated at 160 °C for 6 h. By thermogravimetric analysis it was found that the solvent was practically removed by this heat treatment. It should be noted that all the copolymers were found to be insoluble in DMAc (dimethylacetamide), NMP, hexane, toluene, THF (tetrahydrofuran), and CH_2Cl_2 (dichloromethane) after this process.

Infrared spectra were recorded for these membranes (heated at 160 °C for 6 h) to check for the progress of imidization. As already seen for similar copolyimides [22], bands centered around 3257, 2500, and 1657 cm^{-1} found in the casted copolyamic acid strongly decreased or disappeared with the thermal treatment, and bands at approximately 1774, 1713, 1372, and 738 cm^{-1} increased or appeared with the progress on the imidization reaction, the last one being identificative of BPDA derived imides (see Figure 2). The peaks appearing around 2800 cm^{-1} are due to the aliphatic polyether segments. These changes were not completed for lower temperatures and any ulterior modification was seen at higher temperatures.

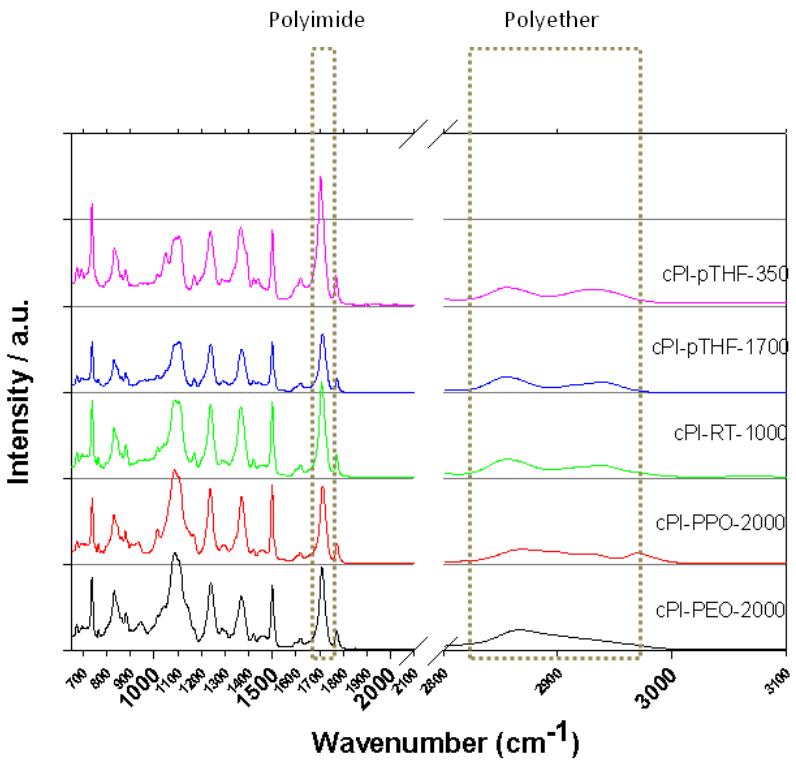

Figure 2. ATR-FTIR Spectra of copoly(ether-imide)s .

For similar copoly(ether-imide)s to the ones presented here, Hangzheng et al. [26] used IR spectra to prove the imidization at 200 °C. Even though the complete imidization of our copolyimides at a temperature as low as 160 °C is actually remarkable, we must mention that this full imidization at relatively low temperatures had already been found by us for copoly(ether-imide)s based on PEO segments [22,27]. Also, two works of Okamoto et al., studying similar copoly(ether-imide)s to the ones presented here, stated that a thermal treatment at 170 °C completely imidizes the precursor poly(amic acid)s to polyimides [18,19] although they did not show any IR spectra to prove the imidization state of the copolymers.

4.3.2 Thermal Stability

Thermogravimetric analysis was performed to evaluate the thermal stability of the copolymers. Dynamic runs using the HiREs mode, in a nitrogen atmosphere, showed a weight loss pattern for all the samples after being treated at 160 °C during 6 h. The resulting thermograms are shown in Figure 3.

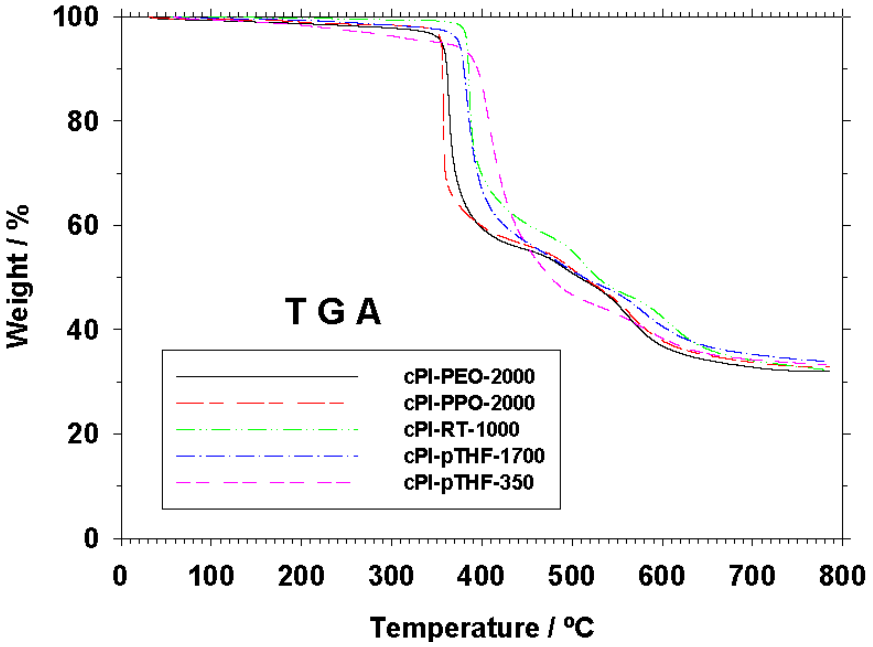

Figure 3. TGA curves in dynamic conditions of copolymers having different aliphatic diamines.

The behavior was similar for the different samples. The initial mass loss (close to 2 % weight from ambient temperature to 100 °C) can be attributed to the absorbed water in the sample. The second step is thought to be due to the loss of the aliphatic part included in the copolymer composition. In all the cases, the temperature of the maximum rate of weight loss was above 300 °C but clearly higher for the copolymers containing tetramethylene oxide units (385, 407, and 382 °C for cPI-RT-1000, cPI-pTHF-350, and cPI-pTHF-1700, respectively) with respect to the polymers containing ethylene oxide (363 °C for cPI-PEO-2000) or propylene oxide (345 °C for cPI-PPO-2000) units, showing the higher thermal stability of the former. After this degradation, a third step was attributed to the generalized degradation of the residual aromatic part. For all copolymers, the residual carbon content at 800 °C was 32−34 %. The differences between the mass losses in the second step for the different copolyimides studied are due to different percentages of polyether blocks in the polymers as evidenced by the good agreement between the experimental loss and what should be expected according to mass balances. This is shown in Figure 4.

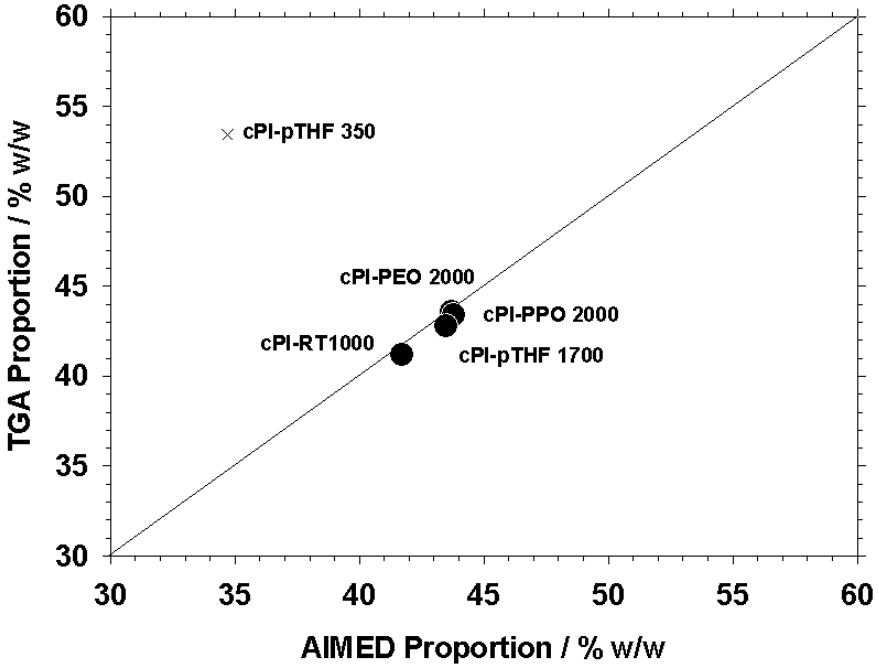

Figure 4. Aliphatic mass losses obtained from TGA versus the corresponding mass proportions according to the manufacture procedure.

Note, however, that cPI-pTHF-350, which has the highest temperature of degradation for this step, it's totally out of line with this correlation. In this case, because of the low molecular weight of the polyether chains, the aromatic polyimide segments are shorter than for the other copolymers and degrade at a lower temperature producing a merging of the degradation of the aliphatic and remaining aromatic portions, which cannot be clearly separated as for the other copolymers. Thus, TGA analyses confirmed that the aliphatic-chain thermal stability is much lower than the thermal stability of the aromatic polyimide segments, and therefore a selective degradation of this part can be performed in these copolymers with long polyether chains, as has been reported for other similar polymers [28,29].

4.3.3 Calorimetric Studies

The samples were heated in a DSC instrument with a cyclic method in order to monitor the changes in the thermal properties of the films with the thermal treatment. In Figure 5 we can see the changes in Tg for the aliphatic component of the copolymers for the different treatment temperatures. Only minor changes are seen that could be due to the increase in the proportion and size of the segregated domains along with the release of the remaining traces of solvent.

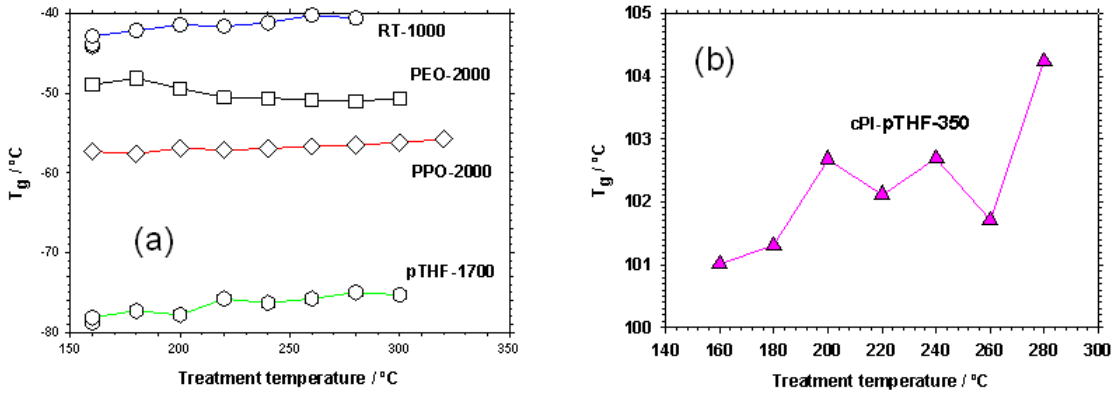

Figure 5. a) Tg of the aliphatic part of copolymers as a function of the thermal treatment. For the sake of readability, Tg of the aliphatic part of cpI-THF-350 is shown in Figure 5(b).

The Tg for the copolymers with approximately 2000 g/mol follows the trend of the corresponding homopolymers: pTHF < PPO < PEO. Copolymer cPI-RT-1000, with shorter chains, has a higher Tg, and for copolymer cPI-pTHF-350, the chains are so short that phases are significantly mixed and Tg reaches a value well above room temperature due to its convolution with the aromatic part of the copolymer.

When the polyether moiety is able to crystallize, the melting enthalpy can be used to evaluate the amount of crystallized aliphatic segments [22]. For the copolymers prepared in this work, cPI-PEO-2000 had a crystallinity lower than 2% after thermal treatments, while cPI-PPO-2000, cPI-RT-1000, cPI-pTHF-350, and cPI-pTHF-1700 were totally amorphous. Thus, from these results, it can be asserted that for all the copolymers studied, at the temperature of measurement of permeability, the polyether segments were totally amorphous (and well above their Tg except for copolymer cPI-pTHF-350 probably because the Tg measured in this case corresponds to a mixture of aliphatic and aromatic portions of the copolymer). In any case, no transitions for the pure aromatic polyimide hard segments were detected by DSC.

4.3.4 Thermomechanical Analysis

Thermomechanical analysis was also carried out in order to detect the glass transition temperature of the aromatic polyimide hard segments, which could not be detected by DSC. It was assumed that a good estimation of Tg corresponds to the temperature when strain is 10 times that of the sample at 100 °C [22]. This criterion could be accepted at least for comparative purposes. The thus-obtained results are shown in Figure 6. The corresponding results for Tg are shown as a function of the copolymer density in Figure 7. The data on permeability and density for the BPDA-ODA

homopolymer are taken from the literature [30]. Note that there is a clear increase of the Tg for the aromatic portion of the copolymers with increasing copolymer densities for polyethers of relatively long chains. This is nevertheless clearly not the case for cPI-pTHF-350. This anomalous fact could be due to the very short length of the pTHF-350 chains and their close interaction with the aromatic chains in the copolymer leading to a very significant mixture of the segments, as already seen by DSC.

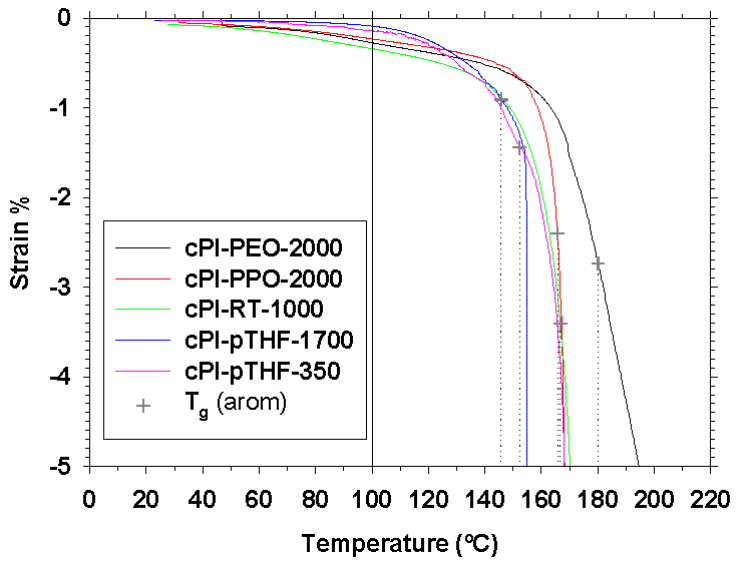

Figure 6. TMA curves of copolyimides. Crosses correspond to the T_g for the aromatic segment. These polymer films were treated at 160 ºC.

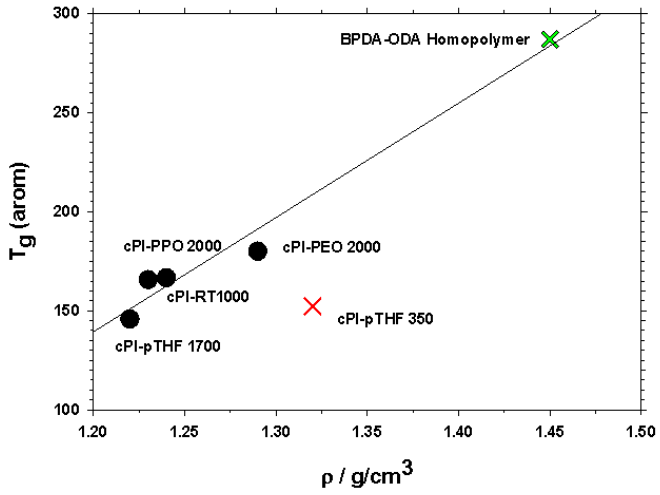

Figure 7. Tg of the aromatic parts of copolymers (as shown in Figure 6) versus the density of these copolymers. Density and Tg for BPDA-ODA homopolymer are shown in the graph. Polymer films were treated at 160 ºC.

For all the copolymers, the Tg of the aromatic polyimide is well above ambient temperature, although lower than the corresponding Tg for a pure aromatic polyimide homopolymer, due to the much lower polymerization degree and, consequently, lower length of the aromatic polyimide segments in the copolymer as compared to the corresponding homopolymer [22]. All samples have the same aromatic part so that the observed differences should only be due to the different mode of packaging of the aliphatic part in the final polymer structure.

For this reason, a better segregation in phases would increase the Tg of the aromatic portion. Under this assumption, it could be observed that the cPI-PEO-2000 sample showed the highest Tg value, followed by the cPI-RT-1000 and PPO-2000 ones. The lowest Tg values were obtained for samples with pTHF, where phase segregation is likely to be poor.

4.3.5 Small-Angle X-ray Scattering

Two parameters can be calculated from these scattering curves: the relative invariant, Q′, as the integral below the curve Iq^2 vs q, which is related to the extent of the phase separation; and the maximum on the scattering curve, q_{max}, related to the size scale of the separated phases, calculated also from the curve Iq^2 vs q. The equations used and the mode of operation of the equipment as well as an outline of it has been explained in previous studies [27]. Actually, the length scale, L, of the phase separation can be accurately evaluated from the curve Iq^2 vs q only for lamellar morphologies [31]. Nevertheless, our aim here is to compare L for some copolymers that are similar in structure. Thus, this procedure will be followed attending to its simplicity. Essentially, to eliminate the influence of the different film thicknesses and electronic density, the relative increment of both parameters is defined as:

$$\Delta Q' = \frac{Q'(T) - Q'(\text{baseline at T})}{Q'(\text{baseline at T})} \tag{3}$$

$$\Delta L = \frac{L(T) - L(\text{baseline at T})}{L(\text{baseline at T})} \tag{4}$$

The obtained results for ΔQ′ and ΔL, are represented in Figures 8 and 9 for the copoly(ether-imides) studied. In the curves shown in these figures, for the sample treated at 160 °C, there is a change in both the relative invariant and the characteristic length of the segregated phases that appears in the range from 170 to 300 °C (the increase is continued until the end of the temperature range tested). After heating at 300 °C, the final length scale for the copolymers lies in between 10 and 13 nm, which is smaller than the values for similar copolymers with longer polyether chains [22].

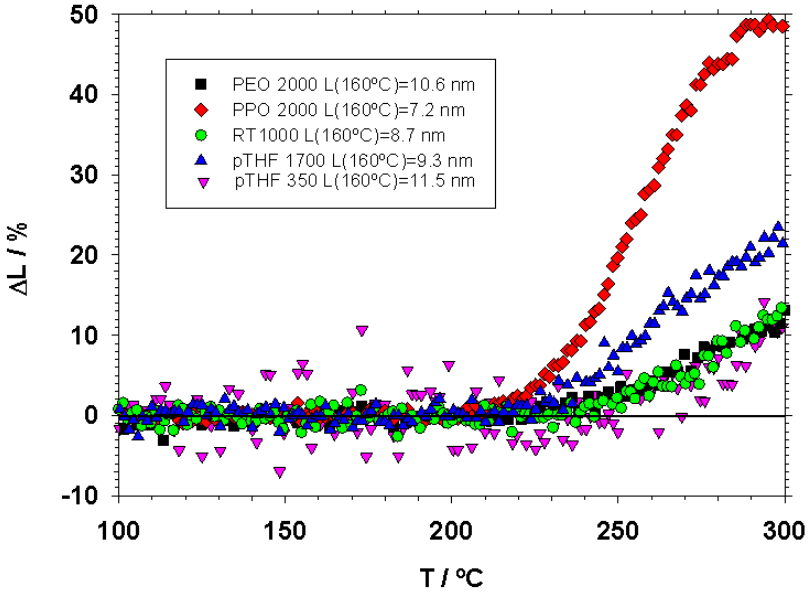

Figure 8. ΔL of copolymers as a function of treatment temperature. The characteristic length for the treatment at 160 ºC is shown in the legend. Polymer films were treated at 160 ºC.

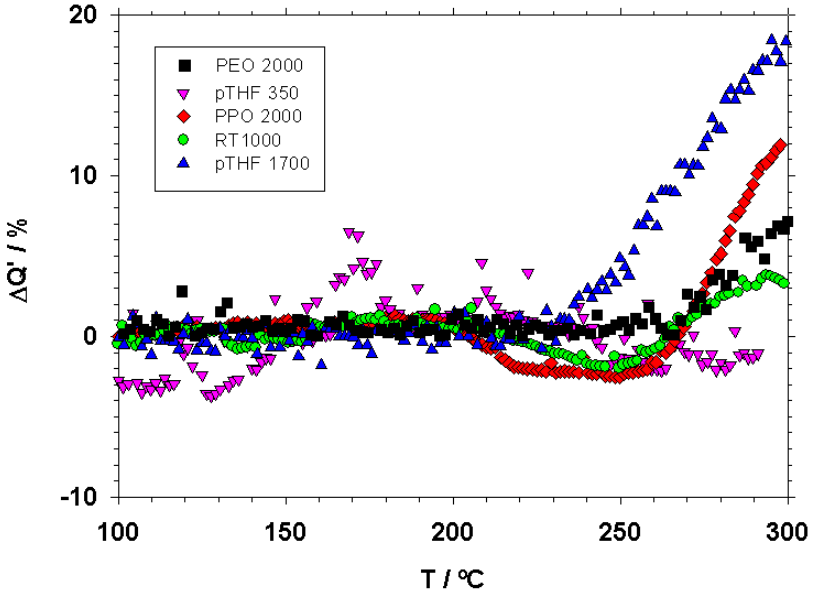

Figure 9. ΔQ' of copolymers as a function of temperature. Polymer films were treated at 160 °C.

4.3.6 Mechanical Properties

To complete the study on the physical properties of these copoly(ether imide)s, mechanical properties were measured in the tensile mode for copolymer films treated at 160 °C for 6 h. The obtained results are shown in Table 2.

Table 2. Mechanical properties of copoly(ether-imide)s.

Mechanical property	cPI-PEO-2000	cPI-PPO-2000	cPI-RT-1000	cPI-pTHF-1700	cPI-pTHF-350
Maximum stress (MPa)	22.1±1.7	13.5±1.9	18.7±1.4	44.4±3.4	75.3±2.0
Strain (%)	115±5	13.2±1.8	33.5±2.1	219±10	9.7±1.1
Modulus (GPa)	0.38±0.04	0.40±0.06	0.36±0.02	0.53±0.08	1.68±0.02

It is worth noting that all the copolymers showed reasonably good mechanical properties. Copolymer cPI-pTHF-1700 had better mechanical properties than copolymers with similar polyether length (cPI-PEO-2000 and cPI-PPO-2000). This is somewhat expected given that for other copolymers based on these polyethers such as polyurethanes, it is well-known that poly(tetramethylene oxide) polyethers produce stronger materials than poly(propylene oxide) or poly(ethylene oxide) polyethers. In the case of copolymer cPI-pTHF-350, because of the extensive mixing of the segments, the copolymer is much more rigid than the other ones as it can be deduced for the value of the modulus, and the properties lie in between the value of the copolymer with longer polyether segments and the values for the pure aromatic polyimide BPDA-ODA [22].

4.3.7 Gas Permeation and Selectivity

Figure 10 presents the permeability coefficients for the O_2, N_2, CH_4, and CO_2 gases in films of cPI-PEO-2000 as a function of the temperature of treatment. It could be observed that all the synthesized copolyimides showed similar trends. Permeability increased with the temperature of treatment of the copolymer, following the sequence:

$$P(CO_2)>P(CH_4)\sim P(O_2)>P(N_2)$$

This is the order of a decrease of the critical temperature of the penetrant gas (i.e., decreasing penetrant condensability). For these types of compounds, the diffusion coefficient is only a weak function of the penetrant size because the polymer sizesieving ability is poor [32]. In our case, as the penetrant size increased, the solubility coefficient increased more strongly than the diffusion

coefficient decreased, which means that larger, more condensable penetrants are more permeable than smaller ones [33]. Therefore, in these materials the relative permeability of each penetrant is largely determined by its solubility.

Figure 11 illustrates the effect of the thermal treatment on the CO_2 permeability. The tendency was quite similar for all the copolymers, with the exception of the sample pTHF-350, which showed very low permeability differences. The increase in permeability was always higher for treatment temperatures over 250 °C, when most of the possible residual solvent is released and the improvement in the phase separation is higher. In the case of films from cPI-PPO-2000, the increase in permeability was especially intense.

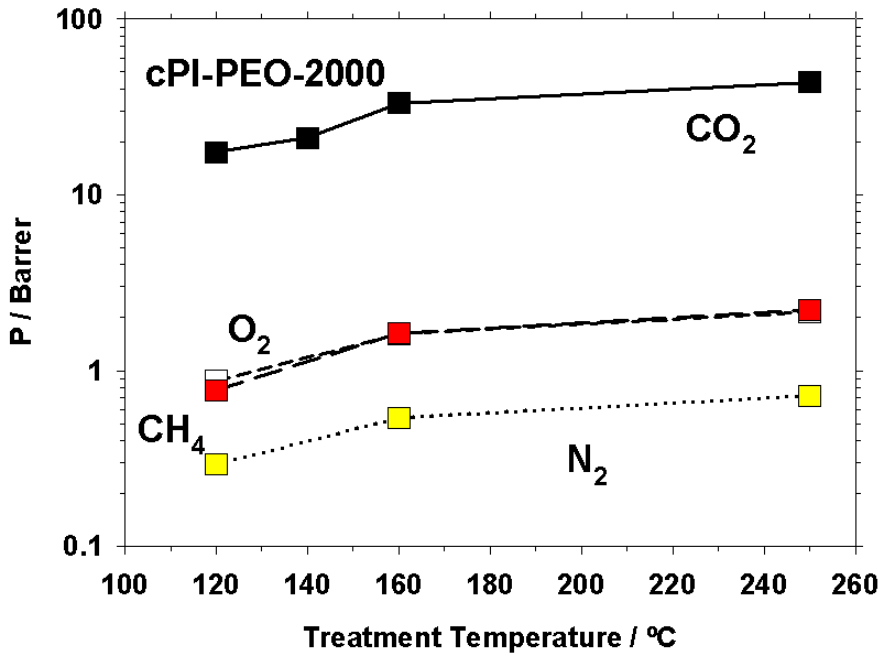

Figure 10. Permeability of the different gases studied as a function of the temperature of treatment for cPI-PEO-2000 copolymer.

For all the copolymers, the selectivity versus diffusivity and the solubility-selectivity versus the diffusivity-selectivity for the different pairs of gases and the temperature treatments are shown in Figures 12−16. For the CH_4/N_2 pair (Figure 15) given that no bound has been proposed yet, a bound is drawn on the basis of some good results from literature [34−39].

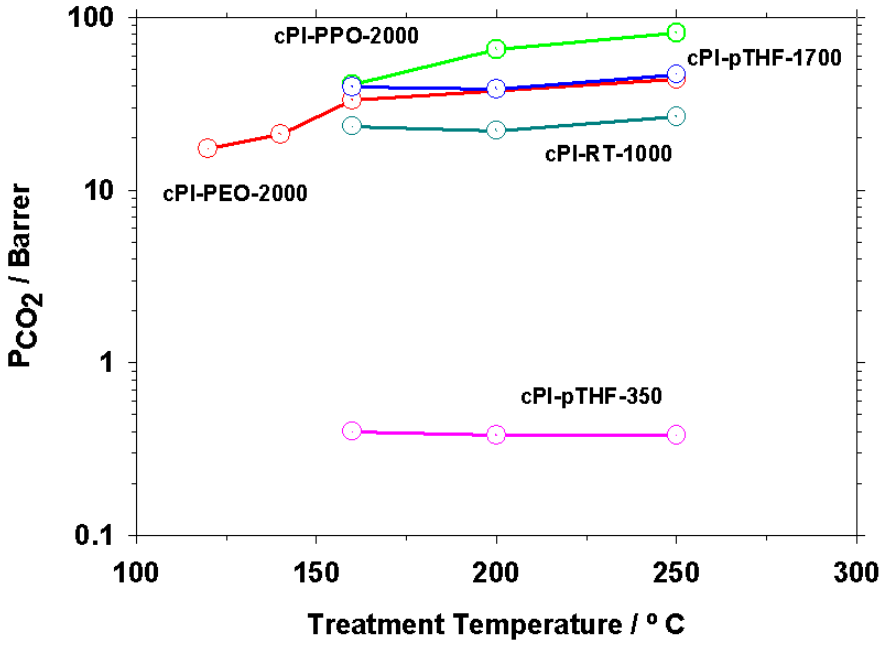

Figure 11. Permeability of CO_2 for different copolyimides as a function of the temperature of treatment.

Note that for all the gas pairs, the permeability of cPI-pTHF-350 was very low corresponding to its very low phase segregation as has been shown in Figures 8 and 9. Regarding the CO_2/N_2 and CO_2/CH_4 gas pairs, cPI-PEO-2000 presented the highest selectivity while the highest permeability appeared for cPI-PPO-2000. Note that both $\Delta Q'$ and ΔL increased strongly with thermal treatment for cPI-PPO-2000. Thus, it seems that the extension of segregation ($\Delta Q'$) and the mean size of the segregated domains (ΔL) increased the permeability of CO_2 and the rest of the gases studied. The selectivity for all the pairs including CO_2 was especially high for cPI-PEO-2000, probably due to specific interactions and to the big surface of its segregated domains, as seen in Figure 8, although neither this dimension nor the invariant (see Figure 9) increased notably with the treatment temperature.

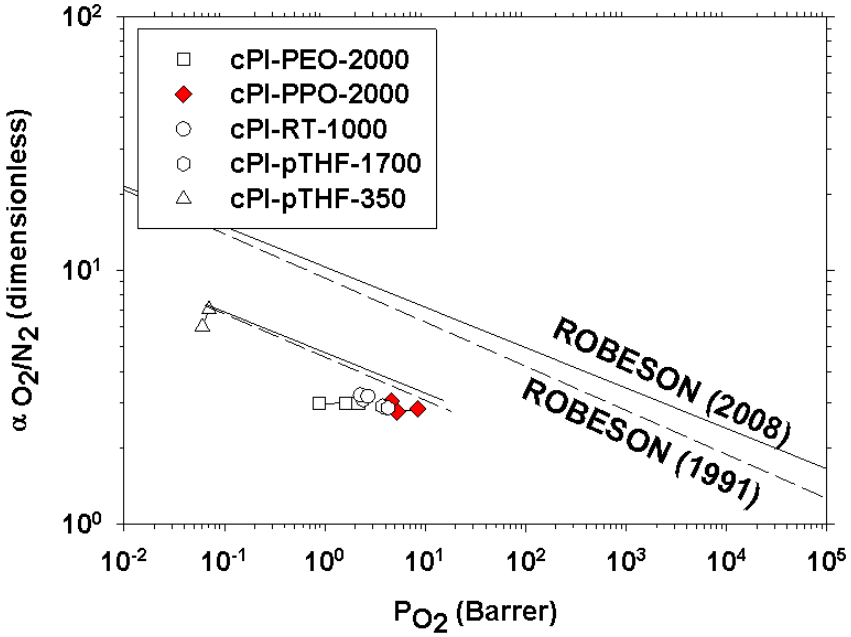

Figure 12. Robeson plot of copolymers for the O_2/N_2 gas pair. The insert shows the corresponding solubility and diffusivity selectivities.

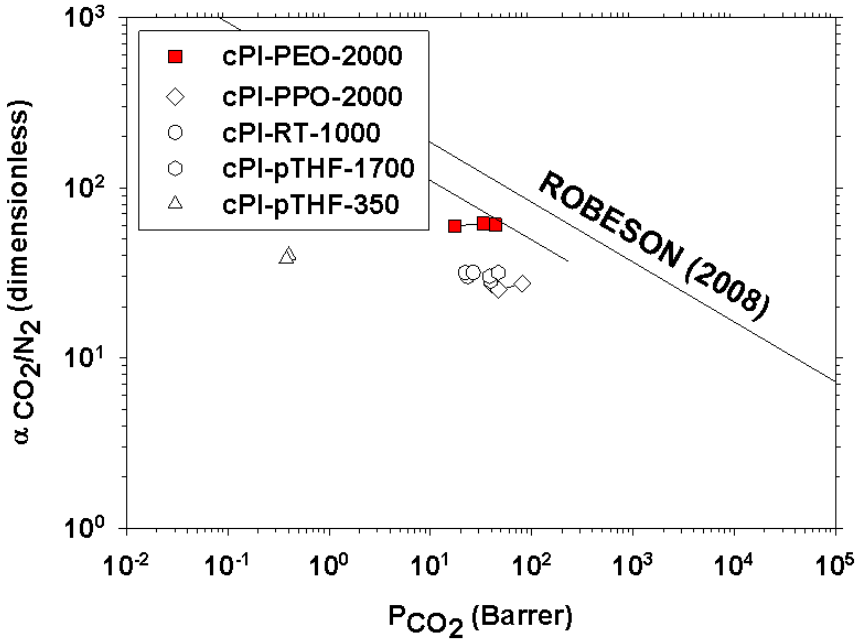

Figure 13. Robeson plot of copolymers for the CO_2/N_2 gas pair. The insert shows the corresponding solubility and diffusivity selectivities.

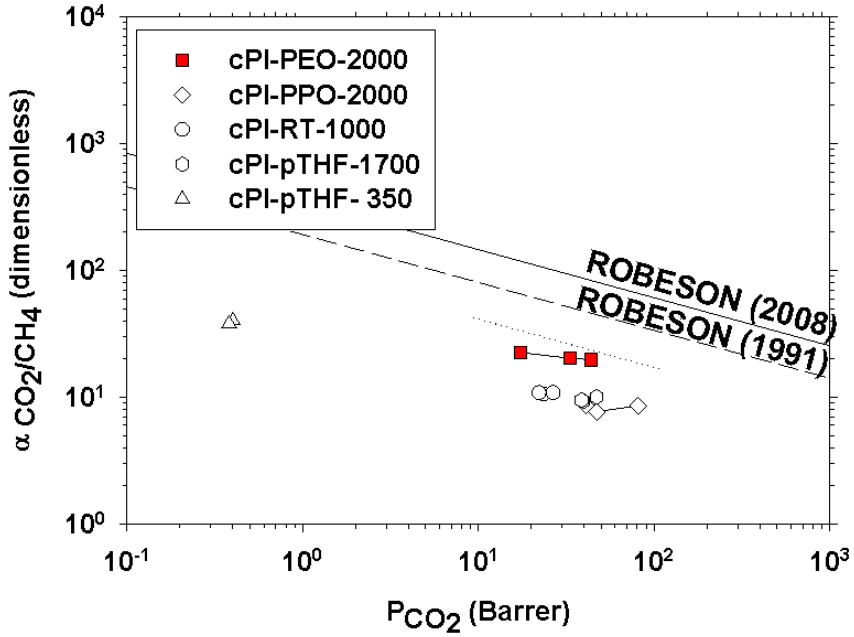

Figure 14. Robeson plot of copolymers for the CO_2/CH_4 gas pair. The insert shows the corresponding solubility and diffusivity selectivities.

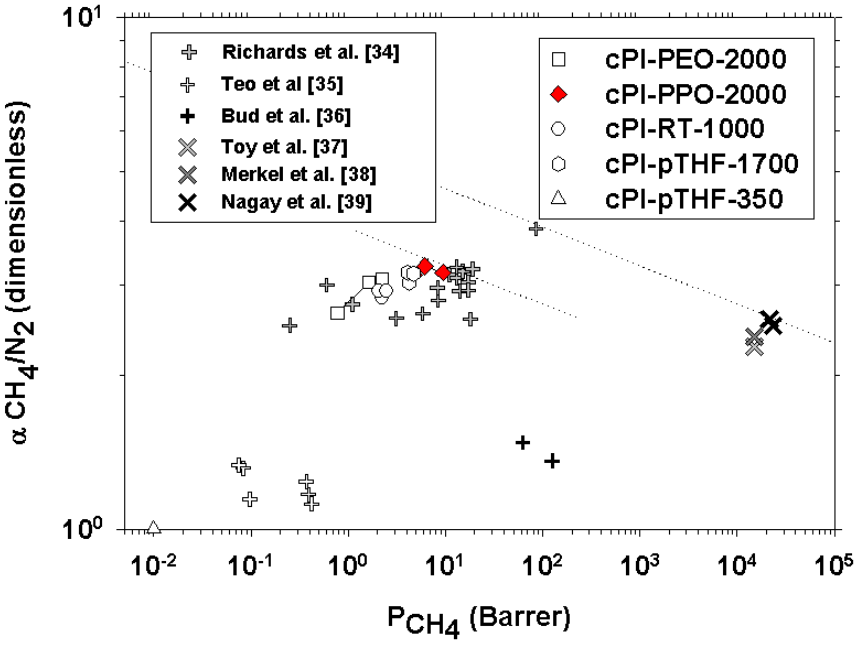

Figure 15. Robeson plot of copolymers for the CH_4/N_2 gas pair.

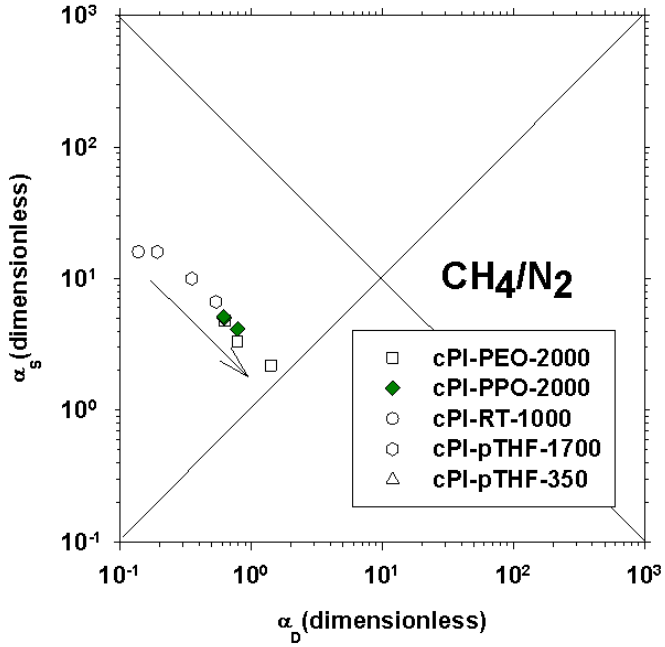

Figure 16. Solubility and diffusivity selectivities of copolymers for the CH_4/N_2 gas pair.

Since the copolyimides studied here can be assumed as consisting of a nonsegregated (continuous) aromatic polyimide phase and a soft segregated (disperse) aliphatic phase, the effective permeability of each copolyimide may be predicted by the Maxwell equation as shown below [4]:

$$P_{eff} = P_C \left[\frac{P_D + 2P_C - 2\phi_D \left(P_C - P_D \right)}{P_D + 2P_C + 2\phi_D \left(P_C - P_D \right)} \right] \tag{5}$$

P_{eff} is the effective permeability, P_C and P_D are the permeability of the continuous phase and of the dispersed phase, respectively, and ϕ_D is the volume fraction of the dispersed phase in the block copolymer. The permeability of CO_2 for a pure PEO is known to be 143 barrer in the amorphous state[41], and it is taken as P_D while the permeability of the copolyimides treated at 120 °C (when segregation has not advanced appreciably, according to Figures 8 and 9) is assumed for P_C. Note that the CO_2 permeability for the BPPA-ODA homopolymer cannot be taken as P_C because the presence of non segregated PEO (thus being a part of the continuous phase) should have an effect in permeability. In any case, this method can be used in order to attain approximate values for ϕ_D (i.e., the fraction of segregated PEO) in cPI-PEO-2000. Because the permeability of pure aliphatic constituents of the from the initial mass balance used to make the polymers or from the TGA

results, taking into account the densities of pure PEO and BPDA-ODA homopolymer, are shown in Figure 17.

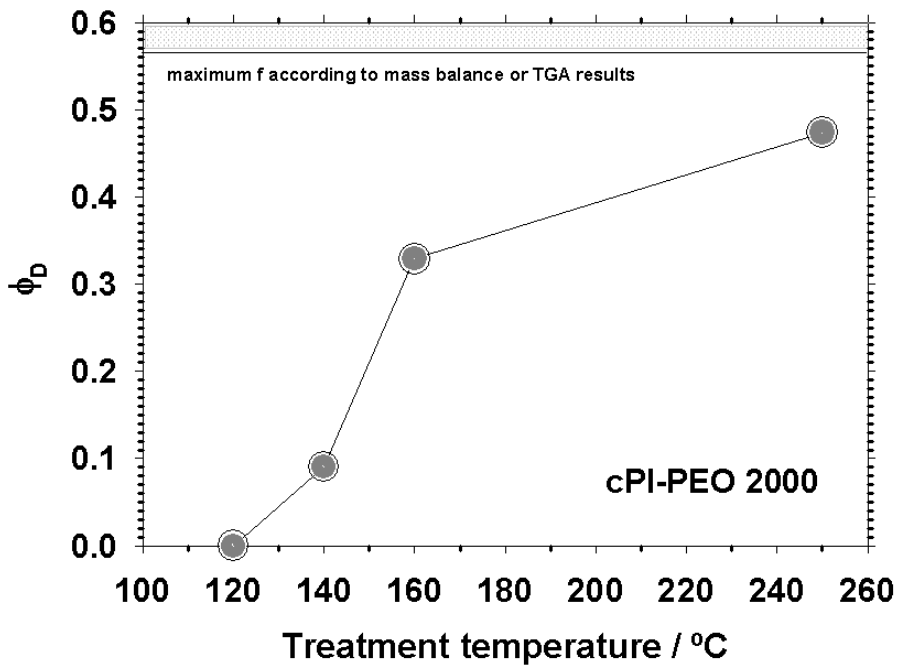

Figure 17. Volume fraction of phase segregated PEO for cPI-PEO-2000 as a function of the treatment temperature.

It is clear that the treatment temperature was so efficient in segregating the PEO moieties that after treatment of the membranes at 250 °C almost all the available PEO was segregated. It is worth noting that the Maxwell equation is accurate only when the components in the medium are mutually independent [42]. Therefore, the fractions shown in Figure 17 could only be an estimation. Obviously, the existence of the simultaneous imidization process (at temperatures below 160 °C) could also lead to erroneous evaluations of fractions. All these possible sources of error do not put into risk the conclusion on the high efficiency of thermal treatment to cause a strong segregation of the aliphatic components of the copolymer. Actually, these percentages are referred to the unknown percentage really existing at 120 °C that could be small but not zero. If alternatively we admitted that at 250 °C all or close to all PEO in the copolymer was segregated, a correction of the baseline would lead to a 8% of segregated PEO at 120 °C.

In terms of permselectivity (see Figures 12−16), the separation performances when the gases involved in the mixtures have different polarity (CO_2/N_2 and CO_2/CH_4) follow the sequence of polarities of the aliphatic portion of the copolymers: PEO-2000 > PPO-2000 > RT-1000/pTHF-1700. In the selectivity versus permeability plots, the copolymer with better performances (closer to

the corresponding Robeson's bound) is identified by a dotted line. Again, the permselectivity for pTHF-350 was very low due to the lack of phase segregation. When polarities are similar, with similar (O_2/N_2) or quite different (CH_4/N_2) sizes, the copolymer sequence follows the evolution of $\Delta Q'$ or ΔL (see Figures 8 and 9). In the case of the CH4/N2 gas pair, the cPI-PPO-2000 copolymer showed the highest permeability along with better selectivity. This extra selectivity that can even overcome the high solubility of the condensable gases that presents cPI-PEO-2000 can only be due to the presence of CH_3 groups contained within the PPO-2000 chain because this group is able to interact in a favorable way with CH_4. The cPI-pTHF-1700 presented the second lowest permeability and selectivity (once more cPI-pTHF-350 was the copolymer that gave the worst gas productivity). cPI-RT-1000 (the copolymer with poly- (tetramethylene oxide) and poly(propylene oxide) in its structure) gave permeability and selectivity values in between those shown by cPI-PPO-2000 and cPI-PEO-2000. On the other hand, the balance of the selectivity by diffusivity versus the selectivity by solubility proved that for all the couples of gases studied in this paper the selectivity was controlled mainly by the solubility term except for the O_2/N_2 pair where the diffusive selectivity played a major role. At this point, it is interesting to remark that the use of higher temperature during the thermal treatment increased the balance between the solubility and the diffusive terms of selectivity.

4.4 Conclusions

Copoly(ether-imide)s have been synthesized by the reaction between an aromatic dianhydride (BPDA), an aromatic diamine (ODA), and various diamine terminated aliphatic polyethers (PEO-2000, PPO-2000, RT-1000, pTHF-1700 and pTHF-350. FTIR showed that full imidization is almost achieved for all copolymers after a thermal treatment at 160 °C, well below the temperature needed to imidize fully aromatic polyimides. On the basis of TGA data, these copolymers proved to be stable under inert atmosphere up to around 300 °C. The TGA plots have determined that it is possible to make a selective degradation of the polyether segments except for the copolymer cPI-pTHF-350, with very short polyether chains. Mechanical properties for these copolymers were good enough to be applied in gas separation applications.

DSC, TMA, and SAXS experiments proved the existence of a phase separated morphology in these copolymers that improved when they were thermally treated at increasing temperatures below the temperature of the onset of decomposition. The phase segregation consisted of a polyether phase (completely amorphous at ambient temperature) and an aromatic polyimide phase with a Tg well above ambient temperature, except for cPI-pTHF-350 that had a very extensive mixing of segments.

For high treatment temperatures, the normalized or relative degree of segregation of the phases followed the sequence pTHF-1700 > PPO-2000 > PEO-2000 > RT-1000 > pTHF-350, whereas the relative increment of size scale of the segregated domains followed the progression PPO-2000 > pTHF-1700 > RT-1000/PEO-2000 > pTHF-350. As a consequence of the thermal treatment, the properties of the copolymers changed as their degree of segregation proceeded. Initially, at intermediate treatment temperatures, the release of the remaining solvent in the imidized copolymers produced a fast improvement in the phase separation, and treatments at higher temperatures (up to the degradation temperature) produced further improvement. After phase segregation, all of the samples show increasing selectivity for the studied pairs of gases. This fact was due to the increasing percentage and size of the domains of the segregated phases that determined the extra permeability and selectivity shown for the films after higher treatment temperatures. In terms of permselectivity, the gas performances when the gases had different polar natures followed the sequence of polarities of the aliphatic part of the copolymers.

Finally, when polarities were similar, the gas productivity sequence followed the trend of the extent of segregation and the size of the segregated domains that were quite similar. For the case of the CH_4/N_2 separation, an interesting reverse selectivity appeared probably due to the higher condensability of CH_4 in the segregated domains and to a possible existence of interactions between CH_4 and the soft segregated aliphatic moieties of the copolymers. The main results pointed to in this work were the effect of the structure and the percentage of the aliphatic diamines used to make the copolymer, the temperature of treatment and also the possibility of adapting polarity and chemical nature of the aliphatic chains, which open a wide range of options for the optimization of these aromatic−aliphatic copolyimides to tailor their functionality to different applications in industrial processes.

4.5 Acknowledgements

We are indebted to the Spanish Junta de Castilla-León for their financing of this work through the GR-18 Excellence Group Action and to the Spanish Ministry of Science and Innovation (MICINN) for the economic support of this work (MAT2008-00619/MAT, CIT-420000-2009-32 and MAT2010-20668/MAT). We also acknowledge financial support from the programme CONSOLIDER, project Multicat.

Authors are thankful for the access to the beamline BM16 at the European Synchrotron Radiation Facility (ESRF) in Grenoble (France). We are grateful to Dr. Ana Labrador and Dr. François Fauth for their help at BM16 station at the ESRF. The help provided by Sara Rodriguez in measuring gas properties is greatly appreciated. Advice from Dr. Jack Preston is greatly appreciated. A. Tena thanks CSIC for the predoctoral JAE fellowship received to carry out this work.

4.6 References

1. L. M. Robeson, Polymer membranes for gas separation. Curr. Opin. Solid State Mater. Sci. 4, (1999), 549–552.
2. P. Pandey, R.S. Chauhan, Membranes for gas separation. Prog. Polym. Sci. 26, (2001), 853-893.
3. W.J. Koros, Gas separation membranes: Need for combined materials science and processing approaches. Macromol. Symp. 188, (2002), 13–22.
4. M. Ulbricht, Advanced functional polymer membranes, Polymer. 47, (2006), 2217–2262.
5. R.W. Baker, Future directions of membrane gas separation technology. Ind. Eng. Chem. Res. 41, (2002), 1393–1411.
6. H. Lin, B.D. Freeman, Materials selection guidelines for membranes that remove CO_2 from gas mixtures. J. Mol. Struct. 739, (2005), 57–74.
7. M.T. Bessonov, M.M. Koton, V.V. Kudryavtsev, L.A. Laius, Polyimides: Thermally Stable Polymers; Consultants Bureau, New York, 1987.
8. D. Wilson, H.D. Stenzenberger, P.M. Hergenrother, Polyimides; Blackie: Glasgow, 1990.
9. M.K. Ghosh, K.L. Mittal, Polyimides: Fundamentals and Applications; Marcel Dekker: New York, 1996.
10. L.M. Robeson, Correlation of separation factor versus permeability for polymeric membranes. J. Membr. Sci. 62, (1991), 165-185.
11. L.M. Robeson, The upper bound revisited. J. Membr. Sci. 320, (2008), 390–400.
12. A. Tena, L. Fernández, M. Sánchez, L. Palacio, A.E. Lozano, A. Hernández, P. Prádanos, Mixed matrix membranes of 6FDA-6FpDA with surface functionalized gamma-alumina particles. An analysis of the improvement of permselectivity for several gas pairs. Chem. Eng. Sci. 65 (6), (2010), 2227–2235.
13. K. Ghosal, R.T. Chen, B.D. Freeman, W.H. Daly, I.I Negulescu, Effects of basic substituents on gas sorption and permeation in polysulfone. Macromolecules 29, (1996), 4360–4369.

14. M. Kawakami, H. Iwanaga, Y. Hara, M. Iwamoto, S.J. Kagawa, Gas permeabilities of cellulose nitrate/poly(ethylene glycol) blend membranes. J. Appl. Polym. Sci. 27, (1982), 2387-2393.
15. J. Li, K. Nagai, T. Nakagawa, S. Wang, Preparation of Polyethyleneglycol (PEG) and Cellulose Acetate (CA) Blend Membranes and Their Gas Permeabilities. J. Appl. Polym. Sci. 58, (1995), 1455-1463.
16. H. Lin, E. van Wagner, J.S. Swinnea, B.D. Freeman, S.J. Pas, A.J. Hill, S. Kalakkunnath, D.S. Kalika, Transport and structural characteristics of crosslinked poly(ethylene oxide) rubbers. J. Membr. Sci. 276(1-2), (2006), 145-161.
17. V.I. Bondar, B.D. Freeman, I. Pinnau, Gas transport properties of poly(ether-b-amide) segmented block copolymers. J. Polym. Sci. Part B: Polym. Phys. 38 (15), (2000), 2051-2062.
18. K. Okamoto, N. Umeo, S. Okamyo, K. Tanaka, H. Kita, Selective permeation of carbon dioxide over nitrogen through polyethyleneoxide-containing polyimide membranes. Chem. Lett. 5, (1993), 225-228.
19. K. Okamoto, M. Fujii, S. Okamyo, H. Suzuki, K. Tanaka, H. Kita, Gas permeation properties of poly(ether imide) segmented copolymers. Macromolecules 28, (1995), 6950-6956.
20. M. Yoshino, K. Ito, H. Kita, K. Okamoto, Effects of hard-segment polymers on CO_2/N_2 gas separation properties of poly(ethylene oxide)-segmented copolymers. J. Polym. Sci. Part B: Polym. Phys. 38, (2000), 1707-1715.
21. D.M. Muñoz, E.M. Maya, J. de Abajo, J, de la Campa, A.E. Lozano, Thermal treatment of poly(ethylene oxide)-segmented copolyimide based membranes: An effective way to improve the gas separation properties. J. Memb. Sci. 323, (2008), 53–59.
22. A. Marcos-Fernandez, A. Tena, A.E. Lozano, J. de la Campa, J. de Abajo, L. Palacio, P. Prádanos, A. Hernández, Physical properties of films made of copy(ether-imide) with long poly(ethylene oxide) segments. Eur. Polym. J. 46, (2010), 2352-2374.
23. E.M. Maya, D.M. Muñoz, A.E. Lozano, J. de Abajo, J.G. de la Campa. Fluorenyl cardo copolyimides containing poly(ethylene oxide) segments: synthesis, characterization, and evaluation of properties. J. Polym. Sci. Part A: Polym. Chem. 46, (2008), 8170–8178
24. J. Brandrup, E.H. Immergut, E.A. Grulke, Polymer handbook (4th ed.); John Wiley & Sons Inc: New York 1999.
25. J. Scheirs, S.W. Bigger, O. Delatycki, Characterizing the solid-state thermal oxidation of poly(ethylene oxide) powder. Polymer. 32, (1991), 2014–2019.
26. C. Hangzheng, X. Youchang, C. Tai-Shung, Synthesis and characterization of poly (ethylene oxide) containing copolyimides for hydrogen purification. Polymer. 51, (2010), 4077-4086.

27. A.Tena, A. Marcos-Fernández, A.E. Lozano, J.G. de la Campa, J. de Abajo, L. Palacio, P. Prádanos, A. Hernández, Thermally treated copoly(ether-imide)s made from BPDA and aliphatic plus aromatic diamines. Dependence of gas separation properties on the aromatic diamine, Journal of Membrane Science, 387–388 (2012) 54-65.
28. J.L. Hedrick, K.R. Carter, H.J. Cha, C.J. Hawker, R.A. DiPietro, J.W. Labadie, R.D. Miller, T.P. Russell, M.I. Sanchez, W. Volksen, D.Y. Yoon, D. Mecerreyes, High-temperature polyimide nanofoams for microelectronic applications, Reactive & Functional. Polymers. 30, (1996), 43-53.
29. J.L. Hendrich, Y. Charlier, R. DiPietro, S. Jayaraman, J.E. McGrath, High Tg Polyimide Nanofoams Derived from Pyromelletic Dianhidride and 1,1-Bis(4-aminophenyl)-1-phenyl-2,2,2-trifluoroethane, Journal of Polymer Science: Part A: Polymer Chemistry. 34, (1996), 2867-2877.
30. J. Zhang , J. Lu, W. Liu, Q. Xue, Thin Solid Films 340 (1999) 106-109, K. Tanaka, H. Kita, K. Okamoto, Gas Permeability and Permselectivity in Polyimides based on 3,3',4,4'-biphenyltetracarboxylic dianhydride, Journal of Membrane Science, 47, (1989), 203-215
31. F.S. Baltá-Calleja, C.G. Vonk, X-ray scattering of synthetic polymers. Elsevier: Amsterdam,1989.
32. R.C. Reid, J.M. Prausnitz, B.E. Poling, The Properties of Gases and Liquids. McGraw Hill: New York, 1987.
33. R. Recio, A.E. Lozano, P. Pradanos, A. Marcos, F. Tejerina, A. Hernandez, Effect of fractional free volume and Tg on gas separation through membranes made with different glassy polymers. J. Appl. Polym. Sci. 107, (2008), 1039–1046.
34. J.J. Richards, M.K. Danquah, S. Kalakkunnath, D.S. Kalika, V.A. Kusuma, S.T. Matteucci, B.D. Freeman, Relation between structure and gas transport properties of polyethylene oxide networks based on crosslinked bisphenol A ethoxylate diacrylate, Chem. Eng. Sci. 64(22), (2009), 4707-4718.
35. L.S. Teo, C.Y. Chen, J.F. Kuo, The gas transport properties of amine-containing polyurethane and poly(urethane-urea) membranes, J. Membr. Sci. 141, (1998), 91-99.
36. P.M. Budd, K.J. Msayib, C.E. Tattershall, B.S. Ghanem, K.J. Reynolds, N.B. McKeown, D. Fritsch, Gas separation membranes from polymers of intrinsic microporosity, J. Membr. Sci. 251, (2005), 263.
37. L.G. Toy, K. Nagai, B.D. Freeman, I. Pinnau, Z. He, T. Masuda, M. Teraguchi, Y.P. Yampolskii, Pure-gas and vapor permeation and sorption properties of poly[1-

phenyl-2-[p-(trimethylsilyl)phenyl]acetylene](PTMSDPA), Macromolecules 33, (2000), 2516-2524.

38. T.C. Merkel, V. Bondar, K. Nagai, B.D. Freeman, Sorption and transport of hydrocarbon and perfluorocarbon gases in poly(1-trimethylsilyl-1-propyne), J. Polym. Sci. Part B: Polym. Phys. 38, (2000), 273-296.
39. K. Nagai, A. Higuchi, T. Nakagawa, Gas permeability and stability of poly(1- trimethylsilyl-1-propyne-co-1-phenyl-1-propyne) membranes, J. Polym. Sci. Part B: Polym. Phys. 33, (1995), 289-298.
40. J.C. Maxwell, A treatise on electricity and magnetism. Vol. 1. London MacMillan Publ.: London, UK, 1873.
41. H. Lin, B.D. Freeman, Gas solubility, diffusivity and permeability in poly(ethylene oxide). J. Membr. Sci. 239, (2004), 105-117.
42. Y. Mi, T. Hirose, Molecular design of high-performance polyimide membranes for gas separations. J Polym Res. 3, (1996), 11-9.

CHAPTER 5

Advances in the design of co-poly(ether-imide) membranes for CO_2 separations. Influence of aromatic rigidity on crystallinity, segregation and gas transport

AlbertoTena[1,3], Angel Marcos-Fernández[1,3], M. de la Viuda[1], Laura Palacio[1,2], Pedro Prádanos[1,2], Angel E. Lozano[1,3], Javier de Abajo[1,3] and Antonio Hernández[1,2]

[1]*Smap UA-UVA-CSIC, Parque Científico Universidad de Valladolid, Paseo de Belén, s/n, 47011 Valladolid, Spain.*

[2]*Dept. Física Aplicada, Facultad de Ciencias, Universidad de Valladolid, Paseo de Belén, 7, 47011 Valladolid, Spain*

[3]*Instituto de Ciencia y Tecnología de Polímeros, CSIC, Juan de la Cierva 3, 28006 Madrid, Spain.*

This chapter has been prepared for submission

Abstract

A series of aliphatic aromatic copoly(etherimide)s, based on an aromatic diamine (ODA), a diamine terminated poly(ethylene oxide) (PEO2000) of a molecular weight of 2000 g/mol and different aromatic dianhydrides (BPDA, BKDA or BTDA and PMDA), has been synthesized. Cast films of these copolymers have been thermally treated and characterized by FTIR-ATR, DSC, TGA, TMA and Mechanical Tester. It has been found that there is a direct relationship between phase segregation, structural properties and permeability for increasing treatment temperatures.

The different rigidity of the dianhydrides used led to some differences in the physicochemical properties of the synthesized copolymers. The order of rigidity of the used dianhydrides is: PMDA> BPDA> BKDA. The T_g of the aliphatic part decreased for higher rigidity dianhidrides, with the PMDA copolymers showing a T_g closer to that of pure PEO. The T_g of the aromatic part were similar, with slightly increasing values when the rigidity of the dianhydride increases. The mechanical properties of the copolymers synthesized in this work were good and decreased when the PEO percentage in the samples was increased.

Results showed that permeability was higher when PEO content increased in the copolymer. Although the permeability mainly increased with the proportion of PEO, a certain influence was found when the dianhydride was varied. When the proportion of PEO in the copolymer exceeded 50%, the permeability values were similar for all samples, and the aromatic portion had no influence. For CO_2/N_2 selectivity, the behavior was similar; it increased with the increase in PEO content and, at lower percentages of PEO, selectivity varied depending on the rigidity of dianhydride used.

Graphical Abstract

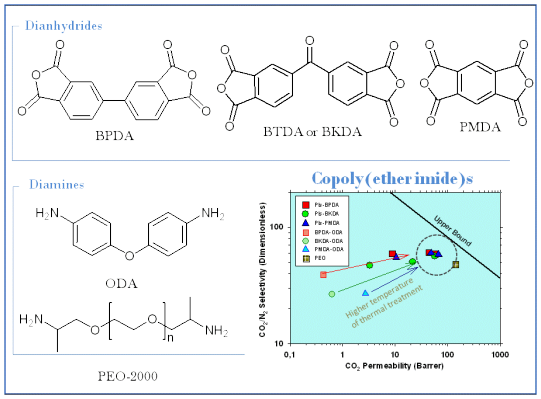

5.1 Introduction

Nowadays, the role of polymeric membranes applied to gas separation is more and more important. Although some of them have already an application in industrial separations [1], research is still necessary to discover new materials and/or to improve the properties of existing polymers to assure them an actual applicability at industrial level. In order to guarantee a real application of a new polymeric material in gas separation, an adequate balance of high permeability and good selectivity must be achieved [2-3].

There are several sources (power plants, steel, cement production plants or the chemical industry) where important amounts of CO_2 are generated, and it is therefore necessary to develop new technologies to curb as far as possible the greenhouse effect. Specifically, one of the most demanding applications is the separation CO_2/N_2 [3-4].

In order to be useful in such gas separation applications, a polymer film should show a preferential affinity for condensable gases such as CO_2 or CH_4 as compared with a mostly ideal gas such as N_2. Moreover, in addition to the criteria of permeability and selectivity, membranes to be used in this type of separations, must give high flow and have good mechanical and thermal resistance.

Glassy polymers and in particular polyimides are well known for their excellent thermal oxidative stability, good organic solvent resistance and exceptional mechanical properties, along with an extraordinary ability to separate complex mixtures of gases in diverse applications [2, 5-6]. Typically these materials present a high selectivity but with a not always sufficiently high permeability [7-8]. It is therefore necessary to increase the affinity of the compounds for condensable gases such as CO_2, or CH_4 and one of the most common approaches to meet these requirements is the use of block-copolymers.

Aromatic-aliphatic block-copolymers usually combine hard and soft blocks. The hard block can be formed by a polymer with well-packed and highly rigid structures; as a result it forms the glassy segment of the polymer chain with usually low free volume. In contrast, the soft block can consist in a polymer with more flexible, low T_g, chains, which can form rubbery segments within the polymer chain normally with high free volume. Also, when aromatic-aliphatic block copolymers are phase-separated, their glassy polymer segments would provide mechanical support. The rubbery segments, due to the nature of the flexible chain structure, allow an efficient transport of gas, giving a good permeability to the copolymer [9-10].

It is known that poly(ethylene oxide) (PEO) compounds give excellent results for the CO_2 separation from other light gases [11-13]. In view of this, block-copolymers combining aromatic and PEO polyimides appear to be a successful route [14-15]. These compounds have also good permselectivity for the couple CO_2/N_2, and usually this is attributed mainly to the high solubility-selectivity [16], which could be due to the existence of strong interactions of CO_2 with the oxyethylene group in PEO. The interaction between CO_2 and PEO has been discussed and used for the development of CO_2 selective membranes previously [17-19]. For these reasons it is necessary to carry on studies for a better understanding of this type of PEO copolymers, in order to reach optimal structures for specific applications. In particular, here we will focus on the influence of the dianhidride on segregation, cristallinity and permselectivity.

5.2 Experimental

5.2.1 Chemicals

The dianhydrides pyromellitic dianhydride (PMDA), 3,3′,4,4′- biphenyltetracarboxylic dianhydride (BPDA), 3,3′,4,4′- benzophenone tetracarbxylic dianhydride (BTDA or BKDA) and the diamine 4,4'-oxydianiline (ODA) were purchased from Aldrich. These products were purified by sublimation at high vacuum just before being used. Polyoxyethylene bis(amine) (Jeffamine ED-2003, n= 41) with nominal molecular weight of 2000 g/mol, was kindly donated by Huntsman® (Holland). This polyether was dried at 70 ºC in vacuum for 5 hours and stored in a desiccator at vacuum until use. Anhydrous N-methylpyrrolidinone (NMP), to be used as polymerization solvent, was purchased from Sigma-Aldrich Co. Figure 1 shows the chemical structure of the monomers.

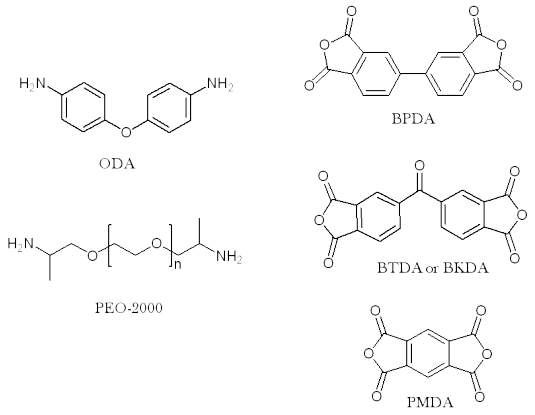

Figure 1.- Chemical structure of the monomers used in this work.

5.2.2 Synthesis of copoly(ether-imide)s

The samples were synthesized by combination of the aliphatic diamine (PEO) with the aromatic diamine (ODA), and different dianhydrides (BPDA, BTDA or BKDA and PMDA). The corresponding copoly(ether-imide) will be nominated by adding the dianhydride abbreviation and the w/w ratio between the diamines aliphatic / aromatic. Thus, BKDA_1/1 refers to the sample BKDA-PEO2000-ODA with an aliphatic-to-aromatic diamine weight ratio of 1:1 which corresponds to a mass proportion of PEO in the final copolymer of around 28 %.

Diamine-terminated poly(oxyethylene oxide) (PEO2000) (*x* mmol), and 4,4'-oxydianiline (ODA) (*y* mmol) in weight ratios 1:1, 2:1, and 4:1 were dissolved in anhydrous NMP (5 mmol (x+y)/10 mL) in a 100 mL three-necked flask blanketed with nitrogen.

Then, the reaction mixture was cooled down to 0 ºC, and under mechanical stirring, a stoichiometric amount of the corresponding dianhydride (BPDA, BKDA or PMDA) (*x*+*y* mmol) was added and the mixture was stirred overnight at room temperature. During this time the dianhydride completely dissolved and the solution reached high viscosity. Table 1 records the proportions of PEO and the acronym for each of the polymers synthesized in this work.

Table 1. Polymers synthesized in this work.

Polymer	*PEO/ODA**	*Acronym*	*PEO content (%w)*	*PEO content (%w)***
BPDA/PEO2000/ODA	1:1	BPDA_1/1	29.2	28,2
	2:1	BPDA_2/1	43.7	43,6
	4:1	BPDA_4/1	58,5	58,2
BKDA/PEO2000/ODA	1:1	BKDA_1/1	28,0	27,5
	2:1	BKDA_2/1	42,4	42,2
	4:1	BKDA_4/1	57,0	56,9
PMDA/PEO2000/ODA	1:1	PMDA_1/1	33,3	31,2
	2:1	PMDA_2/1	48,8	46,4
	4:1	PMDA_4/1	63,6	63,1

* w/w ratio between the diamines aliphatic / aromatic

** Calculated by TGA analysis

5.2.3 Preparation of the copolyimide dense films.

The resultant viscous polyamic acid solution was diluted with NMP to the appropriate viscosity for casting, filtered through a nominal #1 fritted glass funnel, degassed, and cast onto a leveled glass plate. The resulting film was covered with a conical funnel to avoid fast evaporation of the solvent, dried at 80 ºC overnight, and finally treated at different temperatures for 6 hours in a vacuum oven, in order to get a complete imidization. Films of the copolymers of 50-70 μm in thickness were obtained. After that, thermal treatments under inert atmosphere were carried out at different temperatures. All films showed good mechanical properties.

5.2.4 Characterization Methods

Attenuated total internal reflectance-Fourier transform infrared analyses (ATR-FTIR) were performed at room temperature using a PerkinElmer Spectrum One infrared spectrometer equipped with an ATR accessory. 16 scans were performed at a resolution of 4 cm^{-1} and were averaged to get the FTIR spectra.

A Thermal Analysis Q500 instrument was used for thermogravimetric study of the copolymers (TGA). Disc samples, cut from films, with weights between 5 and 15 mg were tested. When running dynamic scans, it was done in Hi-Resolution mode, with an initial heating rate of 10 ºC/min under a flux of nitrogen, where the heating rate is automatically adjusted in response to changes in the rate of weight loss, which results in improved resolution,.

Differential scanning calorimetry (DSC) analyses were carried out in a Mettler Toledo (DSC 822e) calorimeter equipped with a liquid nitrogen accessory. Disc samples cut from films weighting 5–15 mg were sealed in aluminum pans. Samples were heated with the following cyclic method in order to monitor the changes in thermal properties with thermal treatment: from 25 ºC, the sample was heated at 10 ºC/min to a target temperature; once reached, the sample was cooled at the maximum cooling rate accessible for the instrument to -90 ºC, held at this temperature for 15 min and reheated at 10ºC/min to the next target temperature. The procedure was followed until the last treatment temperature was reached and a final run from -90 ºC to 80 ºC was performed. In this way, in each heating run, the thermal properties for the copolymers after treatment to the previously reached temperature were obtained, and a plot of thermal properties versus “instantaneous” thermal treatment could be built.

Thermomechanical (TMA) tests were performed in a Rheometric Scientific instrument model DMTA V. Rectangular test pieces of 3 mm width and 20 mm length were cut from films. A

distance of 10 mm was set between fixation clamps. Runs were carried out from ambient temperature at 2 ºC/min with a static stress of 0.5, 1.5 and 3 MPa for copolymers with weight ratios 4:1, 2:1, and 1:1 respectively. With these stresses, the samples had an initial strain of less than 1% at 50 ºC.

Tensile properties were measured in a MTS Synergie 200 testing machine equipped with a 100 N load cell. Rectangular test pieces of 3.5 mm width and 25 mm length were cut from films. A crosshead speed of 5 mm/min was used. Strain was measured from crosshead separation and referred to 10 mm initial length. At least six samples were tested for each copolymer at room temperature.

The permeability, P, for CO_2 and N_2 was determined by using a permeator with constant volume which uses the *time-lag* operation method. The measurements were carried out at 3 bar and 30 ºC. A sketch of the device and the analyzed method used has been described in previous studies [20].

5.3 Results and discussion

5.3.1 Copoly(ether-imide)s imidization

After the films were dried overnight, they were annealed at different temperatures (160, 200 and 250 ºC) to almost complete removal of the solvent, and infrared spectra (shown in Figure 2) were recorded to check for the progress of imidization. After this process, the polymer films resulted to be insoluble in DMAc (dimethylacetamide), NMP, Hexane, Toluene, THF (tetrahydrofuran) and CH_2Cl_2 (dichloromethane).

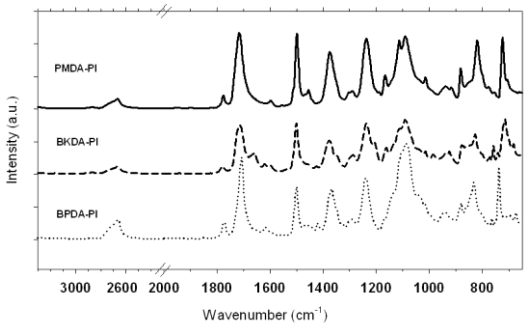

Figure 2.- FTIR spectra for the copolymer with a 1:1 proportion of a diamines, treated at 160 ºC.

Under the commented protocol, the films were almost completely imidized according to their FTIR spectra (within the detection limits of the FTIR technique) at 160 ºC as it was shown in previous studies [21]. For the synthesized copolymers, few differences were observed. Common bands appeared in the spectra: 2880 cm^{-1} (aliphatic C-H stretching), 1774 cm^{-1} (symmetric stretching of C=O imide groups), 1712 cm^{-1} (asymmetric stretching of C=O imide groups), 1370 cm^{-1} (C-N stretching of imide groups), 1250 cm^{-1} (twisting CH_2), 1090 cm^{-1} (C-O stretching), 840 cm^{-1} (rocking CH_2) and 720-750 cm^{-1} (imide ring deformation different for each dianhydride). For the BKDA copolymers a new band appeared at 1660 cm^{-1} which is related to the stretching of the ketone group of the dianhydride BKDA.

5.3.2 Thermal Stability

Thermogravimetric analysis was performed to evaluate the thermal stability of the synthesized copolymers. Dynamic runs in High-Resolution mode, in a nitrogen atmosphere, for fully imidized copolymers (annealed at 160 ºC for 6 hours) showed a weight loss pattern consisting of three consecutive steps (see Figure 3): an initial loss from ambient temperature to 300 ºC; a second loss from 300 ºC to 460-480 ºC; and a third loss from 460-480 ºC to 800 ºC.

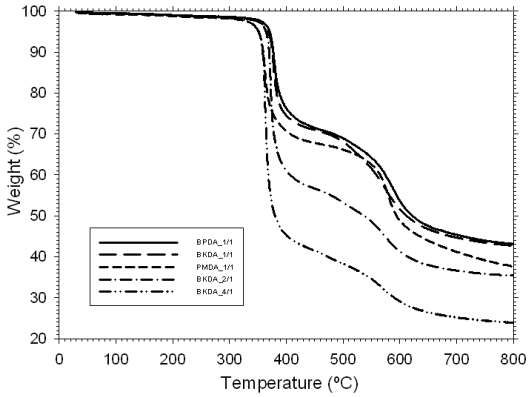

Figure 3.- TGA curves in dynamic conditions of copolymers having different aromatic dianhydride annealed at 160 ºC for 6 h.

The first loss can be attributed to the absorbed water plus the residual solvent trapped in the film. The weight change for this step was in the order of 2 to 2.5 % [22]. The second loss stage, after correcting for the first one, agreed with the theoretical contribution of poly(ethylene oxide) bis(amine) entering the copolymer composition [23], within a 2% error (see Table 1), and it was therefore assigned to the loss of polyether block sequences. The third and final stage of weight loss was due to the thermal decomposition of the remaining aromatic polyimide segments.

TGA analysis confirmed that the polyether chains are much less thermally stable than the aromatic segments, as already found for another copoly(ether-imide)s based on poly(ethylene oxide) [16] and therefore a selective degradation of the polyether moiety can be performed in these copolymers. The temperature of maximum weight loss rate took place between 360-380 ºC for all copolymers. This temperature increased when the amount of aliphatic diamine decreased. Similarly, the char residue at 800 ºC increased with the increase of the aromatic content in the copolymer.

5.3.3 Calorimetric Studies

The samples were heated in a DSC instrument with a cyclic method in order to monitor the changes in their thermal properties with thermal treatment [16]. All the copolymers showed only the T_g, and in some cases T_m, for the poly(ethylene oxide) segments, and no transition for the aromatic polyimide segments could be detected.

Changes in the polyether T_g were observed with thermal treatment as a function of the dianhydride and the amount of PEO. In Figure 4, the change in T_g for the PMDA series is shown. The T_g value decreased always when the PEO content increased, as expected, and for copolymers PMDA_2/1 and PMDA_4/1 the value after treatment at high temperatures, above 250 ºC, reached the expected value [24] for a PEO chain of 2000 g/mol with restricted movement at the chain ends. For copolymer PMDA_1/1 the final value was higher, indicating some degree of mixing of the segments. Similar behavior was found for the PMDA and BKDA series, but the minimum T_g value reached was higher than for the PMDA series, around -50ºC for 2:1 and 4:1 PEO content and between -45 to-50 ºC for 1:1 PEO content.

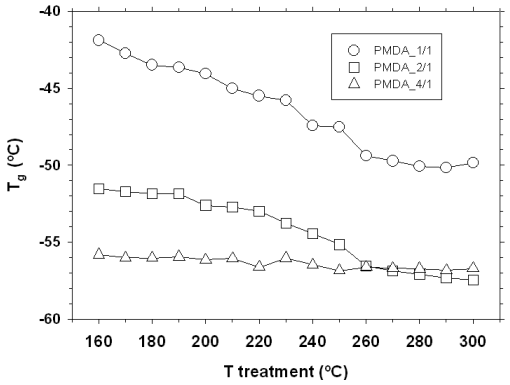

Figure 4.- T_g for PEO in the copolymers of the PMDA series annealed at 160 ºC, 6h, after ‘‘instantaneous” treatment at different temperatures

A clearer picture about the phase-separated structure of these copolymers can be deduced from the melting endotherm of the PEO segments. In Figure 5, the percentage of PEO crystallinity is represented. Copolymers with 1:1 PEO content did not show PEO crystallinity, and for the other PEO contents, the higher the treatment temperature, the higher the amount of crystallized PEO. As expected, series with higher PEO content (4:1) were more crystalline than series with lower PEO content (2:1), but dianhydride had a strong effect on crystallinity. Copolymers based on PMDA dianhydride were more crystalline than copolymers based on BPDA, and the latter were more crystalline than copolymers based on BKDA. Thus, the increase in the rigidity of the structure of the dianhydride, results in a better phase-separated morphology. The sequence of increasing rigidity (and segregation and crystallinity) is (see Figure 1):

BKDA<BPDA< PMDA

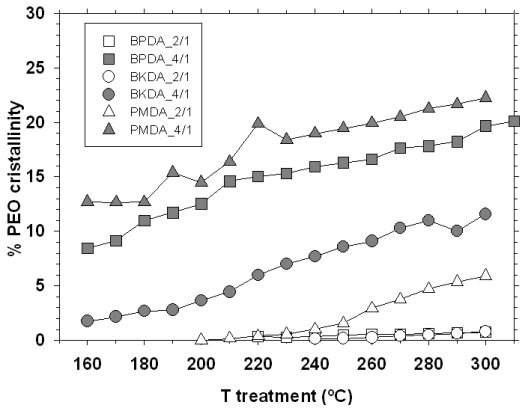

Figure 5.- Percentage of PEO crystallinity for copolymers annealed at 160 ºC, 6h, after ‘‘instantaneous” treatment and different temperatures

The temperature of the maximum of the endotherm is shown in Figure 6. It seems clear that, the melting point did not follow the same tendency as shown by crystallinity (see Figure 5). It also worth to note that the temperature of disappearance of crystalline phase was always below ambient temperature and therefore PEO segments were amorphous at room temperature. Copolymers based on BPDA melted at higher temperature than copolymers based on BKDA and copolymers based on PMDA melted at lower temperature than the others. This result can be explained in terms of the size of the crystals that strongly influence the melting point. It has already been found for similar copolymers, based on diamines of different rigidity, that the diamines with higher rigidity had lower T_g values and lower melting points for the PEO segments [16]. SAXS analysis demonstrated that for these diamines the phase-segregated morphology was better than for a less rigid diamine, and

that the lower melting point was due to a lower size of the segregated aliphatic phase. Thus, for these copolymers based on different dianhydrides, the PMDA (the most rigid dianhydride) copolymers are expected to have the phase-separated structure with the lowest characteristic length (lowest T_m), and the BKDA copolymers to show the highest spacing characteristic lengths (highest T_m). Thus, from the DSC results it can be deduced that PEO segments are in a separated phase of relatively high purity at any PEO content in the copolymer [23].

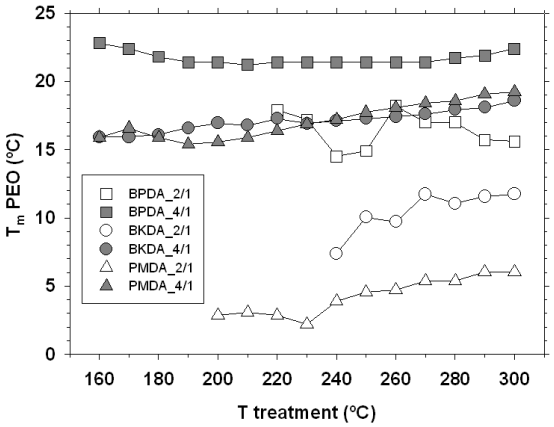

Figure 6.- Temperature on the maximum of the melting endotherm for copolymers annealed at 160 ºC, 6h, after ‘‘instantaneous” treatment and different temperatures

5.3.4 Thermomechanical Analysis

Thermomechanical analysis was carried out in order to detect the glass transition temperature of the aromatic polyimide hard segments, which was not detected by DSC. Several criteria can be chosen to determine the transition temperature. For example, it could be taken as the minimum in the first derivative of the strain vs. temperature curve, or the zero value in the second derivative. With the former criterion, the values were not clearly resolved, so that we decided to choose a different criterion, the temperature when strain is 10 times that of the sample at 100 ºC, which gives lower transition values than the other two mentioned criteria [23]. This criterion can be accepted at least for comparative purposes.

For all the copolymers, the T_g of the aromatic polyimide was well above ambient temperature (from 193 ºC for BKDA_4/1 to 293 ºC for PMDA_1/1), although lower than the corresponding T_g for the corresponding pure aromatic polyimide homopolymer, BPDA-ODA, BKDA-ODA and PMDA-ODA. This is due to the lower polymerization degree in the copolymers and, consequently, lower length of the aromatic polyimide segments as compared to the corresponding homopolymer and to

the possible inclusion of some polyether segments in the polyimide domains [23]. The T_g of the aromatic portion of the copolymer clearly increased when the PEO content decreased (e.g. 213 ºC for PMDA_4/1, 249 ºC for PMDA_2/1 and 293 ºC for PMDA_1/1). All samples have the same aliphatic polyether, thus the differences can only be due to the differences in the aromatic polyimide segments. The order obtained for the copolymers in this work were:

Proportion 1:1 > Proportion 2:1 > Proportion 4:1

PMDA copolymers > BPDA copolymers > BKDA copolymers

The aromatic T_g increased with the rigidity of the dianhydride, so the more rigid PMDA copolymers had higher T_g for the aromatic segments than for the rest of the copolymers.

5.3.5 Mechanical Properties

In general, the mechanical properties were good for copolymers 1:1 and 2:1, and reasonable for copolymers 4:1. As expected, the maximum stress and the modulus decreased when the PEO content increased (see Table 2). The strain was reasonably high for all copolymers except for BPDA_4/1. For this copolymer, the prepared film was the thinnest of all series and therefore, the material was more sensitive to defects that produce a premature failure. No trend in the mechanical properties with respect to the dianhydride was found.

Table 2. Mechanical properties of the copolymers synthesized in this work.

Samples		Strain / %	Modulus / GPa	Stress / MPa
PIs-BPDA	BPDA_1/1	8.4±1.3	1.03±0.16	53±14
	BPDA_2/1	115±15	0.38±0.04	22.1±1.7
	BPDA_4/1	9±2	0.089±0.01	3.2±0.5
PIs-BKDA	BKDA_1/1	56 ± 10	0.89 ± 0.11	66.3 ± 1.0
	BKDA_2/1	270 ± 90	0.59 ± 0.06	36.0 ± 1.1
	BKDA_4/1	390 ± 130	0.127 ± 0.016	19.3 ± 1.8
PIs-PMDA	PMDA_1/1	206 ± 8	0.77 ± 0.07	59 ± 3
	PMDA_2/1	300 ± 60	0.41 ± 0.03	27.1 ± 1.4
	PMDA_4/1	360 ± 80	0.111 ± 0.006	12.0 ± 1.0

For this type of copolymers, it has been shown that decreasing the PEO content in the copolymer increases the mechanical properties, approaching that of the pure aromatic polyimide homopolymer [23].

5.3.6 Gas transport properties

In agreement with our previous results for other similar aliphatic-aromatic copoly(ether imide)s [25-26], the copolymers prepared and studied here showed an improvement in permeation properties with the increase of the temperature of annealing. Results showed a direct correlation between annealing temperature and permeation properties due to the improvement on the phase segregation.

In general, the increase in permeability was much higher for the maximum annealing temperature, when most of the residual solvent was released and the improvement in the phase separation was higher. For samples containing the dianhydride BKDA, the evolution was smaller, resulting probably from a poorer ability to produce phase segregation. Always, at low PEO contents in the copolymer, the effect of the segregation was very significant, see Figure 7. In this Figure and in Figures 8, 9, and 10, the values of permeability and selectivity for the homopolymers BPDA-ODA, BKDA-ODA, PMDA-ODA and for pure PEO are shown in order to obtain a clear comparison. The permeability and selectivity of pure homopolymers were taken from literature [8, 27-28]. Higher segregations produced an increase of the permeability to different gases. According to permeability, the ability of segregation follows this order: PMDA > BPDA > BKDA, in agreement with DSC results.

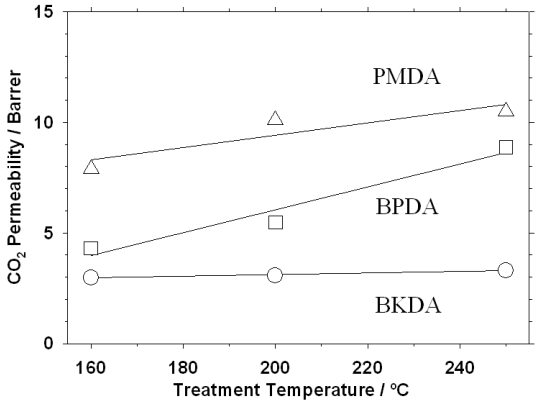

Figure 7.- Evolution of the CO_2 permeability as a function of the temperature of annealing for the copolymers with a weight ratio 1:1 between diamines.

In the case of the samples annealed at 250 ºC, the sample containing the PMDA dianhydride had a carbon dioxide permeability three times that of the sample containing the BKDA dianhydride. Therefore, for low PEO content, the contribution of the aromatic part is quite important to determine the thermal and thermomechanical properties, but also for the contribution to the segregation and permeability.

Figure 8 shows the evolution of CO_2 permeability as a function of the proportion of PEO in the copolymers. In this case, the data have been represented for samples annealed at 250 ºC, when the phase segregation for these polymers is almost complete. As already reported in other copoly(ether-imide)s, the permeability increases when the PEO content in the copolymer increases. When the aliphatic to aromatic diamine weight ratio was 1:1 and 2:1, the highest permeability was obtained for the samples containing PMDA, and the lowest value was obtained for samples containing BKDA. This must be due to their different ability to segregate ability. As mentioned, the BKDA dianhydride is the less rigid, and for this reason the packing between the chains is poorer, leading to a less efficient segregation. The PMDA dianhydride, by contrast, is more rigid and consequently the phase segregation is more efficient. For the dianhydride BPDA intermediate results between them were found.

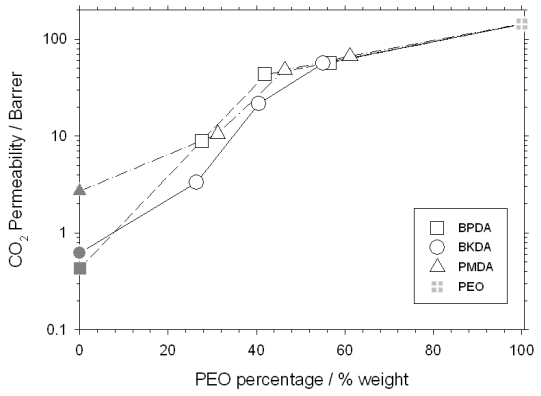

Figure 8.- Evolution of the CO_2 permeability as a function of the PEO content.

Moreover when the PEO content was high, 4:1, the copolymers showed similar behavior. In this case, the permeability was practically the same (assuming that the content is not exactly the same) regardless of the type of dianhydride used. This is probably because the aliphatic phase forms an almost-continuous phase in the polymer with no significant influence of the aromatic phase has on the permeability of the copolymer.

For the selectivity, the trend was analogous to the tendency shown by permeability. Figure 9 describes the evolution of CO_2/N_2 selectivity as a function of PEO content in the copolymer for the samples annealed at 250 ºC. Differences were observed for the 1:1 and 2:1 samples whereas for 4:1 samples, selectivity values were similar for all the dianhydrides.

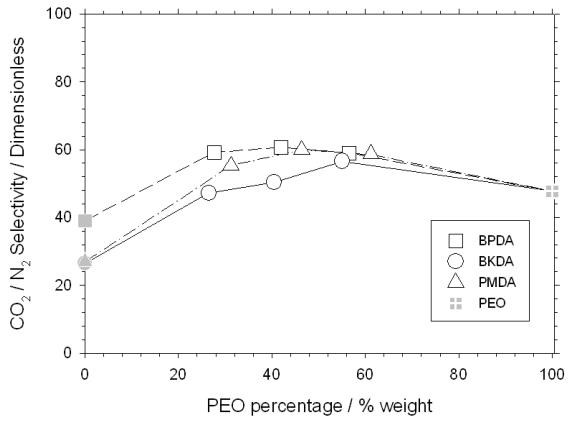

Figure 9.- Evolution of the CO_2/N_2 selectivity as a function of the PEO content.

To facilitate the evaluation of the permeation properties of the copolymers, a very significant and comprehensible way of showing the level of gas separation performance obtained is the Robeson's plot [29]. In this representation, see Figure 10, the distance to the upper bound can give an idea of the compromise between permeation and selectivity of the samples.

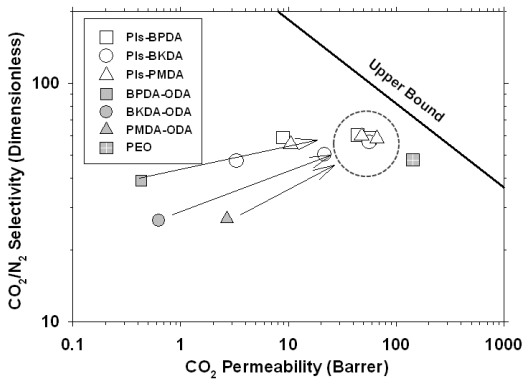

Figure 10.- CO_2 permeability vs CO_2/N_2 for the copolymers synthesized in this work annealed at 250 ºC, and for the homopolymers (BPDA-ODA, BKDA-ODA, PMDA-ODA and PEO). Arrows correspond to increasing the PEO content. PIs refer to the corresponding polyimides.

For these copolymers it can be seen that regardless of the starting aromatic homopolymer, the values obtained for samples with a 4:1 ratio are practically the same, with only the aliphatic portion affecting the permeation properties. Thus, as long as the copolymer is able to undergo complete phase segregation, the behavior will be similar.

A good material would give permeabilities as close as possible to the values of PEO, especially when CO_2 is involved due to the favorable interactions between PEO and carbon dioxide. At the same time, selectivities should be positioned as close as possible to the purely aromatic polyimide. The permeability increased always with the percentage of PEO in the sample, and at higher percentages of PEO, these copolymers gave both high permeability and selectivity that placed them very close to the corresponding upper bound.

5.4 Conclusions

A series of new copoly(ether-imide)s were prepared by the reaction between an aromatic diamine (ODA), an poly(ethylene oxide) diamine (PEO-2000) and different aromatic dianhydrides (BPDA, BKDA and PMDA) of different rigidity. While the aromatic phase contributed to the mechanical and thermal stability of the polymer, the aliphatic phase contributed to high CO_2 permeability.

Compared to pure aromatic polyimides, a relatively low temperature, 160 ºC, was enough to complete imidation. The thermal stability in inert atmosphere was above 300 ºC, with decomposition in two steps, being the PEO segments the less stable units.

These copolymers presented a phase separated structure. The occurrence in DSC of PEO related transitions, and the T_g values obtained, demonstrated the existence of a relatively pure PEO phase with increasing purity at higher treatment temperature, increasing PEO content and increasing rigidity of the dianhydride. PEO segments were amorphous at room temperature, and their melting point depended mainly on the size of the separated phases. TMA measurements proved the existence of an aromatic polyimide phase, with T_g values above 190 ºC that increased with the increase in the rigidity of the dianhydride and the decrease in PEO content. In summary, an improvement of the segregation produced: a more pure PEO phase, which was observed in a lower aliphatic T_g; and a more pure aromatic phase, which likewise, it was observed with a higher aromatic T_g.

Regardless of the PEO proportion, the mechanical and thermal properties of the copolymers were different. Thus, higher dianhydride rigidity produced better mechanical properties and better segregation in phases. The overall mechanical properties depended mainly on PEO content and ranged from good at lower PEO contents to fair at high PEO content.

Permeabilities and CO_2/N_2 selectivity increased with the increase in the temperature of annealing due to the improvement on the phase separation, which (in agreement with DSC results) depended on the PEO content and the rigidity of the dianhydride. For high PEO content, permeability and selectivity values approached quite closely the values for pure PEO, and placed these copolymers close to the Robeson upper bound. For PEO contents below 50 %, the more rigid dianhydride, PMDA, produces better segregation, and in turn higher permeability values. For PEO proportions over 50 %, the permeability obtained were similar regardless of what dianhydride was used. In this case, the permeability only depends on the PEO percentage in the polymer.

These results show that it is possible to obtain PEO copolymers with controlled structures, so the properties can be tuned to some extent by simply varying the aromatic composition in the copolymer. Besides, we can control: cost, processability, solubility and other factors in order to adapt the copolymers to specific applications and processes.

There are different strategies to improve the permselective properties in this kind of PEO copolymers. The first one is to increase the PEO content in the copolymer (keeping good enough mechanical properties for a specific application).The second way would be the formation of copolymers from homopolymers with optimal permeabilities and selectivities for each targeted couple of gases that could segregate at relatively low temperatures.

5.5 Acknowledgements

We are indebted to the Spanish Junta de Castilla León for financing this work through the GR-18 Excellence Group Action and to the Ministry of Science and Innovation in Spain for their economic support of this work (MAT2008-00619/MAT, MAT2010-20668/MAT, MAT2011-25513/MAT and CIT-420000-2009-32). We also acknowledge financial support from the programme Consolider Ingenio 2010 (project CSD-0050-MULTICAT). The help provided by Sara Rodriguez in measuring gas permeability and selectivity is greatly appreciated. A. Tena thanks CSIC for a predoctoral JAE fellowship.

5.6 References

1. R.W. Baker, Future Directions of Membrane Gas Separation Technology, Industrial & Engineering Chemistry Research, 41 (2002) 1393-1411.
2. M.T. Bessonov, M.M. Koton, V.V. Kudryavtsev, L.A. Laius, Polyimides: Thermally Stable Polymers, in, Consultants Bureau, New York, 1987.

3. E. Favre, Carbon dioxide recovery from post-combustion processes: Can gas permeation membranes compete with absorption?, Journal of Membrane Science, 294 (2007) 50-59.
4. R. Bounaceur, N. Lape, D. Roizard, C. Vallieres, E. Favre, Membrane processes for post-combustion carbon dioxide capture: A parametric study, Energy, 31 (2006) 2220-2234.
5. D. Wilson, H.D. Stenzenberger, P.M. Hergenrother, Polyimides, in, Blackie, Glasgow, 1990.
6. M.K. Ghosh, K.L. Mittal, Polyimides: Fundamentals and Applications, in, Marcel Dekker, New York, 1996.
7. D. Ayala, A.E. Lozano, J. de Abajo, C. García-Perez, J.G. de la Campa, K.V. Peinemann, B.D. Freeman, R. Prabhakar, Gas separation properties of aromatic polyimides, Journal of Membrane Science, 215 (2003) 61-73.
8. K. Tanaka, H. Kita, K. Okamoto, A. Nakamura, Y. Kusuki, Gas permeability and permselectivity in polyimides based on 3,3',4,4'-biphenyltetracarboxylic dianhydride, Journal of Membrane Science, 47 (1989) 203-215.
9. T.A. Barbari, W.J. Koros, D.R. Paul, Polymeric membranes based on bisphenol-A for gas separations, Journal of Membrane Science, 42 (1989) 69-86.
10. A. Tena, A.E. Lozano, L. Palacio, A. Marcos-Fernández, P. Prádanos, J. de Abajo, A. Hernández, Gas separation properties of systems with different amounts of long poly(ethylene oxide) segments for mixtures including carbon dioxide, International Journal of Greenhouse Gas Control, 12 (2013) 146-154.
11. H.Z. Chen, Y.C. Xiao, T.-S. Chung, Multi-layer composite hollow fiber membranes derived from poly(ethylene glycol) (PEG) containing hybrid materials for CO_2/N_2 separation, Journal of Membrane Science, 381 (2011) 211-220.
12. Y. Hirayama, Y. Kase, N. Tanihara, Y. Sumiyama, Y. Kusuki, K. Haraya, Permeation properties to CO_2 and N_2 of poly(ethylene oxide)-containing and crosslinked polymer films, Journal of Membrane Science, 160 (1999) 87-99.
13. M. Minelli, M. Giacinti Baschetti, D.T. Hallinan Jr, N.P. Balsara, Study of gas permeabilities through polystyrene-block-poly(ethylene oxide) copolymers, Journal of Membrane Science, 432 (2013) 83-89.
14. K.-i. Okamoto, M. Fujii, S. Okamyo, H. Suzuki, K. Tanaka, H. Kita, Gas permeation properties of poly(ether imide) segmented copolymers, Macromolecules, 28 (1995) 6950-6956.
15. H. Suzuki, K. Tanaka, H. Kita, K. Okamoto, H. Hoshino, T. Yoshinaga, Y. Kusuki, Preparation of composite hollow fiber membranes of poly(ethylene oxide)-containing polyimide and their CO_2/N_2 separation properties, Journal of Membrane Science, 146 (1998) 31-37.

16. A. Tena, A. Marcos-Fernández, A.E. Lozano, J.G. de la Campa, J. de Abajo, L. Palacio, P. Prádanos, A. Hernández, Thermally treated copoly(ether-imide)s made from bpda and alifatic plus aromatic diamines. Gas separation properties with different aromatic diamimes, Journal of Membrane Science, 387–388 (2012) 54-65.
17. A. Car, C. Stropnik, W. Yave, K.V. Peinemann, Pebax®/polyethylene glycol blend thin film composite membranes for CO_2 separation: Performance with mixed gases, Separation and Purification Technology, 62 (2008) 110-117.
18. H. Lin, B.D. Freeman, Gas solubility, diffusivity and permeability in poly(ethylene oxide), Journal of Membrane Science, 239 (2004) 105-117.
19. S.R. Reijerkerk, M.H. Knoef, K. Nijmeijer, M. Wessling, Poly(ethylene glycol) and poly(dimethyl siloxane): Combining their advantages into efficient CO_2 gas separation membranes, Journal of Membrane Science, 352 (2010) 126-135.
20. A. Tena, L. Fernández, M. Sánchez, L. Palacio, A.E. Lozano, A. Hernández, P. Prádanos, Mixed matrix membranes of 6FDA-6FpDA with surface functionalized γ-alumina particles. An analysis of the improvement of permselectivity for several gas pairs, Chemical Engineering Science, 65 (2010) 2227-2235.
21. A. Tena, A. Marcos-Fernandez, L. Palacio, P. Cuadrado, P. Pradanos, J. De Abajo, A.E. Lozano, A. Hernandez, Phase Segregation and Gas Separation Properties of Thermally Treated Copoly(ether-imide) from an Aromatic Dianhydride, an Aromatic Diamine and Various Aliphatic Diamines, Industrial & Engineering Chemistry Research, (2012).
22. J.L. Hedrick, K.R. Carter, H.J. Cha, C.J. Hawker, R.A. DiPietro, J.W. Labadie, R.D. Miller, T.P. Russell, M.I. Sanchez, W. Volksen, D.Y. Yoon, D. Mecerreyes, R. Jerome, J.E. McGrath, High-temperature polyimide nanofoams for microelectronic applications, Reactive and Functional Polymers, 30 (1996) 43-53.
23. A. Marcos-Fernández, A. Tena, A.E. Lozano, J.G. de la Campa, J. de Abajo, L. Palacio, P. Prádanos, A. Hernández, Physical properties of films made of copoly(ether-imide)s with long poly(ethylene oxide) segments, European Polymer Journal, 46 (2010) 2352-2364.
24. D.W. Krevelen, Properties of polymers: their correlation with chemical structure, their numerical estimation and prediction from additive group contributions, Elsevier, 1990.
25. A. Tena, A. Marcos-Fernández, A.E. Lozano, J.G. De La Campa, J. De Abajo, L. Palacio, P. Prádanos, A. Hernández, Thermally segregated copolymers with PPO blocks for nitrogen removal from natural gas, Industrial and Engineering Chemistry Research, 52 (2013) 4312-4322.

26. A. Tena, A. Marcos-Fernández, L. Palacio, P. Prádanos, A.E. Lozano, J. de Abajo, A. Hernández, On the influence of the proportion of PEO in thermally controlled phase segregation of copoly(ether-imide)s for gas separation, Journal of Membrane Science, 434 (2013) 26-34.
27. T.H. Kim, W.J. Koros, G.R. Husk, K.C. O'Brien, Relationship between gas separation properties and chemical structure in a series of aromatic polyimides, Journal of Membrane Science, 37 (1988) 45-62.
28. Z.-K. Xu, L. Xiao, J.-L. Wang, J. Springer, Gas separation properties of PMDA/ODA polyimide membranes filling with polymeric nanoparticles, Journal of Membrane Science, 202 (2002) 27-34.
29. L.M. Robeson, The upper bound revisited, Journal of Membrane Science, 320 (2008) 390-400.

SECTION III

Study of the influence of the structure on the copolymer properties

This section will discuss the influence of the structure on the properties of different copolymers. As in the previous section, the work will focus on the systematic study of the properties of a series of copoly (ether-imide)s based on an aromatic diamine, an aliphatic diamine and an aromatic dianhydride. It was used the same reference structure than in the previous section.

Chapter 6 investigates the effect of the length of the aliphatic diamine on the gas transport properties in polyether based block copolymers with BPDA as aromatic dianhydride and ODA as aromatic diamine, with a weight ratio 2:1 (aliphatic:aromatic) between the diamines (41-46% weight of aliphatic diamine in the final copolymer). The aliphatic diamine, an amine-terminated PEO, varied in length from 900 to 6000 g/mol. In addition, the short length PEOs (900 and 2000) were chain extended with hexamethylene diisocianate (HDI) to a length of approximately 6000 g/mol before copolymerization with the aromatic dianhydride and diamine. A complete characterization of the copolymers was carried out. The relationship with the segregation ability, crystallinity, thermal and mechanical properties, and the gas separation ability was discussed.

Chapter 7 describes the synthesis, and a complete characterization (thermal, segregation, crystallinity, and film properties) of a series of copoly(ether imide)s based on a long aliphatic polyether, PEO6000. The PEO content was increased on the copolymers in order to analyze the influence on the properties. BPDA or BKDA were used as aromatic dianhydride, ODA as aromatic diamine, and PEO6000 as aliphatic diamine, with different weight proportions of PEO6000, from 0 to 70% in the final copolymer.

Chapter 8 presents the analysis of the influence of the PEO percentage on the permeability properties. PEO2000 was used as aliphatic diamine, BPDA as aromatic dianhydride and ODA as aromatic diamine, with different weight proportions of PEO2000, from 0 to 58% in the final copolymer.

Chapter 9 deals with the analysis of the influence of the PEO percentage on the permeability properties. PEO6000 was used as aliphatic diamine, BKDA as aromatic dianhydride and ODA as aromatic diamine. The structural characterization of the structure of these copolymers was already analyzed on chapter 6, and in chapter 9 the relationship between the polymer properties and the influence on the permeability properties was studied. PEO6000 presents high crystallinity, and the influence of the crystallinity on the permeability was thoroughly evaluated.

Chapter 10 presents a study of polypropylene oxide (PPO) as aliphatic diamine on the copolymer properties. BPDA was the aromatic dianhydride, ODA was the aromatic diamine and PPO of

different lengths, PPO2000 and PPO4000, and a mixture of them, was the aliphatic diamine, with different weight proportions of PPO, from 0 to 45% in the final copolymer. In addition, one copolymer was prepared with a more rigid aromatic diamine, BNZ. The influence of the length and content of PPO on the phase segregation ability and the effect on the thermal properties and gas separation behavior was analyzed,

CHAPTER 6

Influence of the PEO length in gas separation properties of segregating aromatic-aliphatic copoly(ether-imide)s

Alberto Tena[1,3], Ángel Marcos-Fernández[1,3], Ángel E. Lozano[1,3], Javier de Abajo[1,3], Laura Palacio[1,2], Pedro Prádanos[1,2], Antonio Hernández[1,2]

[1]*Smap UA-UVA-CSIC, Parque Científico Universidad de Valladolid, Paseo de Belén, s/n, 47011 Valladolid, Spain.*

[2]*Dept. Física Aplicada, Facultad de Ciencias, Universidad de Valladolid, Paseo de Belén, 7, 47011 Valladolid, Spain*

[3]*Instituto de Ciencia y Tecnología de Polímeros, CSIC, Juan de la Cierva 3, 28006 Madrid, Spain.*

This chapter has been submitted to:

Chemical Engineering Science

Abstract

A complete series of aliphatic-aromatic copoly(ether-imide)s has been synthesized in this work. All these copoly(ether-imide)s had the same structure, BPDA-PEO$_X$-ODA, but different lengths of PEO in the final polymer. These copolymers have been thermally treated and characterized by several techniques. A direct relationship between the temperature of treatment, the improvement of phase segregation, and permeability has been demonstrated.

The Maxwell model has been applied to predict permeability (for CO_2, CH_4 and N_2) and it has been found that when the segregated PEO can be considered to be amorphous – it is at high temperatures when crystallinity disappears – the model fits reasonably well. This confirms that the aliphatic and aromatic portions of the copolymer behave approximately as a bi-phase of disperse domains within a continuous matrix.

Results show that permeability is higher when the PEO chains are longer – when there is no crystallinity, or any kind of internal bonds, distorting the results – while selectivity doesn´t depend on the PEO length in the copolymer. Remarkable are the results for the CO_2/N_2 gas pair, with selectivity-versus-permeability very near to the Robeson's upper bound at 30 ºC and even in closer proximity to the corresponding trade off line for higher permeation temperatures.

Graphical Abstract

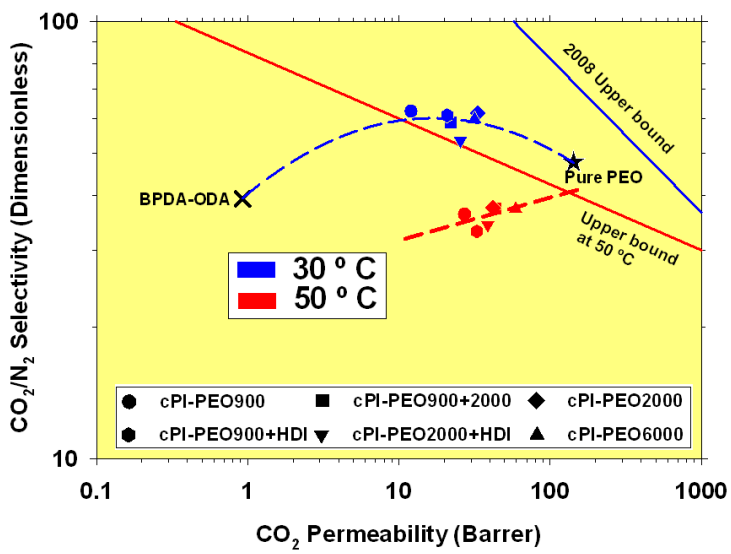

6.1 Introduction

The liberation to the atmosphere of big amounts of greenhouse gases in a short period can lead to global warming. Over a 60 % of the global greenhouse effect is attributable to carbon dioxide [1]. There are several sources — such as power plants, steel, cement production plants or chemical industry— where CO_2 is generated. Among these, coal-fired power plants are the main emitters of CO_2 and are responsible for nearly a 30% of the total CO_2 release. It has been estimated that about half of the electricity will be generated by coal-fired power plants at least until 2035 [2]. This will cause more CO_2 liberated causing a serious intensification of climate change. Hence, it is necessary to develop new technologies to curb as far as possible the emissions of greenhouse gases.

One of the preferred methods to control CO_2 emission is its capture and storage (CCS), including separation, transportation and storage stages [2]. Around a 70 to 80 % of the total costs of CCS is represented by the CO_2 capture. The three main options for CO_2 capture from power plants are: pre-combustion, oxy-fuel combustion, and post-combustion capture [3-5]. Post-combustion capture is the simplest and most suitable way to perform carbon dioxide capture for newly-built as well as for existing coal-fired power plants [6].

Post-combustion capture is fundamentally a separation of CO_2 from flue gas — generally consisting in N_2, CO_2, O_2 and H_2O —, and conventional gas separation technologies, such as chemical absorption, pressure swing adsorption, and membrane separation, could be applied. Of course the separation technique to be used is determined by its effective price [7-9]. The amount of carbon dioxide emitted and captured are, of course, relevant figures in order to make an adequate decision.

A first instance analysis could lead to conclude that chemical adsorption processes are more interesting because they can give high purity at a relatively low price [10-13]. The main disadvantage for chemical absorption is that its cost is still over the target [3] and further cost reduction is quite complicated [14] because the main cost item corresponds to energy consumption. Very different is the situation of gas separation processes using polymeric membranes that are by nature quite flexible processes. Whenever CO_2/N_2 selectivity exceeds 30, permeability of membrane has more influence on the cost than energy consumption which is very low [13]. Moreover, it has been shown that, if the cost of the membrane is low, it is cost-effective to select a material with high selectivity; while if the price of the membrane is high a polymer with a higher CO_2 permeability is more economically effective [12, 15]. All these factors concerning the membrane material leave a very wide range of improvement open in terms of operational cost.

It is also convenient, in order to get appropriate membranes for gas separation, to start with a suitable polymeric material, with adequate flow and good mechanical and thermal resistance. Of course when dealing with CO_2 capture, the polymer membrane must have a high affinity for carbon dioxide, so polymers with adequate permeability values are necessary [16-17].

Glassy polymers and in particular polyimides are well known for their excellent thermal oxidative stability, good organic solvent resistance and exceptional mechanical properties, along with an extraordinary ability to separate complex mixtures of gases in diverse applications [18-20]. Thus, among all the polymeric membranes, it has been widely demonstrated that the use of aromatic polyimides is one of the best alternatives. Typically these materials have a high selectivity while having a not always high enough permeability [21-22].

One of the most common approaches to meet these requirements on CO_2 permeability is to increase the affinity of the polymer to CO_2 by using block-copolymers. Specially promising block-copolymers include both hard and soft blocks. The hard block can have a well-packed and rigid structure; as a result it forms a glassy segment of the copolymer chain with usually low free volume. In contrast, the soft block can consist in more flexible chains that can form rubbery segments on the copolymer chain with habitually high free volume. In this way the glassy polymer segments will provide the mechanical support and in the case of polyimides, thermal resistance. The rubbery segments generally form continuous microdomains through which, due to the nature of the flexible chain structure, gas transport is easy giving a good permeability to the copolymer [23-24].

The use of polyethylene oxide (PEO) compounds for separating CO_2 from other light gases is known [25-26] to give high CO_2 permeability. The interaction between CO_2 and oxyethylene groups has been discussed and used for the development of CO_2 selective membranes by many authors [27-29]. In view of this, the use of block-copolymers combining aromatic polyimides and PEO, appears to be a successful route [30-32]. In effect, these compounds have good permselectivities (permeability-selectivity) results for the couple CO_2/N_2. This was attributed mainly to the high solubility-selectivity due to strong interactions between the oxyethylene group and CO_2 [33-34].

In order to optimize the necessary properties, a good balance between the hard and soft block parts of the copolymer is needed. Previous studies from our group reported that when the copolymer has a percentage of PEO around 50% it has the best properties attending to the necessary mechanical resistance that should be compromised by too high PEO contents [35]. Moreover, the crystallinity of polyether segments is known to increase when the length of PEO increases leading to a decrease

in gas sorption because the crystalline phase acts as a non-sorbing and impermeable barrier reducing the permeability severely. Therefore, in addition to the percentage of PEO, the length of its chain has also an important effect on the permeation properties of the copolymer.

For this reason, we propose here a complete analysis of the influence of PEO length on the properties of separation for a system where both the hard part, in this case the aromatic polyimide BPDA-ODA, and the proportion between soft and hard segments are common in all copolymers to be studied. The length of the PEO chain will be varied from short lengths where all the polyethylene oxide is in amorphous state to percentages as high as to lead to crystallinities over a 40% of the total PEO in the copolymer. Some copolymers have been also synthesized including hexamethylene diisocyanate in order to extend the polyether chain while reducing the increase of crystallinity but improving the phase segregation after thermal treatment. The influence of thermal treatments at different temperatures on PEO segregation and permselectivity will be also analyzed here.

The properties of these copolymers have been analyzed by standard techniques of characterization (DSC, TGA, TMA, mechanical properties and densitometry) and by SAXS. The properties of permeation have been evaluated at temperatures from 30 °C to 50 °C, a temperature high enough so that all samples had the polyethylene oxide chains in an amorphous state. Finally, we have used the Maxwell`s model to predict the permeability to different gases.

6.2 Experimental

6.2.1 Chemicals

3,3′,4,4′-biphenyltetracarboxylic dianhydride (BPDA), and 4,4'-oxydianiline (ODA) were purchased from Sigma-Aldrich Co. These products were purified by sublimation at high vacuum just before being used. Bis(2-aminopropyl) poly(ethylene oxide) with nominal molecular weight of 900 and 2000 g/mol were kindly donated by Huntsman (Holland) (PEO-900 and PEO-2000 from here on). α,ω-Diamine-poly(ethylene oxide) with nominal molecular weight of 6000 g mol^{-1} was kindly donated by Kawaken Fine Chemicals Co., Ltd. (Tokyo, Japan), (PEO-6000 from here on). The polyethers were dried at 70 ºC in vacuum for 5 hours and stored in a desiccator at vacuum until use. Hexamethylenediisocyanate (HDI) was purchased from Sigma-Aldrich and purified by distillation at vacuum before use. Anhydrous N-methylpyrrolidinone (NMP), to be used as polymerization solvent, was purchased from Sigma-Aldrich Co.

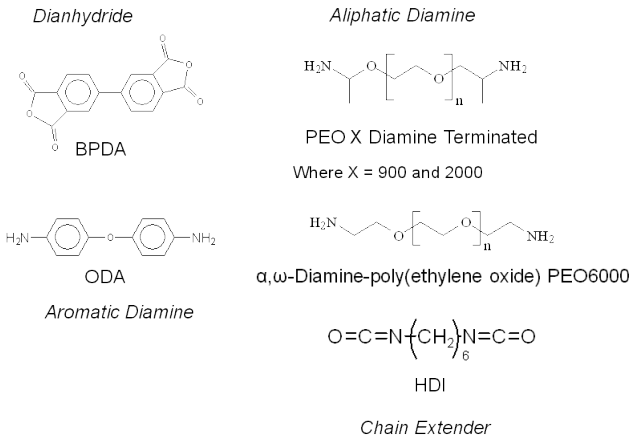

Figure 1. Chemical structure of the monomers.

6.2.2 Synthesis of copoly(ether-imide)s

The polymerization reaction was carried out in a three-neck flask, under N_2 atmosphere and mechanical stirring, following this procedure: PEO (*x* mmol) was dissolved in anhydrous NMP, and when necessary, a certain amount of HDI (*y* mmol) added in order to obtain a PEO oligomer of approximately 6000 g/mol of final molecular weight. Polyether chains included in the synthesized copolymers were: PEO900, PEO900+HDI, PEO2000, PEO2000+HDI, PEO900+PEO2000 (50/50 w/w), and PEO6000. After some minutes of stirring at room temperature, the aromatic diamine (ODA) (*z* mmol) in a weight ratio 2:1 (polyether chain : aromatic diamine), was added to the solution to give a final concentration of 20 mL solvent for 10 meq of amino group. When the solid aromatic diamine was dissolved the precise stoichiometric amount of the BPDA aromatic dianhydride was added at once. The reaction was stirred at room temperature for 12 hours.

From here on the copolymers to be studied will be named by adding cPI to the name of the PEO entering the composition, i.e.: cPI-PEO900, cPI-PEO900+HDI, cPI-PEO2000, cPI-PEO2000+HDI, cPI-PEO900+PEO2000 and cPI-PEO6000.

6.2.3 Preparation of the copolymers dense films

The resultant viscous copolyamic acid solution was diluted with NMP to attain an appropriate viscosity for casting, filtered through a nominal #1 fritted glass funnel, degassed, and cast onto a levelled glass plate. The resulting film was covered with a conical funnel to avoid too fast evaporation of the solvent, dried at 80 ºC overnight, and treated at 120 ºC for 6 hours in a vacuum oven. For the pure aromatic homopolymer (BPDA-ODA), the procedure was similar but the final heat treatment was carried out at 200 °C in a vacuum oven for 24 hours. Films with 40-60 μm in

thickness were obtained. The additional thermal treatments (see Figure 2) for the copolymeric films were carried out under inert atmosphere.

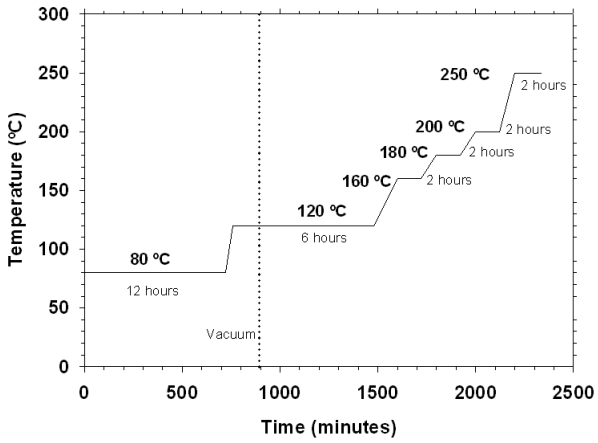

Figure 2. Thermal treatments.

6.2.4 Characterization Methods

Attenuated total internal reflectance-Fourier transform infrared analyses (ATR-FTIR) were performed at room temperature using a PerkinElmer Spectrum One infrared spectrometer equipped with an ATR accessory. IR spectra were the average of 16 scans recorded in the spectral range of 4000–650 cm^{-1} with a 4 cm^{-1} resolution.

A Thermal Analysis Q500 instrument was used for thermogravimetric analysis (TGA). Disc samples cut from films with weights between 5 and 15 mg were tested. When running dynamic scans, it was done in Hi-Resolution mode, where the heating rate is automatically adjusted in response to changes in the rate of weight loss, which results in improved resolution, with an initial heating rate of 10ºC/min under a flux of nitrogen.

Differential scanning calorimetry (DSC) analyses were carried out in a Mettler Toledo (DSC 822e) calorimeter equipped with a liquid nitrogen accessory. Disc samples cut from films weighting 5–15 mg were sealed in aluminium pans. Samples were heated with the following cyclic method in order to monitor the changes in thermal properties with thermal treatment: from 25 ºC, the sample was heated at 10ºC/min to a target temperature; once reached, the sample was cooled at the maximum cooling rate accessible for the instrument to -90 ºC, held at this temperature for 15 min to equilibrate and reheated at 10 ºC/min to the next target temperature. The procedure was followed until the last treatment temperature was reached and a final run from -90 ºC to 80 ºC was

performed. In this way, in each heating run, the thermal properties for the copolymers after "instantaneous" treatment to the previously reached temperature were obtained.

Thermomechanical (TMA) tests were performed in a Rheometric Scientific instrument model DMTA V. Rectangular test pieces of 3 mm width and 20 mm length were cut from films. A distance of 10 mm was set between fixation clamps. Runs were carried out from ambient temperature at 10 ºC/min with a static stress of 3 MPa.

The densities (ρ) of the dense membrane films were determined using a CP225D Sartorius balance, provided with an immersion density kit.

SAXS measurements were performed at the beamline BM16 at the European Synchrotron Radiation Facility (Grenoble, France). Wave length of the X-ray beam was 0.980 Å. Detector calibration was done with silver behenate ($AgC_{22}H_{43}O_2$). Disc samples cut from films were placed in a Linkam hot stage and heated at 10 ºC/min while the SAXS spectra were recorded. Calibration of temperature gave a difference of approximately 7 ºC between the temperature reading at the hot stage display and the real temperature at the sample.

6.2.5 Gas Permeation and Selectivity

The permeability, P, for several gases (namely: O_2, N_2, CH_4 and CO_2) was determined by using a permeator with constant volume and variable pressure which uses the ''time-lag'' operation method. The measurements were carried out at 3 bar at temperatures set from 30 to 50 ºC. The equations used and the mode of operation of the equipment, as well as an outline of it, has been described previously [36].

6.3 Results and Discussion

6.3.1 Copoly(ether-imide)s imidization

Poly(ethylene oxide) chains are prone to oxidation [37], and therefore, a great care was taken to carry out the imidization. The films were heated at 120 ºC for 6 h. After 6 h heating at 120 ºC, the solvent was almost completely removed as proved by thermogravimetric analysis. All the copolymers resulted to be insoluble in DMAc (dimethylacetamide), NMP, Hexane, Toluene, THF (tetrahydrofuran), and CH_2Cl_2 (dichloromethane) after this process.

Infrared spectra were recorded to check for the progress of imidization. As for other described copoly(ether imide)s [33-34, 38], it was possible to observe the IR bands centered around 1774, 1713, 1372 and 738 cm^{-1}, typical for imidized samples, and the peaks appearing around 2800 cm^{-1}, due to the aliphatic polyether segments. There were no noticeable differences between the copolymers with different polyether lengths, or between samples containing PEO and the samples with PEO+HDI.

For similar copoly(ether-imide)s to the ones presented here, Hangzheng et al. [39] used IR spectra to prove the imidization at 200 ºC. Even though the complete imidization of our copoly(ether imide)s at a temperature as low as 120 ºC is actually remarkable, we must mention that this full imidization at relatively low temperatures has already been found by us for copoly(ether-imide)s based on PEO segments [33, 38] and PPO segments (paper in preparation). Also, two works of Okamoto et al., studying similar copoly(ether-imide)s to the ones presented here, stated that a thermal treatment at 170 ºC completely imidize the precursor poly(amic acid)s to polyimides [30] although they did not show any IR spectra to prove the imidization state of the copolymers.

6.3.2 Thermal Stability

Thermogravimetric analysis was performed to evaluate the thermal stability of the synthesized copolymers treated at 120 ºC during 6 hours (Figure 3).

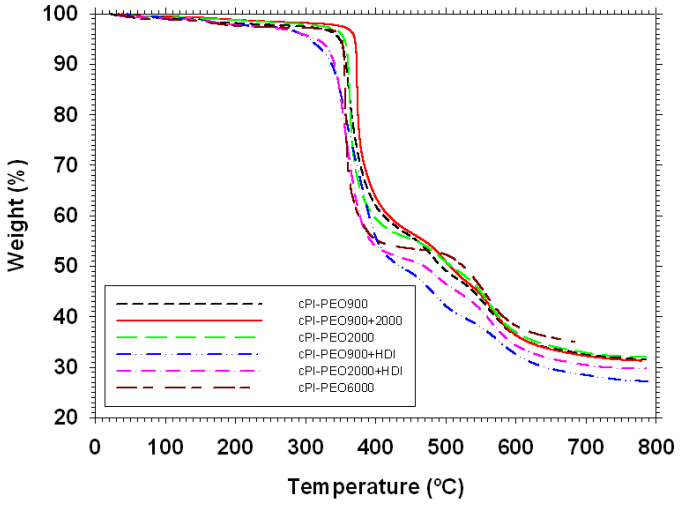

Figure 3. TGA curves in dynamic conditions for the synthesized copolymers.

The behaviour is similar for the different samples. The initial loss from ambient temperature to 100 ºC, can be attributed to the adsorbed water in the sample. A second step approximately from 100 to

250 ºC is due to residual solvent in the film, with a weight loss of 1 to 1.7%. The third step is thought to be due to the contribution of the poly(ethylene oxide) included in the copolymer composition, and it is therefore assigned to the loss of polyether block sequences plus the hexamethylenediisocianate in the case of the copolymers where the polyether chain was extended. The final stage of weight loss is due to the thermal decomposition of the remaining aromatic polyimide segments. For all copolymers, the residual carbon content at 800 ºC was 25-35 %.

The mass loss in this third step for the different copolyimides is close to the percentage of polyether blocks in the feed (see Table 1), proving that it is related to the degradation of this part of the copolymer, as already found previously in other similar copolymers [33-34, 38]. From Figure 3, it is clear that the polyether extended copolymers cPI-PEO900+HDI and cPI-PEO2000+HDI start to degrade at lower temperatures (*circa* 250 ºC) than the other copolymers (*circa* 350 ºC). This is due to the lower stability of the urea groups formed by the reaction of the HDI. This relatively low thermal stability of the urea groups is well known in the field of polyurethanes.

Table 1.- Results obtained by TGA for the prepared copolymers.

Copolymer	**Theoretical PEO weight in the cPI (%)**	**Theoretical PEO+HDI weight in the cPI (%)**	**Experimental polyether weigth loss (%)**	**T of maximum weight loss rate (ºC)**	**Residue at 800ºC (%)**
PEO900	41,4	41,4	42,1	377	33,9
PEO900+2000	42,6	42,6	42,6	372	33,4
PEO2000	43,7	43,7	43.6	363	34,9
PEO900+HDI	42,8	49,3	49,3	368	27,7
PEO2000+HDI	44,5	47,4	47,2	356	31,6
PEO6000	45,7	45,7	45,2	367	32,0

Thus, TGA analysis confirmed that the aliphatic-chain thermal stability is much lower than the thermal stability of the aromatic polyimide segments, and therefore a selective degradation of this part of the chain can be performed in these copolymers.

6.3.3 Calorimetric Studies

The samples were heated in a DSC instrument with a cyclic method in order to monitor the changes in the thermal properties of the films with the thermal treatment. When the polyether moiety is able to crystallize, the melting enthalpy can be used to evaluate the percentages of amorphous-crystalline PEO in the copolymers [38]. No transition related to the aromatic polyimide hard segments was detected by DSC in any case.

A curve with the developed crystallinity for PEO vs. temperature thermal treatment can be built for all copolymers. The melting enthalpy of PEO was taken from literature as 8.67 kJ/mol [40]. In Figure 4 crystallinity is shown for all the copolymers thermally treated at different temperatures. No crystallinity was observed for samples cPI-PEO900 and cPI-PEO900+2000. For cPI-PEO900, the polyether chain is too short to develop crystallinity when the chain ends are linked to the polyimide segments, whereas for cPI-PEO900+2000, the PEO900 chains hamper the crystallization of the longer PEO2000 chains.

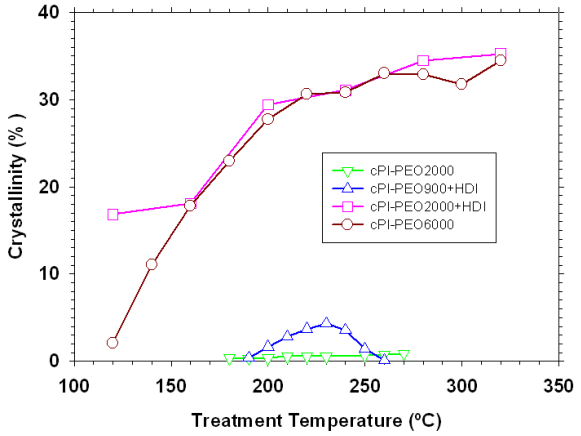

Figure 4. Crystallinity of the aliphatic part of the copolymers. The copolymers that do not appear don't have any crystallinity.

In the case of sample cPI-PEO2000 the crystallinity found was almost negligible, a maximum of 0.9 % after the thermal treatment at 300 ºC, whereas for cPI-PEO6000, crystallinity increases with thermal treatment from almost inexistent in the original sample, heated at 120 ºC, to a 32 % after the thermal treatment at 300 ºC. The maximum increase in crystallinity, up to approximately 250 ºC, happens simultaneously with the release of the residual solvent as shown by TGA. From these data it is clear that lengths over 2000 g mol^{-1} are necessary to develop crystallinity and longer chains develop higher crystallinities.

The samples with extended polyether, cPI-PEO900+HDI and cPI-PEO2000+HDI, have a very characteristic behavior that differs from that shown by cPI-PEO900 and cPI-PEO2000. When the polyether chain is extended with HDI, although all the copolymers contain very similar weights of polyether, the molar ratio of the aromatic reactants over the aliphatic ones increases for the copolymers with extended polyether chains, leading to longer aromatic polyimide blocks. This, in turn, leads to an increase in the incompatibility of the blocks and therefore to a better phase separation, as indicated by the higher crystallinity achieved for polyether extended copolymers. In fact, for cPI-PEO900+HDI, crystallinity appears at 200 ºC whilst the parent copolymer cPI-PEO900 remains amorphous at all thermal treatments, and for cPI-PEO2000+HDI, crystallinity is significant from the beginning, and increases further with thermal treatment, with values that are very similar to those for the cPI-PEO6000.

However, when treated at high temperatures, a different behavior is found for polyether extended copolymers. cPI-PEO900+HDI starts to lose crystallinity above 230 ºC and it completely disappears at 260 ºC, whereas cPI-PEO2000+HDI reaches a pseudo plateau between 200 and 240 ºC and above this temperature crystallinity still has a small increase. Although the trend is just the reverse for these two copolymers, the origin of the behavior is the same. Above 230-240 ºC the urea groups connecting the extended polyether chains start to deteriorate, as shown by TGA, and when this occurs, polyether chains with free chain ends are produced. The chains with low polyether molecular weight, 900 g mol^{-1}, are unable to crystallize and plasticize the PEO phase, decreasing crystallinity until its disappearance, whereas chains with higher molecular weight, 2000 g mol^{-1}, have less restrictions to crystallize and crystallinity increases (it is worth to point out that the starting bis(2-aminopropyl)poly(ethylene oxide) of 2000 g mol^{-1} is highly crystalline).

It is worth noting that here we have been referring to maximal crystallinity that would appear at low enough operation temperatures. It is well known that gases do not easily pass through the crystal structures [41], and for this reason it is important to know the actual crystallinity of our samples at the temperature of permeation measurement (from 30 to 50 ºC). For all the copolymers, except for cPI-PEO6000, the melting point measured by DSC is below 30 ºC after thermal treatment at any temperature, and therefore, PEO chains will be amorphous. For copolymer PEO6000, the melting point reaches a value of 43 ºC after thermal treatment at 300 ºC (approximately 40 ºC after treatment at 250 ºC), thus, when measuring permeation properties at 50 ºC, PEO chains will be amorphous, but at 30 ºC, part of the these PEO chains could still be crystallized.

In figure 5 we can see the changes in the polyether T_g for the different treatment temperatures. Only minor variations are seen, and T_g remains almost unchanged with thermal treatment except for copolymers PEO900+HDI and PEO2000+HDI.

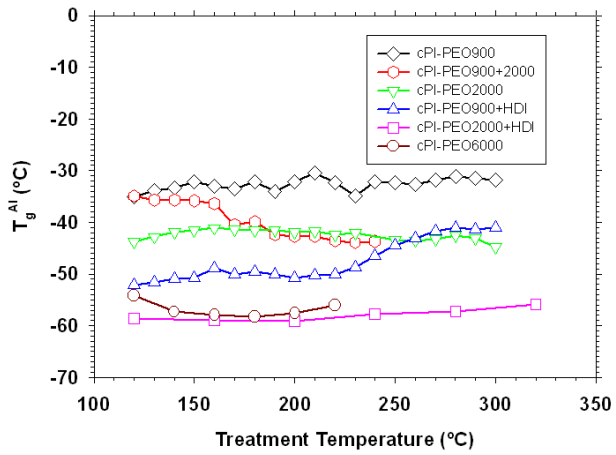

Figure 5. T_g of the aliphatic part of copolymers after ‘‘instantaneous” treatment for the copolymers treated at 160 ºC.

For these two HDI extended copolymers, when urea groups start to degrade for treatments above 220 ºC, T_g increases. This could be interpreted as an increase in the mixing of the rigid polyimide segments in the polyether phase. This increase in T_g is very noticeable for copolymer PEO900+HDI, and coincident with the decrease in crystallinity of the PEO phase. For copolymer PEO2000+HDI the change coincides also with the small increase in crystallinity produced by urea groups degradation, but because of the ability of the PEO chains of 2000 g mol^{-1} to crystallize, the mixing of the aromatic polyimide segments in the PEO phase is very limited and the increase in T_g is very small. If we compare the T_g values after treatment at 200 ºC, where the T_g is practically constant for all the copolymers and the copolymers with extended polyether chain have not started to degrade, it follows the expected trend for the copolymers with un-extended polyether chain, the longer the PEO chain, the lower the T_g:

$$T_g^{al}\ (\text{PEO6000}) < T_g^{al}\ (\text{PEO2000}) < T_g^{al}\ (\text{PEO900})$$

In the case of the copolymers with extended polyether chain, their T_g are well below the values for the copolymers with the parent polyethers, PEO900 and PEO2000, as a consequence of the better phase separation achieved. For PEO2000+HDI the value is similar to the value for PEO6000, and for PEO900+HDI is around 6 ºC higher, probably due to the restrictions imposed by hydrogen bonds between the urea groups, present in a higher concentration in PEO900+HDI compared to

PEO2000+HDI. Yet, T_g for PEO900+HDI is almost 10 ºC lower than for copolymers with PEO2000.

Thus, from these results, it can be affirmed that for all the copolymers studied, at a temperature of permeation of 50 ºC, the polyether segments were totally amorphous and well above their T_g.

6.3.4 Thermomechanical Analysis

Thermomechanical analysis was carried out in order to detect the glass transition temperature of the aromatic polyimide hard segments, which could not be detected by DSC. It was assumed that a good estimation of T_g corresponds to the temperature when strain is 10 times that of the sample at 100 ºC. This criterion could be accepted at least for comparative purposes [38]. The so-obtained results for samples treated at 160ºC for 2 hours in order to develop a phase separated structure are shown in Figure 6.

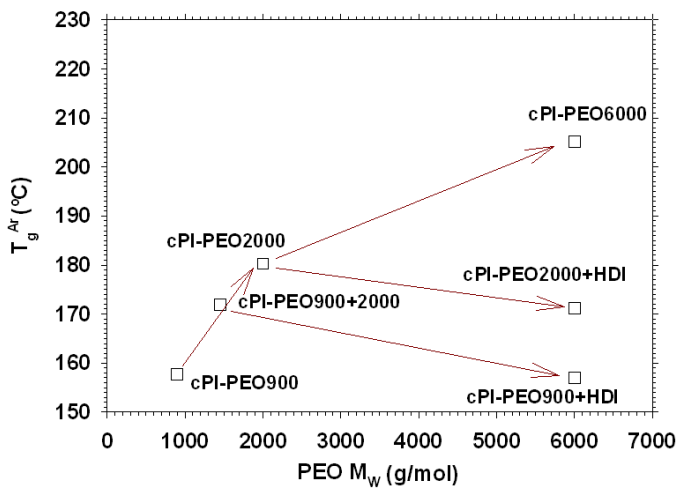

Figure 6. T_g for the aromatic polyimide segments as a function of the PEO length for the copolymers treated at 160 ºC.

All samples have similar content in PEO, but because of the stoichiometry, the longer the polyether chain, the longer the aromatic polyimide would be, and therefore, the higher the T_g^{ar} of the aromatic polyimide segments, as shown in Figure 6. The order is:

$$T_g^{ar}\text{(cPI-PEO900)} < T_g^{ar}\text{(cPI-PEO900+2000)} < T_g^{ar}\text{ (cPI-PEO2000)} < T_g^{ar}\text{ (cPI-PEO6000)}$$

In addition, when PEO chains are shorter, the mixing of PEO segments in the polyimide phase is more likely, and can contribute further to decrease the polyimide T_g by plasticization. This must be the cause of the difference in polyimide T_g for the chain extended polyethers. For cPI-

PEO900+HDI, cPI-PEO2000+HDI, cPI-PEO6000, with theoretically similar polyimide segments length, T_g of polyimide decreases when PEO length decreases (HDI content increases). In these copolymers, although the longer polyimide segments lead to a better phase-separated polyether phase (and bigger domains, as it will be shown latter in SAXS), apparently, the polar urea groups in the polyether chains also produce some mixing in the polyimide phase lowering the T_g. This decrease is of the some order than the increase due to the longer polyimide chains for copolymer cPI-PEO900+HDI, and the T_g value is approximately the same as for the copolymer with the parent polyether, cPI-PEO900, whereas for copolymer cPI-PEO2000+HDI is slightly higher and T_g value is slightly lower than for the copolymer with the parent polyether, cPI-PEO2000.

For all the copolymers, the T_g of the aromatic polyimide is well above ambient temperature, although lower than the corresponding T_g for a pure aromatic polyimide homopolymer (270 ºC[30], 287,3 ºC [42], 305 ºC [38]), due to the much lower polymerization degree and, consequently, lower length of the aromatic polyimide segments in the copolymer as compared to the corresponding homopolymer.

6.3.5 Density

The densities (ρ) of the dense membrane films were determined according to the equation:

$$\rho = \rho_0 \frac{W_{air}}{W_{air} - W_{liq}} \qquad (1)$$

where ρ is the density of the film, W_{air} and W_{liq} are the weights of the film in the air and immersed in an auxiliary liquid (in these measurements, isooctane was used because this polymer is reported to be insoluble in isooctane[43]) and ρ_o is the density of the auxiliary liquid (isooctane). The density for all copolymers is lower than that for the pure aromatic polyimide, BPDA-ODA, which was 1.40 g mL^{-1}, and follows this trend:

ρ(cPI-PEO900)=1.308 > ρ(cPI-PEO900+2000)=1.303 > ρ(cPI-PEO2000)=1.294 > ρ(cPI-PEO6000)=1.281 > ρ(cPI-PEO2000+HDI)=1.276) > ρ(cPI-PEO900+HDI)= 1.266

It is clear that the longer the polyether chain, that is, the better the phase separation, the lower the density should be but, actually, the differences within the copolymers are very small as shown in Figure 7. Copolymers with extended polyether chains, with long polyether chains and well developed phase separation – as well as cPI-PEO6000 –should give low densities. These copolymers should give big free volumes and thus gas should pass through the membrane quite

easily if there were no crystallinity (cPI-PEO6000) and/or hydrogen bonding (HDI extended copolymers).

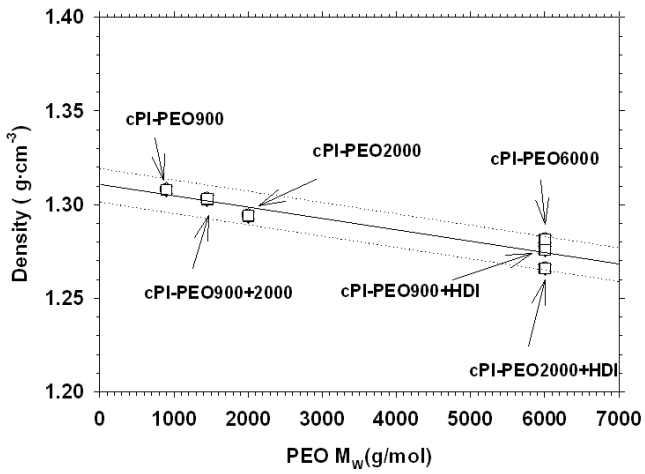

Figure 7. Density as a function of the polymer length.

Note that density decreases when T_g^{ar} increases and T_g^{Al} decreases. The lower densities and lower T_g^{Al} appear due to the ability of the polar groups placed throughout the polymer chains to increase the intermolecular forces increasing the free volume along with the mobility of the PEO chains.

6.3.6 Small-Angle X-ray Scattering

From the curves of scattered intensity I versus the scattering vector ($q = 4\pi(\sin\theta)/\lambda$, λ = wave length, 2θ = scattering angle), two parameters can be evaluated: the relative invariant, Q', as the integral below the curve Iq^2 vs. q, which is related to the extent of the phase separation; and the maximum on the scattering curve, q_{max}, related to the size scale, L, of the separated phases, calculated also from the curve Iq^2 vs. q. The equations used and the mode of operation of the equipment, as well as an outline of it has been explained in previous studies[33].

The scattering profile is very different for the polyether extended copolymers when compared with the copolymers with the parent polyethers. For copolymers cPI-PE900, cPI-PEO2000, cPI-PEO900+2000 and cPI-PEO6000, a single broad peak centered at 0.4-0.6 nm^{-1} appears, as seen in Figure 8 for two selected copolymers. However, for the polyether extended copolymers, cPI-PEO900+HDI and cPI-PEO2000+HDI, the maximum in the scattered intensity is located close to the beam stop (see inset in Figure 8 were these peaks appear clearer).

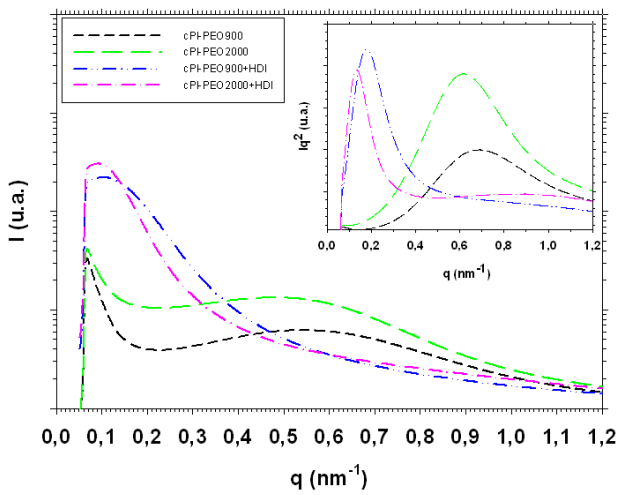

Figure 8. Intensity (logarithmic scale) vs q curves for copolymers cPI-PEO900, cPI-PEO2000, cPI-PEO900+HDI and cPI-PEO2000+HDI. In the insert, the Iq^2 vs q curves for the same copolymers are presented.

In Figure 9, the relative invariant (Q') is plotted versus treatment temperature. Copolymers with the extended polyethers were heated up to 250ºC (before degradation of the urea groups), whereas the others until 300ºC. For copolymer cPI-PEO-900, Q' does not change significantly with temperature, with only a small increase above approximately 165ºC. For this copolymer, with the shortest polyether chain and the shortest polyimide segments of those synthesized here, the segments are partially mixed, as seen in the DSC results, and the phase separated structure almost doesn't improve with thermal treatment. For copolymers cPI-PEO2000, cPI-PEO900+2000 and cPI-PEO6000, at a certain temperature (approximately 180, 170 and 150ºC respectively), Q' increases noticeably up to the final heating temperature, showing a notorious improvement on their phase separated structure. The same improvement is found for the polyether extended copolymers cPI-PEO900+HDI and cPI-PEO2000+HDI, starting in both cases at approximately 180ºC up to the final heating temperature. This improvement is coincident with the increase in PEO crystallinity seen by DSC and, as already mentioned, it is also coincident with the release of the residual solvent in the films.

When the morphology of the phase separated structure is unknown, as in our copolymers, a calculation of the spacing length, L, from the curve I vs. q should be preferred [44]. However, we are more interested on the changes of the spacing scale with temperature than on the absolute value for this length scale of the segregated phases; thus, Iq^2 vs. q curve was used to calculate L attending to the higher accuracy in determining the maximum on this curve.

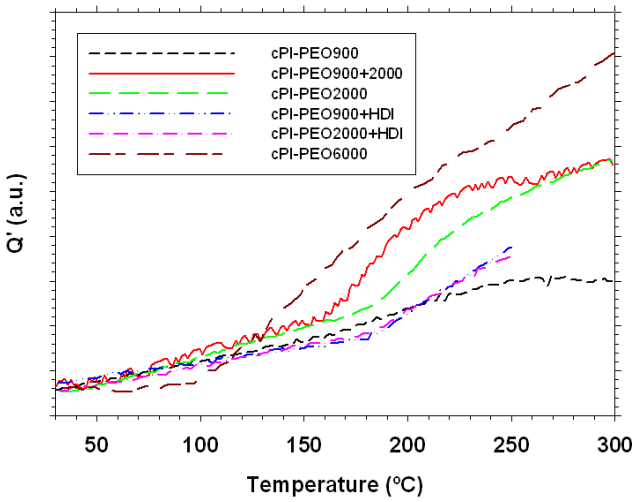

Figure 9. Changes in the relative invariant for the synthesized copolymers treated at 120ºC.

As shown in Figure 10, changes in L take place almost simultaneously to changes in Q'. Big differences are found referring to L between the copolymers with the extended polyether chains and those with the parent polyethers. For copolymers cPI-PEO900, cPI-PEO2000, cPI-PEO900+2000 and cPI-PEO6000, L is initially similar for all of them, *circa* 8 nm, and on heating, grows to a value around 12 nm (i.e. an approximate 50% increment), except for cPI-PEO6000, for which the value reached is almost 19 nm (around 300% increment). This longer L value means bigger PEO domains that are able to crystallize extensively as seen by DSC. Therefore, there is not a trend between L value and polyether length, and only for polyether PEO6000, the L value is clearly above the others. Apart from the strong increase on L for copolymer cPI-PEO6000, it is worth to comment that for copolymer cPI-PEO900, although Q' has a very small increase with temperature, L value changes as much as for copolymers cPI-PEO2000 and cPI-PEO900+PEO2000.

Copolymers with extended polyether chains have a very high L value from the start, around 40 nm for cPI-PEO900+HDI and 50 nm for cPI-PEO2000+HDI, and when Q' increases, the increase in L is very modest, around 8% for both. This large L corresponds to very large PEO domains, and that is the reason why cPI-PEO2000+HDI can reach also very high values of PEO crystallinity, of the order of cPI-PEO6000.

From SAXS data it can be concluded that thermal treatment improves the phase separated structure except for cPI-PEO900, where the segments are mixed in a substantial extent. For this copolymer, however, a significant change in long spacing takes place with thermal treatment. The size scale of the phase separated structure after thermal treatment is similar for copolymers with parent

copolyethers PEO900 and PEO2000, and is much bigger for copolymer based on polyether PEO6000. For copolymers with extended polyether chains, the size scale of the phase separated structure is much bigger than for copolymers with parent polyethers, and even than for copolymer cPI-PEO6000, with similar PEO content, similar total PEO chain length and polyimide segment length, thus, chain extension of relatively short polyether chains is a very effective way to modify the phase separated structure of the copolymers.

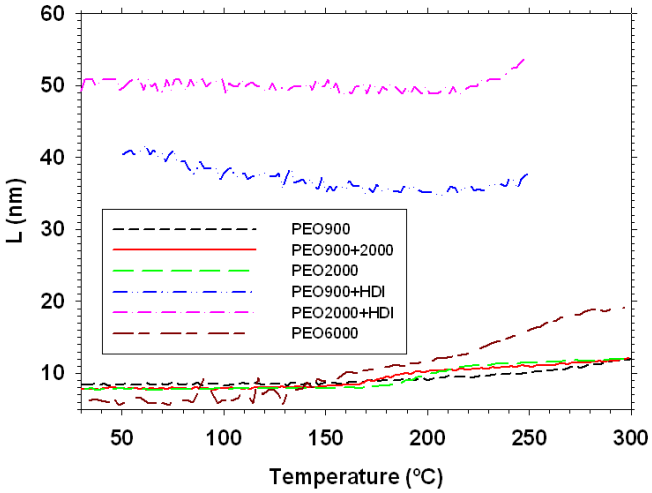

Figure 10. Evolution of L as a function of temperature for the synthesized copolymers.

6.3.7 Permeability properties

6.3.7.1 Behaviour with the thermal treatment

As seen for other aliphatic-aromatic copoly(ether imide)s [34], the results show an improvement in permeation properties after thermal treatment while selectivity remains substantially constant, so that there is a direct relationship between: treatment temperature, phase segregation and permeation properties as can be seen in Figure 11 for the sample cPI-PEO900+2000.

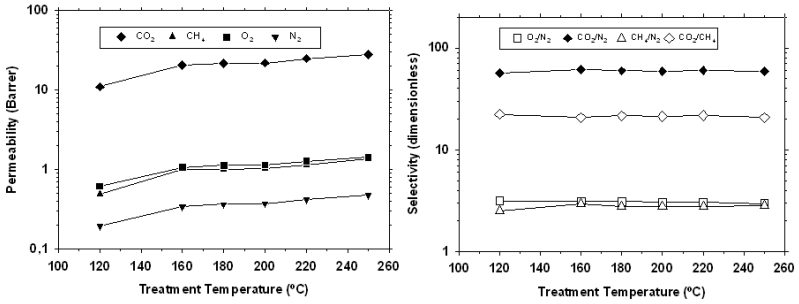

Figure 11. Evolution of the permeability (a) and selectivity (b) as a function of the treatment temperature for cPI-PEO900+2000.

In the case of samples with extended polyether chain, the picture is somewhat different. Figure 12 shows the comparative behavior of sample cPI-PEO900+2000 with samples cPI-PEO900+HDI and cPI-PEO2000+HDI. As already seen, segregation increases with heat treatment, but by TGA and DSC it was clear that at certain temperature, urea groups decompose. When polyether extended copolymers are heated at 200ºC for 2 hours in an oven, urea groups would decompose, producing some mixing of segments and some loss of polyether chains that lead to the observed decrease in CO_2 permeability.

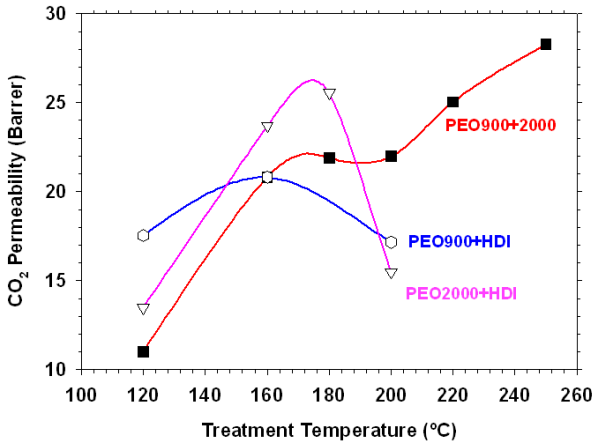

Figure 12. CO_2 permeability as a function of the thermal treatment.

6.3.7.2 Behaviour with the measurement temperature

The movement of gas molecules to penetrate the polymer membranes depends on the thermally activated motion of polymer chains. Not only diffusivity but also solubility is related to the interaction between the polymer chain and the place left to gas condensation. In this sense it is very important to know the properties of the polymers that have a strong influence on the process of separation, such as the free volume. When a polymer is in the crystalline state, the gases hardly penetrate across this structure because the chain movements are very limited giving quite low permeability. The crystals would operate as a non-sorption, impermeable barrier and reduce the permeability severely. On the other hand, when the melting temperature, T_m, is surpassed, the polymer is amorphous, making chains more mobile and thus favoring the permeation of gases through the samples. Therefore, in samples that present or may present crystallinity at work

temperature, it is advisable to conduct a study of their behavior as a function of measurement temperature.

Taking into account the temperature dependence for the diffusion and sorption coefficients, the temperature effect on gas permeability follows an Arrhenius law [45]:

$$P = P_0 exp\left(\frac{E_P}{RT}\right) \quad (2)$$

where E_P is the activation energy of permeation. In Figure 13 the Arrhenius' increase of permeability with the measurement temperature is shown for several gases and the cPI-PEO6000 sample. Several intermediate permeabilities at temperatures from 30 ºC to 50 ºC are shown in the Figure. The activation energy of permeation is shown in Figure 14 as a function of the PEO length. It seems clear that cpI-PEO-6000 has lower activation energy than expected. This could be attributable to its residual crystallinity.

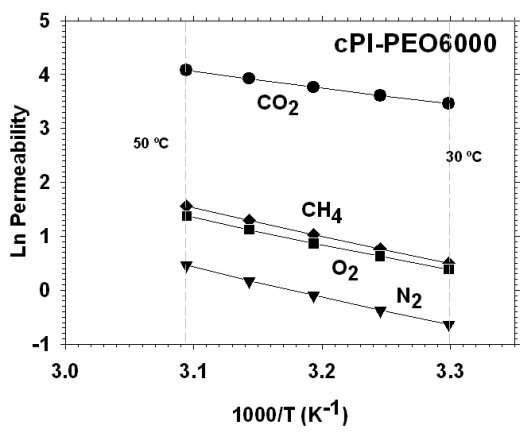

Figure 13. CO_2 permeability as a function of permeation temperature for cPI-PEO6000 membranes treated at 160ºC.

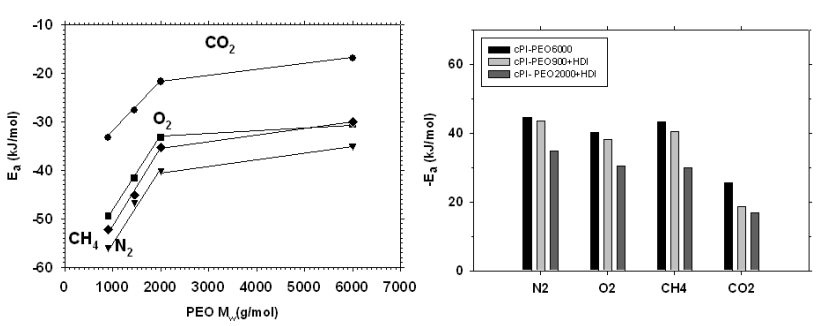

Figure 14. Activation energy as a function of the molecular weight of PEO (a) and for the longest PEO copolymers (b). In the (a) figure only cPI-PEO2000+HDI, among the copolymers with the longest PEO chains, is shown.

6.3.7.3 Permselective properties as a function of the PEO length

Some authors have recently assumed that there should be a maximum length over which permeability decreases [39, 46]. As mentioned above, the amount of crystalline PEO in these samples is important especially for the longest PEO chains (especially cPI-PEO6000). Could this crystallinity be the cause of such an apparent decrease in permeability for copolyetherimides containing very long PEO chains?

In order to analyze the influence of crystallinity in an eventual decrease of permeability for long PEO chains. It is worth to note that at 50 ºC all residual crystallinity would be eliminated for all the copolymers studied guaranteeing that all they are in amorphous state.

Figure 15 shows the results obtained, at the lowest (30 ºC) and the highest (50 ºC) permeation temperature, for the permeability of CO_2 (the trend is similar for all gases tested). The results at 30 °C show that there is a maximum length over which permeability decreases as seen in literature. However, the results at 50 °C show that there is a monotonous increase of permeability for increasing PEO lengths. This is clear for samples containing only pure PEO. For samples with HDI in its structure permeabilities are lower than for the sample cPI-PEO6000. For the polymers with chain extender (HDI) the restriction of chain motion due to possible hydrogen bonds in between urea groups in the soft segments would produce a reduction in the permeability values. The existence of these hydrogen bonds that restrict polyether chain mobility has already been proved in aromatic isocyanate chain extended polyethers [47].

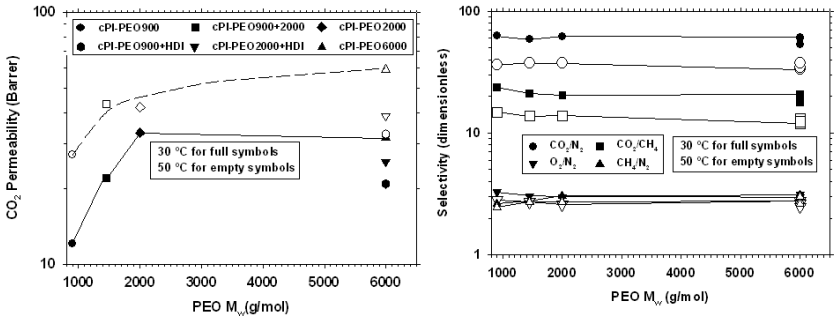

Figure 15. CO_2 permeability (a) and selectivities (b) for some gas pairs as a function of the PEO length, for HDI extended copolymers (treated at 160 ºC) and for the rest of copolymers (treated at 250 ºC).

Therefore it seems clear that when permeation is measured at a high enough temperature to have only amorphous PEO longer chains improves the passage of gases. This indicates that for each length of PEO it is necessary to find an optimum working temperature to get all PEO in amorphous

state, in order to obtain the maximum performance. Referring to selectivities, it seems clear that they can be considered almost constant; what means that for these block-copolymers, the aromatic part determines the selectivity of the sample (as mentioned in this study the proportion of PEO is almost constant). This leads to a clear possibility of controlling permeability without damaging selectivity by simply increasing the length of PEO chains. On the other hand by varying the aromatic part, higher selectivity could, of course, be obtained. Naturally, for the copolymers that are already amorphous at 30 ºC, permeability increases with the permeation temperature while selectivity decreases only very slightly.

6.3.7.4 Permselective properties as a function of the PEO percentage

For all samples the content of PEO is quite similar, ranging from 42 to 45 %, (between 42 and 49 % considering the HDI+PEO content— see Table 1). Consequently the effect of the polyether proportion should be very small in permeability. Here results for both the permeation temperatures of 30 and 50 °C are considered too.

Figure 16a shows the evolution of permeability as a function of the percentage of total polyether in the final polymer. It seems clear that the amount of total polyether or PEO doesn't play a decisive role for this narrow range of percentages, and therefore it is the length of the PEO chains the key parameter.

In the case of samples with chain extender (HDI), that have the highest percentages of polyether in the sample, it can be seen that they don't show the best permeabilities. The reduction of mobility of the chains causes lower permeability [47] and activation energies as seen in Figure 14.

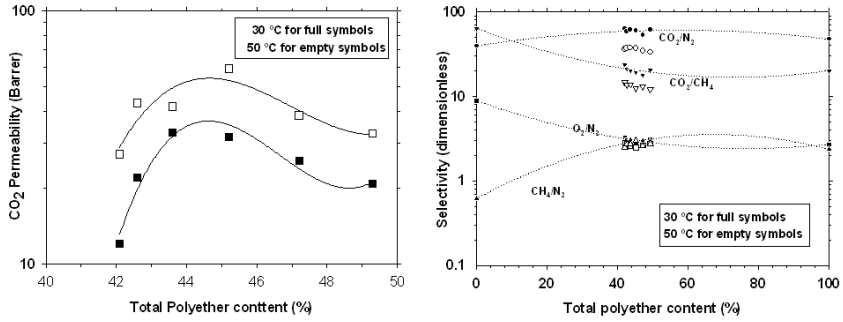

Figure 16. CO_2 permeability (a) and selectivities (b) for some gas pairs as a function of the PEO percentage for HDI extended copolymers (treated at 160 ºC) and for the rest of copolymers (treated at 250 ºC).

It has been carried out an analysis of the influence of the percentage of polyether on the selectivity for different gas pairs. Figure 16b shows the selectivity for the synthesized copolymers and also for the homopolymer BPDA-ODA and for the pure PEO at 30 ºC. It can be seen that all samples show very close selectivities regardless of the percentage of polyether. A comparison of selectivity with those of the pure aromatic polyimide, and pure PEO shows that for the couples O_2/N_2 and CO_2/CH_4 selectivities are between those of both BPDA-ODA and pure PEO. In the case of couples CO_2/N_2 and CH_4/N_2, the samples showed exceptional results, surpassing the selectivities of BPDA-ODA and pure PEO.

6.3.7.5 Robeson's plot

After confirming that the working temperature and the length of the PEO chains, for similar percentages of polyether, play key roles in permeation properties, these permselective properties are themselves considered here on. A visual way of representing the permeability values obtained for different gases are the Robeson's representations [48-49]. In these representations the distance to the so called upper bond gives us an idea of the permeation properties of the samples.

In addition to our copolymers, we have represented the values for pure PEO at 35 ºC [28] and for BPDA-ODA (synthesized in our lab) at 30 ºC. The representative points for our copolymers should be in between these two values. As it's well known, the Robeson's upper bounds depend on the measurement temperature [50]. This is also taken into account when comparing data at 30 and at 50 °C.

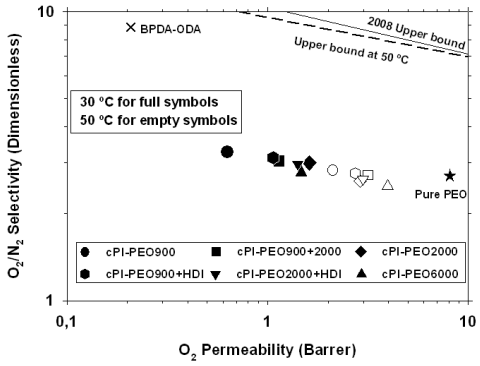

Figure 17. Robeson's plot for O_2/N_2. Full circles correspond to a temperature of permeation of 30 ºC; while hollow ones were measured at 50 ºC.

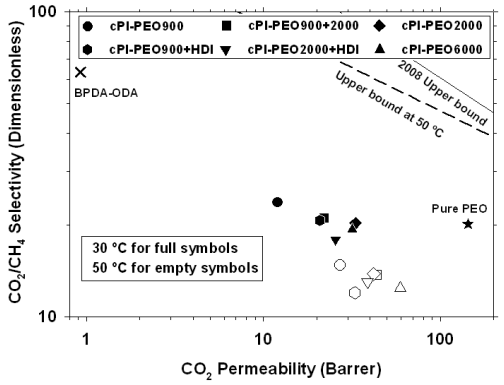

Figure 18. Robeson's plot for CO_2/CH_4. Full circles correspond to a temperature of permeation of 30 ºC; while hollow ones were measured at 50 ºC.

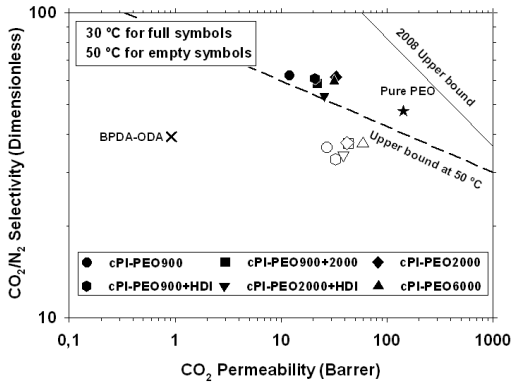

Figure 19. Robeson's plot for CO_2/N_2. Full circles correspond to a temperature of permeation of 30 ºC; while hollow ones were measured at 50 ºC.

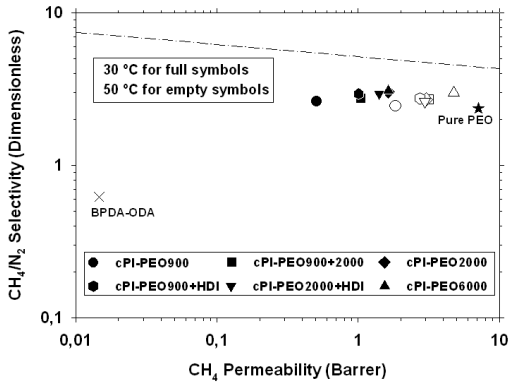

Figure 20. Robeson's plot for CH_4/N_2. Full circles correspond to a temperature of permeation of 30 ºC; while hollow ones were measured at 50 ºC. A pseudo Robeson upper bound has been drawn by us from the best results in literature.

In these Figures, the crosses correspond to BPDA-ODA and the stars to pure PEO. The full circles represent the measurements at 30 °C and the hollow circles represent the measurements at 50 °C. The best permeabilities at 30 °C were given by the cPI-PEO2000 sample; whereas for 50 ºC, the best results are shown by cPI-PEO6000. As already mentioned, the high permeability for cPI-PEO6000 is due to the elimination of all crystallinity in this copolymer at 50 °C. Therefore the high length of cPI-PEO6000 leads to higher permeability.

For couples O_2/N_2 and CO_2/CH_4 (Figure 17 and 18), the results are far from their respective upper bound. For the couple CO_2/N_2 the polymers showed an excellent performance (see Figure 19). Whereas when the measuring temperature was 30 ºC the polymers showed values close to the Robeson's limit, when the measurement temperature was 50 ºC results clearly are even closer to the upper bound for this temperature. For the couple CH_4/N_2 the polymers showed a reverse selectivity getting reasonably good figures. For this couple, there is not a Robeson's plot thus a tentative limit (drawn by us) is shown in Figure 20[34].

6.3.7.6 Permeability prediction

The permeability for the samples BPDA-ODA-PEO with different PEO lengths in the polymer may be predicted by the Maxwell equation as exposed below [51]:

$$P_{eff} = P_C \left[\frac{P_D+2P_C-2\phi_D(P_C-P_D)}{P_D+2P_C+\phi_D(P_C-P_D)}\right] \quad (3)$$

where P_{eff} is the effective permeability, P_C and P_D are the permeability of the continuous phase and the dispersed phase, respectively, and ϕ_D is the volume fraction of the dispersed phase in the block copolymer. In this type of polymers, we should take into consideration that the roles of continuous or disperse phases could be played by the hard (aromatic) or by the soft (aliphatic) segments of the copolymer. We will consider the aliphatic (PEO containing) phase as the continuous phase, because it has already been proven, for this type of system, that when the amount of PEO is higher than 20 %, the disperse phase is the aromatic part [39]. Under these assumptions we built the Maxwell prediction curve. The permeability of pure PEO in the amorphous state is used as the permeability of the soft segments (continuous phase) [28] and the permeability of BPDA-ODA to the hard segments (disperse phase).

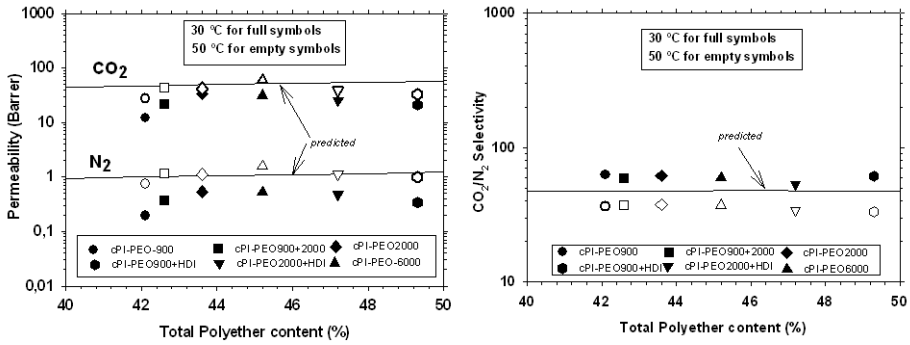

Figure 21. Predicted values for CO_2 and N_2 permeability (a) and CO_2/N_2 selectivity (b) using Maxwell equation along with the corresponding experimental results.

Figure 21 shows the prediction of permeability and selectivity prediction for the CO_2/N_2 gas pair according to the Maxwell model. The model shows a good fit for permeability, although samples with high crystallinity showed a slightly poorer fit, and the polymers with longer PEO have the highest crystallinity. On the other hand, the phase segregation was better for longer PEO chains, thus the model should be better adapted. Referring to selectivity, the fit was acceptable for all samples. This model brings new evidence of the importance of crystallinity in the samples, so for that to get the best fit, it is necessary that the samples are in amorphous state and phase segregation be as high as possible.

6.4 Conclusions

A series of copoly(ether-imide)s with approximately 45% weight of polyether in the final copolymer presenting good gas separation properties have been prepared. These copolymers have been synthesized by the reaction between an aromatic dianhydride (BPDA), an aromatic diamine (ODA) and a diamine terminated poly(ethylene oxide) having a different molecular weight (900, 2000 and 6000 g / mole), or diisocyanate (HDI) extended poly(ethylene oxide) 900 and 2000 with the aim of obtaining a greater length of PEO (approximately 6000 g/mol) but with less tendency to crystallization.

TGA analysis confirmed the weight amount of PEO in the copolymers and showed that the polyether moiety can be eliminated selectively by thermal treatment. Thermal treatment decreased the Tg value for the polyether phase in the completely amorphous copolymers or increased its crystallinity for the copolymers with polyether crystallization capability except for copolymer with

the shortest PEO, cPI-PEO900 for which no change in thermal properties was observed. For the chain extended polyethers, the surprising low Tg value and the higher crystallinity respect to the parent polyethers 900 and 2000 proved that chain extension is an effective way to increase the phase separation in these copolymers. TMA data complemented DSC data and a T_g well above ambient temperature for the aromatic polyimide phase was measured. This T_g increased with the increase of PEO length due to the increase in the aromatic polyimide segment length, but for the copolymers with chain extended polyethers, the value was lower than expected, probably due to some mixing of soft segments in the hard segment phase promoted by the urea groups.

SAXS analysis confirmed the existence of a phase separated morphology in these copolymers that improved when they were thermally treated at increasing temperatures below the temperature of the onset of decomposition. After initial treatment temperatures that released the remaining solvent in the imidized copolymers, a fast improvement in the phase separation was produced at higher temperatures. The size scale of the phase separated structure was initially similar for the copolymers based on the parent polyethers, around 8 nm, and increased simultaneously with the improvement in the phase separation up to a value of 12 to 19 nm. For the copolymer with chain extended polyethers, long spacing was much higher, 40 to 50 nm, with almost no change with treatment temperature. The large size of the phases would explain the DSC results for these copolymers.

Gas permeability for the synthesized copolymers was directly related to the phase separated structure present in the material, with an increase in permeability when treatment temperature, and phase separation, was increased. For copolymers with chain extended polyethers, the degradation of the urea groups led to an increase of segregation but with considerable internal bonding that led to a decrease in permeability. At the same time, selectivity was almost unaffected and remained constant at any treatment temperature. In this way, we could conclude that chain enlarging with HDI is not efficient in increasing permeability.

Temperature is important in the case of polymers that show a high content of crystallized polyether. Thus studies of the behavior of the copolymers as a function of working temperature have been carried out. The amount of crystalline PEO is zero or negligible for these samples when the temperature is 50 ºC. For this reason, in this case, we have analyzed the results of permeability and selectivity for different pairs as a function of the length of PEO at two temperatures of work, a standard 30 ºC and a sufficiently high so that all the PEO is in amorphous state, 50 °C. Thus, it was observed that the greater the length of PEO the higher permeability was observed, because the PEO is in purest state. For samples with HDI results were lower than for the sample with PEO6000

owing to the hydrogen bridges forming urea structures. The results of selectivity for all PEO lengths were similar.

Analyzing the results in terms of percentage of PEO in the samples, the highest results were found for 43.5 % for the measurement at a temperature of 30 °C, which corresponds to the sample PEO2000, and to values close to 45 % when as the temperature is 50 ºC, which coincides with the sample PEO6000. This again highlights the importance of crystallinity, when all the poly(ethylene oxide) is in amorphous state, the best values are for the longest PEO, the 6000 in this case.

Regarding the Robeson's plots, the best results were found for the CO_2/N_2 gas couple. At 30 °C the results are quite close to the Robeson upper bound, and in the case of the measures at 50 °C the permselectivity closely approaches the limit for this temperature. In conclusion it seems clear that this type of polymer is suitable for separations where CO_2 is involved, and especially for the separation CO_2/N_2. This separation has a great importance in the greenhouse effect and makes these membranes good candidates for their application at industrial level. An interesting application of CO_2/N_2 separation is in the purification of coal gas. In this process the working temperatures are high, so this type of materials is presented as an attractive alternative.

We have compared the results with those calculated by using the Maxwell's model. In this case also the percentage of amorphous PEO should be used and crystallinity has to be taken into account for low permeation temperatures. The samples with a low or negligible crystallinity showed a good fit. The need to take into account the truly amorphous portion of PEO makes necessary to optimize both the amount of poly(ethylene oxide) in the sample and the operating temperature for a specific length and amount of PEO.

6.5 Aknowledgements

We are indebted to the Spanish Junta de Castilla León for financing this work through the GR-18 Excellence Group Action and to the Ministry of Science and Innovation in Spain for their economic support of this work (MAT2008-00619/MAT, MAT2010-20668/MAT, MAT2011-25513/MAT and CIT-420000-2009-32). We also acknowledge financial support from the programme Consolider Ingenio 2010 (project CSD-0050-MULTICAT).

Authors thank the access to the beamline BM16 at the European Synchrotron Radiation Facility (ESRF) in Grenoble (France). We are grateful to Dr. Ana Labrador and Dr. François Fauth for their help at BM16 station at the ESRF. The help provided by Sara Rodriguez in measuring gas

permeability and selectivity is greatly appreciated. A. Tena thanks CSIC for a predoctoral JAE fellowship.

6.6 References

1. A. Yamasaki, An Overview of CO_2 Mitigation Options for Global Warming-Emphasizing CO_2 Sequestration Options, Journal of Chemical Engineering of Japan, 36 (2003) 361-375.
2. U.S. EIA, International Energy Outlook in, Washington, DC, 2011.
3. J.D. Figueroa, T. Fout, S. Plasynski, H. McIlvried, R.D. Srivastava, Advances in CO_2 capture technology—The U.S. Department of Energy's Carbon Sequestration Program, International Journal of Greenhouse Gas Control, 2 (2008) 9-20.
4. M.T. Ho, G.W. Allinson, D.E. Wiley, Factors affecting the cost of capture for Australian lignite coal fired power plants, Energy Procedia, 1 (2009) 763-770.
5. H. Yang, Z. Xu, M. Fan, R. Gupta, R.B. Slimane, A.E. Bland, I. Wright, Progress in carbon dioxide separation and capture: A review, Journal of Environmental Sciences, 20 (2008) 14-27.
6. H.J. Herzog, What future for carbon capture and sequestration?, Environmental Science and Technology, 35 (2001) 148-153.
7. J. Klemeš, I. Bulatov, T. Cockerill, Techno-economic modelling and cost functions of CO_2 capture processes, Computers & Chemical Engineering, 31 (2007) 445-455.
8. J. Davison, Performance and costs of power plants with capture and storage of CO_2, Energy, 32 (2007) 1163-1176.
9. S. Hoffmann, M. Bartlett, M. Finkenrath, A. Evulet, T.P. Ursin, Performance and Cost Analysis of Advanced Gas Turbine Cycles With Pre-Combustion CO_2 Capture, ASME Conference Proceedings, 2008 (2008) 663-671.
10. J. Oexmann, C. Hensel, A. Kather, Post-combustion CO_2-capture from coal-fired power plants: Preliminary evaluation of an integrated chemical absorption process with piperazine-promoted potassium carbonate, International Journal of Greenhouse Gas Control, 2 (2008) 539-552.
11. F. Qin, S. Wang, I. Kim, H.F. Svendsen, C. Chen, Study of the Heat of Absorption of CO_2 in Aqueous Ammonia: Comparison between Experimental Data and Model Predictions, Industrial & Engineering Chemistry Research, 49 (2010) 3776-3784.
12. M.T. Ho, G.W. Allinson, D.E. Wiley, Reducing the Cost of CO_2 Capture from Flue Gases Using Pressure Swing Adsorption, Industrial & Engineering Chemistry Research, 47 (2008) 4883-4890.
13. T.C. Merkel, H. Lin, X. Wei, R. Baker, Power plant post-combustion carbon dioxide capture: An opportunity for membranes, Journal of Membrane Science, 359 (2010) 126-139.

14. J.M. Klara, P.J. Capicotto, L.L. Pinkerton, R.L. Schoff, V. Vaysman, Cost and Performance Baseline For Fossil Energy Plants, in: N.E.T. Laboratory (Ed.), 2009.
15. H. Yang, S. Fan, X. Lang, Y. Wang, J. Nie, Economic Comparison of Three Gas Separation Technologies for CO_2 Capture from Power Plant Flue Gas, Chinese Journal of Chemical Engineering, 19 (2011) 615-620.
16. R. Bounaceur, N. Lape, D. Roizard, C. Vallieres, E. Favre, Membrane processes for post-combustion carbon dioxide capture: A parametric study, Energy, 31 (2006) 2220-2234.
17. E. Favre, Carbon dioxide recovery from post-combustion processes: Can gas permeation membranes compete with absorption?, Journal of Membrane Science, 294 (2007) 50-59.
18. M.T.K. Bessonov, M.M.; Kudryavtsev, V.V.; Laius, L.A., Polyimides: Thermally Stable Polymers, in, Consultants Bureau, New York, 1987.
19. D.S. Wilson, H.D.; Hergenrother, P.M., Polyimides, in, Blackie, Glasgow, 1990.
20. M.K.M. Ghosh, K.L., Polyimides: Fundamentals and Applications, in, Marcel Dekker, New York, 1996.
21. D. Ayala, A.E. Lozano, J. De Abajo, C. García-Perez, J.G. De La Campa, K.V. Peinemann, B.D. Freeman, R. Prabhakar, Gas separation properties of aromatic polyimides, Journal of Membrane Science, 215 (2003) 61-73.
22. K. Tanaka, H. Kita, K. Okamoto, A. Nakamura, Y. Kusuki, Gas permeability and permselectivity in polyimides based on 3,3',4,4'-biphenyltetracarboxylic dianhydride, Journal of Membrane Science, 47 (1989) 203-215.
23. T.A. Barbari, W.J. Koros, D.R. Paul, Gas transport in polymers based on bisphenol-A, Journal of Polymer Science, Part B: Polymer Physics, 26 (1988) 709-727.
24. Y. Li, M. Ding, J. Xu, Gas separation properties of aromatic polyetherimides from 1,4-bis(3,4-dicarboxyphenoxy)benzene dianhydride and 3,5-diaminobenzic acid or its esters, Journal of Applied Polymer Science, 63 (1997) 1-7.
25. Y. Hirayama, Y. Kase, N. Tanihara, Y. Sumiyama, Y. Kusuki, K. Haraya, Permeation properties to CO_2 and N_2 of poly(ethylene oxide)-containing and crosslinked polymer films, Journal of Membrane Science, 160 (1999) 87-99.
26. M. Kawakami, H. Iwanaga, Y. Hara, M. Iwamoto, S. Kagawa, Gas permeabilities of cellulose nitrate/poly(ethylene glycol) blends membranes, Journal of Applied Polymer Science, 27 (1982) 2387-2393.
27. A. Car, C. Stropnik, W. Yave, K.V. Peinemann, Pebax®/polyethylene glycol blend thin film composite membranes for CO_2 separation: Performance with mixed gases, Separation and Purification Technology, 62 (2008) 110-117.

28. H. Lin, B.D. Freeman, Gas solubility, diffusivity and permeability in poly(ethylene oxide), Journal of Membrane Science, 239 (2004) 105-117.
29. S.R. Reijerkerk, M.H. Knoef, K. Nijmeijer, M. Wessling, Poly(ethylene glycol) and poly(dimethyl siloxane): Combining their advantages into efficient CO_2 gas separation membranes, Journal of Membrane Science, 352 (2010) 126-135.
30. K.I. Okamoto, M. Fujii, S. Okamyo, H. Suzuki, K. Tanaka, H. Kita, Gas permeation properties of poly(ether imide) segmented copolymers, Macromolecules, 28 (1995) 6950-6956.
31. K.U. Okamoto, N.; Okamyo, S.; Tanaka, K.; Kita, H., Selective permeation of carbon dioxide over nitrogen through polyethyleneoxide-containing polyimide membranes, Chemistry Letters 5(1993) 225-228.
32. H. Suzuki, K. Tanaka, H. Kita, K. Okamoto, H. Hoshino, T. Yoshinaga, Y. Kusuki, Preparation of composite hollow fiber membranes of poly(ethylene oxide)-containing polyimide and their CO_2/N_2 separation properties, Journal of Membrane Science, 146 (1998) 31-37.
33. A. Tena, A. Marcos-Fernández, A.E. Lozano, J.G. de la Campa, J. de Abajo, L. Palacio, P. Prádanos, A. Hernández, Thermally treated copoly(ether-imide)s made from bpda and alifatic plus aromatic diamines. Gas separation properties with different aromatic diamimes, Journal of Membrane Science, 387–388 (2012) 54-65.
34. A. Tena, A. Marcos-Fernandez, L. Palacio, P. Cuadrado, P. Pradanos, J. De Abajo, A.E. Lozano, A. Hernandez, Phase Segregation and Gas Separation Properties of Thermally Treated Copoly(ether-imide) from an Aromatic Dianhydride, an Aromatic Diamine and Various Aliphatic Diamines, Industrial & Engineering Chemistry Research, (2012).
35. A. Tena, A.E. Lozano, L. Palacio, A. Marcos-Fernández, P. Prádanos, J. de Abajo, A. Hernández, Gas separation properties of systems with different amounts of long poly(ethylene oxide) segments for mixtures including carbon dioxide., International Journal of Greenhouse Gas Control, send it (2012).
36. A. Tena, L. Fernández, M. Sánchez, L. Palacio, A.E. Lozano, A. Hernández, P. Prádanos, Mixed matrix membranes of 6FDA-6FpDA with surface functionalized γ-alumina particles. An analysis of the improvement of permselectivity for several gas pairs, Chemical Engineering Science, 65 (2010) 2227-2235.
37. J. Scheirs, S.W. Bigger, O. Delatycki, Characterizing the solid-state thermal oxidation of poly(ethylene oxide) powder, Polymer, 32 (1991) 2014-2019.

38. A. Marcos-Fernández, A. Tena, A.E. Lozano, J.G. de la Campa, J. de Abajo, L. Palacio, P. Prádanos, A. Hernández, Physical properties of films made of copoly(ether-imide)s with long poly(ethylene oxide) segments, European Polymer Journal, 46 (2010) 2352-2364.
39. C. Hangzheng, X. Youchang, C. Tai-Shung, Synthesis and characterization of poly (ethylene oxide) containing copolyimides for hydrogen purification, Polymer, 51 (2010) 4077-4086.
40. D.W. Van Krevelen, Properties of polymers in: third edition, Elsevier, Amsterdam, 1990, pp. 120
41. C. Casado-Coterillo, J. Soto, M. T. Jimaré, S. Valencia, A. Corma, C. Téllez, J. Coronas, Preparation and characterization of ITQ-29/polysulfone mixed-matrix membranes for gas separation: Effect of zeolite composition and crystal size, Chemical Engineering Science, 73 (2012) 116-122.
42. J. Zhang, J. Lu, W. Liu, Q. Xue, Separation of CO_2 and CH_4 through two types of polyimide membrane, Thin Solid Films, 340 (1999) 106-109.
43. J.I. Brandrup, E.H.; Grulke, E.A., Polymer handbook, in, John Wiley & Sons Inc, New York, 1999.
44. F.J. Baltá-Calleja, C.G. Vonk, X-ray scattering of synthetic polymers, Elsevier, 1989.
45. R.E. Kesting, A.K. Fritzsche, Polymeric gas separation membranes, Wiley, 1993.
46. W. Yave, A. Szymczyk, N. Yave, Z. Roslaniec, Design, synthesis, characterization and optimization of PTT-b-PEO copolymers: A new membrane material for CO_2 separation, Journal of Membrane Science, 362 (2010) 407-416.
47. A. Marcos-Fernández, A.E. Lozano, L. González, A. Rodríguez, Hydrogen Bonding in Copoly(ether−urea)s and Its Relationship with the Physical Properties, Macromolecules, 30 (1997) 3584-3592.
48. L.M. Robeson, Correlation of separation factor versus permeability for polymeric membranes, Journal of Membrane Science, 62 (1991) 165-185.
49. L.M. Robeson, The upper bound revisited, Journal of Membrane Science, 320 (2008) 390-400.
50. B.W. Rowe, L.M. Robeson, B.D. Freeman, D.R. Paul, Influence of temperature on the upper bound: Theoretical considerations and comparison with experimental results, Journal of Membrane Science, 360 (2010) 58-69.
51. J.C. Maxwell, A treatise on electricity and magnetism, in: vol. 1, Dover Publications Inc, New York, 1954.

CHAPTER 7

Physical properties of films made of copoly(ether-imide)s with long poly(ethylene oxide) segments

Ángel Marcos-Fernández[1,3], Alberto Tena[1,3], Ángel E. Lozano[1,3], J. G. de la Campa[1,3], Javier de Abajo[1,3], Laura Palacio[1,2], Pedro Prádanos[1,2], Antonio Hernández[1,2]

[1]*Smap UA-UVA-CSIC, Parque Científico Universidad de Valladolid, Paseo de Belén, s/n, 47011 Valladolid, Spain.*

[2]*Dept. Física Aplicada, Facultad de Ciencias, Universidad de Valladolid, Paseo de Belén, 7, 47011 Valladolid, Spain*

[3]*Instituto de Ciencia y Tecnología de Polímeros, CSIC, Juan de la Cierva 3, 28006 Madrid, Spain.*

This chapter has been published in:

European Polymer Journal 46 (**2010**) 2352–2364

DOI: 10.1016/j.eurpolymj.2010.09.040

Abstract

Polyimides having long poly(ethylene oxide), PEO, moieties in the main chain have been synthesized by a classical two-steps polycondensation method with good yield and high molecular weight. In contrast with previous works on this topic, essentially full conversion of the polyamic acid to polyimide was attained by heating at relatively low temperatures (around 160 ºC).

These copolyimides undergo an increase of phase separation between the PEO part and the polyimide one after a thermal annealing. This phase separation increases gas separation properties of membranes made up of these copolymers. An exhaustive study of polymer properties as a function of the thermal treatment has been carried out in order to figure out the origin of this behavior. The analysis performed included TGA, DSC, SAXS and mechanical testing.

The polymers studied in this paper have medium thermal stability. In fact, degradation of the polyether chain under nitrogen takes place at temperatures above 300 ºC. However, their thermal stabilities were much lower under oxidant atmosphere.

Graphical Abstract

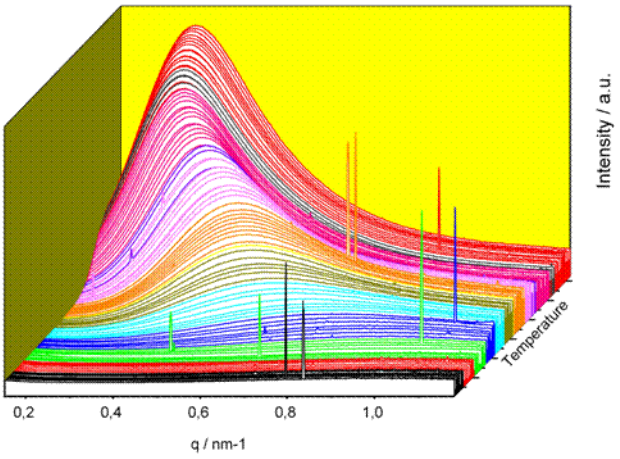

7.1 Introduction

Attending to new social and economical necessities such as energy efficiency, global warming and use of currently non-economical resources, the recovery of CO_2 from mixtures is an important industrial objective in view of several aspects such as natural gas reforming, biomedical applications, synthesis gas processes and clean and efficient coal burning. In particular, some gas purifications to be accomplished using new technologies in the near future are: CO_2/N_2 CO_2/H_2 and CO_2/CH_4.

Polymeric membranes have been used in many gas separation processes for mixtures including CO_2 as those mentioned above, because they offer low energy cost, simplicity of operation, and also they present good thermal and mechanical properties. However, for polymeric membranes it has been shown that there is a trade-off between selectivity and permeability, which means that membranes with high gas permeabilities have low selectivities and viceversa [1].

Diverse polyimides having high permeability to CO_2 (P_{CO2}), have been reported [2], but they use to exhibit low CO_2/N_2 selectivity due to the small difference in the effective molecular size of both gases [3,4]. However, recently reported modified polyimides able to undergo thermal rearrangement processes (TR polymers), exhibited extraordinary gas separation properties, including CO2, due to microcavity evolution after thermal treatment [5-7]. The introduction of polar groups that can interact favorably with CO_2, such as amine [8] or carboxyl [9] groups has also proved to be a very efficient method to increase the CO_2/N_2 or CO_2/CH_4 selectivity.

In this regard, poly(ethylene oxide), PEO, is a very attractive polymer due to the strong affinity of CO_2 towards the oxygen of the oxyethylenic units [10], and there have been many recent studies of polymeric membranes containing PEO or similar polar ether segments in carbon dioxide separations [11–26]. Since PEO does not have the mechanical and thermal resistance required for the preparation of thin membranes, research efforts have been carried to incorporate PEO segments into polyurethanes, polyesters, polyamides and polyimides (PI) [14–26]. Block copolymers containing PEO segments are interesting membrane materials since they exhibit high CO_2 permeability and high polar/non polar gas selectivity. In these materials, CO_2 permeation occurs through the PEO-domains (soft segments) whereas the other domains (the polyimide hard segments) contribute to the mechanical strength [14–26].

Okamoto et al. reported for the first time data of PEO-copolyimides for gas separation [19]. The short, rigid aromatic polyimide segments and the flexible polyalkylene oxide segments were phase-separated into two major domains, which increased the selectivity for CO_2/N_2 gas separation [14,20]. These authors explored the effect of the hard segment of PEO-copolyimides on gas separation properties, and they found that copolyimides containing similar PEO weight percent and different chemical structure of the hard segments exhibited similar CO_2/N_2 selectivity (49–53), but different P_{CO2} (117–238 Barrer) [20].

We previously reported preliminary results concerning the promising CO_2/N_2 separation properties of some thermally treated copolyimide membranes containing different PEO content (28–68 wt.%) [27,28]. It was found that, after a programmed thermal treatment, the studied membranes improved their permeability to CO_2 while the CO_2/N_2 selectivity just suffered a small drop.

In this work, we present the details on the physical characterization, including phase separated morphology, of the previously reported copolyimides [28] and some other related results. The study consists of a systematic evaluation of the physical properties of the synthesized copolyimides after different thermal treatments and its relationship with the evolution of the phase separated structure.

7.2 Experimental

7.2.1 Chemicals

3,3′,4,4′-benzophenonetetracarboxylic dianhydride (BKDA), 3,3′,4,4′-biphenyltetracarboxylic dianhydride (BPDA) and 4,4'-oxydianiline (ODA) were purchased to Aldrich. These products were purified by sublimation at high vacuum just before being used. Polyoxyethylene bis(amine) with nominal molecular weight of 6000 g/mol was kindly donated by Kawaken Fine Chemicals Co., Ltd. (Tokyo, Japan), (PEG-6000 from here on). This polyether was dried at 70ºC in vacuum for 5 hours and stored in a desiccator at vacuum until use. Anhydrous N-methylpyrrolidinone (NMP), to be used as polymerization solvent, was purchased from Sigma-Aldrich Co. Scheme 1 shows the chemical structure of the monomers.

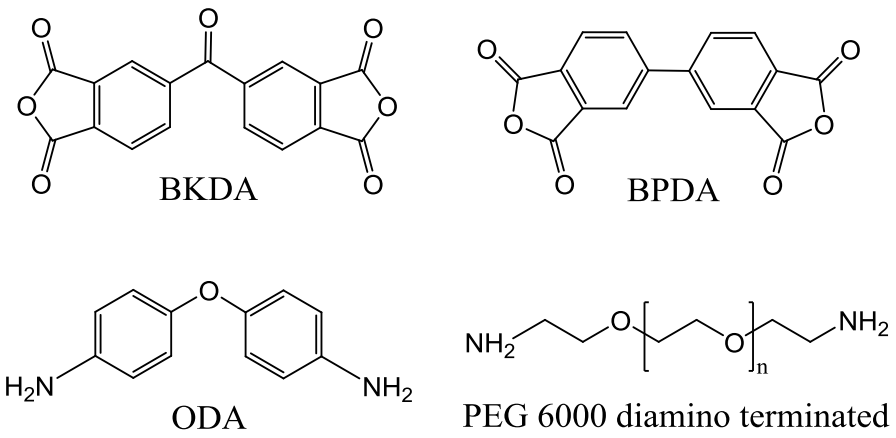

Scheme 1. Chemical structure of the monomers

7.2.2 Synthesis of copoly(ether-imide)s

The procedure for the synthesis of all the polymers in this study was as follows:

- A mixture of polyethyleneoxide bis(amine) 6000 (*x* mmol), PEG-6000, and ODA (*y* mmol) in weight ratios 1:1, 2:1, 4:1 or 6:1 was dissolved in anhydrous NMP (5 mmol (x+y)/10 mL) in a 100 mL three-necked flask blanketed with nitrogen.

- The reaction mixture was cooled down to 0ºC, and under mechanical stirring, a stoichiometric amount of BKDA or BPDA dianhydride (*x*+*y* mmol) was added all at once and the mixture was stirred overnight at room temperature. During this time the dianhydride completely dissolved and the solution reached high viscosity.

- The resultant viscous copolyamic acid solution was diluted with NMP to the appropriate viscosity for casting, filtered through a nominal number 2 fritted glass funnel, degassed, and cast onto leveled glass plates. The resulting films were covered with a conical funnel to avoid fast evaporation of the solvent, dried at 80ºC overnight, and finally treated at 120ºC for 6 hours in a vacuum oven. Films of the copolymers of 85-150 μm in thickness were obtained. After that, thermal treatments under inert atmosphere were carried out at different temperatures.

In addition to the copoly(ether-imide)s, two pure aromatic polyimides, BKDA-ODA and BPDA-ODA were prepared as references using the same procedure. The films from the pure polyimides were thermally treated to produce imidization with a final step at 285ºC for 1 hour.

In table 1, the complete list of the synthesized polymers, and its denomination throughout this paper, can be found.

Table 1. Polymers synthesized in this work

Dianhydride	DP* Imide segment	Mol ratio PEG-6000/ODA	Weight ratio PEG-6000/ODA	Denomination
BKDA	∞	0/100	0/100	BKDA-ODA
BKDA	60.9	30/1	1/1	BKDA 1/1
BKDA	31.0	15/1	2/1	BKDA 2/1
BKDA	16.0	7.5/1	4/1	BKDA 4/1
BKDA	11.0	5.0/1	6/1	BKDA 6/1
BPDA	∞	0/100	0/100	BPDA-ODA
BPDA	60.9	30/1	1/1	BPDA 1/1
BPDA	31.0	15/1	2/1	BPDA 2/1
BPDA	16.0	7.5/1	4/1	BPDA 4/1
BPDA	11.0	5.0/1	6/1	BPDA 6/1

* Theoretical degree of polymerization calculated from the feed ratio

7.2.3 Experimental Methods

Attenuated total internal reflectance-Fourier transform infrared analyses (ATR-FTIR) were performed at room temperature using a PerkinElmer Spectrum One infrared spectrometer equipped with an ATR accessory.

A Thermal Analysis Q500 instrument was used for thermogravimetric analysis (TGA). Disc samples cut from films with weights between 5 and 15 mg were tested. When running dynamic scans, it was done in Hi-Resolution mode, where the heating rate is automatically adjusted in response to changes in the rate of weight loss, which results in improved resolution, with an initial heating rate of 10ºC/min under a flux of nitrogen (in some cases with air, as detailed in the corresponding section).

Differential scanning calorimetry (DSC) analyses were carried out in a Mettler Toledo (DSC 822e) calorimeter equipped with a liquid nitrogen accessory. Disc samples cut from films weighting 5–15mg were sealed in aluminium pans. Samples were heated with the following cyclic method in order to monitor the changes in thermal properties with thermal treatment: from 25ºC, the sample was heated at 10ºC/min to a target temperature; once reached, the sample was cooled at the

maximum cooling rate accessible for the instrument to -90ºC, held at this temperature for 15 min and reheated at 10ºC/min to the next target temperature. The procedure was followed until the last treatment temperature was reached and a final run from -90ºC to 80ºC was performed. In this way, in each heating run, the thermal properties for the copolymers after treatment to the previously reached temperature were obtained, and a plot of thermal properties versus "instantaneous" thermal treatment could be built.

SAXS measurements were performed at the beamline BM16 at the European Synchrotron Radiation Facility (Grenoble, France). Wave length of the X-ray beam was 0.980 Å. Detector calibration was done with silver behenate ($AgC_{22}H_{43}O_2$), and distance L was calculated from the scattering vector ($q=4\pi(\sin\theta)/\lambda$, λ=wave length, 2θ=scattering angle). Disc samples cut from films were placed in a Linkam hot stage and heated at 10ºC/min while the SAXS spectra were recorded. Calibration of temperature gave a difference of approximately 7ºC between the temperature reading at the hot stage display and the real temperature at the sample.

Thermomechanical (TMA) tests were performed in a Rheometric Scientific instrument model DMTA V. Rectangular test pieces of 3 mm width and 20 mm length were cut from films. A distance of 10 mm was set between fixation clamps. Runs were carried out from ambient temperature at 10ºC/min with a static stress of 3 MPa.

Tensile properties were measured in a MTS Synergie 200 testing machine equipped with a 100 N load cell. Rectangular test pieces of 5 mm width and 25 mm length were cut from films. A crosshead speed of 5 mm/min was used. Strain was measured from crosshead separation and referred to 10 mm initial length. At least six samples were tested for each polymer. Tests were conducted at room temperature and in some cases, when PEO was crystalline at ambient temperature, also at approximately 50ºC, as noted in the corresponding table. The samples were heated in situ by blowing hot air transversally to the cross-section side of the specimen in order to avoid stress on the sample. In this case, temperature was measured with a thermometer close to the specimen.

7.3 Results and discussion

7.3.1 Copoly(ether-imide)s imidization

Polyethyleneoxide chains are prone to oxidation [29], and therefore, a great care was taken to carry out the imidization. After the films were dried overnight, they were heated at 120ºC for 6 h to almost completely remove the solvent, and infrared spectra were recorded to check for the progress of imidization. Once treated at 120ºC, the polymer films became insoluble in any organic solvent.

Under the commented protocol, membranes with polyether ratios 4/1 and 6/1 were completely imidized according to their FTIR spectrum, but the films with polyether ratios 2/1 and 1/1 did not undergo a full imidization. These latter films were totally imidized (within the detection limits of the FTIR technique) after a further heating at 160ºC during two additional hours. In figure 1, the FTIR spectra of copolyimide BPDA 1/1 and its corresponding poly(amic acid) precursor are shown.

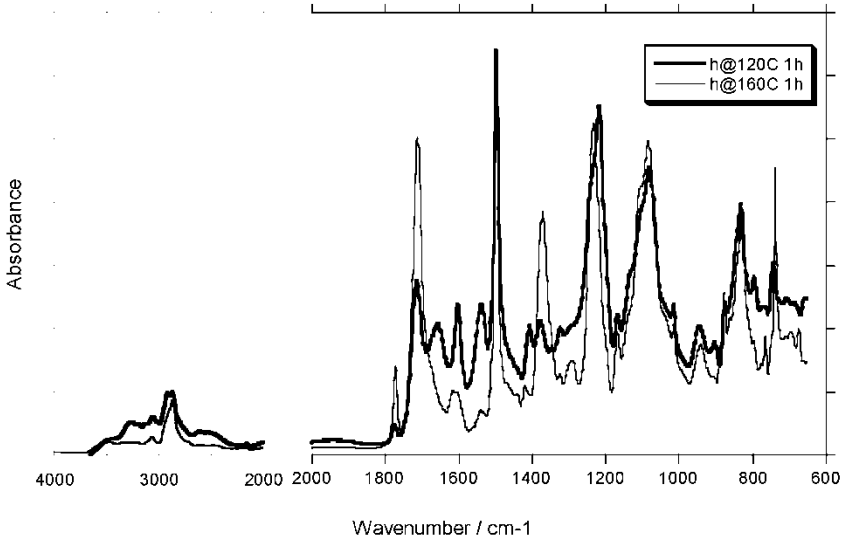

Figure 1. FTIR spectra of copolymer BPDA 1/1 before imidization (thick line) and after the thermal treatment at 160ºC for 2h (thin line).

In this figure, the bands centered around 3257, 2500, 1657, 1603 and 1538 cm^{-1} strongly decrease or disappear, and the bands at 1774, 1713, 1372 and 738 cm^{-1} increase or appear with imidization. The band at approximately 738 cm^{-1} is identificative of BPDA derived imides, and can be found in between 738-742 cm^{-1} in all copolyimides based on BPDA dianhydride [30]. For the BKDA series, a band appears in the FTIR spectrum at 720 cm^{-1} due to imidization. This band is actually broader than that appearing at 738 cm^{-1} due to the BPDA derived imides. The rest of the infrared spectra are

almost identical for both series except for the peak at 1667 cm^{-1} that appears in the BKDA series, due to the ketone group linking the aromatic rings in the dianhydride.

7.3.2 Thermal Stability

Thermogravimetric analysis was performed to evaluate the thermal stability of the synthesized copolymers. Dynamic runs in High-Resolution mode, in a nitrogen atmosphere, showed a weight loss pattern consisting of four consecutive steps (see figure 2): an initial loss of up to 2% weight from ambient temperature to 100ºC; a second loss from 100 to 250ºC; a third loss from 250 to approximately 450ºC; and a fourth loss from 450 to 800ºC.

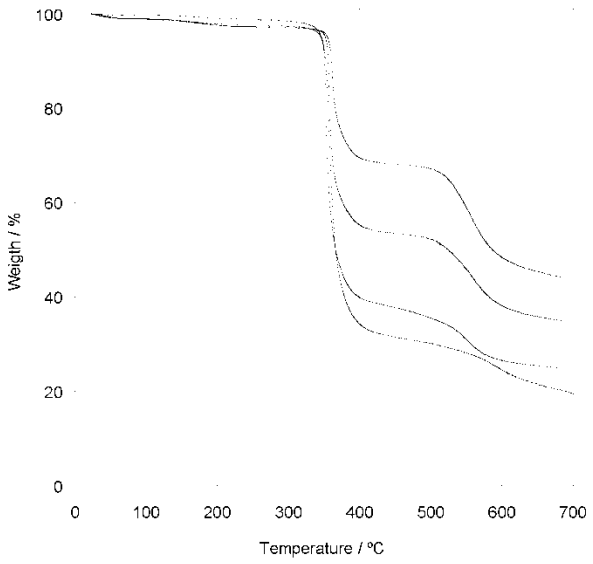

Figure 2. TGA curves in dynamic conditions for copolymers of series BPDA. From top to bottom: 1/1 (treated at 160ºC); 2/1 (treated at 120ºC); 4/1 (treated at 120ºC); 6/1 (treated at 120ºC).

The first loss can be attributed to the adsorbed water in the sample. The second step is thought to be due to both the water from imidization and the solvent trapped in the film. This weight change is very large (4 to 6 % weight) for the 1/1 copolymers, which were partially imidized as exhibited by FTIR. This weight loss step is substantially reduced (to less than 2%) for these copolymers after 2 h treatment at 160ºC. For the rest of the copolymers, this weight loss is also low. If incomplete imidization was the only source for this second weight loss, simple calculations would give a percentage of imidization for the samples treated at 120ºC of 39 to 74%, which is not true based on the FTIR results, that clearly showed that all these samples were virtually fully imidized. The third

loss step, after correcting for the two previous weight decrease steps, agrees with the theoretical contribution of polyethyleneoxide bis(amine) 6000 entering the copolymer composition, within a 2% error (see Table 2) and it is therefore assigned to the loss of polyether block sequences. The fourth and final stage of weight loss is due to the thermal decomposition of the remaining aromatic polyimide segments.

Table 2. Total polyether weight loss obtained by TGA for the prepared copolymers.

Copolymer	**Theoretical polyether weight in the copolymer (%)**	**Experimental polyether weight loss (%)**
BPDA 1/1	30.0	29.8
BPDA 2/1	45.7	45.2
BPDA 4/1	61.9	61.2
BPDA 6/1	70.2	68.5
BKDA 1/1	28.8	28.3
BKDA 2/1	44.2	43.8
BKDA 4/1	60.4	60.3
BKDA 6/1	68.9	69.1

Thus, TGA analysis confirmed that the polyether thermal stability is much lower than the thermal stability of the aromatic polyimide segments, and therefore a selective degradation of the polyether moiety could be performed in these copolymers. Isothermal experiments in nitrogen showed that at temperatures above 325ºC, the PEO chains completely broke down, and that the evolution proceeded faster at higher temperatures. For copolymer BPDA 2/1 for example, heating at 375ºC for 2 h was enough to reach the plateau; at 325ºC, at least 24 h were necessary; and at 300ºC, PEO rests were not completely removed after 60 h. When the plateau was reached, at least 97% of the initial polyether had been removed. The absence of the bands at 2925 and 2854 cm^{-1} in the FTIR spectra of the samples degraded isothermally until the plateau was reached, confirmed the loss of polyether segments.

As mentioned, the copolymers were stable below 300ºC for long times in a nitrogen atmosphere, however, this is totally different in an atmosphere containing oxygen. Actually, a high degree of degradation was observed in air well below this temperature. It is known that polyethers are prone to oxidation [29,31], and these copolymers showed the expected sensitivity to oxygen, not only at high temperatures, but also when undergoing relatively moderate temperatures for long times. In

Figure 3, the isothermal experiment at 160ºC for copolymer BPDA 2/1 is presented. As it can be seen, after an induction period of approximately 17 h, a sharp decay in weight takes place. In a simple experiment, samples of copolymers BKDA 1/1 and BKDA 2/1 were heated for 2 h at several temperatures in nitrogen and in air atmosphere. In Figure 4, the results for the BKDA sample with the 1/1 composition are displayed. It is clear that in nitrogen, temperatures above 300ºC are necessary for a significant breakdown of the PEO chains, whereas in air, a high degree of degradation takes place well below this temperature. The same behavior was observed for copolymer 2/1 when it was subjected to the same thermal treatments in air and in nitrogen.

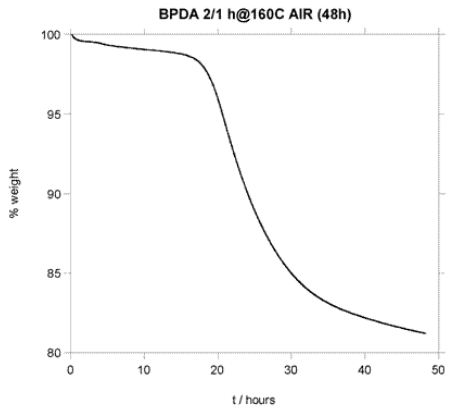

Figure 3. TGA isothermal curve of copolymer BPDA 2/1 at 160ºC in air.

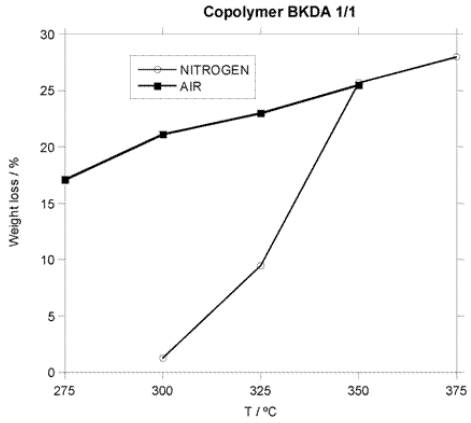

Figure 4. Weight loss for copolymer BKDA 1/1 after thermal treatment at several temperatures for 2 h in air and in nitrogen atmosphere.

7.3.3 Calorimetric Studies

The samples were heated in a DSC instrument with a cyclic method in order to monitor the changes in thermal properties with thermal treatment. In figure 5, the DSC traces show the increase in the PEO melting endotherm after several "instantaneous" treatments for copolymer BPDA 2/1. Eventually, step by step, a curve with the developed crystallinity for PEO vs. "instantaneous" thermal treatment could be built for all copolymers. The melting enthalpy of PEO was taken from literature as 8.67 KJ/mol [32]. In Figures 6 and 7 the results are shown for both the BKDA and BPDA series.

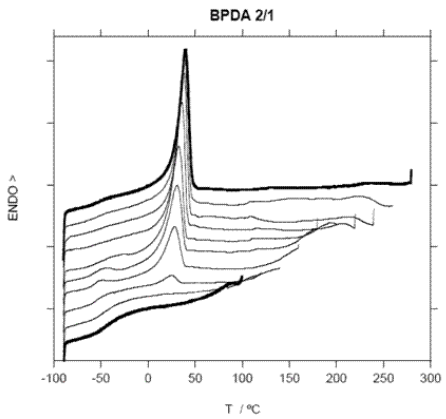

Figure 5. DSC curves for copolymer BPDA 2/1 after "instantaneous" treatment at (from bottom to top): 80, 100, 120, 140, 160, 180, 200, 220, 240 and 260ºC.

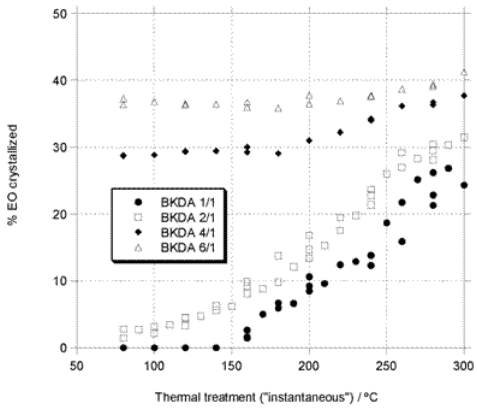

Figure 6. Crystallinity of the PEO segments for the BKDA series as a function of temperature.

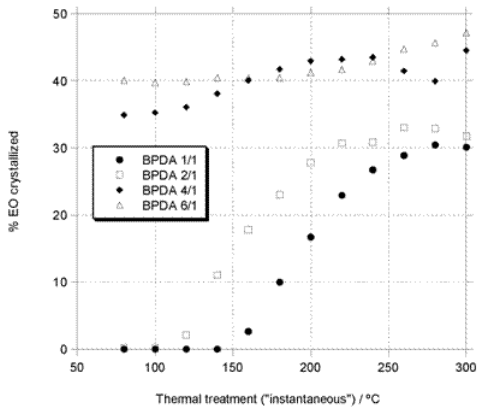

Figure 7. Crystallinity of the PEO segments for the BPDA series as a function of temperature.

From these figures it is apparent, within each series, that for 4/1 and 6/1 copolymers the PEO content is high enough to segregate in a pure phase and to achieve a relatively high crystallinity degree from the beginning. It can be also observed that the higher the PEO content, the higher the crystallinity developed in the BKDA series. The copolymers 1/1 and 2/1, initially with no crystallinity (or only a very small one for BKDA 2/1) after film preparation at 120ºC, started to develop a noticeable crystallinity above approximately 120ºC for 2/1 copolymers and 150ºC for 1/1 copolymers. For copolymers of higher PEO content, a slight increase of crystallinity was also observed at higher temperatures.

When comparing both series, the crystallinity obtained for the copolymers of the same PEO content was slightly higher for the BPDA series. In the copolymers with lower PEO content, those with compositions 1/1 and 2/1, the crystallinity built up more rapidly for the BPDA series. This result can be interpreted as due to a higher thermodynamic incompatibility between the aromatic polyimide segments and the PEO segments for the BPDA series.

For all copolymers, the crystallinity development was simultaneous to the second weight loss found in the TGA experiments, which was presumed to be due to the splitting off of both water caused by the completion of the imidization and residual solvent trapped in the film.

For the lower PEO content copolymers, 1/1 and 2/1, the calorimetric results were consistent with a system of partially mixed PEO and aromatic polyimide segments that, when heated, was driven by the release of residual solvent and completion of imidization towards a more perfectly phase separated system, where part of the PEO segments segregated in a completely pure domain which was able to crystallize. For the higher PEO content copolymers, 4/1 and 6/1, the pure PEO domains

were obtained just from the beginning in a relatively high extent, but higher temperatures were needed to improve phase separation on these systems.

Table 3. Maximum of the endotherm and % of crystalline PEO after heating at 300ºC.

Copolymer	**Polyether content (%)**	**Maximum (ºC)**	**Crystalline PEO (%)**
BPDA 1/1	30.0	37	30
BPDA 2/1	45.7	42	32
BPDA 4/1	61.9	48	44
BPDA 6/1	70.2	51	47
BKDA 1/1	28.8	34	24
BKDA 2/1	44.2	38	31
BKDA 4/1	60.4	45	38
BKDA 6/1	68.9	49	41

The values for the maximum of the melting peak and the percentage of crystalline PEO, after "instantaneous" treatment at 300 ºC, are listed in Table 3. Within each series, on increasing the PEO content the maximum of the melting endotherm and the percentage of crystalline PEO increased. This is most probably due to the restrictions imposed by the rigid polyimide segments, which are more important when its content in the copolymers increases. This fact brings about a more confined environment which disturbs PEO crystallization, resulting in a lower amount of PEO chains free to crystallize and a smaller size of the crystals.

When compared with data reported in the literature, it could be confirmed that, as expected, the melting maxima and the percentage of crystalline PEO were higher for the current copolymers than for PEO-containing block copolymers with a shorter PEO length of approximately 2000 g/mol [14,18,20,22,33-35]. For other systems, when the length of the PEO chain rose to 3400 g/mol or more, the values approach the results we have obtained only when the PEO content in the copolyester [22] and copolyamides [35] were higher than 75 %. For PEO-containing copolyimides, in networks treated at 250 ºC for 1 hour and PEO chains of 3400 g/mol, the maximum percentage of crystalline PEO reached a 30 % for a 80 % PEO content [36], and in the case of linear BPDA and ODA based copoly(ether-imide) treated at 170 ºC for 20 hours with PEO sequences of approximately 9000 g/mol and a 62 % of PEO, endotherm maximum was found at 25 ºC [37], well below our values.

Taking into account these antecedents, it appears evident that the current copolymers, after appropriate thermal treatment, achieve better phase separation than the block copolymers reported in literature so far. Although the existence of a pure PEO phase is clearly proved by these results, it is impossible to establish anything on the composition of the rest of the system by calorimetric studies. It could consist of a homogeneous phase of mixed aromatic polyimide segments and the PEO segments not involved in the formation of PEO crystalline domains, or it could comprise polyimide rich domains with a broader or sharper interface in between both domains. No transition was found for the possible aromatic polyimide segments by DSC, and nothing can be concluded at this point about the nature of the phases other than the pure segregated PEO domains.

7.3.4 Small Angle X-ray Scattering

X-ray scattering experiments were performed at a synchrotron radiation source in order to follow, in real-time conditions, the development of the phase separated structure in these copolymers. In figure 8, the evolution of the scattering (Iq^2 vs. q) with increasing temperature for copolymer BPDA 2/1 is shown as an example. Samples used for SAXS analysis were taken from the films treated at 120 ºC for 6 hours. A single broad peak was obtained when the sample showed scattering. Two parameters were calculated over the scattering curve: the relative invariant, Q', as the integral below the curve Iq^2 vs. q in between the detector limits, related to the extent of the phase separation; and the maximum on the scattering curve, q_{max}, related to the size scale of the separated phases, calculated also from the curve Iq^2 vs. q. It is known that for lamellar systems the length scale (L) of the phase separation can be calculated directly from the curve Iq^2 vs. q, while for other morphologies a calculation of L from the I vs. q curve gives more realistic results [38]. For the current copolymers, we do not investigated if a lamellar morphology is present, but we are more interested on the changes with temperature than on the absolute values, and the representation Iq^2 vs. q highlights the maximum and makes it easier to detect, especially when using automated macros for the processing of the huge amount of data generated in a synchrotron experiment. Therefore this will be the criterion used here to get information on the L value.

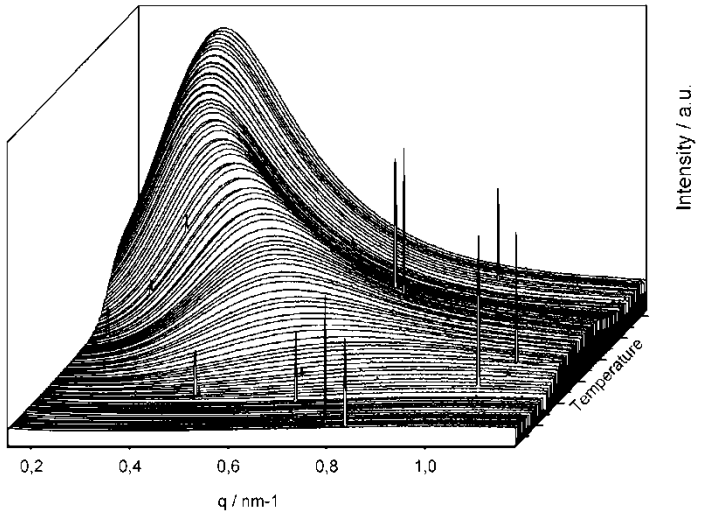

Figure 8. Evolution of the Iq^2-q curves with temperature for copolymer BPDA 2/1.

The obtained results for Q' and q_{max}, after data treatment, are represented in figures 9 to 16. For the BPDA copolymers with compositions 4/1 and 6/1 (figures 13 and 14), the cooling ramp has also been depicted to show the effect of temperature on Q' and q_{max} when no changes on the morphology are taking place. It is evident that the increase in temperature, when there were no changes in the morphology of the system, produced a linear increase in Q' and a linear decrease in q_{max} (increase in L). The difference between the values on the heating ramp and on the cooling ramp gives the real change on the parameter for each temperature.

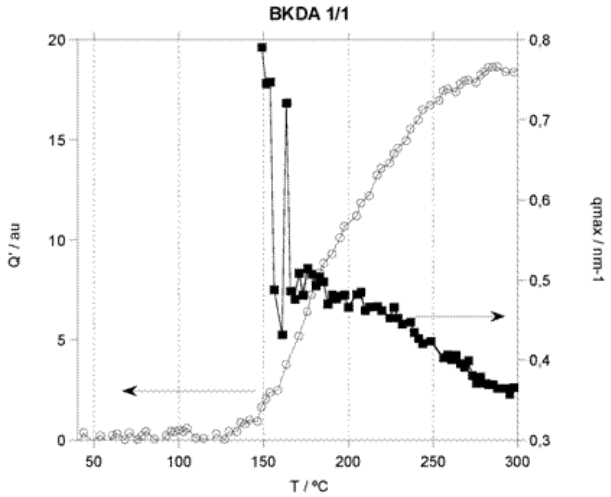

Figure 9. Changes in Q' and q_{max} with temperature for copolymer BKDA 1/1 when heated at 10ºC/min.

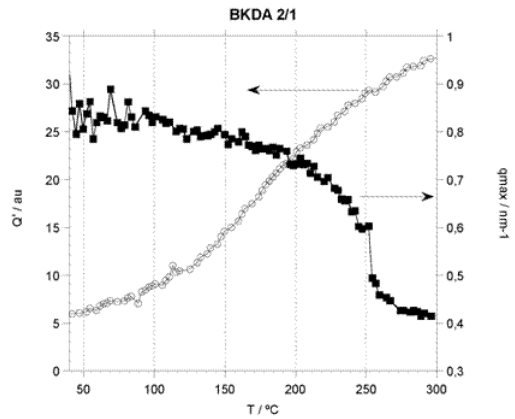

Figure 10. Changes in Q' and q_{max} with temperature for copolymer BKDA 2/1 when heated at 10ºC/min.

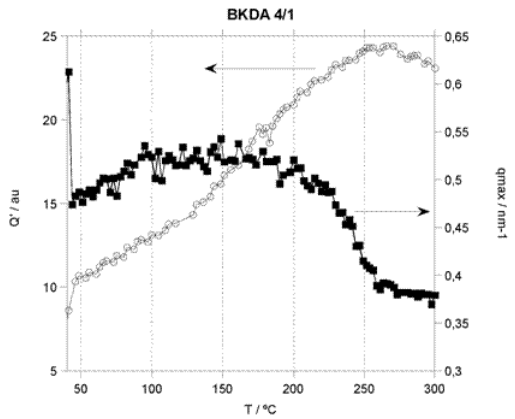

Figure 11. Changes in Q' and q_{max} with temperature for copolymer BKDA 4/1 when heated at 10ºC/min.

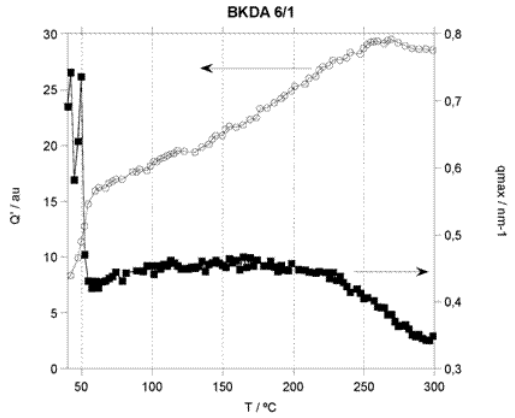

Figure 12. Changes in Q' and q_{max} with temperature for copolymer BKDA 6/1 when heated at 10ºC/min.

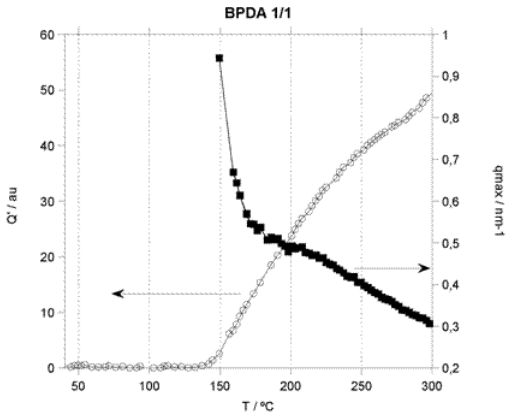

Figure 13. Changes in Q' and q_{max} with temperature for copolymer BPDA 1/1 when heated at 10ºC/min.

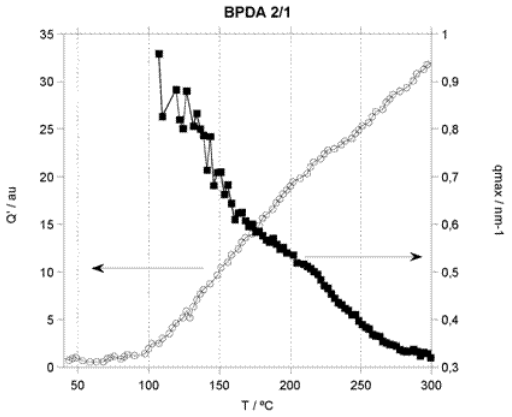

Figure 14. Changes in Q' and q_{max} with temperature for copolymer BPDA 2/1 when heated at 10ºC/min.

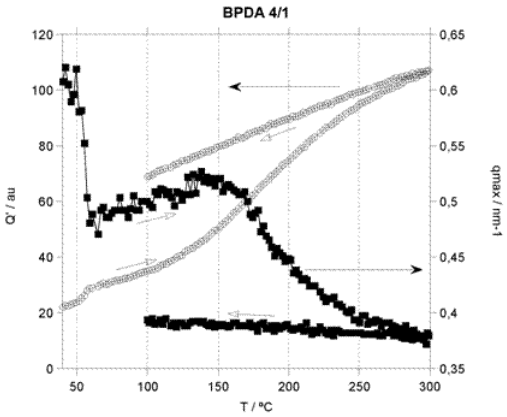

Figure 15. Changes in Q' and q_{max} with temperature for copolymer BPDA 4/1 when heated at 10ºC/min.

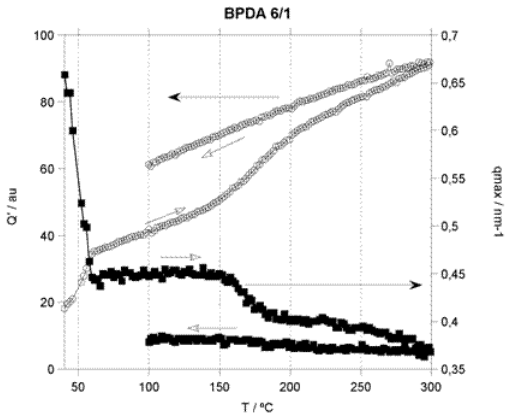

Figure 16. Changes in Q' and q_{max} with temperature for copolymer BPDA 6/1 when heated at 10ºC/min.

For 1/1 copolymers (figures 9 and 13), a defined maximum in the scattering did not appear until reaching a temperature of approximately 150ºC. At the same time that the maximum appeared, the relative invariant, Q' started to grow, and this growth was continuous until practically the maximum temperature of the test is reached, 300ºC. So, once the imidization had been completed and the residual solvent released, a process of phase separation started in the system and the extension and length scale of such separation increased with temperature.

For copolymers 2/1 (figures 10 and 14), above 150 ºC, the behavior was similar, with a steady growth of Q' and a decay of the scattering vector value in the maximum, q_{max}, above 200 ºC and up to approximately 270 ºC, when it practically leveled. For these samples, different to 1/1 samples, the imidization was practically completed, as tested by FTIR at 150 ºC, but as for the 1/1 samples, once the phase separation started at relatively low temperatures, the release of residual solvent was completed while the phase separation proceeds, and it progressed with increasing temperature.

The copolymers 4/1 (figures 11 and 15) and 6/1 (figures 12 and 16) showed an initial phase separated morphology. At low temperatures, around 50 ºC, an initial jump on Q' was detected due to the melting of the PEO crystals. Afterwards, the increase was linear due to the effect of the increase in temperature until approximately 130 ºC for copolymers 4/1 or 140 ºC for copolymers 6/1 and afterwards Q' grew more quickly. At higher temperatures, above 250 ºC, the Q' value decayed for BKDA samples as a consequence of the sample falling out of the holder; but BPDA samples were retained and showed that the growth in Q' was steady until 300 ºC. A significant difference in the response of the two series was that for the BPDA samples, the decay in q_{max} (increase in L) appeared at lower temperatures (above 150 ºC) than for the BKDA samples (above 200 ºC). This result can be interpreted as caused by a higher incompatibility of BPDA with PEO,

which leads to an increase in the length scale of the segregated phase at lower temperatures than for the BKDA samples. This incompatibility was also assumed when analyzing the DSC results.

Once the phase separation appears, with the simultaneous increase on Q' and appearance of a maximum in the scattering curve, the changes in Q' and q_{max} do not necessarily follow the same trend. Q', and therefore phase separation, steadily improved with temperature. However, q_{max} showed inflection points at temperatures when Q' did not show any relevant change. Although tentatively, the changes in q_{max} could be related to the glass transition of the aromatic polyimide segments. However, it should be note out that at this point of the discussion that there is not enough information to entirely explain the changes in q_{max}.

On comparing the SAXS and DSC results, a parallelism between PEO crystallinity and Q' behavior could be found. When crystallinity appeared, Q' started to grow, and when crystallinity increased, Q' increased. Only for copolymers BPDA 1/1 and 2/1, when high treatment temperatures were reached, above 240 ºC for BPDA 1/1 and above 220 ºC for BPDA 2/1, the crystallinity had almost leveled at a plateau whereas the relative invariant still grew. In figures 17 and 18, the PEO crystallinity is compared with the changes in Q' and L for the BKDA 2/1 sample to illustrate this statement.

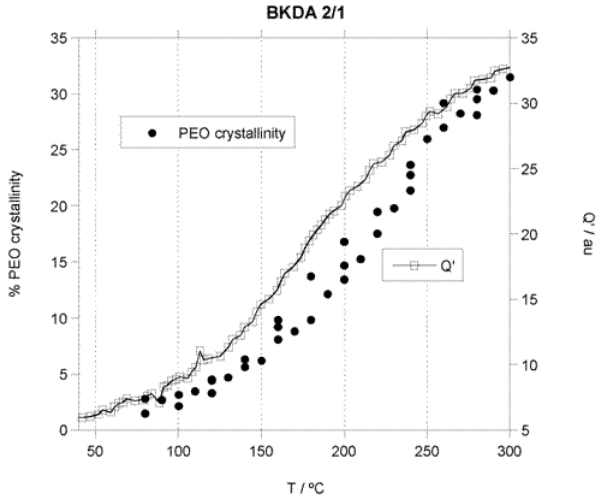

Figure 17. Development of PEO crystallinity compared with the changes in Q' with temperature for sample BKDA 2/1.

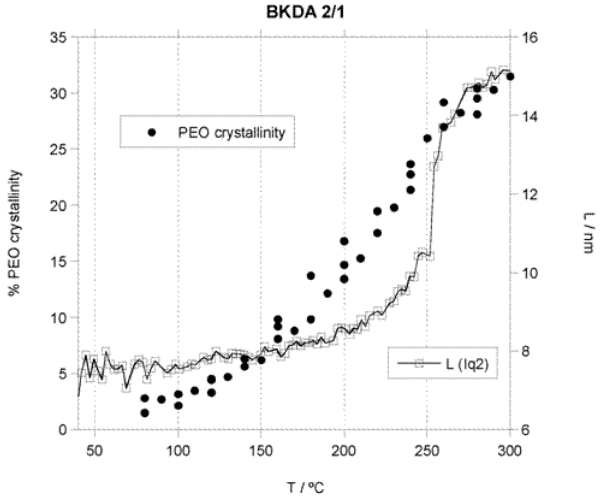

Figure 18. Development of PEO crystallinity compared with the changes in L with temperature for sample BKDA 2/1.

Therefore, for these copolymers, if temperature does not reach a value where degradation occurs, there is a direct relationship between the amount of developed PEO crystallinity and the extent of the phase separation in the system. When studying this type of copolymers, we can then use the amount of PEO crystallinity, at least up to relatively high temperatures, to semiquantitatively evaluate the phase separation achieved by the copolymer.

The size of the domains, L, after thermal heating at 300 ºC was calculated at room temperature from the I vs. q and Iq^2 vs. q curves, and they are listed on table 4. The values span from 20 to 26 nm when calculated from I curve, and from 15 to 22 nm when calculated from Iq^2 curve. These values are comparable to the values found in literature for similar PEO-containing block copolymers with lamellar morphology (comparison with Iq^2 vs. q column). Thus, authors found a 13 nm long spacing value for branched polyimide-PEO (2000 g/mol) [39], and 12-15 nm for aliphatic polyamide-PEO [21].

Apart from the expected higher values when the calculation is done on the plot, no trend was found on the data. Values were sometimes higher for BKDA copolymers and sometimes for BPDA copolymers when the counterparts were compared, and within a series, only for the BPDA series and for the values calculated from the Iq^2 curve a decay appeared in length spacing with the increase on PEO content.

Table 4. Long spacing values measured at ambient temperature after thermal treatment at 300ºC for the copolymers prepared

Copolymer	L / nm (I vs. q)	L / nm (Iq^2 vs. q)
BKDA 1/1	25.1[a]	16.8
BKDA 2/1	19.9	15.1
BKDA 4/1	22.5	16.3
BKDA 6/1	22.7	18.3
BPDA 1/1	25.1[a]	22.2
BPDA 2/1	23.3[a]	18.9
BPDA 4/1	26.3	17.6
BPDA 6/1	21.5	15.4

[a] For these samples, the maximum was not well defined in the scattered intensity and the error in the determination is quite high

7.3.5 Thermomechanical Analysis

Thermomechanical analysis has been also carried out in order to detect the glass transition temperature of the aromatic polyimide hard segments, which were not detected by DSC. Samples were heated at 180 ºC, 220 ºC and 260 ºC for 30 minutes, and the changes on the strain with temperature were measured. As an example, in figure 19, the curves for the copolymer BKDA 1/1 treated at the three mentioned temperatures can be seen.

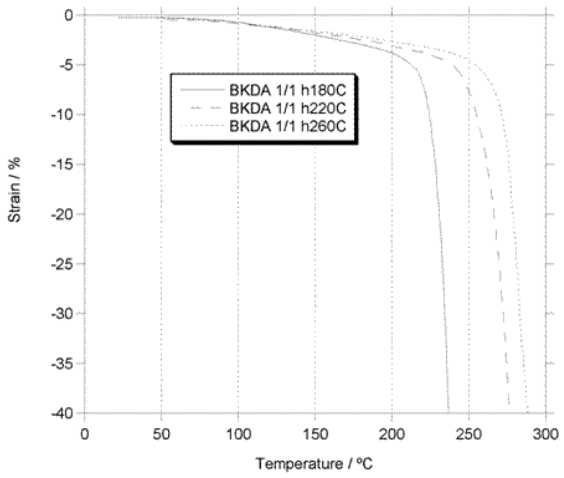

Figure 19. TMA curves for the copolymer BKDA 1/1 treated at several temperatures

Several criteria can be chosen to establish the seek transition temperature. For example, it could be taken as the minimum in the first derivative of the strain versus temperature curve, or the zero value in the second derivative. With the former criterion, the values are not clearly resolved, so that we decided to choose a different criterion, the temperature when strain is 10 times that of the sample at 100 ºC, which gives lower transition values than the other two mentioned criteria. The so obtained results are listed on Table 5.

Table 5. Polyimide hard segment glass transition temperature at different treatment temperatures

Copolymer	**180ºC, 30 m**	**220ºC, 30m**	**260ºC, 30 m**
BKDA 1/1	221 ºC	253 ºC	267 ºC
BKDA 2/1	242 ºC	246 ºC	266 ºC
BKDA 4/1	189 ºC[a]	184 ºC[a]	219 ºC[a]
BKDA 6/1	183 ºC	181 ºC	204 ºC
BPDA 1/1	220 ºC	239 ºC	243 ºC
BPDA 2/1	205 ºC	228 ºC	262 ºC
BPDA 4/1	191 ºC	175 ºC[a]	214 ºC[a]
BPDA 6/1	153 ºC[a]	83 ºC[a]	153 ºC[a]

[a] Sample broke before reaching the established criterion for the strain

For the BPDA 6/1 film, the sample was too thin and broke very early in the test. For the rest, even if the sample breaks before the criterion chosen for the glass transition was accomplished, it is clear that aromatic polyimide hard segment has a transition at temperatures over 175 ºC. The thermal treatment, as expected from the DSC and SAXS results, brought about an increase of the transition temperature. Although it was not possible to correlate directly the changes in q_{max} observed in SAXS with the glass transition of the polyimide segments, it seems clear that the transition temperatures followed the same trend as that observed for q_{max} with the temperature of treatment. This allowed to presume that there should be such a correlation.

Simple theoretical calculations of the polymerization process demonstrated that the length of the polyimide segments decreased when polyether content increased (see table 1). Therefore, in the case of completely phase separated systems, glass transition temperature of the polyimide segments should decrease when polyether content increases. This trend was clearly confirmed for BKDA treated at 220 ºC and at 260 ºC, and for BPDA treated at 180 ºC and at 220 ºC. Nevertheless, such a tendency is only approximately accomplished for BKDA treated at 180 ºC, and for BPDA treated at 260 ºC

Pure aromatic polyimides BKDA-ODA and BPDA-ODA were synthesized in a similar manner to copolyimides, and thermally imidized at 285 ºC for 1 hour. The thermomechanical analysis of this polyimides gave values for the glass transition temperature of 289 ºC and 305 ºC respectively (the corresponding values found in literature, measured by DSC, are 266 ºC [37] and 270 ºC [20] respectively). As expected, theses values are quite higher than those found here for the aromatic polyimide segments in the copolymers. This is very clearly associated to the much lower length of the aromatic polyimide segments in the copolymers, which does not reach the minimum value above which the transition temperature is independent of the length, and also because some polyether segments are mixed with the polyimide segments in the polyimide domains.

7.3.6 Mechanical Properties

The commented SAXS, DSC and thermomechanical studies have shown the changes produced in the morphology of the copolymers during thermal treatment and the changes in thermal properties. To complete the study on the physical properties of these copolyimides, mechanical properties were measured in tensile for the copolymers treated at various temperatures.

In table 6, the values for the imidized copolymers at 160 ºC for 1/1 and 120 ºC for 2/1, 4/1 and 6/1, are listed. For the sake of comparison, the results for the fully aromatic polyimides imidized at 285 ºC, are also included.

Table 6. Mechanical properties of the imidized copolymers and reference fully aromatic polyimides determined at room temperature. [a] Properties measured at approximately 50ºC.

Polymer	**BKDA-ODA**	**BKDA 1/1**	**BKDA 2/1**	**BKDA 4/1**	**BKDA 6/1**
Max.Stress (MPa)	134 ± 7	69 ± 2	21 ± 3	6.4 ± 1.5 *8.0 ± 0.7*[a]	2.0 ± 0.4 *3.1 ± 0.3*[a]
Strain (%)	62 ± 3	131 ± 17	4.5 ± 1.0	3.9 ± 1.2 *19 ± 4*[a]	1.3 ± 0.4 *20 ± 7*[a]
Modulus (GPa)	1.87 ± 0.09	1.24 ± 0.09	0.67 ± 0.04	0.31 ± 0.02 *0.154 ± 0.007*[a]	0.59 ± 0.06 *0.055 ± 0.003*[a]
Polymer	**BPDA-ODA**	**BPDA 1/1**	**BPDA 2/1**	**BPDA 4/1**	**BPDA 6/1**
Max.Stress (MPa)	1.40 ± 30	77 ± 10	31 ± 2	12.6 ± 1.3 *6 ± 2*[a]	1.6 ± 0.7 *3.8 ± 0.2*[a]
Strain (%)	34 ± 20	210 ± 110	10 ± 3	12 ± 3 *37 ± 16*[a]	0.61 ± 0.3 *25 ± 5*[a]
Modulus (GPa)	2.5 ± 0.4	1.13 ± 0.10	0.71 ± 0.05	0.37 ± 0.05 *0.150 ± 0.012*[a]	0.51 ± 0.18 *0.068 ± 0.006*[a]

In general, the mechanical properties are good for copolymers 1/1 and 2/1, fair for copolymers 4/1 and poor for copolymers 6/1. As expected, the maximum stress decreased when PEO content increased.

Referring to the strain, except for the reference fully aromatic polyimides and the copolymers with ratio 1/1, where the curve showed a yielding point followed by a quasi-plateau, for the rest of the copolymers the strain value was small and the sample broke at the value of maximum stress. Strain value was especially small for the 6/1 copolymers, where the high crystallinity of the polyether chains and the low content of aromatic polyimide produced a very brittle copolymer.

The values of the modulus followed the same trend as the maximum stress except for the 6/1 copolymers. In this case, the high crystallinity of PEO chains increased the value of the modulus above the value for 4/1 copolymers. If the tensile tests are carried out at approximately 50ºC for 4/1 y 6/1 copolymers, all polyether chains have melted and are amorphous (it must be remarked that for gas separation, PEO chains have to be amorphous because crystalline PEO is known to present a very low permeability [24,25]), and the elastic moduli will be comparable to the rest of the copolymers, where PEO chains are not crystallized. In this way, and as presumed, when polyether chains are melted, the modulus follows the expected trend, decreasing when polyether content increases. Copolymers 4/1 and 6/1 became soft when PEO chains melted and the strain was increased and the modulus reduced, very strongly for copolymers 6/1.

Mechanical properties were also measured for copolymers 1/1 and 2/1 treated at 180 ºC, 220 ºC and 260 ºC for 30 minutes in nitrogen atmosphere and the corresponding results are shown in table 7. For copolymers 4/1 and 6/1, with reduced mechanical properties, we only measured mechanical properties for different thermal treatments for the series for BKDA and the samples were tested at approximately 50 ºC to avoid the effect of PEO crystallinity.

Apart from some unexpected results, such us the low strain value for BKDA 2/1 and BPDA 2/1 treated at 220 ºC and BKDA 6/1 treated at 180 ºC, the mechanical properties did not change significantly with thermal treatment, probably because there are no significant differences in phase separation upon annealing. Thermal treatment at 180 ºC for 30 minutes was probably enough to achieve a very high degree of phase separation, and a higher temperature did not improve it substantially.

Table 7. Properties of copolymers treated at three different temperatures for 30 minutes.

Copolymer	**BKDA 1/1**			**BKDA 2/1**		
$T_{treatment}$ (ºC)	**180**	**220**	**260**	**180**	**220**	**260**
$Stress_{max.}$ (MPa)	69 ± 3	69 ± 4	69 ± 5	36 ± 7	36 ± 3	39 ± 6
Strain (%)	160 ± 50	150 ± 40	130 ± 20	290 ± 60	80 ± 20	280 ± 40
Modulus (GPa)	1.18 ± 0.08	1.21 ±0.07	1.17 ± 0.06	0.64 ± 0.03	0.66 ± 0.01	0.63 ± 0.04
Copolymer	**BPDA 1/1**			**BPDA 2/1**		
$T_{treatment}$ (ºC)	**180**	**220**	**260**	**180**	**220**	**260**
$Stress_{max.}$ (MPa)	75 ± 4	76 ± 8	77 ± 14	47 ± 4	44 ± 3	55 ± 6
Strain (%)	97 ± 30	110 ± 30	110 ± 16	197 ± 15	70 ± 20	206 ± 15
Modulus (GPa)	1.16 ± 0.08	1.16 ± 0.05	1.10 ± 0.10	0.73 ± 0.09	0.87 ± 0.13	0.70 ± 0.13
Copolymer	**BKDA 4/1[a]**			**BKDA 6/1[a]**		
$T_{treatment}$ (ºC)	**180**	**220**	**260**	**180**	**220**	**260**
$Stress_{max.}$ (MPa)	14 ± 4	12 ± 2	18 ± 4	11 ± 2	10 ± 3	13 ± 2
Strain (%)	640 ± 130	420 ± 110	500 ± 150	14 ± 2	420 ± 40	430 ± 30
Modulus (GPa)	0.161 ± 0.009	0.158 ± 0.010	0.042 ± 0.010	0.052 ± 0.014	0.052 ± 0.010	0.027 ± 0.06

[a] Properties measured at approximately 50 ºC

7.4 Conclusions

A new series of copoly(ethylene oxide-imide)s with long poly(ethylene oxide) segments (6000 g/mol) have been synthesized and characterized in terms of morphology and physical properties.

Complete imidization was achieved at relatively low temperatures (120-160 ºC). This is an evident processing advantage respect to fully aromatic polyimides, for which very high temperatures, generally above 300 ºC, are necessary to achieve almost complete imidization.

These copolymers are stable in nitrogen up to high temperatures, whereas in an oxygen containing atmosphere, degradation takes place at relatively low temperature.

Phase separation, measured as the PEO segments crystallinity, increases with the increase of PEO content in the copolymer, and after treatment at high temperature below degradation temperature, the achieved phase separation increases.

SAXS experiments confirm DSC results and show evidence of phase separation with thermal treatment. For all copolymers, either with no initial phase separation (PEO content 30 % and 45 %) or initially phase separated (60 % and 70 %), domain segregation starts or improves when heated above 150 ºC, which is coincident with the release of the trapped solvent, and the completion of the imidization in the case of the copolymers with the lowest PEO content. At certain temperature, that can be ascribed to the glass transition temperature of the hard polyimide segments, phase separation rate increases. Phase segregation appears slightly earlier for BPDA than for BKDA, and the annealed samples show a slightly better phase separation, due to the higher thermodynamic incompatibility of PEO and BPDA based polyimides. Phase separation scale is 15-20 nm, of the order of similar PEO-containing block copolymers found in literature.

The glass transition temperatures for the aromatic polyimide segments, detected by TMA, were above 150 ºC for the copolymers with high PEO content and above 200 ºC for those with lower PEO content. Thus, it seems clear that thermal treatment increases the transition temperature of the hard domains, which seems to demonstrate that phase separation process also changes the hard segment domains.

As expected, mechanical properties depend on the PEO content, with poorer properties for copolymers with increasing PEO content. The properties resulted good for copolymers with lower PEO content, 30 % and 45 %, fair for 60 % PEO, and poor for 70 % PEO. Thermal treatment at 180 ºC for 30 minutes seems to be enough for a very good phase separation, and thermal treatments at higher temperatures do not have a significant effect on the mechanical properties.

The series of copoly(ether-imide)s prepared in this work have a phase separated morphology and physical properties able to be modulated by thermal treatments, that make them interesting candidates for membranes for CO_2 gas separation applications.

7.5 Acknowledgements

We are indebted to the Spanish Junta de Castilla León for their financing of this work through the GR-18 Excelence Group Action and to the Ministry of Science and Innovation in Spain for their economic support of the work (MAT2008-00619/MAT) and the access to the synchrotron radiation source (experiments 16-2-11 and 16-2-21) in the European Synchrotron Radiation Facility (ESRF)

in Grenoble (France). We are grateful to Dr. Ana Labrador and Dr. François Fauth for their help at BM16 station at the ESRF. A. Tena thanks CSIC for the predoctoral JAE fellowship received to carry out this work. Authors also acknowledge financial support from the programme CONSOLIDER, project Multicat.

7.6 References

1. L.M. Robeson, Correlation of separation factor versus permeability for polymeric membranes, J. Membr. Sci. 62 (1991) 165–185.
2. K. Tanaka, H. Hita, M. Okano and K. Okamoto, Permeability and permselectivity of gases in fluorinated and non-fluorinated polyimides, Polymer, 33 (1992) 585–592.
3. K.Okamoto,K. Tanaka, H. Kita, M. Ishida, M. Kakimoto,Y. Imai, Gas-permeability and permselectivity of polyimides prepared from 4,4_diaminotriphenylamine, Polym. J. 24 (1992) 451–457.
4. K. Tanaka, M. Okano, H. Kita, K. Okamoto, S. Nishi, Effects of trifluoromethyl side-groups on gas-permeability and permselectivity in polyimides, Polym. J. 26 (1994) 1186–1189.
5. H.B. Park, C.H. Jung, Y.M. Lee, A.J. Hill, S.J. Pas, S.T. Mudie, E. Van Wagner, B.D. Freeman, B.S. Cookson. Science, 318, (2007), 254-258.
6. S.H. Han, J.E. Lee, K-J. Lee, H.B. Park, Y.M. Lee, Highly gas permeable and microporous polybenzimidazole membrane by thermal rearrangement, J Membr Sci, 357, (2010), 143-151.
7. H.B. Park, S.H. Han, C.H. Jung, Y.M. Lee, A.J. Hill, Thermally rearranged (TR) polymer membranes for CO_2 separation, J Membr Sci, 359, (2010), 11-24.
8. K. Okamoto, N. Yasugi, T. Kawabata, K. Tanaka, H. Kita, Selective permeation of carbon dioxide through amine-modified polyimide membranes, Chem. Lett. 8 (1996) 613–614.
9. C. Staudt-Bickel, W.J. Koros, Improvement of CO_2/CH_4 separation characteristics of polyimides by chemical crosslinking, J. Membr. Sci. 155 (1999) 145–154.
10. K. Ghosal, R.T. Chen, B.D. Freeman, W.H. Daly, I.I. Negulescu, Effects of basic substituents on gas sorption and permeation in polysulfone, Macromolecules 29 (1996) 4360–4369.
11. M. Kawakami, H. Iwanaga, Y. Hara, M. Iwamoto, S. Kagawa, Gas permeabilities of cellulose nitrate/poly(ethylene glycol) blend membranes, J. Appl. Polym. Sci. 27 (1982) 2387–2393.
12. J.T. Li, K. Nagai, T. Nakagawa, S.Wang, Preparation of polyethyleneglycol (PEG) and cellulose–acetate (CA) blend membranes and their gas permeabilities, J. Appl. Polym. Sci. 58 (1995) 1455–1463.

13. H. Lin, B.D. Freeman, Gas solubility, diffusivity and permeability in poly(ethylene oxide), J. Membr. Sci. 239 (2004) 105–117.
14. M. Yoshino, K. Ito, H. Kita, K. Okamoto, Effects of hard-segment polymers on CO_2/N_2 gas-separation properties of poly(ethylene oxide)-segmented copolymers, J. Polym. Sci., Part B: Polym. Phys. 38 (2000) 1707– 1715.
15. H. Suzuki, K. Tanaka, H. Kita, K. Okamoto, H. Hoshino, T. Yoshinaga, Y. Kusuki, Preparation of composite hollow fiber membranes of poly(ethylene oxide)- containing polyimide and their CO_2/N_2 separation properties, J. Membr. Sci. 146 (1998) 31–37.
16. Y. Hirayama, Y. Kase, N. Tanihara, Y. Sumiyama, Y. Kusuki, K. Haraya, Permeation properties to CO_2 and N_2 of poly(ethylene oxide)-containing and crosslinked polymer films, J. Membr. Sci. 160 (1999) 87–99.
17. V.I. Bondar, B.D. Freeman, I. Pinnau, Gas sorption and characterization of poly(ether-*b*-amide) segmented block copolymers, J. Polym. Sci., Part B: Polym. Phys. 37 (1999) 2463–2475.
18. V.I. Bondar, B.D. Freeman, I. Pinnau, Gas transport properties of poly(ether*b*- amide) segmented block copolymers, J. Polym. Sci., Part B: Polym. Phys. 38 (2000) 2051–2062.
19. K. Okamoto, N. Umeo, S. Okamyo, K. Tanaka, H. Kita, Selective permeation of carbon dioxide over nitrogen through polyethyleneoxide-containing polyimide membranes, Chem. Lett. (1993) 225–228.
20. K. Okamoto, M. Fujii, S. Okamyo, H. Suzuki, K. Tanaka, H. Kita, Gas permeation properties of poly(ether imide) segmented copolymers, Macromolecules 28 (1995) 6950–6956.
21. V. Barbi, S.S. Funari, R. Gehrke, N. Scharnagl, N. Stribeck, SAXS and the gas transport in polyether-block-polyamide copolymer membranes, Macromolecules 36 (2003) 749-758.
22. S.J. Metz, W.H.V. Mulder, M. Wessling, Gas-permeation properties of poly(ethylene oxide) poly(butylenes terephtalate) block copolymers, Macromolecules 37 (2004) 4590-4597.
23. D. Husken, T. Visser, M. Wessling, R.J. Gaymans, CO_2 permeation properties of poly(ethylene oxide)-based segmented block copolymers, J. Membr. Sci. 346 (2010) 194-201.
24. H. Lin, E. Van Wagner, J.S. Swinnea, B.D. Freeman, S.J. Pas, A.J. Hill, S. Kalakkunnath, D.S. Kalika, Transport and structural characteristics of crosslinked poly(ethylene oxide) rubbers, J. Membr. Sci. 276 (2006) 145-161.
25. H. Lin, T. Kai, B.D. Freeman, S. kalakkunnath, D.S. Kalika, The effect of cross-linking on gas permeability in cross-linked poly(ethylene glycol diacrylate), Macromolecules 38 (2005) 8381-8393.

26. H. Lin, B.D. Freeman, Gas and vapour solubility in cross-linked poly(ethylene glycol diacrylate), Macromolecules 38 (2005) 8394-8407.
27. E.M. Maya, D.M. Muñoz, J.G. de la Campa, J. de Abajo, A.E. Lozano, Thermal effect on polyethyleneoxide-containing copolyimide membranes for CO_2/N_2 separation, Desalination 199 (2006) 188–190.
28. D.M. Muñoz, E.M. Maya, J. de Abajo, J.G. de la Campa, A.E. Lozano, Thermal treatment of poly(ethylene oxide)-segmented copolyimide based membranes: An effective way to improve the gas separation properties, J. Membr. Sci. 323 (2008) 53-59.
29. J. Scheirs, S.W. Bigger, O. Delatycki, Characterizing the solid-state thermal oxidation of poly(ethylene oxide) powder, Polymer, 32 (1991), 2014-2019
30. This band is also found in BPDA copolyimides that we have synthesized with 6F diamine, and with poly(propylene oxide)s D4000, D2000, and poly(ethylene oxide)s ED2003, ED900 (Jeffamines).
31. G. Gallet, S. Carroccio, P. Rizzarelli, S. Karlsson, Thermal degradation of poly(ethylene oxide–propylene oxide–ethylene oxide) triblock copolymer: comparative study by SEC/NMR, SEC/MALDI-TOF-MS and SPME/GC-MS, Polymer, 43, (2002), 1081-1094.
32. Van Krevelen DW. Properties of polymers. 3rd ed. Amsterdam: Elsevier Science; 1990 p. 120.
33. A. Arun, R.J. Gaymans, Hydrophilic poly(ethylene oxide)-aramide segmented block copolymers, Eur. Polym J., 45 (2009) 2858-2866.
34. M.A.B. Meador, V.A. Cubon, D.A. Scheiman, W.R. Bennett, Effect of branching on rod-coil block polyimides as membrane materials for lithium polymer batteries, Chem. Mater., 15 (2003) 3018-3025.
35. D. Husken, J. Feijen, R.J. Gaymans, Segmented block copolymers with terephtalic-extended poly(ethulene oxide) segments, Macromol. Chem. Phys, 209 (2008) 525-534.
36. S. Kripotou, P. Pissis, P. Sysel, V. Sindelar, V.A. Bershtein, Structure-property relationships in novel poly(imide-amide)-poly(ethylene glycol) hybrid networks, Polymer 47 (2006) 357-366.
37. J. Fang, K. Tanaka, H. Kita, K.-I. Okamoto, Y. Ito, Positron annihilation properties of copolyimides and copolyamides with microphase-separated structures, J. Polym. Sci., Polym. Phys., 38 (2000) 1123-1132
38. F.S. Baltá-Calleja, C.G.Vonk, X-ray scattering of synthetic polymers. Amsterdam: Elsevier, 1989.
39. C. Xue, M.A.B. Meador, L. Zhu, J.J. Ge, S.Z.D. Cheng, S. Putthanarat, R.K. Eby, A. Khalfan, G.D. Bennett, S.G. Greenbaum, Morphology of PI-PEO block copolymers for lithium batteries, Polymer 47 (2006) 6149-6155.

CHAPTER 8

On the influence of the proportion of PEO in thermally controlled phase segregation of copoly(ether-imide)s for gas separation

Alberto Tena[1,3], Ángel Marcos-Fernández[1,3], Laura Palacio[1,2], Pedro Prádanos[1,2], Ángel E. Lozano[1,3], Javier de Abajo[1,3], Antonio Hernández[1,2]

[1]*Smap UA-UVA-CSIC, Parque Científico Universidad de Valladolid, Paseo de Belén, s/n, 47011 Valladolid, Spain.*

[2]*Dept. Física Aplicada, Facultad de Ciencias, Universidad de Valladolid, Paseo de Belén, 7, 47011 Valladolid, Spain*

[3]*Instituto de Ciencia y Tecnología de Polímeros, CSIC, Juan de la Cierva 3, 28006 Madrid, Spain.*

This chapter has been published in:

Journal of Membrane Science 434 (**2013**) 26-34

DOI: http://dx.doi.org/10.1016/j.memsci.2013.01.036

Abstract

A complete series of aliphatic aromatic copoly(etherimide)s, based on an aromatic dianhydride (BPDA), an aromatic diamine (ODA) and a diamino terminated poly(ethylene oxide) (PEO2000) of 2000 g/mol molecular weight, using different PEO contents, has been synthesized. Cast films of these copolymers have been thermally treated and characterized by FTIR-ATR, DSC, TGA and SAXS. It has been found that there is a direct relationship between phase segregation and permeability for increasing treatment temperatures.

Results show that permeability is higher when PEO content increases in the copolymer. Selectivity for O_2/N_2 and CO_2/CH_4 gas pairs follows the same tendency, while those for CO_2/N_2, and CH_4/N_2 give higher selectivities for intermediate (30-40 %) PEO contents. Especially promising are the results for these two pairs of gases because materials with high permeability with high selectivity can be obtained.

The Maxwell model has been applied to predict permeability (for CO_2, CH_4, O_2 and N_2) from known data for pure BPDA-ODA and neat PEO and it has been found that assuming PEO as the dispersed phase, the use of this equation is adequate for percentages up to approximately a 40 % over which we should assume that it is the aromatic part of the copolymer which plays the role of dispersed phase.

Graphical Abstract

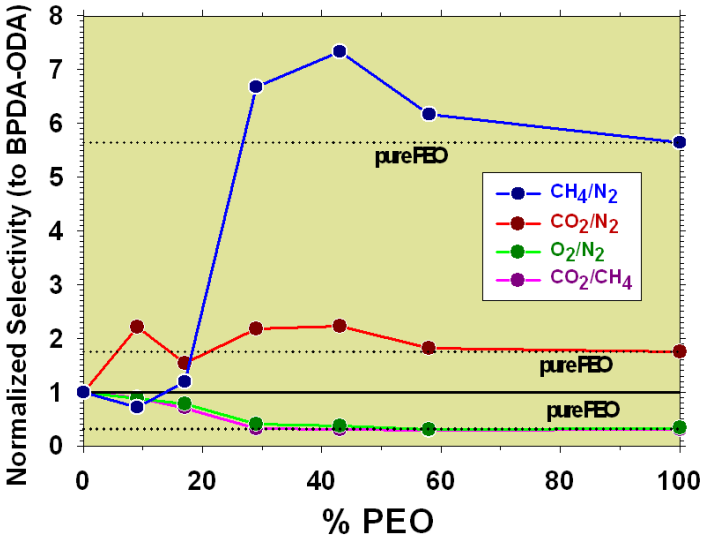

8.1 Introduction

Nowadays, the role of polymeric membranes applied to gas separation is more and more important. Although some of them have already an application in industrial separations[1], the truth is that a lot of research is still necessary to discover new materials and/or to improve the properties of existing polymers to assure them an actual applicability at industrial level.

It is obvious that separations where CO_2 is involved are of great interest now. There are several sources (power plants, steel, cement production plants or the chemical industry) where important amounts of CO_2 are generated, and it is therefore necessary to develop new technologies to curb as far as possible the greenhouse effect. Specifically, one of the most demanding applications is the separation CO_2/N_2. In all cases, in order to guarantee a real application of a new polymeric material in gas separation, an adequate balance of high permeability and good selectivity must be achieved [2-3].

On the other hand, there is an urgent need to change the world's dependence on oil and to find an alternative energy source or to use cleaner fuels [4]. Natural gas appears as an attractive alternative due to its lower carbon footprint as compared with gasoline or coal. Despite the increasing demand of natural gas, the gas reserves have remained reasonably stable because producers have been able to replace most of the drained reserves with new resources [5-6]. Nevertheless, a high percentage of natural gas reserves cannot be used because they are contaminated by nitrogen and thus they do not fit the required specifications for its transport and exploitation [7-9].

In order to be useful in such gas separation applications, a polymer film should show a preferential affinity for condensable gases such as CO_2 or CH_4 as compared with a mostly ideal gas such as N_2. Moreover, in addition to the criteria of permeability and selectivity, membranes to be used in this type of separations, must give high flow and have good mechanical and thermal resistance.

Glassy polymers and in particular polyimides are well known by their excellent thermal oxidative stability, good organic solvent resistance and exceptional mechanical properties, along with an extraordinary ability to separate complex mixtures of gases in diverse applications [10-12]. Thus, among all the polymeric membranes, it has been widely demonstrated that the use of aromatic polyimides is one of the best choices.

Typically these materials have a high selectivity but with a not always sufficiently high permeability [13-14]. It is therefore necessary to increase the affinity of the compounds for

condensable gases such as CO_2, or CH_4 and one of the most common approaches to meet these requirements is the use of block-copolymers.

Aromatic-aliphatic block-copolymers usually combine a hard block and a soft block. The hard block can be formed by a polymer with well-packed and highly rigid structures; as a result it forms the glassy segment of the polymer chain with usually low free volume. In contrast, the soft block can consist in a polymer with more flexible, low Tg, chains, which can form rubbery segments in the polymer chain normally with high free volume. Also, when aromatic-aliphatic block copolymers are phase-separated, their glassy polymer segments would provide mechanical support. The rubbery segments, due to the nature of the flexible chain structure, allow an efficient transport of gas, giving a good permeability to the copolymer [15-16].

It is known that poly(ethylene oxide) (PEO) compounds give excellent results for the CO_2 separation from other light gases [17-18]. In the same way, this category of compounds having oxyethylene groups in the structure showed good permeability for the couple CH_4/N_2[19]. In view of this, the use of these compounds, block-copolymers by combination of aromatic and PEO polyimides, appears to be a successful route [20-22].

These compounds have also good permselectivity for the couples CO_2/N_2 and CH_4/N_2. This was attributed mainly to the high solubility-selectivity[19], which could be due to the existence of strong interactions of CO_2 with the oxyethylene group in PEO. The interaction between CO_2 and PEO has been discussed and used for the development of CO_2 selective membranes previously [23-25]. However CH_4/N_2 separation has not been studied so intensively [26].

It is also necessary for the development of new materials to find a good balance between the hard and soft block segments in order to provide good separation without loss of permeability. For this reason, we propose here a complete study of the influence of composition on the properties of separation for a system composed of hard aromatic polyimide segments (BPDA-ODA), and soft aliphatic polyether segments (PEO).

The properties of such material have been analyzed by standard techniques of characterization (DSC, TGA, TMA, mechanical properties and density). Also, SAXS experiments were performed to study the segregation in the different phases of poly(ether-imide)s. Finally, we have modeled the copoly(ether-imide)s in order to predict their permeability to different gases by applying the Maxwell's equation.

8.2 Experimental

8.2.1 Chemicals

3,3′,4,4′- biphenyltetracarboxylic dianhydride (BPDA), and 4,4'-oxydianiline (ODA) were purchased from Aldrich. These products were purified by sublimation at high vacuum just before being used. Polyoxyethylene bis(amine) (Jeffamine ED-2003, n= 41) with nominal molecular weight of 2000 g/mol, was kindly donated by Huntsman® (Holland). This polyether was dried at 70 ºC in vacuum for 5 hours and stored in a desiccator at vacuum until use. Anhydrous N-methylpyrrolidinone (NMP), to be used as polymerization solvent, was purchased from Sigma-Aldrich Co. Figure 1 shows the chemical structure of the monomers.

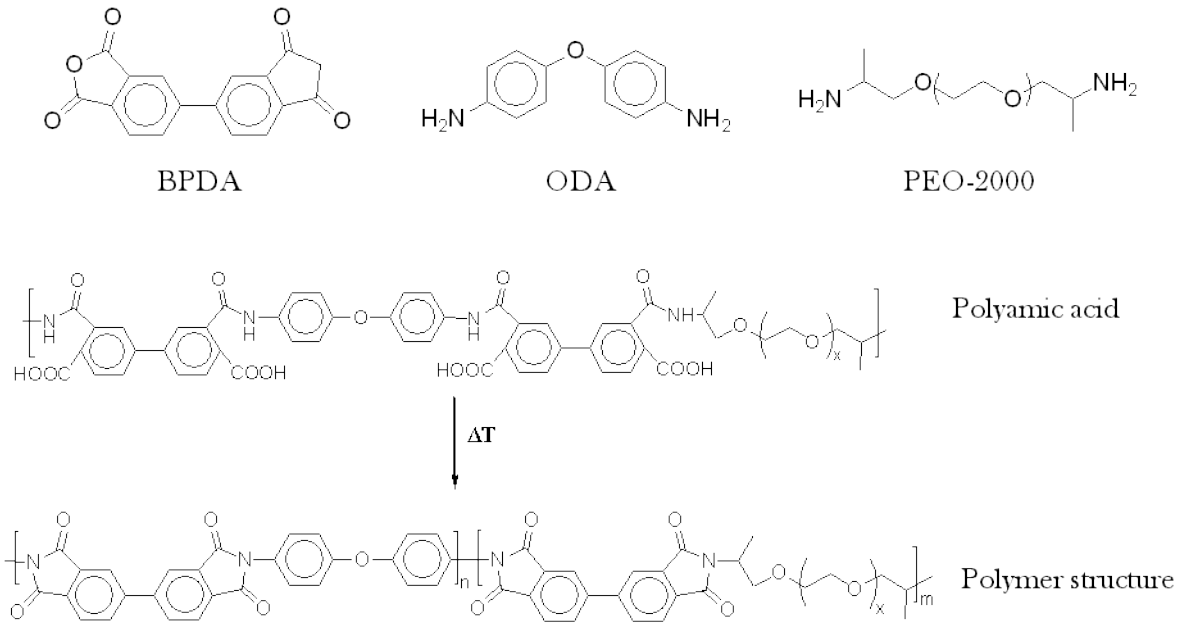

Figure 1. Chemical structure of the monomers and reaction process.

8.2.2 Synthesis of copoly(ether-imide)s

The samples were synthesized by combination of the dianhydride (BPDA) with the aromatic diamine (ODA), and different proportions of the aliphatic diamine (PEO) [20]. The corresponding copoly(ether-imide) will be designated by adding cPI to the w/w percentage of the aliphatic proportion. Thus, cPI-58 designates the sample BPDA-PEO2000-ODA with a weight ratio between the aliphatic and aromatic diamines of 4:1 which corresponds to a mass proportion of PEO in the final copolymer of around 58%.

Diamine-terminated poly(oxyethylene oxide) (PEO2000) (x mmol), and 4,4'-oxydianiline (ODA) (y mmol) in weight ratios 1:4, 1:2, 1:1, 2:1, and 4:1 were dissolved in anhydrous NMP (5 mmol (x+y)/10 mL) in a 100 mL three-necked flask blanketed with nitrogen.

Then, the reaction mixture was cooled down to 0 ºC, and under mechanical stirring, a stoichiometric amount of BPDA dianhydride (x+y mmol) was added and the mixture was stirred overnight at room temperature (see final resulting amounts in table 1). During this time the dianhydride completely dissolved and the solution reached high viscosity.

Table 1. Polymers synthesized in this work

Sample	Acronym	Weight ratio PEO/ODA	Imidization Temperature (°C)
BPDA PEO2000 ODA 4_1	cPI-58	4:1	120
BPDA PEO2000 ODA 2_1	cPI-43	2:1	120
BPDA PEO2000 ODA 1_1	cPI-29	1:1	160
BPDA PEO2000 ODA 1_2	cPI-17	1:2	180
BPDA PEO2000 ODA 1_4	cPI-9	1:4	180

8.2.3 Preparation of the copolyimide dense films

The resultant viscous copolyamic acid solution was diluted with NMP to the appropriate viscosity for casting, filtered through a nominal #1 fritted glass funnel, degassed, and cast onto a leveled glass plate. The resulting film was covered with a conical funnel to avoid fast evaporation of the solvent, dried at 80 ºC overnight, and finally treated at different temperatures for 6 hours in a vacuum oven, in order to get a complete imidization (Table 1). Films of the copolymers of 50-70 μm in thickness were obtained. After that, thermal treatments under inert atmosphere were carried out at different temperatures. All films showed good mechanical properties.

8.2.4 Characterization Methods

Attenuated total internal reflectance-Fourier transform infrared analyses (ATR-FTIR) were performed at room temperature using a PerkinElmer Spectrum One infrared spectrometer equipped

with an ATR accessory. Spectra taken directly from the films were the average of 16 scans at a resolution of 4 cm^{-1}.

A Thermal Analysis Q500 instrument was used for thermogravimetric analysis (TGA). Disc samples cut from films with weights between 5 and 15 mg were tested. When running dynamic scans, it was done in Hi-Resolution mode, where the heating rate is automatically adjusted in response to changes in the rate of weight loss, which results in improved resolution, with an initial heating rate of 10 ºC/min under a flux of nitrogen.

Differential scanning calorimetry (DSC) analyses were carried out in a Mettler Toledo (DSC 822e) calorimeter equipped with a liquid nitrogen accessory. Disc samples cut from films weighting 5–15 mg were sealed in aluminium pans. Samples were heated with the following cyclic method in order to monitor the changes in thermal properties with thermal treatment: from 25 ºC, the sample was heated at 10 ºC/min to a target temperature; once reached, the sample was cooled at the maximum cooling rate accessible for the instrument to -90 ºC, held at this temperature for 15 min and reheated at 10ºC/min to the next target temperature. The procedure was followed until the last treatment temperature was reached and a final run from -90 ºC to 80 ºC was performed. In this way, in each heating run, the thermal properties for the copolymers after treatment to the previously reached temperature were obtained, and a plot of thermal properties versus "instantaneous" thermal treatment could be built.

The densities (ρ) of the dense membrane films were determined using a CP225D Sartorius balance, provided with an immersion density kit.

SAXS measurements were performed at the beamline BM16 at the European Synchrotron Radiation Facility (Grenoble, France). Wavelength of the X-ray beam was 0.980 Å. Detector calibration was done with silver behenate (AgC22H43O2), and the characteristic distance L was calculated from the scattering vector ($q=4\pi(\sin\theta)/\lambda$, λ=wave length, 2θ=scattering angle). Disc samples cut from films were placed in a Linkam hot stage and heated at 10 ºC/min while the SAXS spectra were recorded. Calibration of temperature gave a difference of approximately 7 ºC between the temperature reading at the hot stage display and the real temperature at the sample.

Thermomechanical (TMA) tests were performed in a Rheometric Scientific instrument model DMTA V. Rectangular test pieces of 3 mm width and 20 mm length were cut from films. A distance of 10 mm was set between fixation clamps. Runs were carried out from ambient temperature at 2 ºC/min with a static stress of 3 MPa.

The permeability, P, for O_2, N_2, CO_2 and CH_4 was determined by using a permeator with constant volume and variable pressure which uses the time-lag operation method. The measurements were carried out at 3 bar and 30 ºC. A sketch of the device used has been shown elsewhere [27]. The strategy known as ‘‘time-lag’’ method, attributed to Daynes et al. [28], is very appropriate to determine permeability, diffusivity and indirectly solubility of a sample by a simple, rapid and accurate method working under transitory regime. The method has been successfully applied to polymer permeation by many authors [29-30]. Its theoretical framework, as well as the practical possibilities and limits of the time-lag technique have been abundantly documented [31]. It is nowadays an accepted method to assess the permeability and diffusion coefficients of a gas through a polymer film. Because permeability is a consequence of diffusivity and solubility, this magnitude can be evaluated as

$$S = \frac{P}{D} \tag{1}$$

In this way both P and D and, consequently S, can be evaluated easily by this time-lag method.

8.3 Results and discussion

8.3.1 Copoly(ether-imide)s imidization

After the films were dried overnight, they were heated at different temperatures (see Table 1) to almost completely removal of the solvent, and infrared spectra were recorded to check for the progress of imidization. After this process, the polymer films resulted to be insoluble in DMAc (dimethylacetamide), NMP, Hexane, Toluene, THF (tetrahydrofuran) and CH_2Cl_2 (dichloromethane).

Under the commented protocol, films with diamines ratio 4:1 and 2:1 (cPI-58 and cPI-43) were almost completely imidized according to their FTIR spectra (within the detection limits of the FTIR technique) at 120 ºC. For the sample with the ratio 1:1 (cPI-29), the imidization temperature was increased to160 ºC, and for the polymers with the ratio 1:2 and 1:4 (cPI-17 and cPI-9) complete imidization was reached for temperatures over 180 ºC. In figure 2, the FTIR spectra of copoly(ether-imide) cPI-43 and its corresponding poly(amic acid) precursor are shown.

For all synthesized copolymers, the bands centered around 3260 (O-H stretching from the polyamic acid), 1603 (Amide I band from the polyamic acid) and 1538 (Amide II band from the polyamic

acid) cm-1 strongly decreased or disappeared, and the bands at approximately 1774 (symmetric stretching of C=O imide groups), 1712 (asymmetric stretching of C=O imide groups), 1370 (C-N stretching of imide groups) and 738 (imide ring deformation) cm^{-1} increased or appeared with imidization. The band at approximately 2880 cm^{-1}, related to aliphatic C-H stretching, did not change during imidization and it could be used as reference. The spectra (see Figure 2) for cPI-43 show the differences between the samples with and without imidization, and the lack of differentiation for the samples treated at 120 ºC, 160 ºC and 200 °C. This confirmed that at a temperature of 120 °C imidization was completed for this copolymer as mentioned.

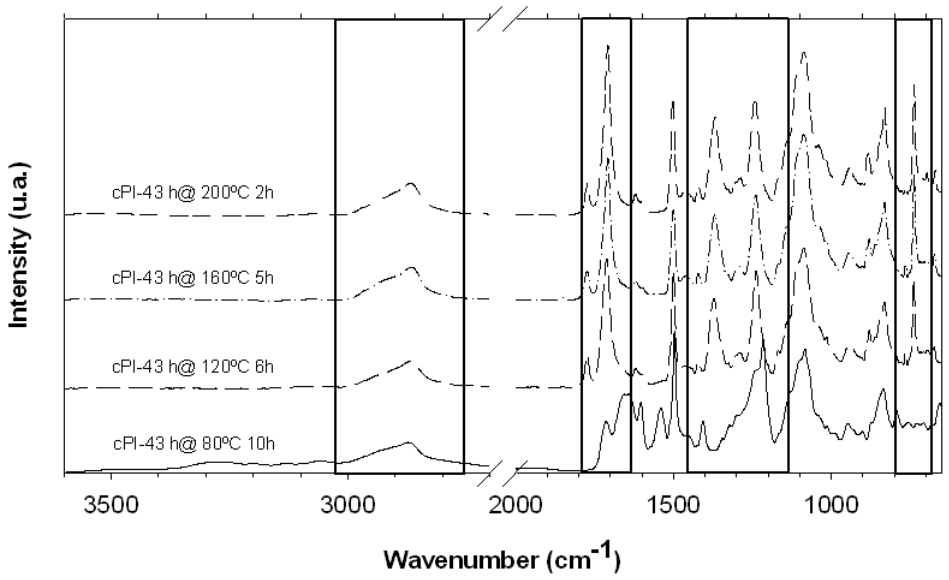

Figure 2. FTIR spectra of copolymer cPI-43 before imidization (80 ºC) and after the thermal treatment at different temperatures (120, 160 and 200 ºC).

The full imidization temperature needed for the copolymers with higher polyether proportions was remarkably lower than that needed for fully aromatic polyimides [20-21]. For the copolymers with low PEO content, cPI-17 and cPI-9, the structure approaches that of a fully aromatic polyimide and higher temperatures were needed to complete the imidization.

8.3.2 Thermal Stability

Thermogravimetric analysis was performed to evaluate the thermal stability of the synthesized copolymers. Dynamic runs in High-Resolution mode, in a nitrogen atmosphere, for fully imidized copolymers (annealed at 120 ºC for 6 hours in the case of cPI-58 and cPI-43 copolymers, at 160 ºC

for 6 hours to cPI-29 and annealed at 180 ºC for 6 hours in the case of copolymers cPI-17 and cPI-9) showed a weight loss pattern consisting of three consecutive steps (see figure 2): an initial loss from ambient temperature to 270-300 ºC; a second loss from 270-300 ºC to 460-470 ºC; and a third loss from 460-470 ºC to 800 ºC.

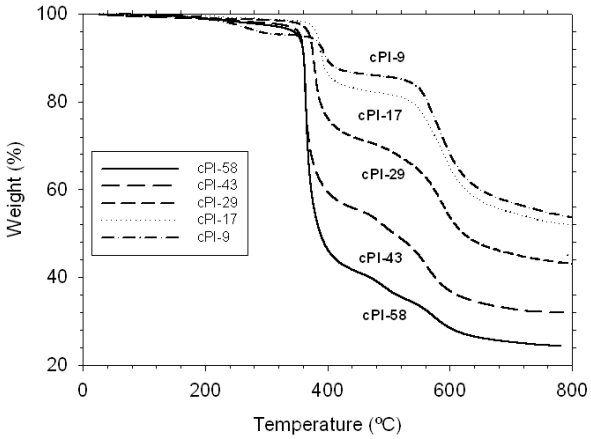

Figure 3. TGA curves in dynamic conditions for PEO based copolymers. From top to bottom: cPI-9 (treated at 180 ºC for 6 hours); cPI-17 (treated at 180 ºC for 6 hours); cPI-29 (treated at 160 ºC for 6 hours); cPI-43 and cPI-58 (treated at 120 ºC for 6 hours).

The first loss can be attributed to the absorbed water plus the residual solvent trapped in the film. The weight change for this step was in the order of 2 to 2.5 % [32]. The second loss stage, after correcting for the first one, agreed with the theoretical contribution of poly(ethylene oxide) bis(amine) entering the copolymer composition [33], within a 3% error (see Table 2), and it was therefore assigned to the loss of polyether block sequences. The third and final stage of weight loss was due to the thermal decomposition of the remaining aromatic polyimide segments.

TGA analysis confirmed that the polyether chains are much less thermally stable than the aromatic segments, as already found for another copoly(ether-imide)s based on poly(ethylene oxide) [19] and therefore a selective degradation of the polyether moiety can be performed in these copolymers.

The temperature of maximum weight loss rate took place between 360-400 ºC for all copolymers. This temperature increased when the amount of aliphatic diamine decreased. Similarly, the char residue at 800 ºC increased with the increase of the aromatic content in the copolymer.

Table 2. Results obtained by TGA for the prepared copolymers. The residue of the BPDA-ODA homopolymer at 800ºC was 64% [34].

Copolymer	Theoretical polyether weight in the copolymer (%)	Experimental polyether weigth loss (%)	Temperature of maximum weight loss rate / ºC	Residue at 800ºC / %
cPI-58	58,5	58,2	365	24,9
cPI-43	43,7	43.6	363	34,9
cPI-29	29,2	25,6	377	46,7
cPI-17	17,5	16,2	382	52,6
cPI-9	9,7	9,1	394	56,1

8.3.3 Calorimetric Studies

The samples were heated in a DSC instrument with a cyclic method in order to monitor the changes in thermal properties with thermal treatment [19]. All the copolymers showed only the Tg and Tm for the poly(ethylene oxide) segments, and no transition for the aromatic polyimide segments could be detected. No significant changes in the polyether Tg were observed with thermal treatment giving results from -55 to -52 ºC, as could be expected for a PEO chain of 2000 g/mol with restricted movement at the chain ends. From this result it can be deduced that PEO segments are in a separated phase of relatively high purity at any PEO content in the copolymer. This phase separated structure will be unambiguously confirmed later by SAXS.

However, there were changes in the Tm of the PEO segments in the copolymers, which increased with decreasing PEO percentages (with the exception of cPI-58 that showed the highest melting point) as shown in Figure S1 (supplementary information) where Tm is plotted as a function of the treatment temperature (the temperature instantaneously reached by the DSC) for the copolymers studied. An increase in the temperature of treatment increased slightly Tm for most of the copolymers.

The same trend was found for the melting enthalpy of PEO segments. If a value of 8.67 kJ/mol is taken for the melting enthalpy of PEO [35], the amount of crystallized PEO, in the samples studied in this paper, increased when the PEO contained in the copolymers decreased (0.9, 6.2, 8.5 and 8.7% for cPI-43, cPI-29, cPI-17 and cPI-9) except for cPI-58, which reached a maximum value of PEO crystallinity of around 12%. For copolymer cPI-58, PEO content was high enough to produce

a well separated phase of pure PEO, whereas for the rest of the copolymers, when PEO content decreased the length of the aromatic polyimide segments increased, augmenting the thermodynamical incompatibility of the segments, and therefore, giving a purer PEO phase. Anyway, the mixing of polyimide segments in the PEO phase was very limited as demonstrated by the similar Tg of the amorphous part of the PEO phase for these copolymers. For all the copolymers, the amount of crystallizable PEO segments increased with the increase on the temperature of thermal treatment, showing that phase separation improved with thermal treatment. In addition, it is worth noting out that, at the temperature of measurement of permeabilities and selectivities, 30 ºC, the PEO present in the copolymers would be melted and in amorphous state.

8.3.4 Thermomechanical Analysis

Thermomechanical analysis was carried out in order to detect the glass transition temperature of the aromatic polyimide hard segments, which was not detected by DSC. Several criteria can be chosen to determine the transition temperature. For example, it could be taken as the minimum in the first derivative of the strain vs. temperature curve, or the zero value in the second derivative. With the former criterion, the values were not clearly resolved, so that we decided to choose a different criterion, the temperature when strain is 10 times that of the sample at 100 ºC, which gives lower transition values than the other two mentioned criteria [33]. This criterion can be accepted at least for comparative purposes. In Figure S2 in the supplementary information, the TMA curves for these copolymers are shown.

For all the copolymers except cPI-58, the Tg of the aromatic polyimide was well above ambient temperature, although lower than the corresponding Tg for the pure aromatic polyimide homopolymer, BPDA-ODA. This is due to the lower polymerization degree in the copolymers and, consequently, lower length of the aromatic polyimide segments as compared to the corresponding homopolymer and to the possible inclusion of some polyether segments in the polyimide domains [33]. The obtained values for the copolymers in this work were

180.1 ºC for cPI-43 (treated at 180ºC 6h) < 203.1 ºC for cPI-29 (treated at 180ºC 6h) < 220.7 for cPI-17 (treated at 160ºC 6h) < 231.6 ºC for cPI-9 (treated at 120ºC 6h)

For copolymer cPI-58, the material was too soft after PEO melting and failed at the testing conditions at approximately 75ºC.

The Tg of the aromatic portion of the copolymer clearly increased when the PEO content decreased. All samples have the same aromatic polyimide, and the same aliphatic polyether, thus the

differences can only be due to different lengths for the aromatic polyimide segments, longer at lower PEO content in the sample.

From the thermomechanical data, the Young modulus can be measured to estimate the mechanical properties of the copolymers. For the stress applied in the test, 3 MPa, the strain at 60ºC, temperature at which PEO segments are amorphous, was below 1% except for cPI-58, that reached approximately 9% strain. This low strain is in the region of elasticity of these materials where the stress follow a linear relationship with the strain and Young modulus can be determined. The calculated values are the following:

0.037 GPa for cPI-58 < 0.39 GPa for cPI-43 < 0.52 GPa for cPI-29 <

0.81 GPa for cPI-17 < 1.40 GPa for cPI-9

The Young modulus increases, as expected, with the increase in aromatic polyimide content. There is a steep decrease from cPI-43 to cPI-58, probably due to a change in the morphology of the material, from a co-continous morphology for cPI-43 to a morphology with almost isolated polyimide hard segments for cPI-58. The Young modulus for cPI-43 is similar to the value measured for this material treated at 160ºC, which showed good mechanical properties [37]. For this type of copolymers, it has been shown that decreasing the PEO content in the copolymer increases the mechanical properties, approaching that of the pure aromatic polyimide homopolymer [33], and therefore, it can be said that this copolymers present good mechanical properties except for copolymer cPI-58, very soft when PEO segments are melted.

8.3.5 Small Angle X-ray Scattering

X-ray scattering experiments were performed at a synchrotron radiation source in order to follow, in real-time conditions, the irreversible development of the phase separated structure in these copolymers [19, 33] caused by their thermal treatment.

As mentioned elsewhere [19, 33] it is possible to obtain, from the SAXS spectra, both the relative invariant and the characteristic length of the segregated phases, Q' and L, as shown, for example, in Figures S3 and S4 in the supplementary information for copolymer cPI-43. Initially, the linear increase in Q' is due to a thermal effect and not to an improvement in phase separation and the extrapolated line can be used as the reference initial state for the phase separated morphology. To eliminate the influence of the different film thicknesses and electronic density, the relative invariant [Q'_r = Q'(T)/ Q'(baseline at T)] and length [L_r = L(T)/ L(baseline at T)] were calculated. In this

way, the relative improvement in the phase separation and in the long spacing of the morphology can be compared for all the copolymers. The resulting curves for Q'_r, Figure 4 left, showed that there is a clear increase of phase segregation in the temperature range from 170 to 300 °C (the increase is continued until the end of the test temperature range) except for cPI-58, for which phase separation reached almost its maximum and practically did not change with temperature. For copolymer cPI-29 the relative change was the highest of the series, almost a 100% increase in Q'_r.

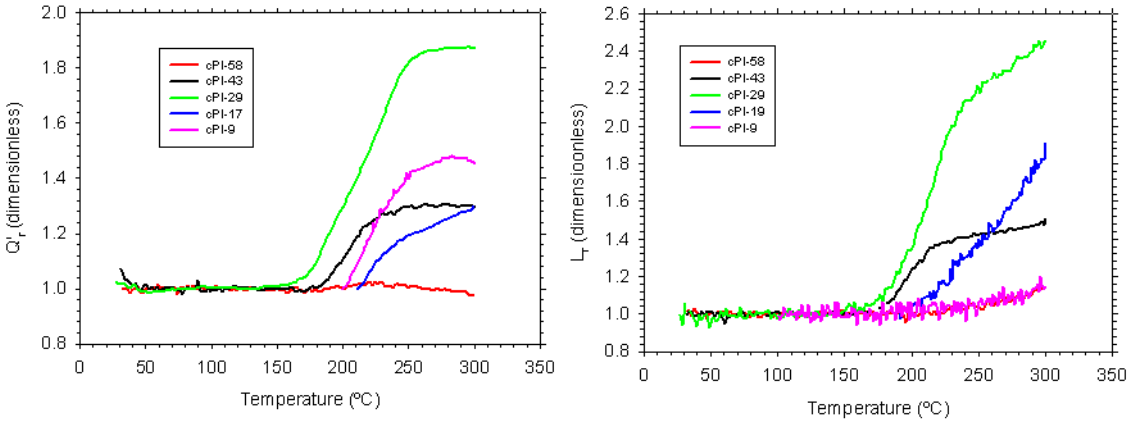

Figure 4. Evolution of Q'_r and L_r as a function of the temperature of treatment for the copolymers studied.

From the results obtained for L we get an idea on the size scale of the phase separated morphology. In this case, the highest values were observed for sample cPI-9 (more than 20 nm) followed by cPI-17 (around 17.5 nm) and the rest of the samples (L around 14 nm). For the range of PEO content studied in this work, it seems that the size scale of the phase separated structure is similar for intermediate contents of PEO (58% to 29%) whereas at lower contents, L increased when PEO content decreased. Moreover, it seems clear that when the copolymers were treated at higher temperatures, the segregated domains became bigger. The relative increase in L (that is, the increase in L_r) was very low for cPI-9 and cPI-58, the copolymers with the lowest and with the highest PEO content in the studied interval, and was high for the rest, specially for cPI-29, the copolymer with the highest increase in Q'_r.

8.3.6 Density

The densities (ρ) of the dense membrane films were determined according to the equation:

$$\rho = \rho_0 \frac{W_{air}}{W_{air} - W_{liq}} \tag{2}$$

where ρ is the density of the film, W_{air} and W_{liq} are the weights of the film in the air and immersed in an auxiliary liquid (in these measurements, isooctane was used because this polymer is reported to be insoluble in isooctane [36]) and ρ_o is the density of the auxiliary liquid (isooctane).

The so measured density was always between the values of pure aromatic polyimide (BPDA-ODA, which is 1.39 g/ml [14]), and the density value for the aliphatic diamine (which is 1,068 g/ml, data provided by Huntsman®):

BPDA-ODA (1,39 g/cm^3) > cPI-9 (1,33 g/cm^3) > cPI-17 (1,34 g/cm^3) > cPI-29 (1,32 g/cm^3) > cPI-43 (1,29 g/cm^3) > cPI-58 (1,24 g/cm^3) > PEO (1,07 g/cm^3)

As expected, the density decreased as the PEO content increased.

8.3.7 Gas transport properties

In agreement with our previous results for other similar aliphatic-aromatic copoly(ether imide)s [19, 37], the copolymers prepared and studied here showed an improvement in permeation properties with the thermal treatment. Results show a direct correlation between: treatment temperature, phase segregation and permeation properties.

Figure 5 shows the permeability (for: CO_2, CH_4, O_2 and N_2) through the copolymer cPI-29 (w/w ratio between diamines 1:1) (29 % of PEO content) as a function of thermal treatment. The trend is quite analogous for all the copolymers showing an enhancement of the permeability with the thermal treatment.

When these data were compared with the results obtained by SAXS, it was clear that the improvement in phase separation lead to better permeation properties. In general, the increase in permeability was much higher for the maximum treatment temperatures, when most of the remaining solvent was released and the improvement in the phase separation was higher.

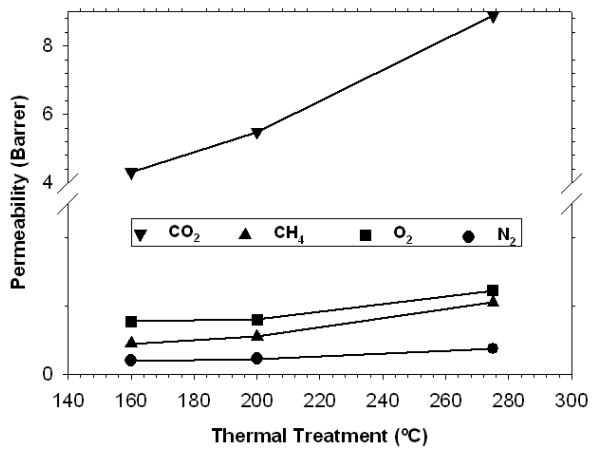

Figure 5. Permeability versus treatment temperature for the copolymer cPI-29.

A very significant and clear way of showing the level of gas separation performance obtained is the Robeson's plot [38-39]. In these representations, Figure 6 and Figures S5 to S7 in the supplementary information, the distance to the limit can give an idea of the compromise between permeation and selectivity of the samples. In these figures (for the different gas pairs) the values of permeability and selectivity for the homopolymer BPDA-ODA and for pure PEO are shown. The permeability and selectivity of a pure BPDA-ODA membrane were measured by us because values found in literature were highly inconsistent [40]. In the case of the other homopolymer, PEO, permeability and selectivity values were taken from data published by Lin and Freeman [24]. In such representations the points corresponding to our samples should be placed in between the representative points for the homopolymers. Actually, this is clearly seen in the Figures.

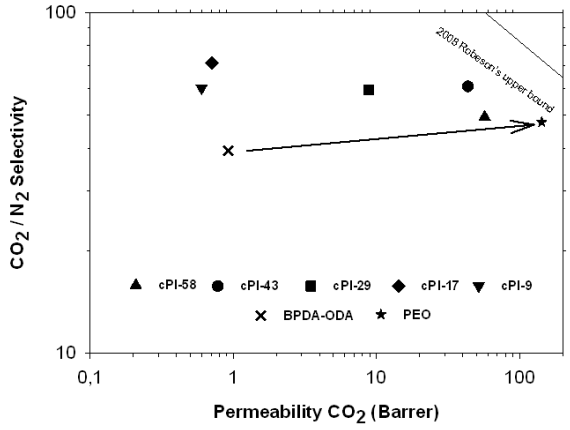

Figure 6. Robeson's plot for the CO_2/N_2 gas pair. The cross figure corresponds to BPDA-ODA and the star figure to PEO.

A good material would give permeabilities as close as possible to the values of PEO, especially when CO_2 is involved due to the favorable interactions between PEO and carbon dioxide. At the same time, selectivities should lie as close as possible to the purely aromatic polyimide. In the materials shown in this work, the treatment temperature and the percentage of PEO can be controlled and should allow the modulation of the permeability-selectivity balance.

For O_2/N_2 separations (Figure S5) and CO_2/CH_4 (Figure S6), as expected, permeability and selectivity were between those for the two homopolymers. For the CH_4/N_2 (Figure S7) and CO_2/N_2 (Figure 6) gas pairs, most of the cPIs showed high selectivities that were even over those for BPDA-ODA and pure PEO (for these gas pairs the selectivity of PEO is over that of BPDA-ODA). The permeability increased always with the percentage of PEO in the sample. Thus, for these pairs, some cPIs with high percentages of PEO gave both high permeability and selectivity that place them very close to the corresponding upper bound. It is worth noting here that for the CH_4 and N_2 pair, CH_4 was more permeable than N_2 giving an inverse selectivity (usually N_2 is more permeable in glassy polymers). No Robeson's limit has been yet proposed, and a tentative line has been drawn by us on the basis of some of the most interesting inverse selectivity polymers [19].

Referring now to the results obtained for the CO_2/N_2 pair, Figure 6, it can be said that in general this type of block-copolymer substantially improves the selectivity found for other types of compounds such as polyacetylenes, polyarylates, polycarbonates, polysulfones, aromatic polyimides or polyethylene oxide. Permeability is not extraordinarily high, although actually only totally rubbery polymers and some polyimides based on the 6FDA dianhydride give higher values but with substantially lower selectivities [41].

In order to analyze in some detail the effect of the proportion of polyether in these block copolymers, permeability is shown as a function of the percentage of PEO in Figure 7. The values for 0 % and 100 % PEO are also shown. In this Figure, it is possible to observe a sigmoidal trend between BPDA-ODA and pure PEO values. In effect, permeabilities were near that of the pure aromatic polyimide between 0 % and 20 % of PEO, while from 40 % to 100 % of PEO permeabilities tended to that of pure PEO. This could be also an indication of a change in the morphology of the copolymers between 17 and 29% PEO content.

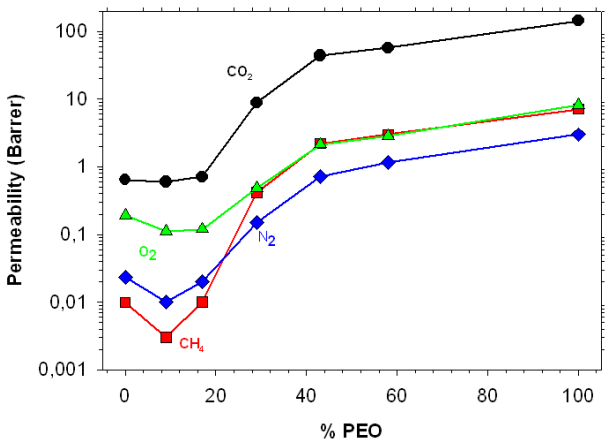

Figure 7. Permeability as a function of the percentage of PEO.

Results on selectivity are shown in Figure 8 as a function of the PEO content. As pointed out above for permeability, the selectivity values of these polymers were intermediate between those of BPDA-ODA and PEO for the couples CO_2/CH_4 and O_2/N_2. In this case, as mentioned above, the selectivity for pure aromatic polyimide was higher than for pure PEO, what was not the case for the couples CH_4/N_2 and CO_2/N_2, where the differences in solubility probably play an important role. As already commented, for these gas pairs, the selectivity was sometimes higher than those of the homopolymers. Thus, although permeability increased with the percentage of PEO it does not mean necessarily that a better permselectivity compromise would be achieved.

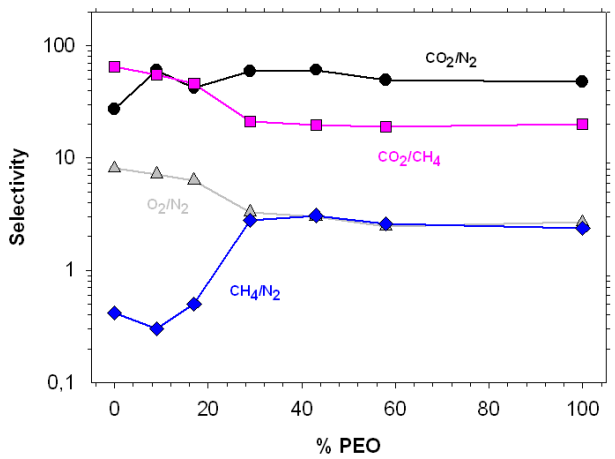

Figure 8. Selectivity variation as a function of percent of PEO.

Due to this especial behavior of selectivity, although cPI-43 was less permeable than cPI-58, its distance from the Robeson limit for couples O_2/N_2, CO_2/N_2 and CH_4/N_2 was lower than for cPI-58. For the couple CO_2/CH_4 the best values were obtained for cPI-58, the sample with the higher content of PEO.

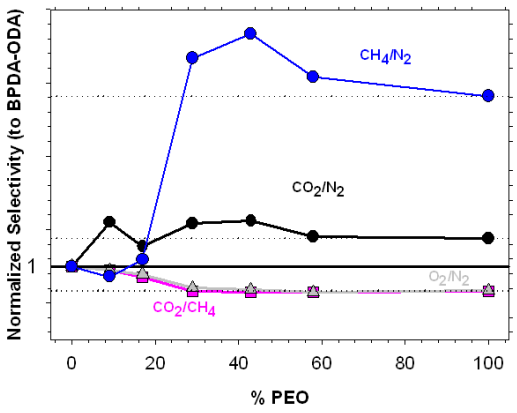

Figure 9. Selectivity distance from BPDA-ODA selectivity values as a function of the proportion of PEO.

Figure 9 shows the selectivity for the copolymers normalized to the value of the BPDA-ODA homopolymer (value 1 and solid line). The so normalized values for the pure PEO are also indicated (dashed lines). Now, it is clear that for CH_4/N_2 and CO_2/N_2 pairs, the selectivity of the copolymers with PEO percentages in the range from 30 to 40% gave the best results (even better than those for both pure aromatic polyimide, BPDA-ODA, or pure PEO). The rigidity of the structure formed, together with the effect of $-CH_3$ and CH_4 condensability and the interaction with the oxygen of the polymer chain should be the cause of this atypical effect. In the case of the CH_4/N_2 couple the presence of big amounts of PEO clearly favored the permeation of CH_4 giving inverse selectivities as it can be seen in Figures S7 and 8. In the case of the couple CO_2/CH_4, because both gases are similar in nature, the selectivity was lower than for the pure aromatic polyimide. Similarly, for O_2/N_2, where none of the gases has a specific interaction with PEO and the separation is mainly due to the different sizes of the molecules, selectivity was clearly lower than for the pure BPDA-ODA.

8.3.8 Permeability modeling

These copolyimides consisting of an aromatic polyimide part (hard segments) and an aliphatic polyether one (soft PEO chains), and having the ability to be phase-segregated by thermal

treatment, can be modeled approximately as a system formed by a disperse phase embedded in a continuous matrix.

It has been demonstrated that for such systems, the permeability for the samples with different PEO percentages in the polymer can be predicted by the Maxwell equation as shown below [42]:

$$P_{eff} = P_C \left[\frac{P_D + 2P_C - 2\phi_D \left(P_C - P_D \right)}{P_D + 2P_C + \phi_D \left(P_C - P_D \right)} \right] \tag{3}$$

Being P_{eff} the effective permeability, P_C and P_D the permeability of the continuous and disperse phase, respectively, and ϕ_D the volume fraction of the dispersed phase in the block copolymer.

In this type of polymers, the continuous phase can be the aromatic or the aliphatic segments depending on the relative amount of them. For this reason, we simulate two different predictions depending on which segment is taken as the continuous or the disperse phase.

Figures S8 and S9 in the supplementary information show the permeability predicted for the different gases. It is observed that for low PEO percentages the model assuming that PEO is the disperse phase fits the experimental data. On the other hand, the model assuming that PEO is the continuous phase works better for high PEO content.

8.4 Conclusions

A series of copoly(ether-imide)s presenting good gas separation properties have been prepared. These copolymers have been synthesized by the reaction between an aromatic dianhydride (BPDA), an aromatic diamine (ODA) and a diamine terminated poly(ethylene oxide) having a molecular weight of 2000 g/mole (PEO-2000), with different percentages of PEO.

It has been proved that higher PEO contents need lower temperatures to carry out the imidization process. These temperatures are notably lower than those needed for pure aromatic polyimides. Thermal properties demonstrated the existence of a phase separated structure with a defined T_g (and melting point) for the polyether phase, similar for all the copolymers, and a defined T_g for the polyimide phase. The T_g value of the aromatic phase, well above ambient temperature for these copolymers except for the copolymer with 58% PEO content, increased with the length of the aromatic polyimide segments (that is, for lower PEO contents). A clear increase in the

crystallization of PEO with the decrease in PEO content was observed except for the copolyimide with the highest PEO content.

SAXS experiments confirmed the phase separated structure and demonstrated the improvement on the phase separation with the increase in the treatment temperature. This segregation increased the permeability and its value clearly depended on the composition. As expected, when the PEO percentage was higher, the permeability increased.

With respect to selectivity, different behaviors were found. When the two gases were of the same nature as it is the case of O_2/N_2 and CO_2/CH_4 pairs, selectivity followed a predictable trend going from that of the pure BPDA-ODA copolymer to that of neat PEO in a gradual way. In the case of the CH_4/N_2 and CO_2/N_2 couples, the highest selectivity was found for a PEO content of 30-40 %. At these compositions, selectivities were better than for pure aromatic polyimide and for pure PEO.

Especially interesting were the values found for the CO_2/N_2 pair, which showed a selectivity-permeability balance that placed these copolymers very close to the Robeson upper bound. Also, very high permeabilities with high selectivities were found for these copolymers when the CH_4/N_2 couple of gases were considered. It is interesting to note out that all the copolymers had reasonably good mechanical properties except for the copolymer with 58% PEO content, that resulted very soft.

Finally, we have compared the results obtained in this work with those calculated by using the Maxwell model for mixtures. For PEO content below 20%, the behavior approached to a system with a continuous aromatic polyimide phase, whereas for PEO contents above 40%, it could be assumed that PEO was the continuous phase.

8.5 Acknowledgements

We are indebted to the Spanish Junta de Castilla León for financing this work through the GR-18 Excellence Group Action and to the Ministry of Science and Innovation in Spain for their economic support of this work (MAT2008-00619/MAT, MAT2010-20668/MAT, MAT2011-25513/MAT and CIT-420000-2009-32). We also acknowledge financial support from the programme Consolider Ingenio 2010 (project CSD-0050-MULTICAT).

Authors thank the Spanish Ministry of Economy and Competitivity for the economical support to access beamline BM16 at the European Synchrotron Radiation Facility (ESRF) in Grenoble (France). We are grateful to Dr. Ana Labrador and Dr. François Fauth for their help at BM16 station at the ESRF. The help provided by Sara Rodriguez in measuring gas permeability and selectivity is greatly appreciated. A. Tena thanks CSIC for a predoctoral JAE fellowship.

8.6 References

1. R.W. Baker, Future directions of membrane gas separation technology, Industrial and Engineering Chemistry Research, 41 (2002) 1393-1411.
2. R. Bounaceur, N. Lape, D. Roizard, C. Vallieres, E. Favre, Membrane processes for post-combustion carbon dioxide capture: A parametric study, Energy, 31 (2006) 2220-2234.
3. E. Favre, Carbon dioxide recovery from post-combustion processes: Can gas permeation membranes compete with absorption?, Journal of Membrane Science, 294 (2007) 50-59.
4. S. Pacala, R. Socolow, Stabilization Wedges: Solving the Climate Problem for the Next 50 Years with Current Technologies, Science, 305 (2004) 968-972.
5. R. Egging, F. Holz, S.A. Gabriel, The World Gas Model: A multi-period mixed complementarity model for the global natural gas market, Energy, 35 (2010) 4016-4029.
6. 6. B.T.W. Low, Yan; Chung, Tai-Shung;, Polymeric Membranes for Energy Applications, in, John Wiley & Sons, 2002.
7. R.H.V. Hugman, E.H.; Springer, P.S., Chemical Composition of Discovered and Undiscovered Natural Gas in the U.S. Lower-48, in: Executive Summary, Tight Sands and Gas Processing Department, 1993.
8. C. Tannehill, Nitrogen Removal Requirements for Natural Gas, Gas Research Institute Topical Report, in: Purvin & Gertz, Gas Research Institute, 1999.
9. C.C. Tannehill, C. Galvin, Business characteristics of the Natural Gas Conditioning Industry, in: Topical Report to GRI, 1993.
10. M.T.K. Bessonov, M.M.; Kudryavtsev, V.V.; Laius, L.A., Polyimides: Thermally Stable Polymers, in, Consultants Bureau, New York, 1987.
11. M.K.M. Ghosh, K.L., Polyimides: Fundamentals and Applications, in, Marcel Dekker, New York, 1996.
12. D.S. Wilson, H.D.; Hergenrother, P.M., Polyimides, in, Blackie, Glasgow, 1990.
13. D. Ayala, A.E. Lozano, J. De Abajo, C. García-Perez, J.G. De La Campa, K.V. Peinemann, B.D. Freeman, R. Prabhakar, Gas separation properties of aromatic polyimides, Journal of Membrane Science, 215 (2003) 61-73.

14. K. Tanaka, H. Kita, K. Okamoto, A. Nakamura, Y. Kusuki, Gas permeability and permselectivity in polyimides based on 3,3',4,4'-biphenyltetracarboxylic dianhydride, Journal of Membrane Science, 47 (1989) 203-215.
15. T.A. Barbari, W.J. Koros, D.R. Paul, Gas transport in polymers based on bisphenol-A, Journal of Polymer Science, Part B: Polymer Physics, 26 (1988) 709-727.
16. Y. Li, M. Ding, J. Xu, Gas separation properties of aromatic polyetherimides from 1,4-bis(3,4-dicarboxyphenoxy)benzene dianhydride and 3,5-diaminobenzic acid or its esters, Journal of Applied Polymer Science, 63 (1997) 1-7.
17. Y. Hirayama, Y. Kase, N. Tanihara, Y. Sumiyama, Y. Kusuki, K. Haraya, Permeation properties to CO_2 and N_2 of poly(ethylene oxide)-containing and crosslinked polymer films, Journal of Membrane Science, 160 (1999) 87-99.
18. M. Kawakami, H. Iwanaga, Y. Hara, M. Iwamoto, S. Kagawa, Gas permeabilities of cellulose nitrate/poly(ethylene glycol) blends membranes, Journal of Applied Polymer Science, 27 (1982) 2387-2393.
19. A. Tena, A. Marcos-Fernández, A.E. Lozano, J.G. de la Campa, J. de Abajo, L. Palacio, P. Prádanos, A. Hernández, Thermally treated copoly(ether-imide)s made from bpda and alifatic plus aromatic diamines. Gas separation properties with different aromatic diamimes, Journal of Membrane Science, 387–388 (2012) 54-65.
20. K.I. Okamoto, M. Fujii, S. Okamyo, H. Suzuki, K. Tanaka, H. Kita, Gas permeation properties of poly(ether imide) segmented copolymers, Macromolecules, 28 (1995) 6950-6956.
21. K.I. Okamoto, N. Umeo, S. Okamyo, K. Tanaka, H. Kita, Selective permeation of carbon dioxide over nitrogen through polyethyleneoxide-containing polyimide membranes, Chemistry Letters 5(1993) 225-228.
22. H. Suzuki, K. Tanaka, H. Kita, K.I. Okamoto, H. Hoshino, T. Yoshinaga, Y. Kusuki, Preparation of composite hollow fiber membranes of poly(ethylene oxide)-containing polyimide and their CO_2/N_2 separation properties, Journal of Membrane Science, 146 (1998) 31-37.
23. A. Car, C. Stropnik, W. Yave, K.V. Peinemann, Pebax®/polyethylene glycol blend thin film composite membranes for CO_2 separation: Performance with mixed gases, Separation and Purification Technology, 62 (2008) 110-117.
24. H. Lin, B.D. Freeman, Gas solubility, diffusivity and permeability in poly(ethylene oxide), Journal of Membrane Science, 239 (2004) 105-117.

25. S.R. Reijerkerk, M.H. Knoef, K. Nijmeijer, M. Wessling, Poly(ethylene glycol) and poly(dimethyl siloxane): Combining their advantages into efficient CO_2 gas separation membranes, Journal of Membrane Science, 352 (2010) 126-135.
26. K.A. Lokhandwala, I. Pinnau, Z.J. He, K.D. Amo, A.R. DaCosta, J.G. Wijmans, R.W. Baker, Membrane separation of nitrogen from natural gas: A case study from membrane synthesis to commercial deployment, Journal of Membrane Science, 346 (2010) 270-279.
27. J. Marchese, M. Anson, N.A. Ochoa, P. Prádanos, L. Palacio, A. Hernández, Morphology and structure of ABS membranes filled with two different activated carbons, Chemical Engineering Science, 61 (2006) 5448-5454.
28. H.A. Daynes, The process of diffusion through a rubber membrane, in, Proc. R. Soc. London 97, London, 1920, pp. 286–307.
29. J. Crank, The mathematics of diffusion, Clarendon Press, Oxford [England] :, 1975.
30. D.R. Paul, A.T. DiBenedetto, Diffusion in amorphous polymers, Journal of Polymer Science Part C: Polymer Symposia, 10 (1965) 17-44.
31. S.W. Rutherford, D.D. Do, Review of time lag permeation technique as a method for characterisation of porous media and membranes, Adsorption, 3 (1997) 283-312.
32. J.L. Hedrick, K.R. Carter, H.J. Cha, C.J. Hawker, R.A. DiPietro, J.W. Labadie, R.D. Miller, T.P. Russell, M.I. Sanchez, W. Volksen, D.Y. Yoon, D. Mecerreyes, R. Jerome, J.E. McGrath, High-temperature polyimide nanofoams for microelectronic applications, Reactive and Functional Polymers, 30 (1996) 43-53.
33. A. Marcos-Fernández, A. Tena, A.E. Lozano, J.G. de la Campa, J. de Abajo, L. Palacio, P. Prádanos, A. Hernández, Physical properties of films made of copoly(ether-imide)s with long poly(ethylene oxide) segments, European Polymer Journal, 46 (2010) 2352-2364.
34. S.-H. Hsiao, Y.-J. Chen, Structure–property study of polyimides derived from PMDA and BPDA dianhydrides with structurally different diamines, European Polymer Journal, 38 (2002) 815-828.
35. D.W. Van Krevelen, Properties of polymers in: third edition, Elsevier, Amsterdam, 1990, pp. 120
36. J. Brandrup, E.H. Immergut, E.A. Grulke, A. Abe, D.R. Bloch, Polymer Handbook (4th Edition), in, John Wiley & Sons, 1999.
37. A. Tena, A. Marcos-Fernández, L. Palacio, P. Cuadrado, P. Prádanos, J. de Abajo, A.E. Lozano, A. Hernández, Phase Segregation and Gas Separation Properties of Thermally Treated Copoly(ether-imide) from an Aromatic Dianhydride, an Aromatic Diamine, and Various Aliphatic Diamines, Industrial & Engineering Chemistry Research, 51 (2012) 3766-3775.

38. L.M. Robeson, Correlation of separation factor versus permeability for polymeric membranes, Journal of Membrane Science, 62 (1991) 165-185.
39. L.M. Robeson, The upper bound revisited, Journal of Membrane Science, 320 (2008) 390-400.
40. K. Tanaka, H. Kita, M. Okano, K.I. Okamoto, Permeability and permselectivity of gases in fluorinated and non-fluorinated polyimides, Polymer, 33 (1992) 585-592.
41. C.E. Powell, G.G. Qiao, Polymeric CO_2/N_2 gas separation membranes for the capture of carbon dioxide from power plant flue gases, Journal of Membrane Science, 279 (2006) 1-49.
42. J.C. Maxwell, A treatise on electricity and magnetism, in: vol. 1, Dover Publications Inc, New York, 1954.

8.7 Supporting Information

Supplementary data associated with this chapter can be found in the next DOI:

http://dx.doi.org/10.1016/j.memsci.2013. 01.036.

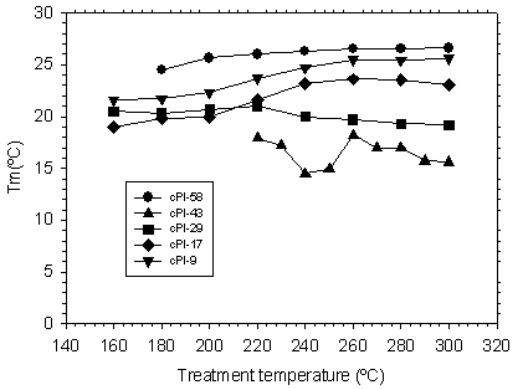

Figure S1. Melting temperatures as a function of the treatment temperature.

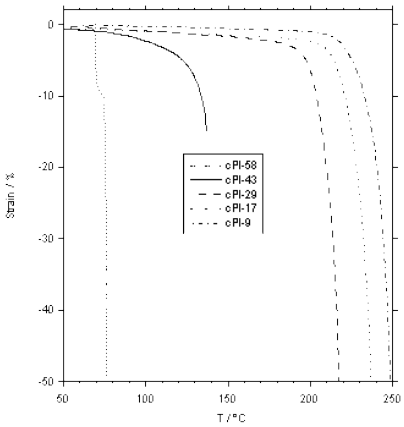

Figure S2. TMA curves for the synthesized copolymers.

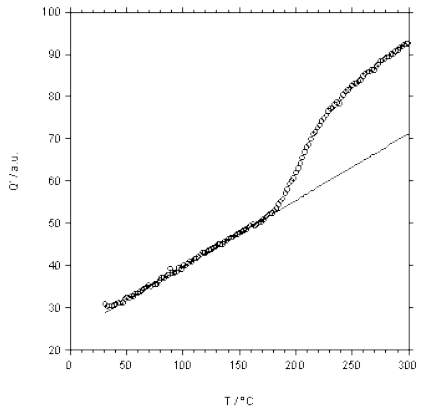

Figure S3. Change in Relative Invariant (Q'; dots) and baseline (line) with temperature for sample cPI-43.

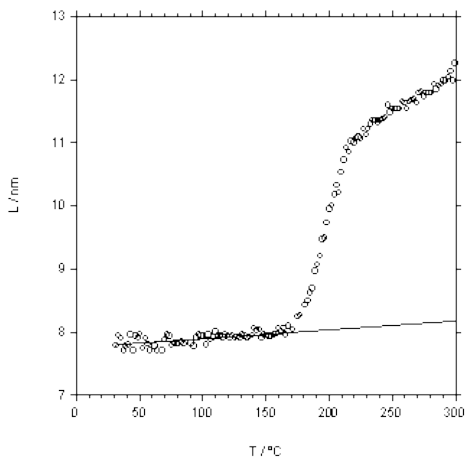

Figure S4. Change in Long spacing (L; dots) and baseline (line) with temperature for sample cPI-43.

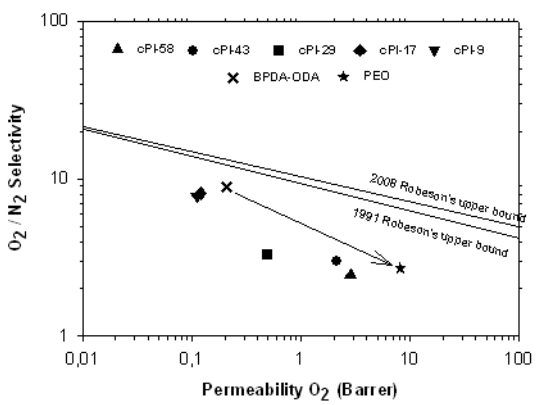

Figure S5. Robeson's plot for the O_2/N_2 gas pair. The cross figure corresponds to BPDA-ODA and the figure star to PEO (treatment temperature: 275 °C for cPI-9, cPI-17 and cPI-29, and 250 °C for cPI-43 and cPI-58).

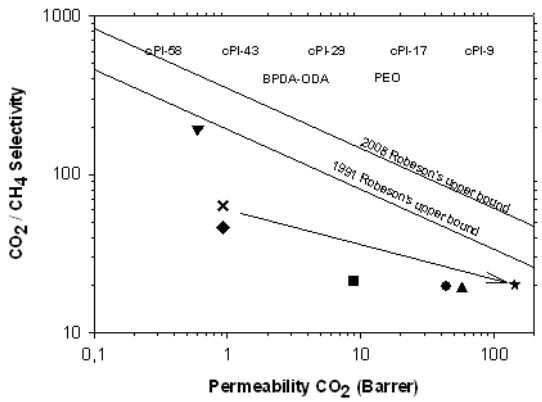

Figure S6. Robeson's plot for the CO_2/CH_4 gas pair. The cross figure corresponds to BPDA-ODA and the star figure to PEO.

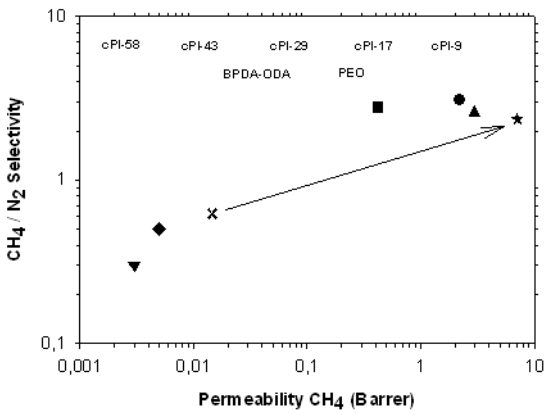

Figure S7. Robeson's plot for the CH_4/N_2 gas pair. The cross figure corresponds to BPDA-ODA and the star figure to PEO.

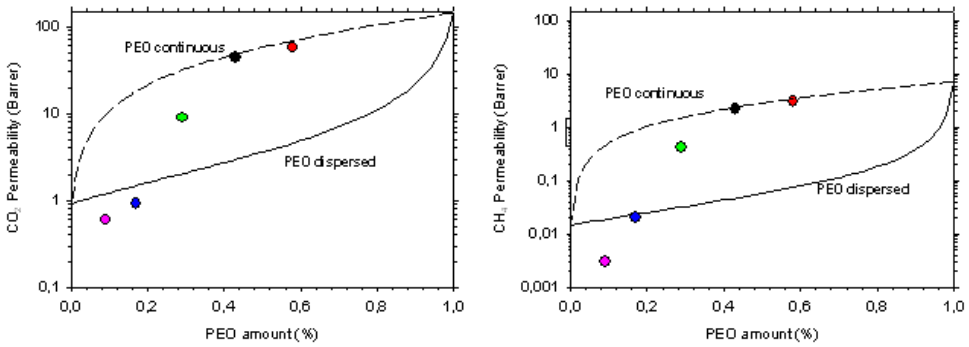

Figure S8. Predicted values for CO_2 (left) and CH_4 (right) using Maxwell equation and comparison with the experimental data for the samples at maximum treatment temperature (at 275 °C for cPI-9, cPI-17 and cPI-29, and 250 °C for cPI-43 and cPI-58).

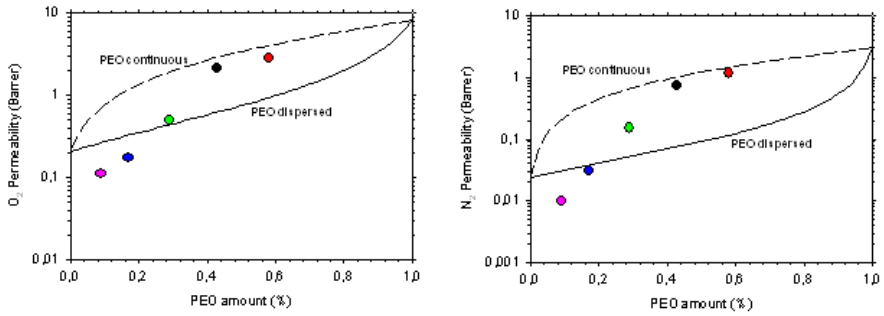

Figure S9. Predicted values for O_2 (left) and N_2 (right) using Maxwell equation and comparison with the experimental data for the samples at maximum treatment temperature (at 275 °C for cPI-9, cPI-17 and cPI-29, and 250 °C for cPI-43 and cPI-58)

CHAPTER 9

On the influence of the proportion of PEO in thermally controlled phase segregation of copoly(ether-imide)s for gas separation

Alberto Tena[1,3], Ángel E. Lozano[1,3], Laura Palacio[1,2], Ángel Marcos-Fernández[1,3], Pedro Prádanos[1,2], Javier de Abajo[1,3], Antonio Hernández[1,2]

[1]*Smap UA-UVA-CSIC, Parque Científico Universidad de Valladolid, Paseo de Belén, s/n, 47011 Valladolid, Spain.*

[2]*Dept. Física Aplicada, Facultad de Ciencias, Universidad de Valladolid, Paseo de Belén, 7, 47011 Valladolid, Spain*

[3]*Instituto de Ciencia y Tecnología de Polímeros, CSIC, Juan de la Cierva 3, 28006 Madrid, Spain.*

This chapter has been published in:

International Journal of Greenhouse Gas Control, 12 (**2013**) 146-154.

DOI: http://dx.doi.org/10.1016/j.ijggc.2012.10.014

Abstract

A complete series of aliphatic aromatic copolyimides has been synthesized. In this case all the samples had the same structure, BKDA-PEO6000-ODA, but different percentage of PEO in the final polymer. These copolymers have been thermally treated and characterized by several techniques. A direct relationship between temperature of treatment and both phase segregation and permeability improvement has been demonstrated.

Results show that the permeability is higher when higher the PEO content is, but otherwise the selectivity does not follow the same trend. Notable is the case of the CO_2/N_2 couple of gases that show selectivity-versus-permeability very near the upper bound of Robeson especially when permeation is done at 50 ºC.

The Maxwell model has been applied to carry out the prediction of permeability (for CO_2, CH_4, O_2 and N_2) and it has been found that depending on the percentage of amorphous PEO in the polymer, the model reproduces well the experimental tendency.

Graphical Abstract

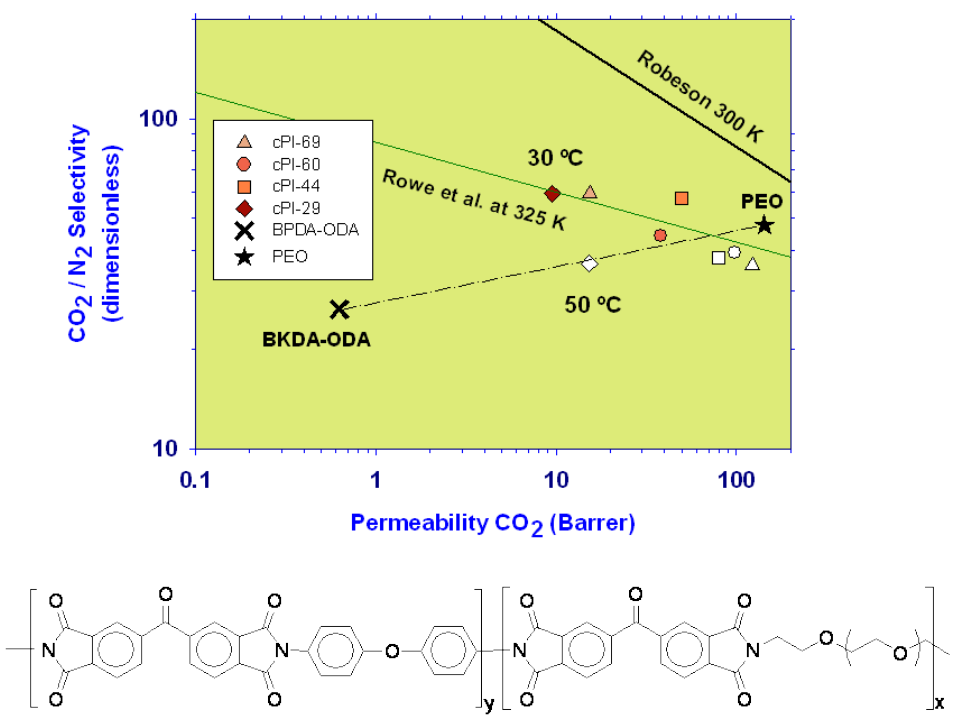

9.1 Introduction

The augment of carbon dioxide concentration in atmosphere due to the use of fossil fuels has caused a global warming that due to its potential dangerous effects requires resolved actions [1]. The 60 % of total CO_2 emissions are produced by power generation facilities and industrial factories. Of course research should focus on the optimization of clean energy sources and on the more efficient use of energy. However, it is also necessary to reduce CO_2 levels, so carbon capture and storage (CCS) must be considered as an urgent issue [2]. CO_2 can be captured by a variety of methods, which can be classified as post-combustion, pre-combustion and oxy-combustion ones [3-4]. Among these methods, Postcombustion appears as one of the most attractive alternatives [5]. This process can be applied to different sources: power, steel, cement or petrochemical plants etc. [6]. In this process the flue gas after the combustion step must be concentrated and purified to meet the transport and storage specifications [7].

The role of polymeric membranes applied to gas separation is increasingly gaining importance [8]. Currently they are presented as a good alternative for this type of processes [9-10] when compared with the processes that have been used up to now [11-13].

The amount of CO_2 in the flue gas ranges from low (4%) to high (30 %) concentrations and therefore the applied technology should consider these differences [5, 14]. Other compounds in the flue are O_2, H_2, CO, NO_x or SO_x, although the most frequent is N_2, which appears in the coal power plants, where CO_2 concentrations are typically around 15% [6, 15-16].

Polymers to be applied for this type of separation should have an adequate balance of permeability and selectivity [17]. But, it is also necessary to have a high gas flow and good mechanical and thermal resistance.

Glassy polymers and in particular polyimides are well known for their excellent thermal oxidative stability, good organic solvent resistance and exceptional mechanical properties, along with an extraordinary ability to separate complex mixtures of gases in diverse applications [18-20].

Typically these materials have a high selectivity but they sometimes do not exhibit sufficiently high permeability [21-22]. In order to increase the selectivity to CO_2, it is convenient to increase the affinity of the material for this gas. One of the most common approaches to meet these requirements is the use of block-copolymers having moieties able to interact with a certain gas.

Block-copolymers can combine hard and soft blocks. The hard block can consist in a polymer with well-packed rigid structure; while the soft segments usually contain more flexible chains. The hard segments are glassy while the soft segments behave as rubbery polymers with relatively high free volume fractions. In this way the glassy polymer segments will provide the mechanical resistance. The rubbery segments generally form continuous nanodomains with high gas permeability [23-24].

It is widely known that CO_2 is highly soluble in polyethylene oxide (PEO) and thus it has been used to separate carbon dioxide from other light gases [25-26]. In view of this, the use of block-copolymers combining aromatic diamines with aliphatic ones based on PEO (Jeffamines), appears to be a promising route [27-29]. These compounds have good permselectivity for the couple CO_2/N_2 [30], which was attributed mainly to the high solubility-selectivity due to the existence of strong interactions between the hydrophilic and rubbery domains of the oxyethylene groups in PEO and CO_2. The role of the interaction between CO_2 and ethylene oxide (EO) groups in CO_2 selectivity has been discussed and used for the development of new membranes [31-33].

In addition, it is necessary to reach a good balance between the hard and soft block segments in order to provide good gas separation balance without loss of permeability. For this reason, it is proposed here a complete study of the influence of composition on the properties of separation for a system where both the hard part, in this case the aromatic polyimide (ODA rich phase), and the soft section, the aliphatic (rich in the diamine polyethylene oxide, PEO-6000), are common to all structures.

9.2 Experimental

9.2.1 Chemicals

3,3′,4,4′- Benzophenonetetracarboxylic dianhydride (BKDA), and 4,4'-oxydianiline (ODA) were purchased from Aldrich. These products were purified by sublimation at high vacuum just before being used. α,ω-Diamine-poly(ethylene oxide) with nominal molecular weight of 6000 g/mol, were kindly donated by Kawaken Fine Chemicals Co., Ltd. (Tokyo, Japan), (PEO-6000 from here on). This polyether was dried at 70 ºC in vacuum for 5 hours and stored in a desiccator at vacuum until use. Anhydrous N-methylpyrrolidinone (NMP), to be used as polymerization solvent, was purchased from Sigma-Aldrich Co. Figure 1 shows the chemical structure of the monomers.

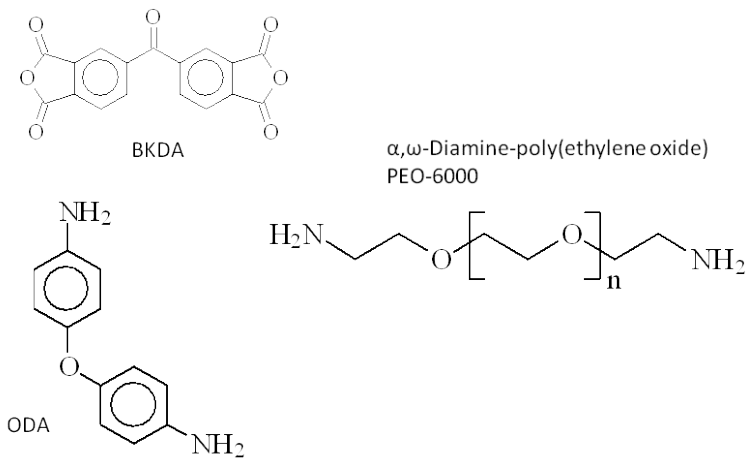

Figure 1. Structure of the monomers used to build up the poly(ether-imide)s.

9.2.2 Synthesis of copoly(ether-imide)s

The samples were synthesized by combination of the dianhydride (BKDA) with an aromatic amine (ODA), and changing the proportion of the aliphatic amine (PEO-6000). The corresponding copoly(ether-imide) will be designated by adding cPI before the figures corresponding to the weight proportion of PEO. cPI-69 should be an example for the sample BKDA PEO-6000 ODA with a 6:1 w/w relation between the aliphatic and aromatic diamines, that correspond to a w/w PEO proportion of a 69%.

The first step for the synthesis of all the polymers here was to make a mixture of poly(ethylene oxide) (PEO-6000) (x mmol), and 4,4'-oxydianiline (ODA) (y mmol), in weight ratios 1:1, 2:1, 4:1, and 6:1, dissolved in anhydrous NMP (5 mmol (x+y)/10 mL) in a 100 mL three-necked flask blanketed with nitrogen.

Then, the reaction mixture was cooled down to 0 ºC, and under mechanical stirring, a stoichiometric amount of BKDA dianhydride (x+y mmol) was added and the mixture was stirred overnight at room temperature (see final resulting amounts of PEO-6000 in the samples in table 1). During this time the dianhydride completely dissolved and the solution reached high viscosity.

Table 1. Polymers synthesized in this work.

Sample	Treatment Temperature (ºC)	% Crystallized PEO/ % Total PEO	% Amorphous PEO/ polymer
cPI-69	180	49,0	36,1
	220	49,0	36,1
	260	55,0	32,1
cPI-60	180	0,90	59,9
	220	21,0	48,4
	260	31,0	42,0
cPI-44	180	0,0	43,8
	220	0,0	43,8
	260	1,0	39,4
cPI-29	180	0,0	28,3
	220	0,0	28,3
	260	0,0	28,3

9.2.3 Preparation of the copolyimide dense films

The resultant viscous copolyamic acid solution was diluted with NMP to the appropriate viscosity for casting, filtered through a nominal #1 fritted glass funnel, degassed, and cast onto leveled a glass plate. The resulting film was covered with a conical funnel to avoid fast evaporation of the solvent, dried at 80 ºC overnight, and finally thermally treated under inert atmosphere at different temperatures (see Figure 2 for a description of the different thermal treatments). Films of the copolymers of 80-100 μm in thickness were obtained.

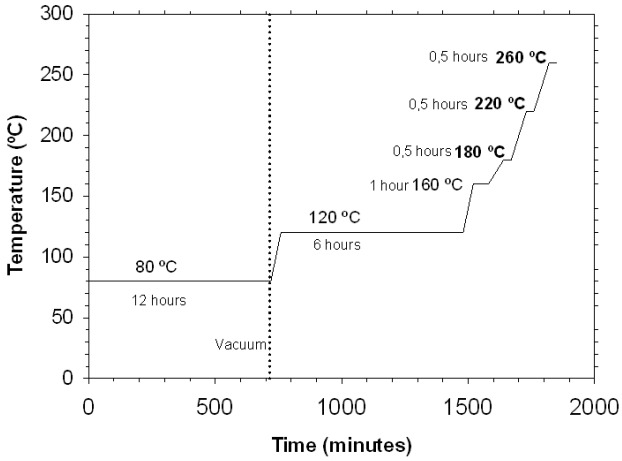

Figure 2. Sketch of the thermal treatment protocol.

9.2.4 Physical Characterization

Some of the physical characteristics of these copolymers have been shown in a previous paper [34]. For example, Attenuated total internal reflectance-Fourier transform infrared analysis (ATR-FTIR) has been used to verify the complete removal of solvent as well as imidization process, verifying that all the treated samples were completely imidized [34]. Thermomechanical analysis (TMA) was used to attain the Tg of the aromatic part of the sample, showing that for all the copolymers, the Tg of the aromatic polyimide is well above ambient temperature [34].

Small Angle X-ray Scattering (SAXS) proved that the systems suffer intense phase segregation after being thermally treated which increase for increasing percentage of PEO [34]. Moreover, mechanical properties of these membranes have been found to be good enough to allow their application to gas separation, although their mechanical resistance decreases slightly as the percentage of PEO increases [34].

On the other hand, from the standpoint of polymeric characterization, the use of thermogravimetric analysis (TGA) determined the thermal stability of the samples, and differential scanning calorimetry (DSC) was employed to determine the Tg and Tm of the aliphatic part of the sample and to determine the percentage of crystalline PEO in the sample.

Some results obtained by these techniques will be summarized below in order to correlate them with the gas transport and separation properties of such membranes.

9.2.5 Gas permeation

The permeability, P, for He, O_2, N_2, CO_2 and CH_4 were determined by using a barometric permeator using a constant volume technique which uses the time-lag operation method. The measurements were carried out at 30 ºC and 50 ºC and the applied pressure was 3 bar. A sketch of the device used has been shown elsewhere, [35]. The strategy known as time-lag method, attributed to Daynes et al. [36], is very appropriate to determine permeability, diffusivity and solubility of a sample by a simple, rapid and accurate method working under transitory regime. The method has been successfully applied to determine polymer gas permeation by many authors [37-38]. Its theoretical framework along with as the practical possibilities and limits of the technique have been abundantly documented, [39]. This system is nowadays an accepted method to assess the permeability and diffusion coefficients of gases through a polymer film.

9.3 Results and Discussion

9.3.1 Thermal Stability

Dynamic thermogravimetric runs in high-resolution mode have been performed in a nitrogen atmosphere for fully imidized copolymers (annealed at 220 ºC for 0,5 hours). TGA graphs showed a weight loss pattern consisting of three consecutive steps (see figure 3); an initial loss from ambient temperature to 300-350 ºC; a second loss from 300-350 ºC to 460-470 ºC; and a third loss from 460-470 ºC to 700 ºC.

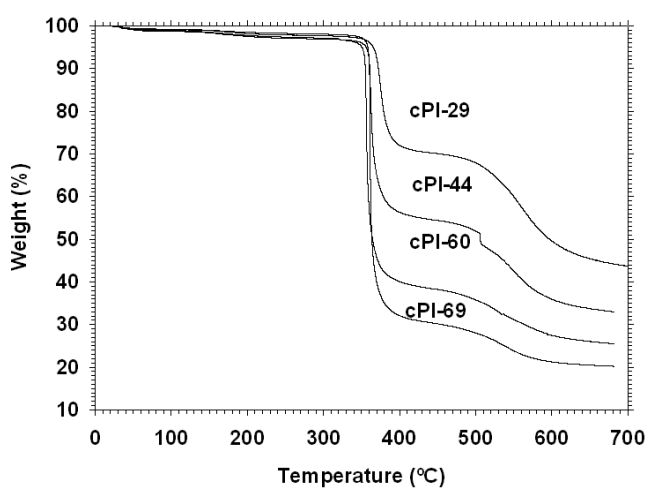

Figure 3. TGA curves in dynamic conditions for PEO based copolymers.

The first loss can be attributed to the absorbed water plus the solvent trapped in the film. This weight change is in range from 2 to 2.5 % [40]. The second loss step, after correcting for the previous weight decrease step, agrees with the theoretical contribution of α,ω-diamine-poly(ethylene oxide) in the copolymer composition [34], within a 3 % error (see Table 2) and it is therefore assigned to the weight loss due to the degradation of polyether block sequences. The differences between the weight losses should be due to the different mass percentages of PEO in the copolymers. The third and final stage of weight loss is due to the thermal decomposition of the remaining aromatic polyimide segments.

Table 2. Results obtained by TGA for the prepared copolymers.

Copolymer	**Theoretical polyether weight in the copolymer (%)**	**Experimental polyether weigth loss (%)**	**Temperature of maximum weight loss rate / ºC**	**Residue at 700ºC / %**
cPI-69	68,9	69,1	364	20,5
cPI-60	60,4	60,3	357	26,1
cPI-44	44,2	43,8	364	33,8
cPI-29	28,8	28,3	366	44,5

TGA analysis confirmed that the polyether thermal stability is much lower than the thermal stability of the aromatic polyimide segments, as already found for other copoly(ether-imide)s based on poly(ethylene oxide), and therefore a selective degradation of the polyether moiety could be performed in these copolymers. Other authors have also found that poly(propylene oxide) segments can be selectively degraded in: triblock [41-42], linear [43] and grafted [44] copolyimides to produce nanofoams.

The temperature of maximum weight loss rate was between 355-365 ºC for all copolymers. Of course, the char residue at 700 ºC is higher for the copolymers with more proportion of aromatic diamines, which leaves a higher residual content.

9.3.2 Calorimetric analysis

The samples were heated in a DSC instrument with a cyclic method in order to monitor the changes in thermal properties with the temperature of treatment [45]. All copolymers showed only the Tg and Tm corresponding to the poly(ethylene oxide) segments, and no transition for the aromatic polyimide segments could be detected. However, it was possible to obtain the Tg of the aromatic block by TMA. No significant changes in polyether Tg with thermal treatment took place, and thus Tg, for all the poly(ether-imide)s, was between -55 and -52 ºC.

Tg of the polymers is known to depend mainly on composition and length [46], although here composition seems to play a limited role on Tg. However, there were changes in the Tm of the copolymers. The Tm in the polymer is related with its crystallinity, and correlated with the purity of the PEO domains, because only pure PEO could crystallize. A clear correlation appears between the percentage of poly(ethylene oxide) in the sample and the Tm of the polymer. It is known that in dispersed materials, the melting point is strongly influenced by the size of the domains (and correspondingly of the crystals); thus, higher melting point for cPI-69 copolymer means that the size of the PEO domains is bigger than those for the rest of the copolymers. Figure 4 shows the changes in the Tm and the percentage of maximal crystallinity for PEO chains as a function of the treatment temperature (the temperature instantaneously reached by the DSC) for the copolymers studied.

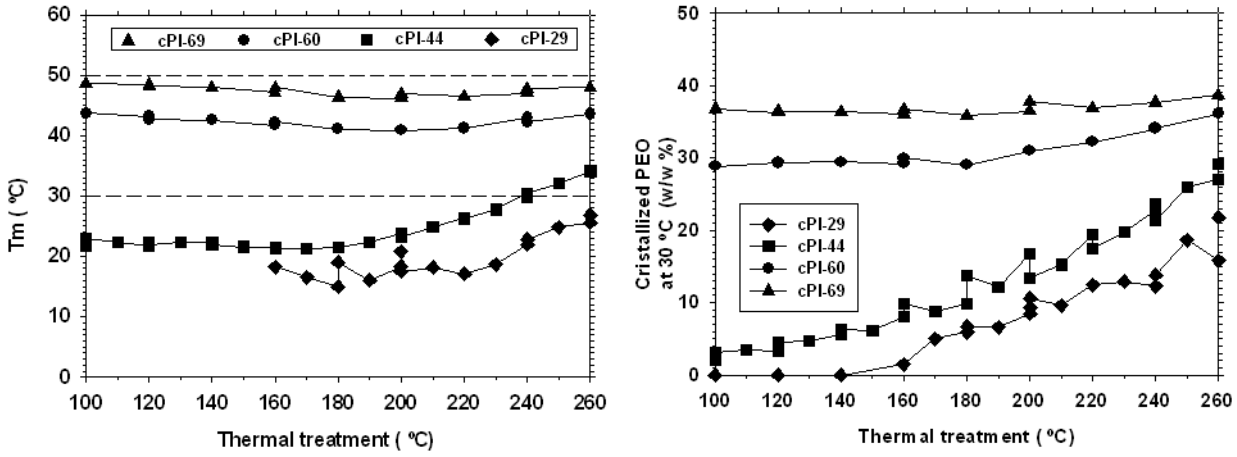

Figure 4. Tm (a) and maximal crystallinity (b) for the PEO portion of the copolymers as a function of the treatment temperature.

If a value of 8.67 kJ/mol is taken for the melting enthalpy of PEO [47], the amount of crystallized PEO, in the samples studied in this paper can be calculated as shown in Table 3. Note that the amount of crystallized PEO increases when its percentage does.

The amount of PEO-6000 crystallized in each sample for each heat treatment is relevant in what refers to gas permeability because the crystals act as obstacles to the passage of gas through the polymer. Under this assumption, it can be seen that if the sample is kept at 50 °C the percentage of crystallized poly(ethylene oxide) would be zero. At 30 ºC the amount of crystallized PEO for the samples cPI-29 and cPI-44 should be very low or negligible, while for the samples cPI-60 and cPI-69 the percentage of crystallized polyether is relatively important (see Table 3).

Table 3. Percentage of crystallized PEO at 30 ºC calculated by DSC.

Sample	**Treatment Temperature (ºC)**	**% Crystallized PEO/ % Total PEO**	**% Amorphous PEO/ polymer**
cPI-69	180	49,0	36,1
	220	49,0	36,1
	260	55,0	32,1
cPI-60	180	0,90	59,9
	220	21,0	48,4
	260	31,0	42,0
cPI-44	180	0,0	43,8
	220	0,0	43,8
	260	1,0	39,4
cPI-29	180	0,0	28,3
	220	0,0	28,3
	260	0,0	28,3

9.3.3 Gas transport properties

9.3.3.1 Behaviour with the temperature of measurement

The behavior of the polymers is strongly influenced by the percentage of amorphous or crystalline PEO in the sample. By DSC it was determined that samples contain a high percentage of crystalline PEO-6000 and that this crystallinity augments when the PEO content increases (higher phase segregation).

It is therefore very important to check the permeation performance as a function of the measurement temperature because high temperatures would lower the presence of such microcrystals in the segregated domains that could act as barriers hampering the passage of gases through the film.

Arrhenius' representation can help us to understand the behavior of the samples as a function of temperature. In effect, the dependence of gas diffusion on temperature can be expressed in terms of an Arrhenius type relationship that considers the movement of the gas molecules through a membrane as a thermally activated process [48]. Mathematically, the temperature dependence of diffusion is given as:

$$D = D_0 \, exp\left(\frac{E_D}{RT}\right) \tag{1}$$

where D_0 is the pre exponential factor and E_D is the activation energy of diffusion. The activation energy term depends on the size of the penetrant and not on its mass [37]. Taking into account the temperature dependence for the diffusion and sorption coefficients, the temperature effect on gas permeability is given as [48]:

$$P = P_0 \, exp\left(\frac{E_P}{RT}\right) \tag{2}$$

where E_P is the activation energy of permeation , which is the algebraic sum of E_D and ΔH_s. In general, permeability increases when temperature does. The results, for cPI-60, are shown in a plot of the natural logarithm of Permeability versus 1000/T in Figure 5. In this Figure it can be seen that there is a change in the trend when the measurement temperature is above 50 °C (1000/T-3.09). This demonstrates that samples must be in the same state at these high temperatures and that all PEO chains should be already in amorphous state.

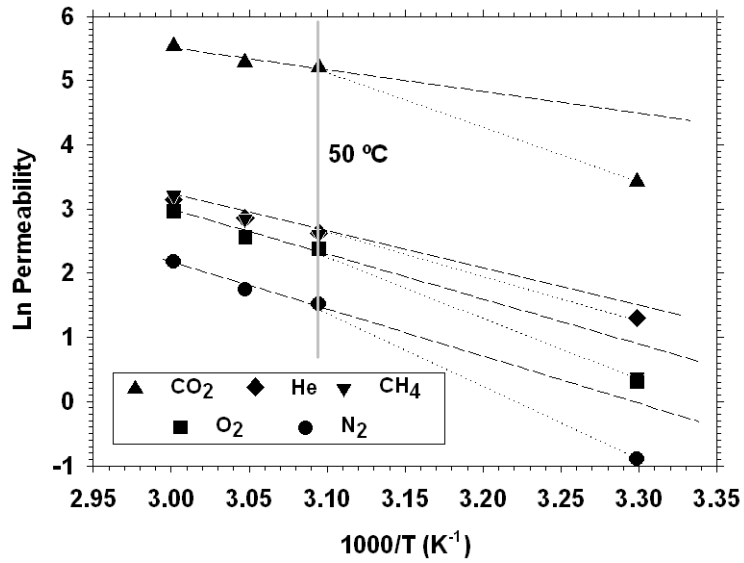

Figure 5. Arrhenius plot for the permeability of the gases studied.

In the same way, it is possible to make a representation of the ideal selectivity (the ratio of pure gas permeabilities), presented in Figure 6. There, we can clearly see that the change in tendency for temperatures over 50 ºC appears clearly. This is especially obvious for the CO_2/He couple probably because helium, due to its small size, is less affected by the PEO crystals.

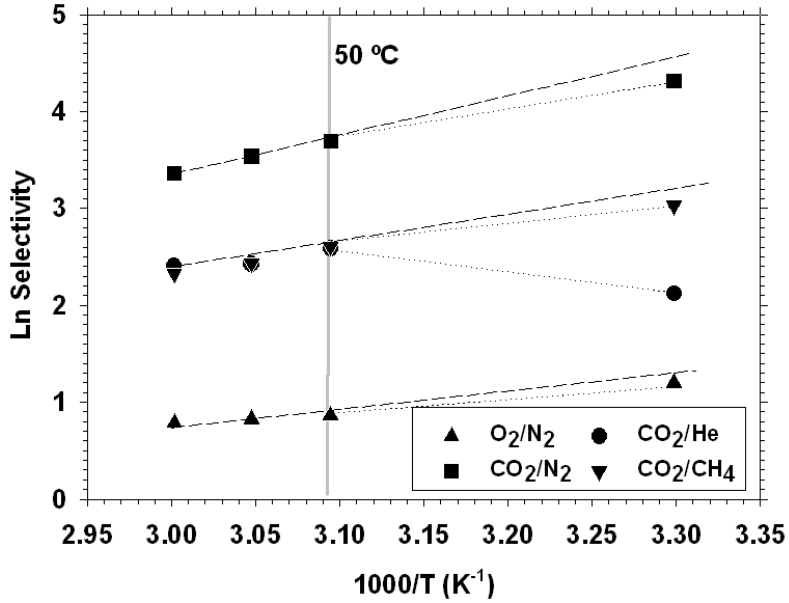

Figure 6. Natural logarithm of selectivity as a function of 1000/T.

9.3.3.2 Behaviour with the thermal treatment

Results show an improvement in permeability when the temperature of treatment is high. Therefore a correlation appears between high segregation and high permeability because both terms are caused by the thermal treatment of the copolymers. This correlation was already shown by us for other aliphatic-aromatic copoly(ether imide)s [45].

Figure 7 presents the permeability of different gases for the copolymer cPI-29 as a function of thermal treatment for two measurement temperatures: 30 (black symbols) and 50 ºC (white symbols).

The figure shows that when the samples are measured at 50 °C higher permeabilities are obtained because then we can assume that most of the PEO in the copolymer is in amorphous state. In general, permeability increases for high treatment temperatures, when most of the remaining solvent is released and the improvement in phase separation is higher. The same trend was observed for all the copolymers.

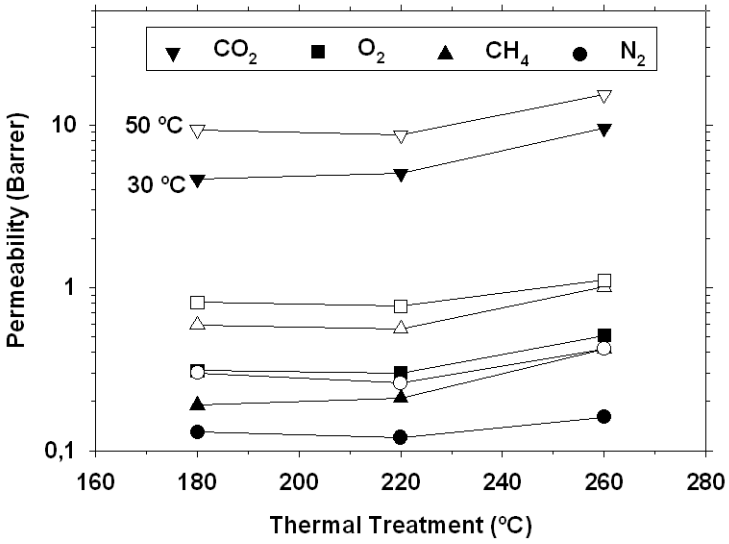

Figure 7. Permeability versus treatment temperature for the copolymer cPI-29 (1Barrer= 3.348 x 10^{-19} kmol·m / (m^2·s·Pa)).

9.3.3.3 Permeation properties as a function of the PEO percentage

Figure 8 shows the CO_2 permeability obtained for copolymers with different percentages of PEO for different samples thermally treated at the maximum temperature of 260 °C. When permeability is measured at 30 ºC there is a maximum permeability at approximately a 40 % of PEO followed by a steep decrease in permeability. This behavior fully disappears when permeation is measured at 50 ºC and a monotonous increase in permeability is obtained.

This is due to the hindering role of the increasing proportion of crystalline PEO appearing in the segregated domains for the copolymers containing high percentages of polyether chains.

It has been already mentioned that PEO crystals are practically impermeable to the passage of gases, so that if the total percentage of PEO in the sample is substituted by the percentage in the amorphous state (represented by white squared symbols in Figure 8), It can be observed that there is indeed a clear direct trend also at 30 °C between the permeability and the percentage of polyethylene oxide in the sample.

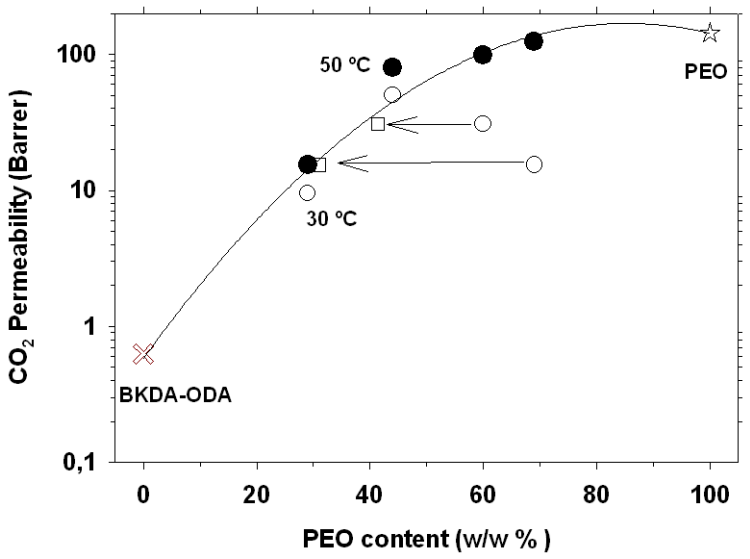

Figure 8. CO_2 permeability for samples treated at 260 ºC containing different percentages of PEO.

There representation also shows the values of the BKDA-ODA homopolymer [49] and pure PEO [32] at 35 °C (0 and 100% of PEO in the sample, respectively). It is clearly evident that the permeability values obtained for the samples are between them.

Recent works suggest that it should be a maximal length of PEO in the samples [50-51]. Our results suggest that that the apparent presence of such a maximum could be due to the presence of high crystallinity for long PEO chains. Thus, the correct strategy should be to increase the temperature of the permeation experiment to avoid the presence of these PEO crystals.

Similarly, Figure 9 shows the selectivity for several gas pairs as a function of the percentage of PEO. Particularly noteworthy is the behavior for the couple CO_2/N_2, where the selectivity values are over those exhibited for both the BKDA-ODA and PEO homopolymers. As expected, when the measurement temperature is higher, the selectivity decreases a little.

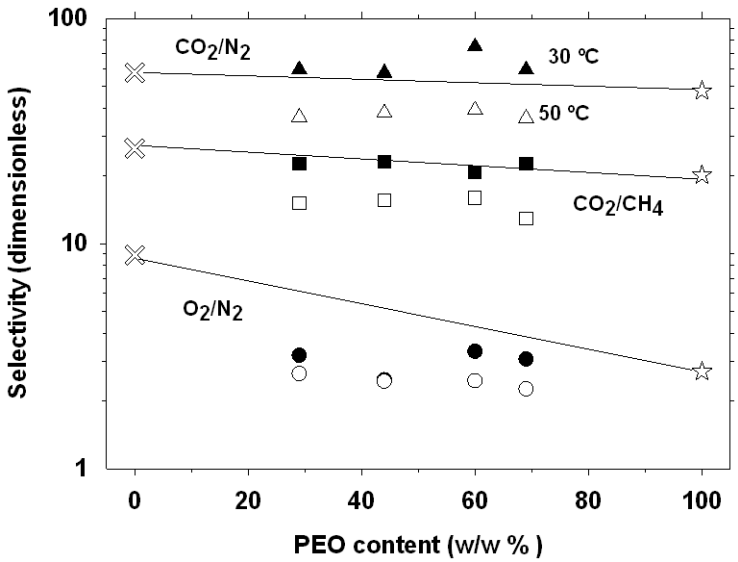

Figure 9. Selectivity for some gas pairs at 30 ºC (black squares) and 50 ºC (white symbols).

9.3.3.4 Robeson's plots

A visual way of illustrate and compare the permeability versus selectivity performances of a membrane for different gases are the corresponding Robeson's plots [52-53]. In these diagrams, in which the selectivity is shown as a function of the permeability of the most permeable gas in the couple, there is an upper bound which is called Robeson trade-off limit. The distance to this limit gives us an idea of the permeation properties of the samples. It has been shown in this paper that by measuring the samples at 50 °C permeability increases substantially with a very moderate decrease in selectivity due to the elimination of most or all the crystals of PEO from the copolymer. In order to present permselectivity at 50 ºC it is necessary to take into account that the corresponding

Robeson limit depends also on the temperature of measurement [54]. These charts are shown for some couples of gases in Figures 10-12. In this case in addition to our results the values of permeability and selectivity for PEO [32] and BKDA-ODA [49] at 35 ºC have been represented. In this way, assuming that our samples are mixtures of both the homopolymers BKDA-ODA and BKDA-PEO, the obtained gas separation properties should be intermediate between the values for these two polymers. It is worth noting that BKDA-PEO has very poor mechanical properties thus PEO data can be used assuming that BKDA-PEO should have permselectivities quite similar to that of pure PEO.

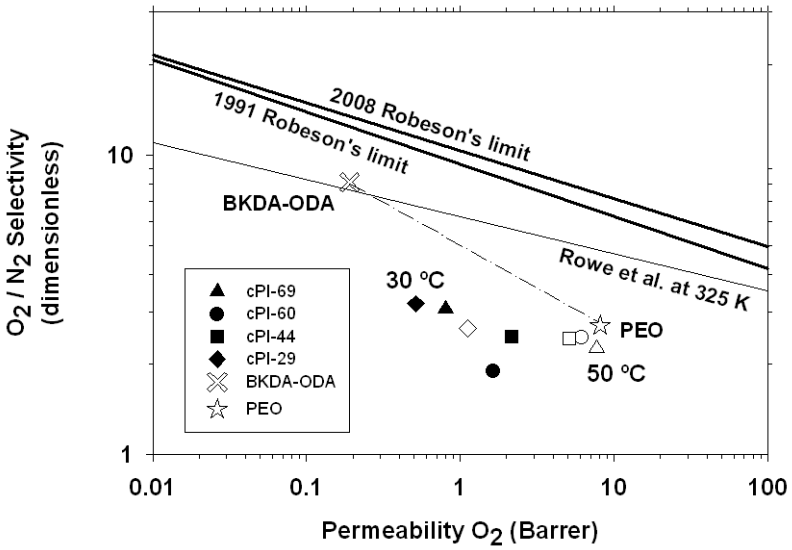

Figure 10. Robeson's plot for the O_2/N_2 gas pair.

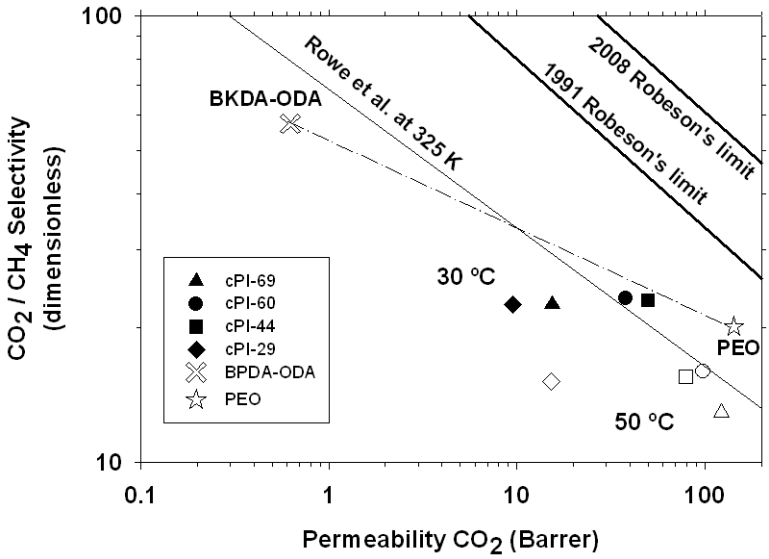

Figure 11. Robeson's plot for the CO_2/CH_4 gas pair.

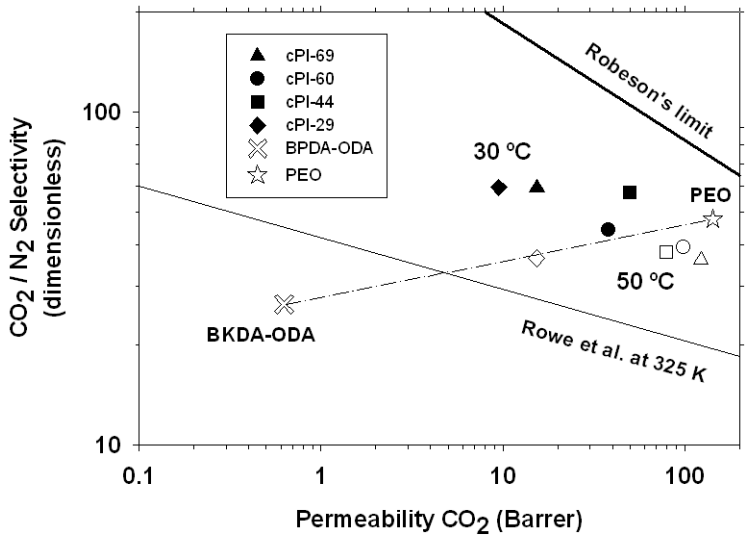

Figure 12. Robeson's plot for the CO_2/N_2 gas pair.

Our aim with these copolymers is, as mentioned, to combine aliphatic blocks to provide high permeability plus aromatic blocks that should supply excellent mechanical strength. Thus, a good result would approach as far as possible to the PEO permeability. For separations where similarly condensable gases (O_2/N_2 or CO_2/CH_4) selectivity of the copolymers should not change too much because then the selectivity is mainly determined by the aromatic portion of the copolymer. For gas

mixtures with very different condensability (CO_2/N_2 for example) the selectivity is even improved by the presence of PEO due to their easy condensability in the PEO moieties.

For both O_2/N_2 and CO_2/CH_4 separations, as expected, the performances of the membranes made out of the BKDA-ODA-PEO-6000 are between the two values corresponding to the homopolymers. In the CO_2/CH_4 case, the selectivity doesn't change substantially (it is actually determined by solubility which is similar for these gases). On the other hand, for the O_2/N_2 couple, selectivity even decreases with higher content of polyethylene oxide. In both cases permeability increases clearly when the content of polyethylene oxide increases. This increase in permeability is stronger for permeation experiments performed at 50 ºC although the distance to the corresponding upper bound is quite similar. Note that, for the gas pairs, results are below those for the pure homopolymers.

In any case, it is worth noting the particularly good permselectivity for the CO_2/N_2 gas couple. For this pair of gases, the selectivity is even over that of pure BKDA-ODA homopolymer. The corresponding permeabilities increase with the percentage of PEO in the sample, in such a way that for the samples with large proportions of polyether, selectivity versus permeability approaches the Robeson's upper bound at 30 ºC. The theoretical limit proposed by Rowe et al, [54] at 50 ºC is even more closely approached by the copolymers with high content of PEO as can be seen in Figure 12. The selectivity found for CO_2/N_2 substantially enhances that found for other polymers [55].

Thus, it has been proved that it is possible to modulate the permeability and the selectivity of block copolymers having PEO chains by controlling the amount of their soft and hard constituents. The presence of PEO blocks enhances permeability while a high selectivity for gas pairs containing CO_2 (principally for CO_2/N_2) is retained. Also, the presence of the aromatic polyimide part ensures good mechanical properties.

9.3.3.5 Permeability modeling

For this type of copolyimides consisting of an aromatic polyimide (hard part) and an aliphatic polyimide (soft PEO part), the permeability for the sample BKDA-ODA-PEO with different PEO percentages in the polymer may be predicted by the Maxwell equation as exposed below [56]:

$$P_{eff} = P_C \left[\frac{P_D + 2P_C - 2\phi_D \left(P_C - P_D \right)}{P_D + 2P_C + 2\phi_D \left(P_C - P_D \right)} \right] \qquad (3)$$

where P_{eff} is the effective permeability, P_C and P_D are the permeability of the continuous and the dispersed phase respectively and ϕ_D is the volume fraction of the dispersed phase in the block

copolymer. In this type of polymers, we should consider that the continuous phase could be the aromatic or the aliphatic one. We will consider PEO phase to be the continuous phase when the amount of PEO is higher than 20% because it has been established that for these PEO contents the consideration of the aromatic part as the continuous phase would make the model deviate from experimental results [50]. It is worth to note that the Maxwell model assumes that there is a mixture without interaction of impenetrable domains (disperse phase) within a continuous phase. Of course the role should be interchanged for some proportions near the 50 % proportion. Moreover within the range of compositions when the roles are reversing it is not at all a question of pure distinguishable and separated disperse and continuous phases and obviously the equation doesn't fit the results.

The permeability of pure PEO in the amorphous state is used as the permeability of the soft segments [32] and the permeability of the aromatic homopolymer BKDA-ODA as that for the hard segments [49].

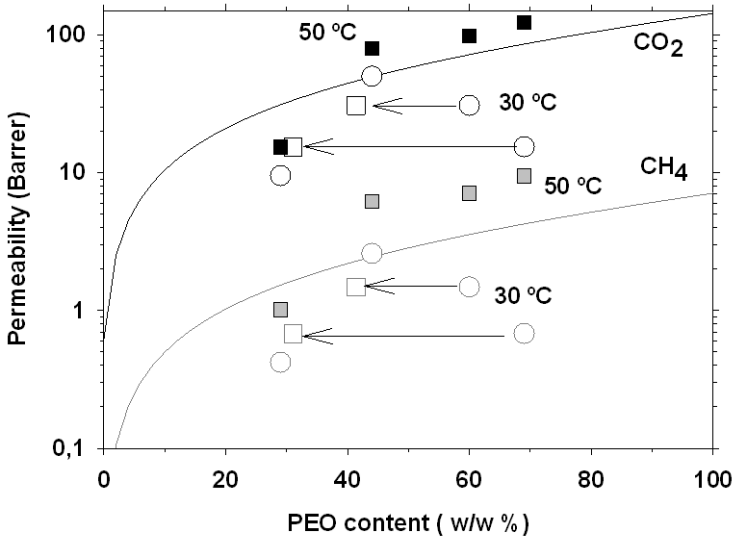

Figure 13. Predicted values for CO_2 and CH_4 permeabilities by using Maxwell equation. Empty squares correspond to the content of amorphous PEO.

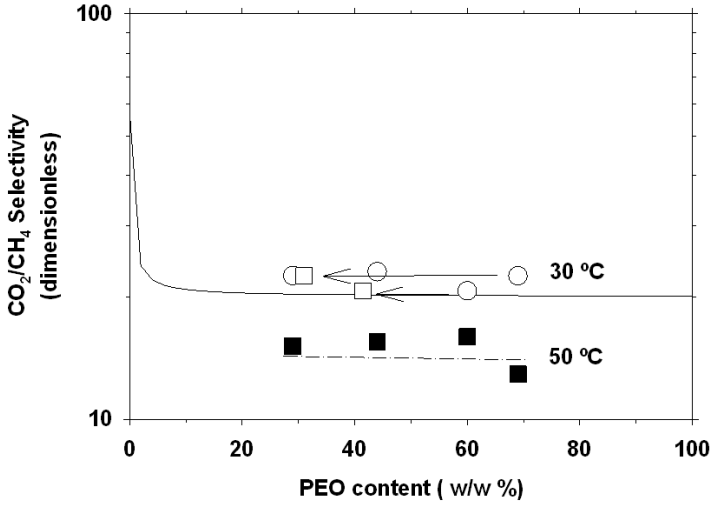

Figure 14. Predicted values for CO_2/CH_4 selectivity using Maxwell equation. Empty squares correspond to the content of amorphous PEO.

Figure 13 and Figure 14 show the permeability and selectivity prediction for the CO_2 and CH_4. The model is clearly more precise to predict permeabilities than selectivities and gives better results once the portion of crystallinity has been substracted. Of course both of them are only approximately fitted but at least the model reproduces the tendency. It is also clear that the corrected results for experiments done at 30 ºC fit better the model than those for 50 ºC because the permeabilities of the homopolymers used in Equation (3) have been taken at ambient temperature.

9.4 Conclusions

A series of copoly(ether-imide)s presenting good gas separation properties have been prepared. These copolymers have been synthesized by the reaction between an aromatic dianhydride (BKDA), an aromatic diamine (ODA) and a diamine terminated poly(ethylene oxide) having a molecular weight of 6000 g/mole (PEO-6000), in a different percentage of PEO in the final copolymer.

TGA analysis confirmed the exact amount of PEO present in the material and showed that it can be selectively eliminated from the rest of the sample. DSC proved that the Tg values for the aliphatic blocks are quite similar, which means that the structure of PEO in the copolymers is alike. Nevertheless, the melting temperature associated to the PEO chains is different decreasing when the segregated domains are smaller. The maximal crystallinity is higher for copolymers containing

larger percentages of PEO while the real crystallinity can be relatively high at low temperatures of operation. The permeability increases with the percentage of PEO in amorphous state (i.e. for percentages corrected to take into account the crystallinity of the samples).

The thermal treatment of the samples improved phase segregation, which as well produced an increasing permeability. Permeability and selectivity are between those for the homopolymers except for the CO_2/N_2 pair of gases. Although permeability increases with increasing percentage of PEO, the selectivity for the CO_2/CH_4, remains almost constant while for O_2/N_2 it decreases slightly. For the CO_2/N_2 gas couple, results for high PEO percentages at 30 °C are quite close to the Robeson bound. In the case of the measurements at 50 °C, the permeability-selectivity values approach even more closely to the limit for this temperature. In conclusion, it seems clear that these copolymers are suitable for separations where CO_2 is involved and non-condensable gases are involved, especially for the separation CO_2/N_2. These separations have a great importance in the remediation of greenhouse effect and make these membranes good candidates for their application at industrial level.

We have also compared the experimental results with those calculated by using the Maxwell's model. In this case, the percentage of amorphous PEO should be used and the crystallinity has to be taken into account for low permeation temperatures. If these corrections are made the model fits relatively well the permeability experimental results and it is also reasonably valid to be used to justify the found selectivities in spite of the clear simplifications assumed. The need to take into account the truly amorphous portion of PEO makes necessary to optimize both the amount of poly(ethylene oxide) in the sample and the operating temperature of these materials for a specific length and amount of PEO.

9.5 Acknowledgements

We are indebted to the Spanish Junta de Castilla León for financing this work through the GR-18 Excellence Group Action and to the Ministry of Science and Innovation in Spain for their economic support of this work (MAT2008-00619/MAT, MAT2010-20668/MAT, MAT2011-25513/MAT and CIT-420000-2009-32). We also acknowledge financial support from the program Consolider Ingenio 2010 (project CSD-0050-MULTICAT). The help provided by Sara Rodriguez in measuring gas permeability and selectivity is greatly appreciated. A. Tena thanks CSIC for a predoctoral JAE fellowship.

9.6 References

1. J.T.D. Houghton, Y.; Griggs, D.J.; Noguer, M.; van der Linden, P.J.; Dai, X.; Maskell, K.; Johnson, C.A., Climate Change 2001: The Scientific Basis, Cambridge University Press, New York, 2001.
2. O.M.B. Davidson, Special Report on Carbon Dioxide Capture and Storage, International Panel on Climate Change, Geneva, Switzerland, 2005.
3. J.D. Figueroa, T. Fout, S. Plasynski, H. McIlvried, R.D. Srivastava, Advances in CO_2 capture technology-The U.S. Department of Energy's Carbon Sequestration Program, International Journal of Greenhouse Gas Control, 2 (2008) 9-20.
4. B.D. Metz, O.; de Coninck, H. ; Loos, M. ; Meyer L. , IPCC Special Report on Carbon Dioxide Capture and Storage, United Kingdom 2005.
5. J. Davison, K. Thambimuthu, Technologies for capture of carbon dioxide, in, International Energy Association (IEA), Vancouver, Canada, 2004.
6. R. Steeneveldt, B. Berger, T.A. Torp, CO_2 capture and storage: Closing the knowing-doing gap, Chemical Engineering Research and Design, 84 (2006) 739-763.
7. E. de Visser, C. Hendriks, M. Barrio, M.J. Mølnvik, G. de Koeijer, S. Liljemark, Y. Le Gallo, Dynamis CO_2 quality recommendations, International Journal of Greenhouse Gas Control, 2 (2008) 478-484.
8. R.W. Baker, Future directions of membrane gas separation technology, Industrial and Engineering Chemistry Research, 41 (2002) 1393-1411.
9. H.J. Herzog, What future for carbon capture and sequestration?, Environmental Science and Technology, 35 (2001) 148-153.
10. W.J. Koros, Evolving beyond the thermal age of separation processes: Membranes can lead the way, AIChE Journal, 50 (2004) 2326-2334.
11. M. Krumbeck, Post combustion capture from coal, CSLF CCS Workshop Paris, in, 2007.
12. J. Gibbins, H. Chalmers, Carbon capture and storage, Energy Policy, 36 (2008) 4317-4322.
13. I.G.G.R.D. Programme, CO_2 capture ready plants, UK, 2007/4.
14. E. Favre, Membrane processes and postcombustion carbon dioxide capture: Challenges and prospects, Chemical Engineering Journal, 171 (2011) 782-793.
15. R. Bounaceur, N. Lape, D. Roizard, C. Vallieres, E. Favre, Membrane processes for post-combustion carbon dioxide capture: A parametric study, Energy, 31 (2006) 2220-2234.
16. GCEP, An assessment of carbon capture technology and research opportunities, Standford University Global Climate & Energy Project (GCEP) Standford University 2005.

17. E. Favre, Carbon dioxide recovery from post-combustion processes: Can gas permeation membranes compete with absorption?, Journal of Membrane Science, 294 (2007) 50-59.
18. M.T.K. Bessonov, M.M.; Kudryavtsev, V.V.; Laius, L.A., Polyimides: Thermally Stable Polymers, Consultants Bureau, New York, 1987.
19. M.K.M. Ghosh, K.L., Polyimides: Fundamentals and Applications, Marcel Dekker, New York, 1996.
20. D.S. Wilson, H.D.; Hergenrother, P.M., Polyimides, Blackie, Glasgow, 1990.
21. D. Ayala, A.E. Lozano, J. De Abajo, C. García-Perez, J.G. De La Campa, K.V. Peinemann, B.D. Freeman, R. Prabhakar, Gas separation properties of aromatic polyimides, Journal of Membrane Science, 215 (2003) 61-73.
22. K. Tanaka, H. Kita, K. Okamoto, A. Nakamura, Y. Kusuki, Gas permeability and permselectivity in polyimides based on 3,3',4,4'-biphenyltetracarboxylic dianhydride, Journal of Membrane Science, 47 (1989) 203-215.
23. T.A. Barbari, W.J. Koros, D.R. Paul, Gas transport in polymer based on bisphenol-A, Journal of Polymer Science, Part B: Polymer Physics, 26 (1988) 709-727.
24. Y. Li, M. Ding, J. Xu, Gas separation properties of aromatic polyetherimides from 1,4-bis(3,4-dicarboxyphenoxy)benzene dianhydride and 3,5-diaminobenzic acid or its esters, Journal of Applied Polymer Science, 63 (1997) 1-7.
25. Y. Hirayama, Y. Kase, N. Tanihara, Y. Sumiyama, Y. Kusuki, K. Haraya, Permeation properties to CO_2 and N_2 of poly(ethylene oxide)-containing and crosslinked polymer films, Journal of Membrane Science, 160 (1999) 87-99.
26. M. Kawakami, H. Iwanaga, Y. Hara, M. Iwamoto, S. Kagawa, Gas permeabilities of cellulose nitrate/poly(ethylene glycol) blend membranes, Journal of Applied Polymer Science, 27 (1982) 2387-2393.
27. K.I. Okamoto, M. Fujii, S. Okamyo, H. Suzuki, K. Tanaka, H. Kita, Gas permeation properties of poly(ether imide) segmented copolymers, Macromolecules, 28 (1995) 6950-6956.
28. K.U. Okamoto, N.; Okamyo, S.; Tanaka, K.; Kita, H., Selective permeation of carbon dioxide over nitrogen through polyethyleneoxide-containing polyimide membranes, Chemistry Letters 5(1993) 225-228.
29. H. Suzuki, K. Tanaka, H. Kita, K. Okamoto, H. Hoshino, T. Yoshinaga, Y. Kusuki, Preparation of composite hollow fiber membranes of poly(ethylene oxide)-containing polyimide and their CO_2/N_2 separation properties, Journal of Membrane Science, 146 (1998) 31-37.

30. K.I. Okamoto, N. Yasugi, T. Kawabata, K. Tanaka, H. Kita, Selective permeation of carbon dioxide through amine-modified polyimide membranes, Chemistry Letters, (1996) 613-614.
31. A. Car, C. Stropnik, W. Yave, K.V. Peinemann, Pebax®/polyethylene glycol blend thin film composite membranes for CO_2 separation: Performance with mixed gases, Separation and Purification Technology, 62 (2008) 110-117.
32. H. Lin, B.D. Freeman, Gas solubility, diffusivity and permeability in poly(ethylene oxide), Journal of Membrane Science, 239 (2004) 105-117.
33. S.R. Reijerkerk, M.H. Knoef, K. Nijmeijer, M. Wessling, Poly(ethylene glycol) and poly(dimethyl siloxane): Combining their advantages into efficient CO_2 gas separation membranes, Journal of Membrane Science, 352 (2010) 126-135.
34. A. Marcos-Fernández, A. Tena, A.E. Lozano, J.G. de la Campa, J. de Abajo, L. Palacio, P. Prádanos, A. Hernández, Physical properties of films made of copoly(ether-imide)s with long poly(ethylene oxide) segments, European Polymer Journal, 46 (2010) 2352-2364.
35. J. Marchese, M. Anson, N.A. Ochoa, P. Prádanos, L. Palacio, A. Hernández, Morphology and structure of ABS membranes filled with two different activated carbons, Chemical Engineering Science, 61 (2006) 5448-5454.
36. H.A. Daynes, The process of diffusion through a rubber membrane, Proceedings of the Royal Society London, 1920.
37. J. Crank, The Mathematics of Diffusion, s.e.C. Press (Ed.), Clarendon Press, Oxford, 1975.
38. D.D. Paul, A.T., Gas and vapor solubility in crosslinked poly(ethylene glycol diacrylate), diffusion in amorphous polymers,. J. Polym. Sci., 10 (1965) 17–44.
39. S.W. Rutherford, D.D. Do, Review of time lag permeation technique as a method for characterisation of porous media and membranes, Adsorption, 3 (1997) 283-312.
40. J.L. Hedrick, T.P. Russell, J. Labadie, M. Lucas, S. Swanson, High temperature nanofoams derived from rigid and semi-rigid polyimides, Polymer, 36 (1995) 2685-2697.
41. J.L. Hedrick, K.R. Carter, H.J. Cha, C.J. Hawker, R.A. DiPietro, J.W. Labadie, R.D. Miller, T.P. Russell, M.I. Sanchez, W. Volksen, D.Y. Yoon, D. Mecerreyes, R. Jerome, J.E. McGrath, High-temperature polyimide nanofoams for microelectronic applications, Reactive and Functional Polymers, 30 (1996) 43-53.
42. J.L. Hedrick, Y. Charlier, R. Dipietro, S. Jayaraman, J.E. McGrath, High Tg polyimide nanofoams derived from pyromellitic dianhydride and 1,1-bis(4-aminophenyl)-1-phenyl-2,2,2-trifluoroethane, Journal of Polymer Science, Part A: Polymer Chemistry, 34 (1996) 2867-2877.

43. T. Philip Gnanarajan, N. Padmanabha Iyer, A. Sultan Nasar, G. Radhakrishnan, Preparation and properties of poly(urethane-imide)s derived from amine-blocked-polyurethane prepolymer and pyromellitic dianhydride, European Polymer Journal, 38 (2002) 487-495.
44. T.T. Moore, R. Mahajan, D.Q. Vu, W.J. Koros, Hybrid membrane materials comprising organic polymers with rigid dispersed phases, AIChE journal, 50 (2004) 311-321.
45. A. Tena, A. Marcos-Fernández, A.E. Lozano, J.G. de la Campa, J. de Abajo, L. Palacio, P. Prádanos, A. Hernández, Thermally treated copoly(ether-imide)s made from bpda and alifatic plus aromatic diamines. Gas separation properties with different aromatic diamimes, Journal of Membrane Science, 387–388 (2012) 54-65.
46. Y. Hu, M. Rogunova, V. Topolkaraev, A. Hiltner, E. Baer, Aging of poly(lactide)/poly(ethylene glycol) blends. Part 1. Poly(lactide) with low stereoregularity, Polymer, 44 (2003) 5701-5710.
47. D.W. Van Krevelen, Properties of polymers in: third edition, Elsevier, Amsterdam, 1990, pp. 120
48. R.E.F. Kesting, A. K. , Polymeric gas separation membranes, in, John Wiley & Sons, New York, 1993.
49. K. Tanaka, H. Kita, M. Okano, K.-i. Okamoto, Permeability and permselectivity of gases in fluorinated and non-fluorinated polyimides, Polymer, 33 (1992) 585-592.
50. C. Hangzheng, X. Youchang, C. Tai-Shung, Synthesis and characterization of poly (ethylene oxide) containing copolyimides for hydrogen purification, Polymer, 51 (2010) 4077-4086.
51. W. Yave, A. Szymczyk, N. Yave, Z. Roslaniec, Design, synthesis, characterization and optimization of PTT-b-PEO copolymers: A new membrane material for CO_2 separation, Journal of Membrane Science, 362 (2010) 407-416.
52. L.M. Robeson, Correlation of separation factor versus permeability for polymeric membranes, Journal of Membrane Science, 62 (1991) 165-185.
53. L.M. Robeson, The upper bound revisited, Journal of Membrane Science, 320 (2008) 390-400.
54. B.W. Rowe, L.M. Robeson, B.D. Freeman, D.R. Paul, Influence of temperature on the upper bound: Theoretical considerations and comparison with experimental results, Journal of Membrane Science, 360 (2010) 58-69.
55. C.E. Powell, G.G. Qiao, Polymeric CO_2/N_2 gas separation membranes for the capture of carbon dioxide from power plant flue gases, Journal of Membrane Science, 279 (2006) 1-49.
56. J.C. Maxwell, A treatise on electricity and magnetism, in: vol. 1, Dover Publications Inc, New York, 1954.

CHAPTER 10

Thermally Segregated Copolymers with PPO Blocks for Nitrogen Removal from Natural Gas

Alberto Tena[1,3], Ángel Marcos-Fernández[1,3], Ángel E. Lozano[1,3], J. G. de la Campa[1,3], Javier de Abajo[1,3], Laura Palacio[1,2], Pedro Prádanos[1,2], Antonio Hernández[1,2]

[1]*Smap UA-UVA-CSIC, Parque Científico Universidad de Valladolid, Paseo de Belén, s/n, 47011 Valladolid, Spain.*

[2]*Dept. Física Aplicada, Facultad de Ciencias, Universidad de Valladolid, Paseo de Belén, 7, 47011 Valladolid, Spain*

[3]*Instituto de Ciencia y Tecnología de Polímeros, CSIC, Juan de la Cierva 3, 28006 Madrid, Spain.*

This chapter has been published in:

Industrial & Engineering Chemistry Research 52, (**2013**), 4312−4322

DOI: dx.doi.org/10.1021/ie303378k

Abstract

Copoly(ether imide)s formed by the reaction of an aromatic dianhydride (BPDA), an aromatic diamine (ODA or BNZ), and α,ω-bis(2-aminopropyl polypropylene oxide)s with molecular weights of 2000 and 4000 g/mol were obtained, characterized, and studied as gas separation membranes. All of the copoly(ether imide)s studied showed a low imidization temperature, well below 200 °C. They also underwent a phase segregation process, as confirmed by SAXS, when they were thermally treated. The segregation was found to increase permeability without any significant decrease of selectivity for almost all of the gas pairs studied (O_2/N_2, CO_2/CH_4, and CO_2/N_2). For the CH_4/N_2 pair, a strong increase in selectivity was obtained upon segregation, along with a rising permeability. This excellent gas productivity for the mixture CH_4/N_2 is probably due to a combined effect of a specific interaction and an increase in solubility of CH_4 in the soft segregated domains of the copolymer.

Methane permeabilities over 20 barrer and CH_4/N_2 selectivities close to 4.2 for an applied pressure of 1 bar were attained. The changes in permselectivity with permeation temperature were observed to follow an Arrhenius correlation, which adds a certain tunable permeability versus selectivity to these materials. Thus, it is possible to attain high selectivities (for relatively low temperatures) or high permeabilities (for comparatively high temperatures). The proportion of PPO in the final polymer has a significant influence on the segregation extent and domains, so that both the selectivity and permeability improved when the proportion of polyether in the final polymer was high. The mechanical properties were good for all of the proportions and/or densities tested. All of the copolymers studied showed a high resistance to plasticization and to the action of solvents and aggressive media. The high permselectivities and resistance to plasticization and solvents suggest that the membranes obtained could be advantageously used in natural gas extraction and purification.

10.1 Introduction

The growing global demand for energy results in a persistent tension with the limited supply of fossil-fuel-derived products. Despite the increased attention to a wide range of sources of renewable and nonrenewable energy, liquefied petroleum continues to dominate the world consumption of energy [1]. In this context, there is an urgent need to change the world's dependence on oil by searching for cleaner fuels as an alternative energy source [2]. The ideal solution to ensure the sustainability of energy is full utilization of renewable resources for power generation and transportation. The combustion of natural gas derivatives and hydrogen as fuels is vital to reduce emissions of greenhouse gases and global warming in the period of change in the pattern of world energy consumption [3]. Because of the lack of infrastructure for hydrogen storage and distribution, natural gas (or methane derived from fossil fuels) is often seen as a fuel source bridge to a hydrogen economy.

Natural gas has a lower carbon footprint than gasoline or coal and is used increasingly as a source of energy. Despite the increasing demand for natural gas, the gas reserves have remained reasonably stable because producers have been able to replace most of the drained reserves with new resources over time [3,4]. In addition to natural gas, methane (i.e., biomethane) can be generated from the anaerobic digestion of biomass by microorganisms [5,6]. In all cases, the removal of impurities is necessary to increase the heating value, to meet the requirements of pipes, to reduce the volume of gas transported, to prevent corrosion of pipes inside the gas distribution network, and to reduce air pollution. Actually, natural gas will be accepted for transport by pipeline only if it contains less than a specified amount of nitrogen, typically between 4% and 6% (w/w) [7−9]. Nitrogen content can be lowered by pressure-swing adsorption (PSA) using molecular sieves that preferentially adsorb nitrogen [9,10], but cryogenic distillation is the only process used on a large scale. In fact, only in the United States are there cryogenic plants (a total of around 30) operating for the removal of this excess nitrogen [8]. Such plants require high capital and energy costs. It is therefore necessary to search for new sources of purification. Approximately 17% of natural gas reserves in the United States do not meet pipeline specifications because of high nitrogen content [8,11]. About 40% of these reserves would require new suitable gas processing technology, especially for gas containing more than 15% nitrogen [7,8]. Moreover, many small gas wells are closed because of the absence of a technology that could be applied to the small-scale separation of nitrogen.

Consequently, a very important research and development effort is being conducted to obtain new materials that allow for efficient nitrogen versus methane separation using polymeric membranes. The use of polymeric membranes in gas purification processes is mainly due to their high

applicability, good mechanical properties, low cost, and simple operation. Observing the separation of methane from nitrogen, in the case of glassy polymers, nitrogen is usually more permeable, whereas in the case of rubbery polymers, methane is frequently more permeable than nitrogen. Obtaining suitable nitrogen permeable membranes does not seem feasible. A nitrogen/methane selectivity of at least 15 should be required to make this type of membrane economically viable; the highest selectivity available with current polymers is only about [2−3,12,13]. On the other hand, for a methane-permeable membrane to be viable, a methane/nitrogen selectivity of 4 to 6 would suffice [14]. The best measure of the ability of a membrane to separate two gases, for example, e nitrogen and methane, is the ratio of their permeabilities, called the membrane selectivity, which can be written as the product of the ratio of diffusivities and solubilities.

$$\alpha_{i/j} = \frac{P_i}{P_j} = \left[\frac{D_i}{D_j}\right]\left[\frac{S_i}{S_j}\right] = (\alpha_D)(\alpha_S) \tag{1}$$

In polymer materials, diffusion coefficients decrease with increasing molecular size of the gas because large molecules interact with more segments of the polymer chain than small molecules. For this reason, the diffusive selectivity, α_D, always favors permeation of small molecules such as nitrogen (kinetic diameter = 3.64 Å) over larger ones such as methane (kinetic diameter = 3.80 Å). The sorption coefficient of gases in a polymer generally increases with increasing condensability. Hence, the sorption selectivity, α_S, favors sorption of the more condensable gas (methane, with a boiling point of 111 K) over the less condensable gas (nitrogen, with a boiling point of 77 K). It follows that the effects of the diffusivity and sorption selectivity terms for the separation of nitrogen−methane mixtures in eq. 1 are divergent [12,15]. The magnitude of the diffusivity selectivity term depends on whether the polymer in the selective layer of the membrane is above or below its glass transition temperature. Below the glass transition temperature, the polymer chains are essentially fixed, and only very limited movement is possible. The polymer is then a rigid, tough glassy material, and the effect on the relative mobility of differences in the sizes of the permeating gases is relatively large. If the polymer is above its glass transition temperature, motion of the polymer chains is increased significantly. The polymer is then rubbery and elastic, and the effect of molecular size on relative permeant mobility is reduced. Normally, the ratio D_{N_2}/D_{CH_4} is between 1.5 and 2.0 for rubbery polymers and between 3 and 6 for glassy polymers [13,16].

For nitrogen and methane, the solubility selectivity term, S_{CH_4}/S_{N_2}, usually lies between 2.5 and 5 for both rubbery and glassy polymers. It follows from the preceding discussion that glassy polymers tend to permeate nitrogen preferentially, with a maximum expected N_2/CH_4 selectivity of ~2.5, and similarly, rubbery polymers will tend to permeate methane preferentially, with a maximum

expected CH_4/N_2 selectivity of ~3.5 [16]. Therefore, it is necessary to search for polymeric materials with the ability to carry out the separation of nitrogen and methane, as well as withstand the conditions of solvents, temperatures, and pressures present in the wells.

In this article, we report the preparation and characterization of gas separation membranes obtained from a series of new aromatic−aliphatic copolyimides with segregated blocks. These copolymers permeate methane preferentially because of the elastomeric properties of the segregated aliphatic chains. The aliphatic block consists of flexible chains of poly(propylene oxide) (PPO), which has specific affinity for methane that helps to increase its permeability while exhibiting very good mechanical properties and stability.

10.2 Experimental section

10.2.1 Chemicals

3,3′,4,4′-Biphenyltetracarboxylic dianhydride (BPDA), 4,4′-diaminobiphenylbenzidine (BNZ), and 4,4′-oxidianiline (ODA) were purchased from Aldrich. These reagents were purified by sublimation under high vacuum just before being used. Bis(2-aminopropyl) poly(propylene oxide) samples with nominal molecular weights of 2000 g/mol (Jeffamine D2000, denoted PPO-2000) and 4000 g/mol (Jeffamine D4000, denoted PPO-4000) were kindly donated by Huntsman Europe (Everberg, Belgium). These polyethers were dried at 70 °C in a vacuum for 5 h and stored in a desiccator under a vacuum until use. The total amine content obtained by titration was 1.01 mequiv/g for PPO-2000 and 0.48 mequiv/g for PPO-4000. Anhydrous N,N′-dimethylacetamide (DMAc), used as the polymerization solvent, was purchased from Sigma-Aldrich Co. Figure 1 shows the chemical structures of the monomers.

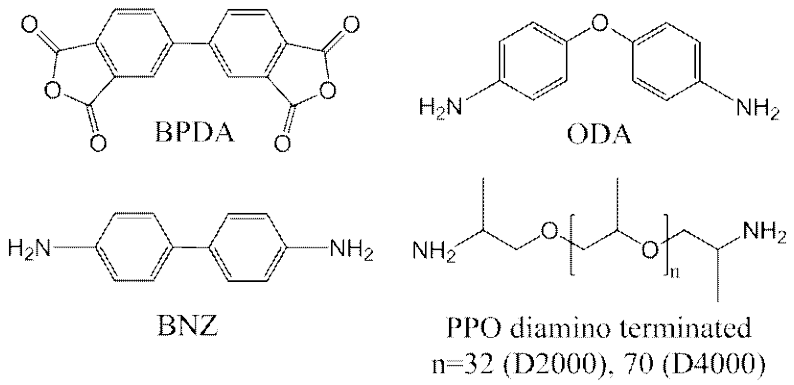

Figure 1. Chemical structure of the monomers.

10.2.2 Synthesis of Copoly(ether imide)s

The procedure for the synthesis of all of the polymers in this study was as follows: A mixture of bis(2-aminopropyl) poly(propylene oxide) (x mmol) and aromatic diamine (y mmol) in a weight ratio of 2:1, 1:1, or 1:2 was dissolved in anhydrous N,N′-dimethylacetamide (DMAc) [5 mmol of (x + y)/10 mL] in a 100 mL three-necked flask blanketed with nitrogen. The reaction mixture was cooled to 0 °C; under mechanical stirring, a stoichiometric amount of BPDA dianhydride (x + y mmol) was added all at once; and the mixture was stirred overnight at room temperature. During this time, the dianhydride completely dissolved, and the solution reached high viscosity.

The resultant viscous copolyamic acid solution was diluted with DMAc to the appropriate viscosity for casting, filtered through a nominal number 1 fritted glass funnel, degassed, and cast onto a leveled glass plate. The resulting films were covered with a conical funnel to avoid fast evaporation of the solvent, dried at 80 °C overnight, and finally treated at 120 °C for 5 h in a vacuum oven. Films of the copolymers that were 50−70 μm in thickness were obtained. After that, thermal treatments under inert atmosphere were carried out at different temperatures. Table 1 provides a complete list of the synthesized polymers and the symbols by which they are identified throughout this article.

Table 1. Polymers synthesized ii

Diamines	Weight ratio PPO/ODA	Denomination
PPO-2000 ODA	2/1	cPI-PPO-2000 (2/1)
PPO-4000 ODA	2/1	cPI-PPO-4000 (2/1)
PPO-4000 ODA	1/1	cPI-PPO-4000 (1/1)
PPO-4000 ODA	1/2	cPI-PPO-4000 (1/2)
PPO2000-PPO4000 ODA	2/1	cPI-PPO-2000+4000 ODA (2/1)
PPO2000-PPO4000 BNZ	2/1	cPI-PPO-2000+4000 BNZ (2/1)

10.2.3 Experimental Methods

Attenuated total internal reflectance-Fourier transform infrared (ATR-FTIR) analyses were performed at room temperature using a Perkin-Elmer Spectrum One infrared spectrometer equipped with an ATR accessory.

A TA Instruments Q500 system was used for thermogravimetric analysis (TGA). Disk samples cut from films with weights between 5 and 15 mg were tested. Dynamic scans were run in high-resolution mode, where the heating rate was automatically adjusted in response to changes in the rate of weight loss, resulting in improved resolution, with an initial heating rate of 10 °C/min under a flux of nitrogen.

Differential scanning calorimetry (DSC) analyses were carried out in a Mettler Toledo (DSC 822e) calorimeter equipped with a liquid nitrogen accessory. Disk samples cut from films weighing 5−15 mg were sealed in aluminum pans. Samples were heated with the following cyclic method to monitor the changes in thermal properties with thermal treatment: From 25 °C, the sample was heated at 10 °C/min to a target temperature. Once this target was reached, the sample was cooled at the maximum cooling rate to −90 °C, held at this temperature for 15 min, and reheated at 10 °C/min to the next target temperature. The procedure was followed until the last treatment temperature was reached, and a final run from −90 to 80 °C was performed. In this way, in each heating run, the thermal properties of the copolymers after treatment to the previously reached temperature were obtained, and a plot of thermal properties versus "instantaneous" thermal treatment was built.

SAXS measurements were performed at beamline BM16 of the European Synchrotron Radiation Facility (Grenoble, France). The wavelength of the X-ray beam was 0.980 Å. Detector calibration was performed with silver behenate ($AgC_{22}H_{43}O_2$). Disk samples cut from films were placed in a Linkam hot stage and heated at 10 °C/min as the SAXS spectra were recorded. Calibration of temperature gave a difference of approximately 7 °C between the temperature reading at the hot-stage display and the actual temperature at the sample.

Thermomechanical analysis (TMA) was performed with a Rheometric Scientific model DMTA V instrument. Rectangular test pieces of 3-mm width and 20-mm length were cut from films. A distance of 10 mm was set between fixation clamps. Runs were carried out from ambient temperature at 2 °C/min with a static stress of 1 MPa.

Tensile properties were measured in a MTS Synergie 200 testing machine equipped with a 100 N load cell. Rectangular test pieces of 3-mm width and 25-mm length were cut from films. A crosshead speed of 5 mm/min was used. Strain was measured from crosshead separation and referred to the 10-mm initial length. At least six samples were tested for each polymer. Tests were conducted at room temperature.

The densities of the dense membrane films were determined using a Sartorius balance (model SARTORIUS CP225D) and a density kit according to the Archimedean principle with the aid of the equation

$$\rho = \left(\frac{W_{air}}{W_{air} - W_{liq}}\right) \times \rho_o \tag{2}$$

where ρ is the density of the film; W_{air} and W_{liq} are the weights of the film in air and in an auxiliary liquid, respectively (in this case, isooctane was used because this type of polyether has been reported to be insoluble in isooctane) [17]; and ρ_o is the density of the auxiliary liquid.

The permeability, P, for O_2, N_2, CO_2, and CH_4 was determined using a permeator with a constant volume and variable pressure that uses the time-lag operating method. The measurements were carried out at 3 bar and 30 °C. A sketch of the device used has been shown elsewhere [18,19]. The strategy known as the time-lag method, attributed to Daynes [20], allows the determination of the permeability, diffusivity, and solubility of a sample by a simple, rapid, and accurate method working in the transitory regime. The method has been successfully applied to polymer permeation by others [21,22]. Its theoretical framework, as well as the practical possibilities and limits of the technique, have been abundantly documented [23]. It is currently an accepted method for assessing the permeability and diffusion coefficients of a gas through a polymer film. To summarize, the classical treatment postulates, among other hypotheses, that Fick's law holds, with a constant diffusion coefficient for a constant thickness membrane. Consequently, this treatment assumes that there is no swelling of the membrane by the permeant. When these conditions hold, the transitory response at the downstream part of a membrane to a pressure step at the upstream part enables the time lag, t_0, to be computed easily. This parameter is linked to the diffusion coefficient, D, of the permeant through the simple expression [21]

$$t_0 = \frac{\Delta x^2}{6D} \tag{3}$$

where Δx is the thickness of the membrane. The amount of gas transmitted through the membrane at time t was calculated from the readings of the permeate pressure, p_2, on the low-pressure side. The permeability coefficient can be obtained directly from the flow rate into the downstream volume upon reaching steady state. Finally, the solubility coefficient, S, was obtained from the directly measured diffusivity and permeability as follows

$$S = \frac{P}{D} \tag{4}$$

10.3 Results and discussion

10.3.1 Copoly(ether imide)s Imidization

Copoly(ether imide)s were readily prepared from the dianhydride BPDA, the amino-terminated PPO, and an aromatic diamine (ODA or BNZ), following the common procedure at low temperature in a solution of DMAC, as explained in the preceding section.

Polymer films were obtained by casting the final polymer solutions and applying a heating protocol to achieve solvent evaporation and imidization. After the films had dried overnight, they were heated at 120 °C for 12 h to almost completely remove the solvent, and infrared spectra were recorded to check for the progress of imidization. Films with a polyether ratio of 2/1 were almost completely imidized according to their FTIR spectra (within the detection limits of the FTIR technique). Further heating at 160 °C for 2 h gave completely imidized films. For copolymers with polyether ratios of 1/1 and 1/2, it was necessary to reach higher temperatures for complete imidization, and treatment at 200 °C for 2 h resulted in fully imidized films. All of the copolymers were found to be insoluble in DMAc (dimethylacetamide), N-methylpyrrolidone (NMP), hexane, toluene, THF (tetrahydrofuran), and CH_2Cl_2 (dichloromethane) after this process.

In Figure 2, the FTIR spectra of copoly(ether imide) with PPO-4000 (2/1) and its corresponding poly(amic acid) precursor are shown. As can be seen, the bands of carboxylic acid and amide centered around 3260, 2550, 1650, 1603, and 1538 cm^{-1} strongly decreased or disappeared, and the bands at approximately 1774, 1712, 1370, and 738 cm^{-1} increased or appeared upon imidization. The same spectra as in Figure 2 with only minor variations in the relative intensities of the peaks were recorded for all of the fully imidized copolymers except for cPI-PPO-2000 + 4000 BNZ (2/1). For this copolymer, the change in aromatic diamine from ODA to BNZ resulted in the appearance of a new peak at 814 cm^{-1} and the disappearance of the peak at 1239 cm^{-1}. The remarkably low temperature needed for full imidization in these copolymers has been previously described by us in detail for similar copoly(ether imide)s based on poly(ethylene oxide) [24,25].

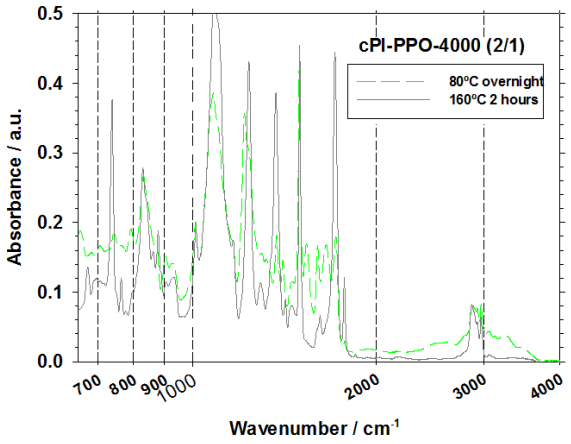

Figure 2. FTIR spectra of cPI-PPO-4000 (2/1) before (continuous line) and after (dashed line) the thermal treatment at 160 ºC for 2h.

10.3.2 Thermal Stability

Thermogravimetric analysis was performed to evaluate the thermal stability of the synthesized copolymers. Dynamic runs in high-resolution mode, in a nitrogen atmosphere, for fully imidized copolymers (annealed at 160 °C for 2 h in the case of PPO-2000 2/1, PPO-4000 2/1, PPO-2000 + 4000 ODA 2/1, and PPO-20004000 BNZ 2/1 copolymers and annealed at 200 °C for 2 h in the case of copolymers PPO-4000 1/1 and PPO-4000 1/2) showed a weight loss pattern with three consecutive steps (see Figure 3): an initial loss from ambient temperature to 270−300 °C; a second loss from 270−300 °C to 460−470 °C; and a final loss from 460−470 to 800 °C.

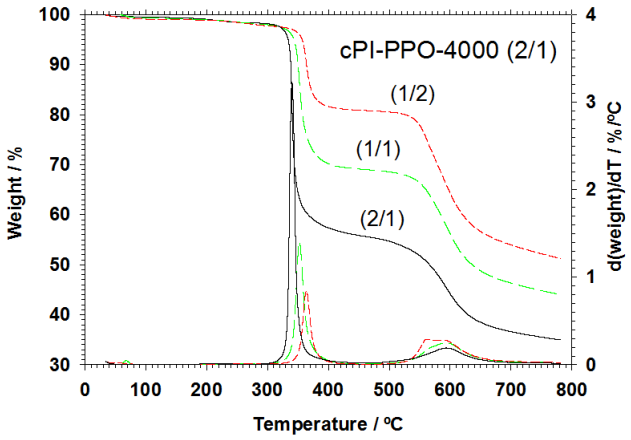

Figure 3. TGA curves in dynamic conditions for PPO-4000 based copolymers. From bottom to top: cpI-PPO-4000 (2/1) (treated at 160 ºC for 2 hours); cPI-PPO-4000 (1/1) (treated at 200 ºC for 2 hours); and cPI-PPO-4000 (1/2) (treated at 200 ºC for 2 hours).

The first loss can be attributed to the elimination of absorbed water plus the removal of the solvent trapped in the film. In some cases, the completion of total imidation can contribute partially to this mass loss. The weight change was 2−2.5%. The second loss step agrees with the theoretical contribution of PPO entering the copolymer composition, within 3% error (see Table 2), and it is therefore assigned to the loss of polyether block sequences. The third and final stage of weight loss is due to the thermal decomposition of the remaining aromatic polyimide segments.

Table 2. Results obtained by TGA for the prepared copolymers.

Copolymer	**Theoretical polyether weight in the copolymer / %**	**Experimental polyether weigth loss / %**	**Temperature of maximum weight loss rate / ºC**	**Residue at 800ºC / %**
cPI-PPO-2000 (2/1)	43.8	42.6	345	34.3
cPI-PPO-4000 (2/1)	45.1	43.5	340	35.5
cPI-PPO-4000 (1/1)	29.8	29.7	352	44.9
cPI-PPO-4000 (1/2)	17.8	17.3	364	52.4
cPI-PPO-2000+4000 ODA (2/1)	44.6	44.3	344	35.3
cPI-PPO-2000+4000 BNZ (2/1)	43.5	42.2	345	37.9

TGA confirmed that the thermal stability of the polyether segments was much lower than the thermal stability of the aromatic polyimide segments, as already found for copoly(ether imide)s based on poly(ethylene oxide) of different lengths [24,25], and therefore, a selective degradation of the polyether moiety could be performed in these copolymers. Other authors have also found that poly(propylene oxide) segments can be selectively degraded in triblock [26,27], linear, and grafted [29] copolyimides to produce nanofoams. The temperature of maximum weight loss rate was 340−345 °C for all copolymers with a 2/1 proportion between polyether and aromatic amines. The char residue at 800 °C was similar for these copolymers, at around 35%, except for the copolymer based in BNZ, which left a slightly higher residual content. When the relative content of aromatic amine increased, the temperature of maximum weight loss rate (and the char residue at 800 °C) increased slightly.

10.3.3 Calorimetric Studies

Samples were heated in a DSC instrument by a cyclic method to monitor the changes in their thermal properties after different thermal treatments. In a standard run, a sample was heated from room temperature to a certain temperature, then cooled to −90 °C at the highest rate attainable by the instrument, held at −90 °C for 15 min, and reheated to the next target temperature. In this way, in each heating step, the thermal transitions after instantaneous heating to the temperature reached in the previous step was detected.

Table 3. Polymer properties at ambient temperature for the films treated at 200 ºC[a] (250 ºC for the aliphatic T_g) for 2h.

	T_g / ºC aliphatic	**T_g / ºC aromatic[b]**	**Density / g/cm^3**	**Strain / %**	**Modulus / GPa**
cPI-PPO-2000 (2/1)	- 60.1	191.5	1.23	8.3± 4.6	0.40 ± 0.05
cPI-PPO-4000 (2/1)	- 69.1	225.7	1.21	1.7 ± 0.5	0.51 ± 0.06
cPI-PPO-4000 (1/1)	- 71.6	240.1	1.27	6.8 ± 2.1	0.997 ± 0.17
cPI-PPO-4000 (1/2)	- 71.5	236.9	1.29	20.3 ± 8.4	1.24 ± 0.20
cPI-PPO-2000+4000 ODA (2/1)	- 68.3	231.5	1.22	3.44 ± 0.6	0.654 ± 0.05
cPI-PPO-2000+4000 BNZ (2/1)	- 63.8	188.7	1.24	3.41 ±2.6	0.950 ± 0.18

[a]Treatment temperature of 250 °C for the aliphatic T_g. [b]T_g for the aromatic part of the copolymer was calculated from the TMA data.

All copolymers showed only the glass transition, T_g, for the poly(propylene oxide) segments, and no transition for the aromatic polyimide segments could be detected. No significant changes in the T_g value of polyether appeared upon thermal treatment except for the copolymers cPI-PPO-4000 (1/1) and cPI-PPO-4000 (1/2). For these copolymers, the initial T_g value was lower probably because of some retention of solvent that, when removed at higher temperatures, would lead to an increase in T_g. Obviously, the final values should correspond to the T_g of the polyether (PPO) which, of course, varies with the length of the polyether and the rigidity of the polymer, as shown in Table 3.

In Figure 4, the T_g of PPO is shown versus its percentage in the copolymer, as evaluated from TGA. It can be seen that T_g remained almost constant and quite similar to that of the pure PPO until relatively high percentages of PPO [30], when there was a steep increase in T_g. The high Tg values could result from the increase of the intermolecular forces appearing because of the proximity of the polar groups of the polymer chains, which should appear when there is enough PPO confined within the aromatic chains.

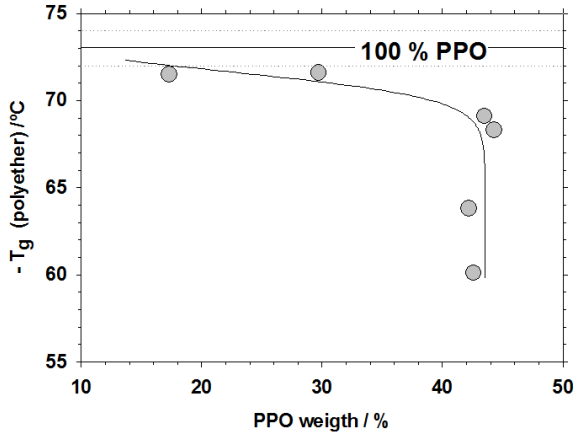

Figure 4. Polyether T_g as a function of the percentage of PPO as evaluated from TGA. The pure PPO T_g is taken from literature.

10.3.4 Density

The results for density are reported in Table 3. For the sake of comparison, the density of pure BPDA-ODA is 1.39 g/mL [30]. The sequence of decreasing densities was found to be

PPO 4000 (1/2) > PPO 4000 (1/1) > PPO 2000+4000 BNZ (2/1) ≈ PPO 2000 (2/1) ≈ PPO 2000+4000 ODA (2/1) ≈ PPO 4000 (2/1)

Note that increasing the proportion of PPO decreased the density of the copolymers.

10.3.5 Small-Angle X-ray Scattering

X-ray scattering experiments were performed at a synchrotron radiation source to follow, under real-time conditions, the development of the phase-separated structure in these copolymers. Two parameters were calculated from the scattering curves [intensity versus scattering vector q, with $q = 4\pi(\sin\theta)/\lambda$, where λ is the wavelength and 2θ is the scattering angle]: the relative invariant, Q', as the integral below the curve Iq^2 versus q related to the extent of the phase separation and the maximum on the scattering curve, qmax, related to the size scale of the separated phases according to Bragg's law. Q' can be correlated with the electron density of the phases (assuming there are two phases) as

$$Q' = k\,\Delta\rho^2\,\phi(1-\phi) \tag{5}$$

where ϕ is the fraction of one of the phases, $\Delta\rho$ is the difference in the electron densities of the two phases, and k is a constant related to the experimental geometry and the Thomson scattering factor. Changes in Q′ can arise from changes in the extent of phase segregation or from changes in the density difference between the phases. q_{max} is related to the length scale L, which refers to the separation of domains or heterogeneities in the material. In the simplest analysis for lamellar phases, the scattering can be treated according to Bragg's law as simply

$$L = \frac{2\pi}{q_{max}} \tag{6}$$

For morphologies that are not truly lamellar, calculation from the curve of I versus q is preferred [31]. In our case, we were interested not in the absolute value for this length scale of the segregated phase but rather in the change of this scale with the treatment temperature. Thus, this procedure was followed because of its higher accuracy in determining the maximum of the scattering curve.

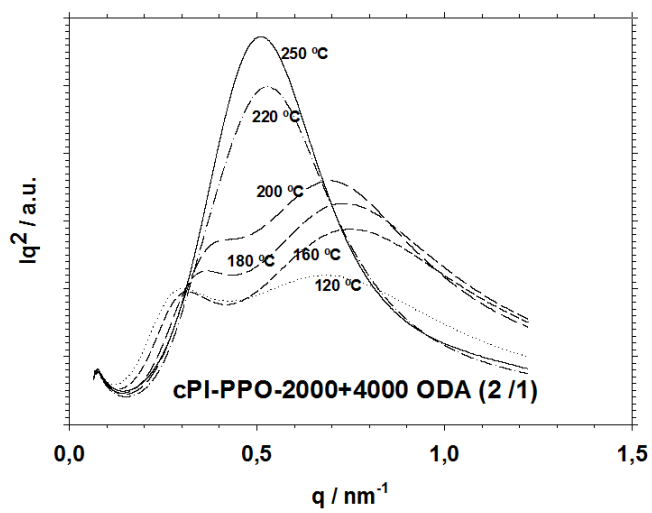

Figure 5. Scattering curves (Iq^2 vs. q) for copolymer cPI-PPO-2000+4000 ODA (2/1) at different temperatures.

A single broad peak was obtained for some of the copolymers [cPI-PPO-2000 (2/1) and cPI-PPO-2000 + 4000 BNZ (2/1)], but two peaks and/or shoulders were obtained for the others [cPI-PPO-4000 (2/1), cPI-PPO-4000 (1/1), cPI-PPO-4000 (1/2), and cPI-PPO-2000 + 4000 ODA (2/1)]. In Figure 5, the evolution of the Iq^2 versus q plot with treatment temperature is shown for cPI-PPO-2000 + 4000 ODA (2/1). For this copolymer, the presence of the two scattering maxima is very clear. For copolymer cPI-PPO-4000 (2/1), there was a shoulder close to the beam stop in addition to the clear maximum at higher scattering vector (lower interdomain distance). For copolymer cPI-PPO-4000 (1/1), a peak was evident close to the beam stop, and when higher temperatures were

reached, a new maximum appeared at higher scattering vector. Finally, for copolymer cPI-PPO-4000 (1/1), a high scattering intensity, not defined as a peak, was present close to the beam stop, and when higher temperatures were reached, a shoulder appeared at higher scattering vector values. We have no explanation for the two different characteristic interdomain distances in these copolymers that, because of the broadness of the peaks, cannot be due to high-order peaks.

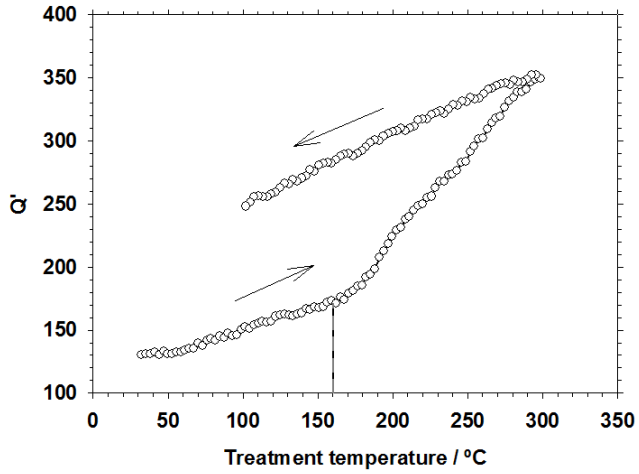

Figure 6. Changes in the Invariant (Q') by heating and cooling for the copolymer PPO-2000+4000 (2/1).

In all cases, at a certain temperature between 170 and 200 °C, the invariant increased (see Figure 6), and phase separation improved. When the invariant increased, for the copolymers showing a single peak, the maximum of the peak, in the vicinity of 10 nm, shifted to longer spacing. For copolymers with two maxima and/or shoulders, they moved to longer spacings, except for copolymer cPI-PPO-2000 + 4000 ODA (2/1). In this case, the peak at longer scattering vector (shorter spacing), also around 10 nm, shifted to longer spacing, whereas the peak closer to the beam stop (seen as a shoulder in some cases), initially around 40 nm, shifted to shorter spacing and finally merged with the other peak. Panels a and b of Figure 7 show the evolution with temperature of Q′ and L, respectively, for all of the copolymers. The samples were measured in situ (SAXS cell) from polymer films previously heated to 160 °C for 6 h. Note that, to eliminate the influence of the film thickness and electronic density, the relative values Q'_r = [Q′(T)/Q′(baseline at T)] – 1 and L_r = [L(T)/L(baseline at T)] − 1 are shown in Figure 7.

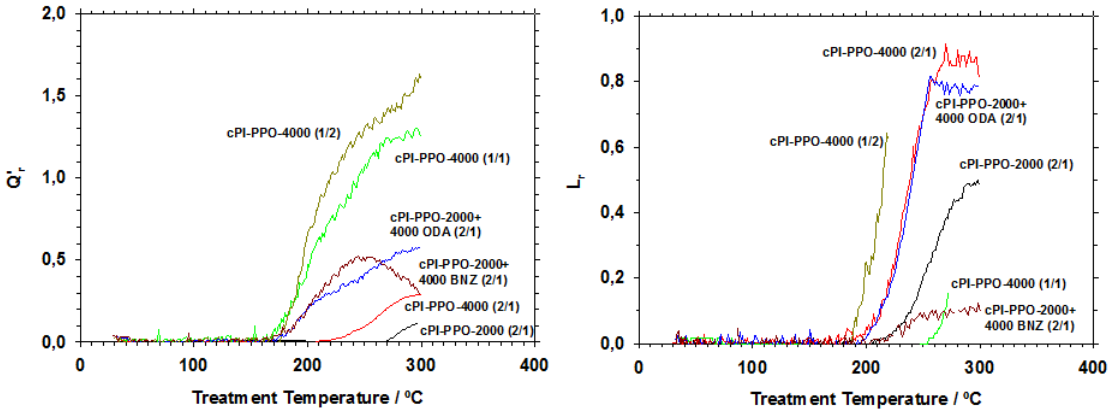

Figure 7. (a) Q′r and (b) Lr as functions of temperature for the copolymers used. Polymer films were previously treated at 160 °C for 2 h.

The influence of the different backgrounds and of the differences in the corresponding baselines was also removed by this procedure. It is important to note that the parameters Q'_r and L_r refer to the increases in the invariant and characteristic length, respectively, from those at low temperatures. It can be seen that Q'_r increased with the treatment temperature, reaching higher relative increments of Q'_r as the proportion of the PPO decreased (density increased). This is due to the rigidity of the polymeric chain. At lower PPO contents in the copolymer, the polymeric chain is more rigid, and when casted from solution, more mixing of the segments is produced and a poorer initial phase segregation is present.

This tendency is clearly shown in Figure 8.a. L_r was found to be greater for longer polyether chains, which seems logical. In this case, the highest values were observed for the samples cPI-PPO-4000 (2/1) and cPI-PPO-2000 + 4000 ODA (2/1). All together, Lr increased with increasing percentages of PPO (decreasing densities), thus giving larger segregated domains when the percentage of PPO increased, as seen in Figure 8b. As the treatment temperatures were higher, the segregated domains became larger as well. It is worth noting that it was impossible to determine Lr for cPI-PPO-4000 (1/1) for the entire range of temperatures, because the peak merged to the beam stop. In addition, for cPIPPO-4000 (1/2), we detected only a shoulder that never developed into a maximum. From the SAXS results, the presence of a phase-separated morphology in these copolymers that improved with thermal treatment was evident (as seen in the increase in the relative invariant).

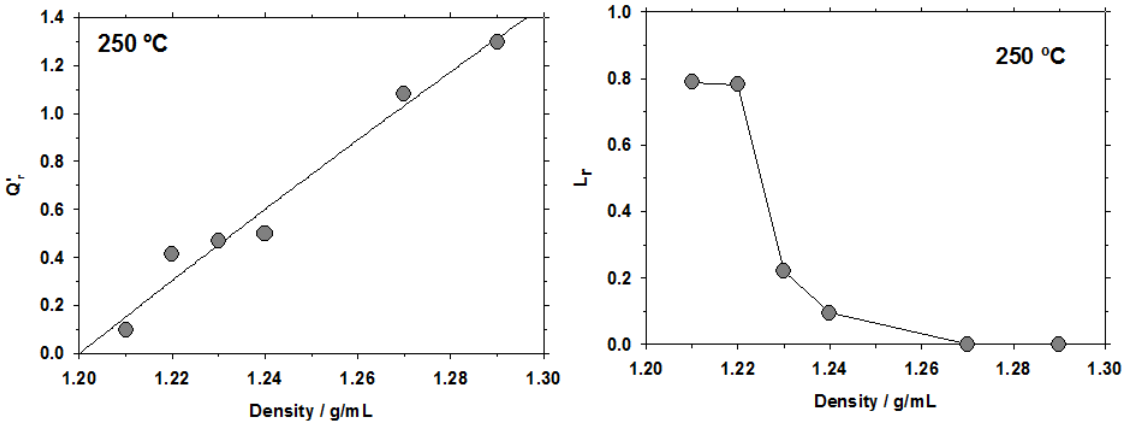

Figure 8. (a) Q′r and (b) Lr as functions of the density of the copolymer for membranes treated at 250 °C for 1 h.

10.3.6 Thermomechanical Analysis

Thermomechanical analysis was also carried out to detect the glass transition temperatures of the aromatic polyimide hard segments, which were not detected by DSC. The criterion to determine the T_g value of the polyimide segments was to identify as such the temperature when the strain was 10 times that of the sample at 100 °C [24]. The corresponding results for the T_g values of membranes treated at 200 °C and their densities are reported in Table 3.

For all of the copolymers, the T_g value of the aromatic polyimide was well above ambient temperature, but much lower than the corresponding T_g value for the pure aromatic homopolymer BPDA-ODA, (287.3 °C), because of the lower polymerization degree and, consequently, the smaller length of the aromatic polyimide segments in the copolymer as compared to the corresponding homopolymer and also because of the possible inclusion of some polyether segments in the polyimide domains [24].

All samples had the same aromatic polyimide part, so the differences can only be due to different modes of packing of the aliphatic part in the final polymer structure and its proportion in the final copolymer. For the copolymers with the same proportion, better segregation into phases will increase the T_g value for the aromatic chain. Actually, the T_g values for the aromatic portions of the copolymers follow a trend quite similar to that of Q'_r, which means that higher phase segregation led to a higher stiffness of the remaining aromatic portion. Of course, this stiffness was always below that of the pure aromatic homopolymer BPDA-ODA. It is worth noting that there was an increase in the size of the segregated domains, L, as detected by SAXS, when the samples were

heated over Tg of the aromatic part of the copolymer in question. This should be a consequence of the segmental freedom of the aromatic portions of the copolymer chains above T_g, which would leave more room for the formation of large domains of segregated PPO.

10.3.7 Mechanical Properties

SAXS, DSC, and thermomechanical studies showed the changes produced in the morphologies of the copolymers during thermal treatment and the changes in their thermal properties. To complete the study of the physical properties of these copoly(ether imide)s, mechanical properties were measured in tensile mode for the copolymers treated at 200 °C for 2 h. The thus-obtained results are included in Table 3.

According to these results, all of the copolymers showed reasonably good mechanical properties, although, of course, they were poorer than those of the aromatic homopolymer. The polyimide hard (aromatic) domains are responsible for the mechanical resistance at the early stages of the test; therefore, the differences are due only to the packing between the aromatic and aliphatic parts. It is worth noting that less dense copolymers (with higher percentages of PPO) were found to have worse mechanical properties.

10.3.8 Gas Transport Properties

10.3.8.1 Permeability and Selectivity

As mentioned, the CH_4 and N_2 pair of gases is especially interesting to apply to these membranes in natural gas extraction. The copolymers studied here showed reverse selectivity because CH4 is preferentially permeated despite its larger size (see Table 4).

Table 4. Transport properties and molecular parameters of the penetrant gases.

	Kinetic Diam. d_K **/ Å**	**Collision Diam.** d_C **/ Å**	**Critical Temp.** T_c **/ K**	**Lennard-Jones Temp.** ε/k **/ K**
CO_2	3.3	3.94	304	195
O_2	3.46	3.47	154.2	107
N_2	3.64	3.8	126	71
CH_4	3.8	3.76	190.5	149

This unusual behavior can only be due to the very high solubility of condensable gases in the aliphatic−aromatic copolyimides [19]. As reported for other aliphatic−aromatic copoly(ether imide)s [25,32,33], the results indicated an improvement in permeation properties after thermal treatment, so that there is a direct relationship among treatment temperature, phase segregation, and permeation properties. Figure 9 shows the selectivity versus permeability plot for the CH_4/N_2 pair of gases. In this case, selectivity and permeability increased with the temperature of treatment and the proportion of PPO in the copolymer. Up to now, no Robeson limit has been determined for the CH_4/N_2 pair even though it has been effectively determined for the N_2/CH_4 pair, and thus, in this figure, the dashed line corresponds to a pseudobound traced by taking into account some of the polymers that present a CH_4 permeability higher than the N_2 permeability [19]. Note that some of the copolymers with highest proportions of PPO treated at high temperatures had very high permeabilities for CH_4 with no less high selectivities. For the O_2/N_2, CO_2/CH_4, and CO_2/N_2 gas pairs, there was an increase in permeability without a significant change in selectivity, with values relatively distant from the corresponding Robeson's bound line (this can be seen in the Supporting Information).

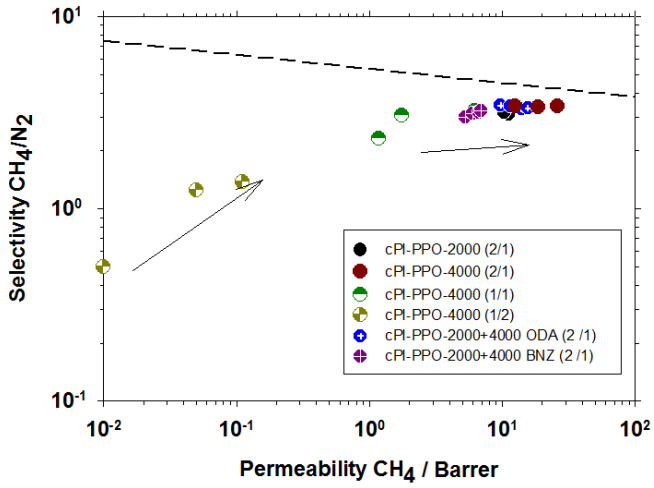

Figure 9. Robeson's plot for the CH4/N2 gas pair. Arrows point to increasing temperatures and proportions of PPO. The applied pressure was 3 bar.

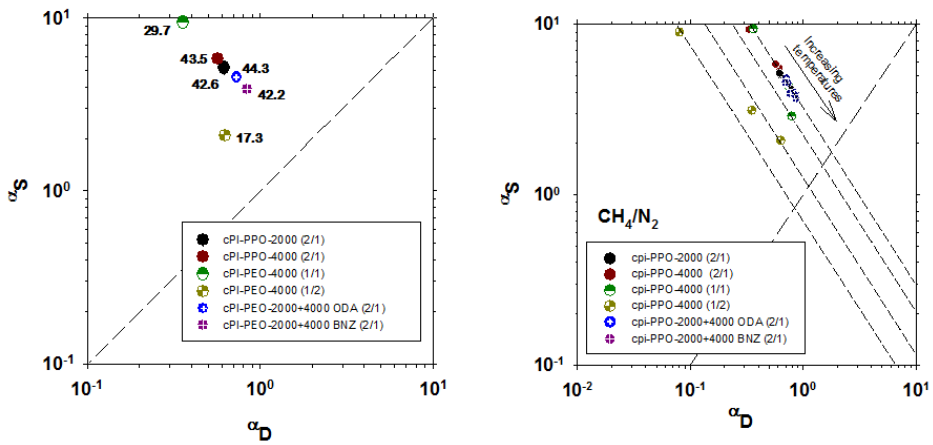

Figure 10. Selectivity by solubility as a function of selectivity by diffusivity for (a) different percentages of PPO and (b) different temperatures.

The evolution of the balance of diffusivity and solubility selectivity is shown in Figure 10. It seems clear that this balance strongly leans toward solubility control, probably because of the strong affinity between the copolymer and methane caused by the presence of $-CH_3$ groups within the PPO chains. For CH_4 and N_2 and the rest of the pairs of gases analyzed, except for O_2/N_2 (see again the Supporting Information), there was no clear tendency with density or percentage of PPO, as can be seen in Figure 10a. There was a clear tendency to go toward more balanced compromises between solubility and diffusivity as the temperature of treatment increased, for this and the other gas pairs studied. This is clearly shown in Figure 10b, where the solid line corresponds to a perfect equilibrium of the two factors whereas the dashed lines correspond to the more direct way to reach it. It seems clear that increasing the sizes of the segregated domains by treating the films at higher temperatures increased the equilibrium of solubility and diffusivity selectivity for all densities (i.e., for all of the copolymers). The permeability of methane increased very strongly with the percentage of PPO, which seems to confirm the existence of a specific PPO$-CH_4$ affinity. As a consequence of this rapid increase in CH_4 permeability, an inverse CH_4/N_2 selectivity was obtained. This was the only selectivity that increased with increasing percentage of PPO, whereas for the rest of the gas pairs studied, the selectivity decreased with increasing PPO content. Permeability, in turn, increased for all of the gases and membranes studied.

The two copolymers including mixed PPO diamines (i.e., PPO-4000 and PPO-2000) showed different permeabilities because one of them was prepared with ODA as the aromatic diamine whereas the other was made with BNZ. The difference in the permeabilities of the two copolymers might be due in part to the differences in packing and segregation of the two copolymers, which

was higher for the less rigid aromatic diamine (ODA) [19]. The permeability of the different gases studied followed the sequence

$$CO_2 > CH_4 \geq O_2 > N_2$$

This represents the order of decreasing penetrant condensability, as described by the critical temperatures of the gases (see Table 4). For this type of compound, the diffusion coefficient is only a weak function of penetrant size, because the polymer-size sieving-ability is poor [34]. As the penetrant size increases, the solubility coefficient increases more strongly than the diffusion coefficient decreases, which means that larger, more condensable penetrants are more permeable than smaller ones [35]. Therefore, the relative permeability of each penetrant is largely determined by its solubility. Regarding the effect of temperature on permeability and selectivity, it is clearly shown that the tendency of increasing permeability was more irregular for the 1/1 and 1/2 proportions than for the 2/1 proportion. For the 2/1 proportion, a notably constant selectivity was obtained, whereas the other proportions showed more variability and lower selectivity. The tendency was quite similar for all of the gases, with better permeation properties after improvement of the phase separation. Note that the tendency was to give higher CH_4 permeability and CH_4/N_2 selectivity when the proportion of aliphatic diamine in the polymer increased. For the other pairs of gases, although permeability increased, the corresponding selectivity decreased for increasing contents of PPO. This difference might be due to the key effect of the affinity of methane for the methyl groups in the aliphatic chains.

10.3.8.2 Effects of Pressure and Temperature

As mentioned previously, the copolymers studied here showed very low solubilities in most organic solvents, which gives them a high resistance to many aggressive media. This also means that their resistance to plasticization could be high as well. This was actually confirmed for all of the gases used here, as shown, for example, in Figure 11 for the pair CH_4/N_2. Thus, plasticization was very limited, because hysteresis in both permeability and selectivity was negligible and selectivity was almost constant [36].

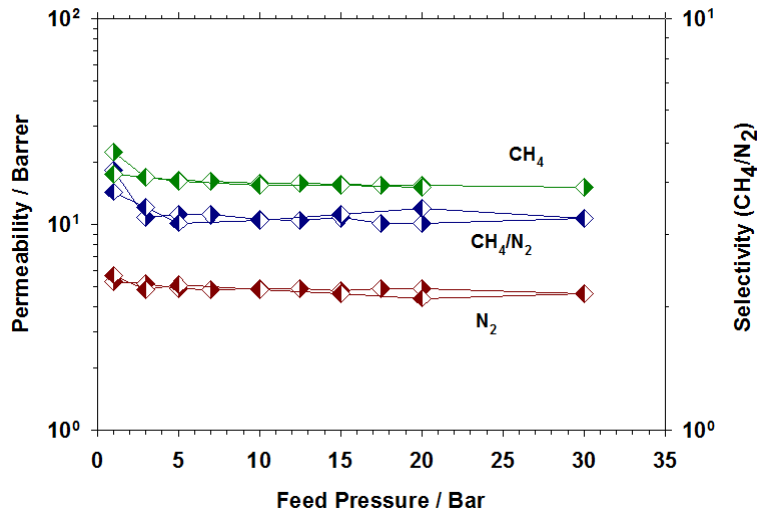

Figure 11. Pressurization and depressurization evolution of (a) permeability and (b) selectivity for the CH_4/N_2 pair of gases for sample cPI-PPO-4000 (2/1) treated at 160 °C.

The dependence of gas diffusion on temperature can be expressed in terms of an Arrhenius-type relationship that considers the movement of the gas molecules through a membrane as a thermally activated process [37]. Mathematically, the temperature dependence of diffusion is given by

$$D = D_0 exp\left(\frac{E_D}{RT}\right) \tag{7}$$

where D_0 is the pre-exponential factor and E_D is the activation energy of diffusion. The activation energy term depends on the size of the penetrant and not on its mass [21,37]. Also, it is well known that diffusion is the most temperature-sensitive transport process, in comparison to solubility and permeability [38]. Taking into account the temperature dependence for the diffusion and sorption coefficients, the temperature effect on gas permeability is given by [37]

$$P = P_0 exp\left(\frac{E_P}{RT}\right) \tag{8}$$

where E_P is the activation energy of permeation and is the algebraic sum of E_D and ΔH_s. In general, permeability increases with increasing temperature. However, there are exceptions, especially near the glass transition temperature of the polymer, where opposite trends have been observed. Experiments with CO_2 permeation through a polyimide membrane showed decreased permeability with increased temperature [39]. The same behavior was also observed for butane permeation through polyimide polymers. These observations were explained in terms of pressure effects on the

polymer under isothermal operating conditions. The high stress caused by the applied gas pressure was stated to cause a transition in the polymer from a rubbery state to a glassy state.

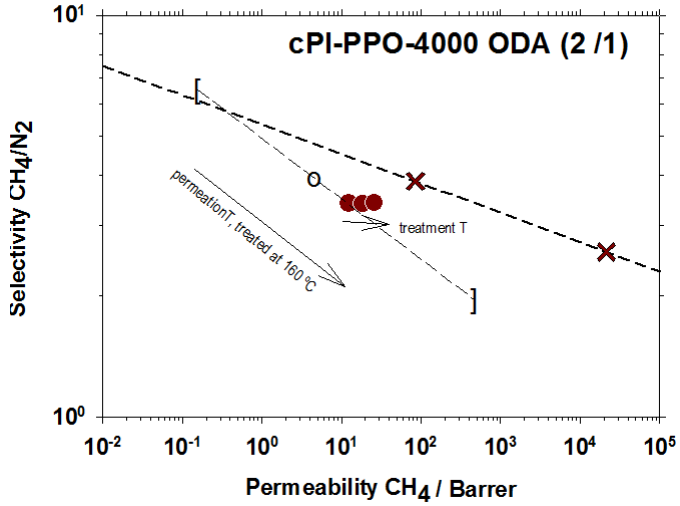

Figure 12. Evolution of permeability and selectivity for CH_4/N_2 for sample cPI-PPO-4000 (2/1) treated at 160 °C for different temperatures of permeation according to the fitted Arrhenius behavior. Only the range from aliphatic to aromatic Tg values is shown between brackets. The circle on the solid line corresponds to a permeation temperature of 0 °C. Crosses correspond to the data recorded to draw a pseudobound line. The points outside the solid line correspond to samples treated at 200 and 250 °C.

The predictions of the Arrhenius plot extrapolated to cover the whole range from the T_g value of the aliphatic chains to that of the aromatic part of the copolymer are also shown in the Robeson plot of Figure 12. The best results from the literature [40,41] that were used to construct the tentative upper bound for this pair of gases are shown as well. If it is assumed that neither the permeation activation energy nor the corresponding pre-exponential value changes substantially along the range between the two glass transitions (of the aliphatic and aromatic portions of the copolymer), the balance of permeability and selectivity could be finely tuned by simply changing the temperature of permeation, giving very high selectivities (for relatively low temperatures) or notably high permeabilities (for comparatively high temperatures). Of course, the Robeson bound changes with temperature [42] in such a way that most of the increase in permeability and decrease in selectivity caused by performing permeation experiments at higher temperatures is balanced by a decrease in the Robeson bound.

10.4 Conclusions

New aromatic−aliphatic copolyimides incorporating PPO have been prepared. FTIR spectroscopy showed that almost complete imidization was achieved at temperatures as low as 120 °C for most of the copoly(ether imide)s and that this process was wholly achieved after treatment at 160 °C, which is well below the temperature needed to fully imidize aromatic polyimides. As indicated by the TGA data, these copolymers were stable in inert atmosphere up to 300 °C, with a selective degradation of the polyether segments at higher temperatures.

DSC, TMA, and SAXS experiments confirmed the existence of a phase-separated morphology in these copolymers, with an amorphous PPO phase at ambient temperature and an aromatic polyimide phase with a Tg value well above room temperature. A relationship was found between segregation into phases determined by SAXS and permeation properties, so that, as the phase segregation increased, the permeability increased as well without a strong decrease of selectivity.

An exceptional behavior was found for the separation of methane and nitrogen. Very high inverse selectivity and permeability were found for this pair of gases. Methane permeabilities over 20 barrer and selectivities (CH_4/N_2) close to 4.2 could be measured for an applied pressure of 1 bar. The proportion of PPO was found to have a high influence in the final polymer, so that both the selectivity and permeability improved when the proportion of polyether in the final copolymer was high. The changes in permeability and selectivity for different temperatures of permeation were confirmed to fit an Arrhenius correlation that adds the possibility of tuning permselectivity, which can be translated into the achievement of very high selectivities (for temperatures below ambient) or notably high permeabilities (for higher temperatures).

To improve the permselectivity of these materials, three approaches can be outlined. The first is to improve the molecular packing of the final polymer by varying the stiffness of the aromatic diamine. The second would be to incorporate longer aliphatic diamines that should give larger segregated domains, keeping in mind that the mechanical properties of the resulting copolymer should be preserved. The last possibility to be taken into account is the elimination by controlled pyrolysis of the aliphatic polymer, increasing the permeability even more. This option should also require careful control of the procedure to avoid collapse of the created structure. Finally, we confirmed that these copolymers, which have high resistance to different solvents and aggressive media, present excellent performance when the feed pressures are high, showing a high resistance to the plasticization processes. The behavior of these copolymers at different temperatures of permeation was also analyzed and compared with the changing permselectivity “tradeoff” curves.

Both the high permeability and selectivity, along with their solvent and plasticization resistance, make these poly(ether imide)s containing PPO very good candidates for their industrial use in the purification of natural gas that has a high nitrogen content.

10.5 Acknowledgments

We are indebted to the Spanish Junta de Castilla León for financing this work through the GR-18 Excellence Group Action and to the Ministry of Science and Innovation in Spain for their economic support of this work (MAT2008-00619/ MAT, CIT-420000-2009-32, and MAT2010-20668/MAT). We also acknowledge financial support from the programme Consolider Ingenio 2010 (Project CSD-0050-MULTICAT). The authors are grateful for access to beamline BM16 at the European Synchrotron Radiation Facility (ESRF) in Grenoble, France. We are also grateful to Dr. Ana Labrador and Dr. François Fauth for their help at BM16 station at the ESRF. The help provided by Sara Rodriguez in measuring gas permeability and selectivity is greatly appreciated. A.T. thanks CSIC for a predoctoral JAE fellowship.

10.6 References

1. S. Pacala, R. Socolow, Stabilization Wedges: Solving the Climate Problem for the Next 50 Years with Current Technologies, Science, 305 (2004) 968-972.
2. M.Z. Jacobson, Review of solutions to global warming, air pollution, and energy security, Energy & Environmental Science, 2 (2009) 148-173.
3. R. Egging, F. Holz, S.A. Gabriel, The World Gas Model: A multi-period mixed complementarity model for the global natural gas market, Energy, 35 (2010) 4016-4029.
4. B.T.W. Low, Yan; Chung, Tai-Shung, Polymeric Membranes for Energy Applications, in, John Wiley & Sons, 2002.
5. J.L. Walsh, C.C. Ross, M.S. Smith, S.R. Harper, Utilization of biogas, Biomass, 20 (1989) 277-290.
6. F. Vedrenne, F. Béline, P. Dabert, N. Bernet, The effect of incubation conditions on the laboratory measurement of the methane producing capacity of livestock wastes, Bioresource Technology, 99 (2008) 146-155.

7. R.H.V. Hugman, E.H.; Springer, P.S., Chemical Composition of Discovered and Undiscovered Natural Gas in the U.S. Lower-48, in: Executive Summary, Tight Sands and Gas Processing Department, 1993.
8. C. Tannehill, J.G. Strickland, H. Meyer, High N_2 gas - snap shot of the present requirements for the future, in, Gas Processors Association, Nashville, TN, USA, 1999, pp. 230-233.
9. M. Mitariten, Economic N_2 removal, Hydrocarbon Engineering, 9 (2004) 53-57.
10. M. Mitariten, New technology improves nitrogen-removal economics, Oil and Gas Journal, 99 (2001) 42-44.
11. C. Tannehill, Nitrogen Removal Requirements for Natural Gas, Gas Research Institute Topical Report, in: Purvin & Gertz, Gas Research Institute, 1999.
12. R.W. Baker, Membrane Technology and Applications, in: n. edition (Ed.), John Wiley & Sons Ltd, Chichester, England, 2004.
13. Y.P. Yampolskii, I.; Freeman, B.D. , Materials Science of Membranes for Gas and Vapor Separation, in, John Wiley & Sons Ltd., Chichester, England, 2006, pp. 251–270.
14. R.W. Baker, K. Lokhandwala, Natural gas processing with membranes: An overview, Ind. Eng. Chem. Res., 47 (2008) 2109-2121.
15. S.A. Stern, Polymers for gas separations: the next decade, Journal of Membrane Science, 94 (1994) 1-65.
16. K.A. Lokhandwala, I. Pinnau, Z.J. He, K.D. Amo, A.R. DaCosta, J.G. Wijmans, R.W. Baker, Membrane separation of nitrogen from natural gas: A case study from membrane synthesis to commercial deployment, Journal of Membrane Science, 346 (2010) 270-279.
17. J.I. Brandrup, E.H.; Grulke, E.A., Polymer handbook, in, John Wiley & Sons Inc, New York, 1999.
18. J. Marchese, M. Anson, N.A. Ochoa, P. Prádanos, L. Palacio, A. Hernández, Morphology and structure of ABS membranes filled with two different activated carbons, Chemical Engineering Science, 61 (2006) 5448-5454.
19. A. Tena, L. Fernández, M. Sánchez, L. Palacio, A.E. Lozano, A. Hernández, P. Prádanos, Mixed matrix membranes of 6FDA-6FpDA with surface functionalized γ-alumina particles. An analysis of the improvement of permselectivity for several gas pairs, Chemical Engineering Science, 65 (2010) 2227-2235.
20. H.A. Daynes, The process of diffusion through a rubber membrane, in, Proc. R. Soc. London 97, London, 1920, pp. 286–307.
21. J. Crank, The mathematics of diffusion / by J. Crank, Clarendon Press, Oxford [England] :, 1975.

22. D.R. Paul, A.T. DiBenedetto, Diffusion in amorphous polymers, Journal of Polymer Science Part C: Polymer Symposia, 10 (1965) 17-44.
23. S.W. Rutherford, D.D. Do, Review of time lag permeation technique as a method for characterisation of porous media and membranes, Adsorpt.-J. Int. Adsorpt. Soc., 3 (1997) 283-312.
24. A. Marcos-Fernández, A. Tena, A.E. Lozano, J.G. de la Campa, J. de Abajo, L. Palacio, P. Prádanos, A. Hernández, Physical properties of films made of copoly(etherimide) s with long poly(ethylene oxide) segments, European Polymer Journal, 46 (2010) 2352-2364.
25. A. Tena, A. Marcos-Fernández, A.E. Lozano, J.G. de la Campa, J. de Abajo, L. Palacio, P. Prádanos, A. Hernández, Thermally treated copoly(ether-imide)s made from bpda and alifatic plus aromatic diamines. Gas separation properties with different aromatic diamimes, Journal of Membrane Science, 387–388 (2012) 54-65.
26. Y. Charlier, J.L. Hedrick, T.P. Russell, S. Swanson, M. Sanchez, R. Jérôme, Crosslinked polyimide foams derived from pyromellitic dianhydride and 1,1-bis(4-aminophenyl)-1-phenyl-2,2,3-trifluoroethane with poly(α-methylstyrene), Polymer, 36 (1995) 1315-1320.
27. J.L. Hedrick, K.R. Carter, H.J. Cha, C.J. Hawker, R.A. DiPietro, J.W. Labadie, R.D. Miller, T.P. Russell, M.I. Sanchez, W. Volksen, D.Y. Yoon, D. Mecerreyes, R. Jerome, J.E. McGrath, High-temperature polyimide nanofoams for microelectronic applications, Reactive and Functional Polymers, 30 (1996) 43-53.
28. T. Philip Gnanarajan, N. Padmanabha Iyer, A. Sultan Nasar, G. Radhakrishnan, Preparation and properties of poly(urethane-imide)s derived from amine-blockedpolyurethane prepolymer and pyromellitic dianhydride, European Polymer Journal, 38 (2002) 487-495.
29. J.S. Do, B. Zhu, S.H. Han, C. Nah, M.H. Lee, Synthesis of poly(propylene glycol)-grafted polyimide precursors and preparation of nanoporous polyimides, Polymer International, 53 (2004) 1040-1046.
30. K. Tanaka, H. Kita, K. Okamoto, A. Nakamura, Y. Kusuki, Gas permeability and permselectivity in polyimides based on 3,3',4,4'-biphenyltetracarboxylic dianhydride, Journal of Membrane Science, 47 (1989) 203-215.
31. F.J. Baltá-Calleja, C.G. Vonk, X-ray scattering of synthetic polymers, Elsevier, 1989.
32. A. Tena, A. Marcos-Fernandez, L. Palacio, P. Cuadrado, P. Pradanos, J. De Abajo, A.E. Lozano, A. Hernandez, Phase Segregation and Gas Separation Properties of Thermally Treated Copoly(ether-imide) from an Aromatic Dianhydride, an Aromatic Diamine and Various Aliphatic Diamines, Industrial & Engineering Chemistry Research, (2012).

33. A. Tena, A.E. Lozano, L. Palacio, A. Marcos-Fernández, P. Prádanos, J. de Abajo, A. Hernández, Gas separation properties of systems with different amounts of long poly(ethylene oxide) segments for mixtures including carbon dioxide, in press, (2012).
34. R.C. Reid, J.M. Prausnitz, B.E. Poling, The properties of gases and liquids, McGraw-Hill, 1987.
35. R. Recio, A.E. Lozano, P. Pradanos, A. Marcos, F. Tejerina, A. Hernandez, Effect of fractional free volume and T-g on gas separation through membranes made with different glassy polymers, J. Appl. Polym. Sci., 107 (2008) 1039-1046.
36. A. Bos, High pressure CO_2/CH_4 separation with glassy polymer membranes—aspects of CO_2-induced plasticization, in, University of Twente, Netherlands, 1996.
37. R.E. Kesting, A.K. Fritzsche, Polymeric gas separation membranes, Wiley, 1993.
38. R.W. Rousseau, Handbook of separation process technology, J. Wiley, 1987.
39. L.M. Costello, W.J. Koros, Thermally stable polyimide isomers for membrane based gas separations ar elevated-temperatures, J. Polym. Sci. Pt. B-Polym. Phys., 33 (1995) 135-146.
40. K. Nagai, A. Higuchi, T. Nakagawa, Gas permeability and stability of poly(1-trimethylsilyl-1-propyne-co-1-phenyl-1-propyne) membranes, Journal of Polymer Science, Part B: Polymer Physics, 33 (1995) 289-298.
41. J.J. Richards, M.K. Danquah, S. Kalakkunnath, D.S. Kalika, V.A. Kusuma, S.T. Matteucci, B.D. Freeman, Relation between structure and gas transport properties of polyethylene oxide networks based on crosslinked bisphenol A ethoxylate diacrylate, Chemical Engineering Science, 64 (2009) 4707-4718.
42. B.W. Rowe, L.M. Robeson, B.D. Freeman, D.R. Paul, Influence of temperature on the upper bound: Theoretical considerations and comparison with experimental results, Journal of Membrane Science, 360 (2010) 58-69.

10.7 Supporting Information

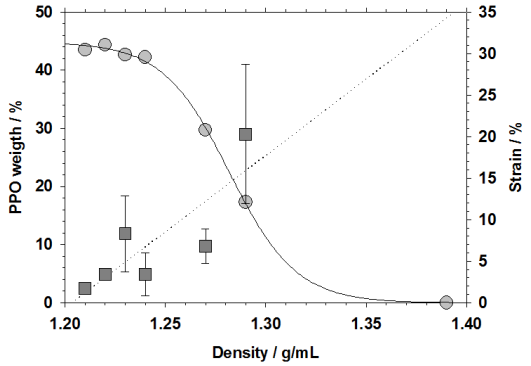

PPO weight percentage and strain for the copolymers as functions of density.

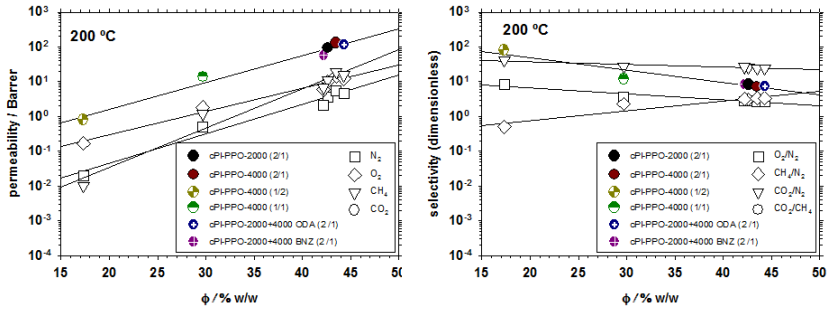

Permeability and selectivity as functions of PPO percentage for membranes treated at 200 °C.

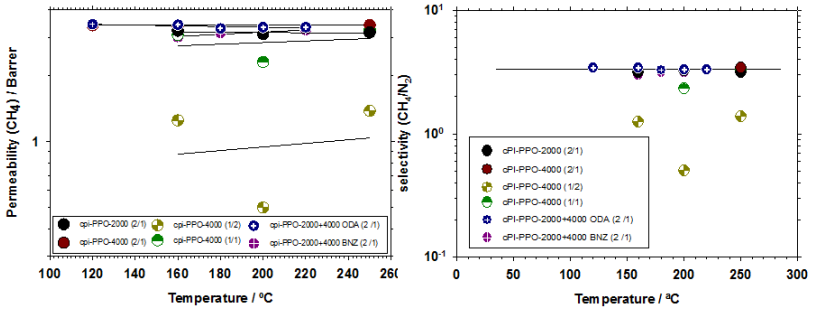

Permeability of CH_4 and CH_4/N_2 selectivity versus treatment temperature for all copolymers studied.

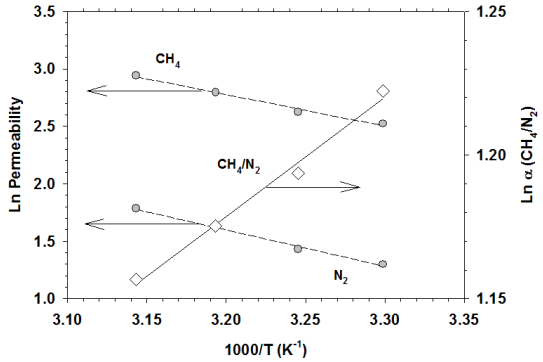

Arrhenius plot for the CH_4/N_2 pair for sample cPI-PPO-4000 (2/1) treated at 160 °C.

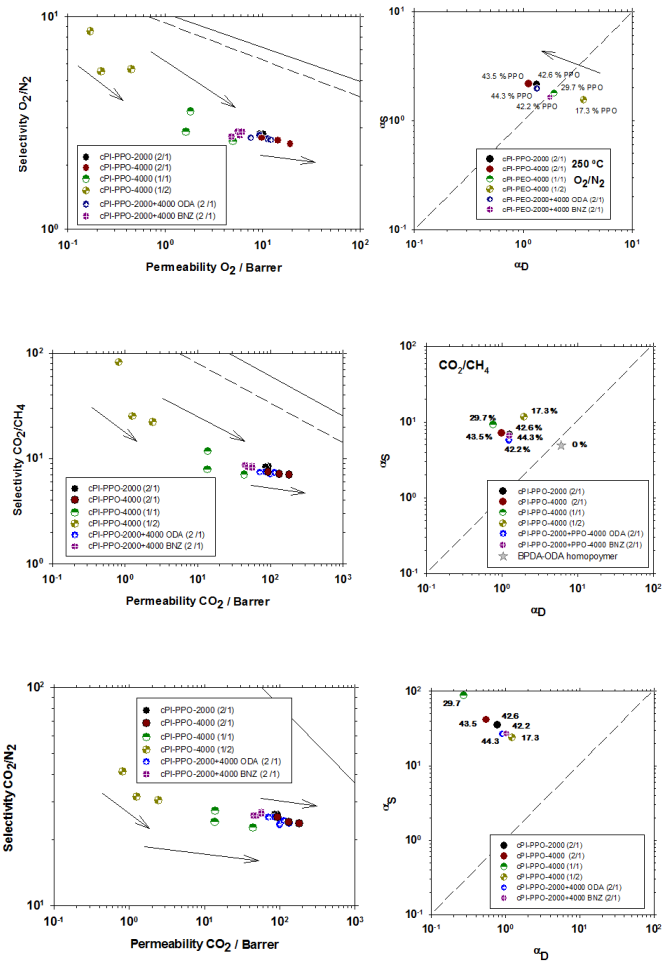

Robeson's plots for the O_2/N_2, CO_2/CH_4, and CO_2/N_2 gas pairs, along with corresponding selectivity by solubility as a function of the selectivity by diffusivity (membranes treated at 250 °C).

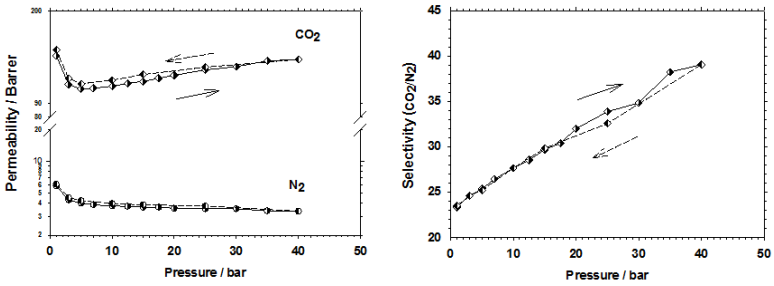

Pressurization and depressurization evolutions of permeability and selectivity for the CO_2/N_2 pair of gases for sample cPI PPO- 4000 (2/1) treated at 160 °C.

SECTION III. Prediction of the permeability properties.

The complexity and the cost of preparation for some polymer systems produces a need for the advance in theoretical models able to reproduce the experimentally results, and make a good prediction about polymers that could be interesting from the point of view of the gas separation applications. In this sense, this section, studies different predictive models for the permeability properties. *Chapter 11* describes the applications of different model, and among them the model based on the Effective Medium Approximation (EMA) that it was proved here to succeed in predicting the main features of the experimental results for all mixture proportions, taking as the starting point the sole input of pure homopolymer permeabilities. Specifically, this method was able to calculate the volume fraction for the maximum increase of permeability, a common feature for all the studied segregated copolymer membranes.

CHAPTER 11

Prediction of Gas Permeability of Block-Segregated Polymeric Membranes by an Effective Medium Model

Alberto Tena[1,3], Mónica de la Viuda[1,3], Laura Palacio[1,2], Pedro Prádanos[1,2], Ángel Marcos-Fernández[1,3], Ángel E. Lozano[1,3], Antonio Hernández[1,2]

[1]*Smap UA-UVA-CSIC, Parque Científico Universidad de Valladolid, Paseo de Belén, s/n, 47011 Valladolid, Spain.*

[2]*Dept. Física Aplicada, Facultad de Ciencias, Universidad de Valladolid, Paseo de Belén, 7, 47011 Valladolid, Spain*

[3]*Instituto de Ciencia y Tecnología de Polímeros, CSIC, Juan de la Cierva 3, 28006 Madrid, Spain.*

This chapter has been submitted to:

Journal of Membrane Science (under revision)

Abstract

A complete series of aliphatic aromatic copoly(ether-imide)s, based on aromatic dianhydrides (BPDA, BKDA or PMDA) and mixtures of an aromatic diamine (ODA) and an aliphatic diamine terminated poly(ethylene oxide) PEO(2000) (Mw=2000 g/mol) or PEO(6000) (Mw= 6000 g/mol), has been synthesized using different PEO contents. Cast films of these copolymers have been thermally treated to ensure the segregation of the linear PEO chains from the aromatic portion of these copoly(ether-imide)s.

Gas permeability (O_2, N_2, CO_2 and CH_4) of membranes, made from these copolymers with different proportions of PEO, were compared with the predictions of various electrical or thermal conductivity models adapted to gas permeability. Several of these models, from Maxwell-Garnet to percolation theory, proved to be inaccurate. Nevertheless, the model based on the Effective Medium Approximation (EMA) is proved here to succeed in predicting the main features of the experimental results for all mixture proportions, taking as the starting point the sole input of pure homopolymer permeabilities. Specifically, this later method was able to calculate the volume fraction for the maximum increase of permeability, a common feature for all the studied segregated copolymer membranes. The model was even able to predict the permeabilities of a three phase system consisting in the aromatic (BKDA-ODA) phase plus a mixture of amorphous PEO(6000) and crystalline PEO(6000).

11.1 Introduction

Nowadays, the role of polymeric membranes applied to gas separation is being more and more important. Although some of these materials have been used in industrial separations[1], it is well known that a lot of research is still necessary to discover or refine materials having an equilibrium of properties making them suitable to be employed in applications demanded nowadays by the industry. In all cases, an adequate balance of high permeability and good selectivity must be achieved [2-3].

In order to be useful in gas separation applications where one or several of the gases to separate is a condensable gas such as CO_2 or CH_4, the polymeric membrane should show a preferential affinity for them. In addition, these membranes must have good mechanical and thermal resistance.

Glassy polymers and in particular polyimides are well known by their excellent thermal oxidative stability, good organic solvent resistance and exceptional mechanical properties, along with an extraordinary ability to separate complex mixtures of gases in diverse applications [4-6]. Thus, it has been widely recognized that the use of aromatic polyimides is one of the best alternatives to be chosen among all the polymeric membranes for gas separation applications [7].

Typically, these materials have good selectivity and not very high permeability [8-9]. It could therefore be interesting to increase the affinity of the material matrix for condensable gases such as CO_2, or CH_4 as one of the most effective approaches.

Aromatic-aliphatic block-copolymers usually combine a hard block and a soft block. The hard block can be formed by a polymer with well-packed and highly rigid structures; as a result it forms a glassy phase with usually low free volume. In contrast, the soft block can consist in a polymer with more flexible, low T_g, chains, which can form a rubbery phase having high free volume. Also, when aromatic-aliphatic block copolymers are phase-separated, for instance, by an adequate thermal treatment, their glassy polymer parts could provide mechanical support. The rubbery segments, due to the nature of the flexible chain structure, should allow an efficient transport of gas, giving a good permeability to the material [10-11]. Among all the block copolymers, those having chains of polyethylene oxide (PEO) or polypropylene oxide (PPO) show outstanding features to be employed in gas separation applications.

The synthesis of new PEO systems using different aromatic diamines showed that an increase of rigidity in the hard part promoted the phase segregation process [12]. When the temperature of treatment of the films increased, phase segregation improved [13]. Analogous trends have been proved when diverse types of aromatic dianhydrides of different rigidity were employed [14]. These processes depended also on the type of polyether used, because the phase segregation and the final properties of the membranes can also vary depending on the nature of the soft part [15].

Mechanical properties of the membranes tended to worsen when the amount of polyether increased, because the amount of the hard part (which provides the mechanical strength of the final polymer) decreased. At the same time, the segregation and the permeation properties improved [16-17].

Polyethers such as PEO can experience easy crystallization processes when the molecular weight exceeds a certain value [16]. In gas separation this increase of crystallinity is undesirable because ordered structures have low or null permeation capacity. When PEO is in amorphous state, it can be said that the permeability increases with the length of the aliphatic part, mainly due to the improvement in phase segregation [16]. It is clearly important to find a good balance between the hard and the soft block segments in order to provide good permeability without having a dramatic loss in mechanical properties.

Many composite systems, as for example mixed matrix membranes, MMM, have been modeled to correlate the overall permeability with those of the component phases by applying Maxwell-Garnet, MG, based treatments. Herein, we have applied this treatment to phase segregated membranes and we have found difficulties to model, within this theoretical frame, the range of intermediate concentrations. In this paper it is demonstrated that more symmetric schemes as the effective medium approximations, EMA, reproduce well enough the composition ranges where none of the phases, forming the material, can be considered as dispersed in a continuous matrix.

11.2 Experimental

The segregated copoly(etherimide)s whose permeabilities are modeled here have been synthetized, thermally segregated and characterized previously by our group [12, 15-16, 18]. A brief summary of these aspects is provided below.

11.2.1 Chemicals

3,3′,4,4′- Biphenyltetracarboxylic dianhydride (BPDA); 3,3′,4,4′-benzophenone tetracarboxylic dianhydride (BTDA or BKDA); pyromellite dianhydride (PMDA), and 4,4'-oxydianiline (ODA) were purchased from Aldrich. These products were purified by sublimation at high vacuum just before use. Polyoxyethylene bis(amine) (Jeffamine ED-2003, n= 41) with nominal molecular weight of 2000 g/mol, was kindly donated by Huntsman® (Holland) (PEO-2000 from here on). α,ω-Diamine-poly(ethylene oxide) with nominal molecular weight of 6000 g/mol, were obtained from Kawaken Fine Chemicals Co., Ltd. (Tokyo, Japan), (PEO-6000 from here on). These polyethers were dried at 70 ºC in vacuum for 5 hours and stored in a desiccator at vacuum until use. Anhydrous N-methylpyrrolidinone (NMP), used as the polymerization solvent, was purchased from Sigma-Aldrich Co.

11.2.2 Synthesis of copoly(ether-imide)s

The samples were synthesized by combination of a dianhydride (BPDA, BKDA or PMDA) with mixtures of an aromatic diamine (ODA), and diverse proportions of an aliphatic diamine (PEO). The corresponding copoly(ether-imide)s will be designated by adding cPI to the w/w percentage of the aliphatic proportion.

Diamine-terminated poly(oxyethylene oxide) – PEO(2000) or PEO(6000) — (x mmol), and 4,4'-oxydianiline (ODA) (y mmol) in several weight ratios were dissolved in anhydrous NMP (5 mmol (x+y)/10 mL) in a 100 mL three-necked flask blanketed with nitrogen.

Then, the reaction mixture was cooled down to 0 ºC, and under mechanical stirring, a stoichiometric amount of the dianhydride (x+y mmol) was added. The mixture was maintained overnight at room temperature. During this time the dianhydride was completely dissolved and the solution reached high viscosity.

In Figure 1 the corresponding structures of the aromatic and aliphatic homopolymers corresponding to the copoly(ether-imide)s synthetized are shown along with their densities

Acronym	Structure	Density g/mL
PEO		1.085[a]
BPDA-ODA	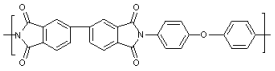	1.366[b]
BKDA-ODA	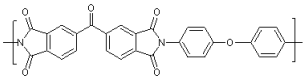	1.374[b]
PMDA-ODA	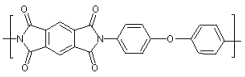	1.395[b]

Figure 1. Structure of the aromatic and aliphatic components of the copolyimide thermally segregated membranes studied here along with their densities. ([a]) Data from the manufacturer and ([b]) Tanaka et al. [7].

11.2.3 Preparation of the copolyimide dense films.

The resultant viscous copolyamic acid solution was diluted with NMP to the appropriate viscosity for casting, filtered through a nominal #1 fritted glass funnel, degassed, and cast onto a leveled glass plate. The resulting film was covered with a conical funnel to avoid fast evaporation of the solvent, dried at 80 ºC overnight, and finally treated at several temperatures from 160 to 250 ºC (275 ºC for the BKDA containing films) for 6 hours until 200 ºC and 30 min over this temperature in a vacuum oven, in order to achieve a complete imidization. Films of copolymers having 50-70 μm in thickness were obtained. After that, thermal treatments under an inert atmosphere were carried out at different temperatures.

11.2.4 Characterization of the membranes.

All the copoly(eherimide)s studied here were treated at different temperatures (as mentioned above) and the resulting films extensively characterized [12-18]. They were and phase segregation was confirmed by Small-Angle X-ray Scattering (SAXS) observing that this process increases with temperature. Glass transition temperatures, crystallinity and mechanical properties were obtained by using Differential Scanning Calorimetry (DSC), Thermo Gravimetric Analysis (TGA), Thermo Mechanical Analysis (TMA) and Dynamic Mechanical Analysis (DMA). All the films showed good mechanical properties.

Permselectivities were obtained by using “time lag” permeators at 3 bar and 30 ºC (some measurements were done at 50 ºC when crystallinity was present in the case of PEO-6000).

11.3 Theory

The membranes composed by two or more different phases should have permeability values placed between those for pure phases. Copolyimides consisting in an aromatic polyimide part (hard segments) and an aliphatic polyether one (soft PEO chains) should be modeled as a system formed by two intermixed phases.

It has been generally [16, 19] found that for intermediate volume fractions there is a range where none of the Maxwell predictions are accurate. It has been also noticed that low PEO proportions are well predicted by the Maxwell model assuming that PEO is the dispersed phase although for high PEO proportions the Maxwell model with PEO as the continuous phase fits better the experimental results. Of course there is a range where neither the PEO rich nor the aromatic rich phases can be taken as disperse or discontinuous. This intermediate range has resisted all attempts to be predictable or even understood.

A revision will be made here of some of the main models that can be used to predict permeabilities for different proportions of a multiphase gas separation membrane. This revision cannot be exhaustive as far as there are a huge plethora of models more or less similar to each other which were originally proposed for electric or thermal conductivity or for mechanical properties [20-22]**.** The models will, of course, be adapted to gas permeation attending to the well-known analogy existent between the transport processes [23].

11.3.1 Maxwell-Garnet Models

The Maxwell approximation, [24-25] also known as the Clausius-Mossotti approximation, is one of the most widely used methods for calculating the bulk dielectric properties of inhomogeneous materials [26-27]. It is useful when one of the components can be considered as a host in which inclusions of the other component or components are embedded. It involves an exact calculation of the field induced in the uniform host by a single spherical or ellipsoidal inclusion and an approximate treatment of its distortion by the electrostatic interaction between the different inclusions. This distortion is caused by the charge dipoles and higher multipoles induced in the other inclusions. The induced dipole moments cause the longest range distortions and their average effect is included in the Maxwell approximation which results in a uniform field inside all the inclusions.

These approaches have been extensively used to study the properties of two-component mixtures in which both, the host and the inclusions, are isotropic materials with scalar dielectric coefficients. Nevertheless, relaying in the known analogies of transport phenomena, this theoretical frame has been used to model: electrical conductivity, thermal conductivity and elasticity parameters. They have been also extensively used for permeation modeling.

For gas separation processes, it has been demonstrated that systems consisting in a disperse phase embedded in a continuous matrix can be described in terms of these models that have been called Maxwell-Garnet or Maxwell-Eucken models. Within the frame of these theoretical schemes, the effective permeability is:

$$P_{eff} = \left[\frac{P_d + 2P_c - 2\phi_d \left(P_c - P_d \right)}{P_d + 2P_c + \phi_d \left(P_c - P_d \right)} \right] \tag{1}$$

Where P_{eff} is the effective permeability, P_c and P_d are the permeabilities of the continuous and disperse phase, respectively, and ϕ_d is the volume fraction of the dispersed phase in the block copolymer.

In our study, of course the continuous phase can be the aromatic or the aliphatic rich portions depending on the composition of the copolymer. For this reason, it should be necessary to make two different predictions depending on which segment is taken as the continuous phase or the disperse one. This is necessary because Equation (1) is not symmetric and if the roles of the filler and the continuous phase are swapped, different results are obtained.

Bruggeman [28] introduced a popular approximation that is now widely known as the differential scheme or the Bruggeman equation. Bruggeman proceeds from the premise that the fields of neighboring particles can be taken into account by adding the dispersed particles incrementally, taking the surrounding medium to be the existing composite at each stage.

Translated to gas permeability, the Bruggeman equation says that the effective permeability of an inhomogeneous medium is given by:

$$\frac{P_d - P_{eff}}{P_d - P_c} \left(\frac{P_c}{P_{eff}} \right)^{1/d} = 1 - \phi_d \tag{2}$$

where d = 3 for spherical fillers [29].

The Bruggeman equation is appropriate for composites containing spherical particles with a very wide size distribution. Ideally, the size distribution should be wide enough so that any two spheres of comparable size are far from each other. Note that Equation (2) needs to be solved numerically and it is also asymmetric, in the sense commented when referring to Equation (1), i.e. it is not single valued.

Some models have been applied without any pursued symmetry between filler and continuous matrix because they are intended for low content of filler within a continuous matrix. Most of these models lead to divergences in permeability for filler contents over a certain value. They belong to this class, for example, the models due to Bruggeman [28], Bötcher [30] and de Loor [31] and corresponding to Equations (3) to (5) [32]:

$$P_{eff} = P_c \left(1-\phi_d\right)^{-3} \tag{3}$$

$$P_{eff} = P_c \left(1-\phi_d\right)^{-1} \tag{4}$$

$$P_{eff} = P_c \left(1-\phi_d\right)\left(1-2\phi_d\right)^{-1} \tag{5}$$

The Lewis and Nielsen model [33-35], originally proposed for the elastic modulus of particulate composites, gives:

$$P_{eff} = P_c \left[\frac{1 + A\phi_d \dfrac{\left(P_d/P_c\right)-1}{\left(P_d/P_c\right)+A}}{1-\psi\phi_d \dfrac{\left(P_d/P_c\right)-1}{\left(P_d/P_c\right)+A}} \right] \tag{6}$$

$$\psi = 1 + \phi_d \left(\frac{1-\bar{\phi}_d}{\bar{\phi}_d^2} \right) \tag{7}$$

The values of A and $\bar{\phi}_d$ were given for many geometric shapes and orientations [36-38]. A is 2 for spheres in a unidirectional transport, $\bar{\phi}_d$ is 0.64 for random close packing of uniform spheres. $\bar{\phi}_d$ is the maximum ϕ_d that is the maximum packing volume fraction for a given inclusion size and shape.

The Pal model [39] assumes that:

$$\frac{P_d - P_{eff}}{P_d - P_c}\left(\frac{P_c}{P_{eff}}\right)^{1/d} = \left(1 - \frac{\phi_d}{\bar{\phi}_d}\right)^{\bar{\phi}_d} \tag{8}$$

where d = 3 as in Equation (2) for spheres like for the original work of Bruggeman (Equation (2)).

Equations (6) to (8) belong also to the divergent or low filler fraction models.

11.3.2 Effective Medium Theory

Actually, when both phases are not continuous and there is a random dispersion of them, the Maxwell approach is not reasonable. Within the frame of the Maxwell's model, the continuous and discontinuous phases must be first identified because Equations (1) to (8) are not symmetric as mentioned. Systems where the formation of an internal network in the structure is observed are more accurately represented with the effective medium theory (EMT) that treats the contributions of each phase equally. As the equation of Maxwell, EMT is derived from the solution of the Laplace equation applied to a single sphere surrounded by a continuous medium, and subjected to a steady-state concentration gradient around the spheres. Maxwell assumed that the local distortions to the concentration distributions around the dispersed spheres did not affect their neighbors. The essence of EMT, however, lies in the assumption that for a completely random distribution of components, the effect of local distortions to the concentration distribution caused by individual inclusions could be averaged in such way that over a sufficiently large volume (or ensemble) the concentration distribution within the material could be approximated by a material having an uniform concentration distribution and permeability P_{eff} [40-41].

Effective medium approximations or effective medium theory (sometimes abbreviated as EMA or EMT) are physical models that describe the macroscopic properties of composite materials, which are developed from averaging the multiple values of the constituents that directly make up the composite material. At the constituent level, the values of the materials vary and are inhomogeneous. Precise calculation of the many constituent values is nearly impossible. The EMA methodologies are based [28] on a self-consistent procedure in which a grain of one of the components is assumed to have a convenient shape (usually spherical or ellipsoidal) and to

be embedded in an effective medium whose properties are determined self-consistently [27, 41]. EMA treats equally both the components as shown in its fundamental equation, [42]:

$$\phi_d \frac{P_d - P_{eff}}{P_d + 2P_{eff}} + \phi_c \frac{P_c - P_{eff}}{P_c + 2P_{eff}} = 0 \tag{9}$$

Note that this frame can be extended to n phases by using:

$$\sum_{i=1}^{n} \phi_i \frac{P_i - P_{eff}}{P_i + 2P_{eff}} = 0 \tag{10}$$

Although the distinction of dispersed and continuous phases losses its meaning as far as the two phases are treated in the same way and the roles of both the phases could be interchanged and the predicted overall permeability would not change, we will continue naming disperse phase to the PEO domains and continuous phase to the aromatic rich one. Equation (9) can be solved to:

$$P_{eff} = \frac{1}{4}\left(\gamma + \sqrt{\gamma^2 + 8P_d P_c}\right) \tag{11}$$

with

$$\gamma = \left(3\phi_d - 1\right)P_d + \left(3\phi_c - 1\right)P_c \tag{12}$$

of course using the identity $\phi_c = 1 - \phi_d$. All these EMA calculations are particularly appropriate for composites and polycrystals in which the grains of the various components are randomly and symmetrically distributed, so that none of the components is identifiable as a host in which the others are preferentially embedded.

Because of the asymmetry of the assumed geometry, and the approximation, the results are likely to differ somewhat from the unevaluated (symmetric) EMA. This geometrical distinction may be easily understood by noting that the EMA and MG approximations are exact for two different microgeometries [26]. The EMA becomes exact in a hierarchical geometry where the two components play symmetrical geometric roles [43]. In contrast, the MG approach is exact for a geometry where the entire space is filled with equal spheres, each with identical ratio, such that one component is the core material and the other is the coating material (the host).

11.3.3 Modifications of the Maxwell models

Modifications of the Maxwell model have been done in two main directions. Firstly, the original asymmetric model has been modified to be symmetrical. And also the model has been modified to take into account the appearance of different phases corresponding, for example, to the interfaces between the matrix and the disperse phases or to take into account the differences of: size, isotropy etc. In this work, we will only mention in some detail the modifications addressed to make the approach symmetric and to take into account the possible presence of more phases.

The Levy model was originally proposed as a purely mathematical averaging of the Maxwell–Eucken model with each of the two phases being treated as continuous [44]. This model was recently given a physical interpretation by Wang et al. [45]. In terms of gas permeability the model states that:

$$P_{eff} = P_c \left[\frac{P_d + 2P_c - 2\left(P_c - P_d\right)F}{P_d + 2P_c + \left(P_c - P_d\right)F} \right] \tag{13}$$

$$F = \frac{\left(2/g\right) - 1 + 2\phi_d - \sqrt{\left[\left(2/g\right) - 1 + 2\phi_d\right]^2 - \left(8\phi_d / g\right)}}{2} \tag{14}$$

$$g = \frac{\left(P_c - P_d\right)^2}{\left(P_d + P_c\right)^2 + \frac{P_d P_c}{2}} \tag{15}$$

which is symmetrical and single valued although, as we will see below, it is actually too symmetrical.

In order to treat three-phase-systems the Maxwell-Garnet model has been modified as:

$$P_{eff} = \left[\frac{P_d + 2P_c - 2\phi_d\left(P_c - P_d\right)}{P_d + 2P_c + \phi_d\left(P_c - P_d\right)} \right] = P_c \left[\frac{2\left(1 - \phi_d\right) + \left(1 + 2\phi_d\right)\left(P_d / P_c\right)}{\left(2 + \phi_d\right) + \left(1 - \phi_d\right)\left(P_d / P_c\right)} \right] \tag{16}$$

with

$$P_d = P_{in}\left[\frac{2(1-\phi_k)+(1+2\phi_k)(P_k/P_{in})}{(2+\phi_k)+(1-\phi_k)(P_k/P_{in})}\right] \tag{17}$$

P_{eff} is the permeability of the ensemble continuous phase plus disperse phase, P_d is the permeability of a single core plus interfacial shield particle and P_{in} is the permeability of the interfacial shield covering the particle core that has a permeability P_k. ϕ_d is the volume fraction of inclusions and ϕ_k is the fraction of the core in the core+shield system. This model has been developed to take into account the existence of such shields covering inclusions in mixed matrix membranes [46-48].

The Felske model [49] has been proposed for such complex (three phases) inclusions. This model gives:

$$P_{eff} = P_c\left[\frac{2(1-\phi_d)+(1+2\phi_d)(\alpha/\beta)}{(2+\phi_d)+(1-\phi_d)(\alpha/\beta)}\right] \tag{18}$$

$$\alpha = \frac{(2+\delta^3)P_k - 2(1-\delta^3)P_{in}}{P_c} \tag{19}$$

$$\beta = 1+2\delta^3-(1-\delta^3)\frac{P_k}{P_{in}} \tag{20}$$

And δ is the ratio of outer-shield to core radii.

The Felske model gives almost the same results than the modified Maxwell model and although it is somewhat simpler, it has the same limitations than the original Maxwell model [50].

As done by Lewis and Nielsen, $\overline{\phi}_d$ can be introduced in the Felske model to give [34, 50]:

$$P_{eff} = P_c\left[\frac{1+2\dfrac{\alpha-\beta}{\alpha+2\beta}\phi_d}{1+\dfrac{\alpha-\beta}{\alpha+2\beta}\psi\phi_d}\right] \tag{21}$$

with ψ given by Equation (7).

11.3.4 Percolation Models

The original problem was proposed [51] for the fluid flow in a porous medium. It has been applied to many other related problems including many phenomena in physics, chemistry and materials science [52].

A two phase system formed by inclusions dispersed in a continuous matrix can be modeled by a (3D) lattice in which each site can be occupied or empty with certain complimentary probabilities. In mathematics, percolation theory describes the behavior of connected clusters in such a random graph. In terms of gas permeability, an occupied site has a permeability P_d while an unoccupied site has a permeability P_c. The fundamental premise of percolation theory is the appearance of a sharp increase in the effective permeability of the disordered media at a critical volume fraction known as the percolation threshold ϕ_t at which long-range connectivity of the system appears.

When $P_d \neq 0$, $P_c = 0$, and $\phi_d < \phi_t$, no macroscopic conducting pathway exists and no permeation happens through the composite phase. When $\phi_d > \phi_t$, however, the system becomes permeable as a connected path appear through the composite material. The existence of a critical percolation threshold for electrical conductivity has been demonstrated for a wide variety of fillers, all at concentrations below the maximum packing fraction, $\bar{\phi}_d$ [53]. The percolation threshold in an actual composite material is in general a function of the lattice structure of the phases, and ranges from $\phi_t \approx 0.2$ for a face-centered cubic arrangement to $\phi_t \approx 0.7$ for a honeycomb arrangement and it can be exactly calculated for certain simple lattices [42].

Electrical conductivity has been treated frequently within percolation models [54] but also thermal conductivity has been modeled as percolative [55-56]. However, many researchers have reported that no percolation appears in thermal conductivity [57]. It may be noted that in contrast to the electrical conductivity, the concentration dependence of thermal conductivity does not show any swift leap that could be interpreted as a percolation threshold. This is because thermal conductivity of the dispersed filler is usually comparable to that of the polymer matrix. Given that this is even more certain for the gas permeabilities through disperse and continuous phases in a composite, we could find difficult to justify the appearance of percolation in the systems to be studied here. Nevertheless, as will be seen below, there is actually a sudden increase in the effective permeability of our two phase systems, thus we will adapt and try to use the most promising percolation model proposed for the thermal

conductivity. This model was proposed by Zhang et al. [58-59] and translated to permeability says that:

$$P_{eff} = P_d \left(\frac{P_t}{P_d} \right)^{\left[\frac{1-\phi_d}{1-\phi_t} \right]^N} \tag{22}$$

P_t is the permeability at the threshold (percolation) composition given by ϕ_t and N is the percolation exponent. This model contains actually 3 parameters to be fitted. Although the values of P_t and ϕ_t can be obtained by an analysis of the experimental data, n has to be fitted or evaluated for some fixed point.

11.3.4 Volume fractions

In all cases it is important to remember that the fractions to be used in the above equations are volume ones rather than mass fractions which are more customarily used for dosing purposes. The corresponding volume fractions can be evaluated from the weight fractions by

$$\phi_d = \frac{\omega_d / \rho_d}{\omega_d / \rho_d + (1-\omega_d)/\rho_c} \tag{23}$$

ω_d is the weight fraction and ρ_d is the density of filler and ρ_c is the density of the matrix. The densities that we will use in the next section are shown in Figure 1.

11.4 Results and Discussion

In Figure 2 the CO_2 permeability of the copolyimide BPDA-ODA-PEO(2000) thermally treated to 250 ºC as a function of the volume fraction of PEO (ϕ_d) is shown. The predictions of Equations: (1) (Maxwell); (2) (Brugeman); (9), (11) and (12) (EMA) and of Equations (13), (14) and (15) (Levy) are shown. It seems clear that the EMA model reproduces well all the main features of experimental data. It seems clear that the presence of an inflexion point in the experimental data is only predicted by the EMA and the Levy models. The vertical double line in Figure 2 corresponds to the volume fraction of PEO for this inflexion point.

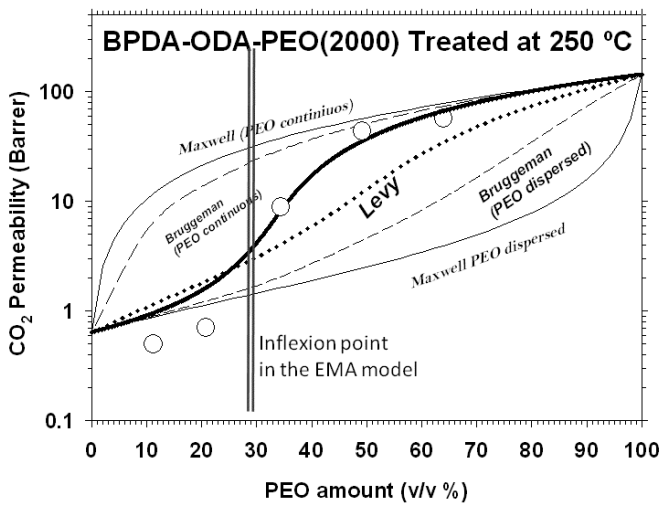

Figure 2. Comparison of some models for the effective permeability of CO_2 for a maximum thermally segregated polyimide. The Bruggeman model corresponds to Equation (2) with d=3. The EMA model corresponds to the s-shaped continuous line.

When Equations (11) and (12) are taken into account it is seen that an inflexion point always appears, within the EMA model when log P_{eff} is plotted versus ϕ_d. This inflexion point can be calculated by solving $d^2\log(P_{eff})/d\phi_d^2 = 0$ and corresponds to the volume fraction of the disperse phase at which P_{eff} increases at its maximum pace. This happens when:

$$\hat{\phi}_d = \frac{1-2\lambda}{3(1-\lambda)} \quad \text{or for all } \phi_d \text{ when } \lambda = 1 \tag{24}$$

Here

$$\lambda = \frac{P_d}{P_c} \tag{25}$$

It is worth remembering that the roles of continuous and disperse phases could be interchanged.

The behavior of the function given in Equation (24) is shown in Figure 3. Note that the maximum increase of P_{eff} happens for $\hat{\phi}_d \approx 1/3$ if $P_d >> P_c$ (or $\hat{\phi}_d \approx 2/3$ if $P_c >> P_d$). Moreover only when $P_d = P_c/2$ or $P_c = P_d/2$ there is a maximum increase of P_{eff} at $\hat{\phi}_d = 0$ or $\hat{\phi}_d = 1$. In any case, this inflexion point cannot appear within the range $1/3 < \hat{\phi}_d < 2/3$. Note that according to the

Levy model this inflexion would appear at $\hat{\phi}_d = 1/2$. This is the justification to our attribution of an excessive symmetry to this model.

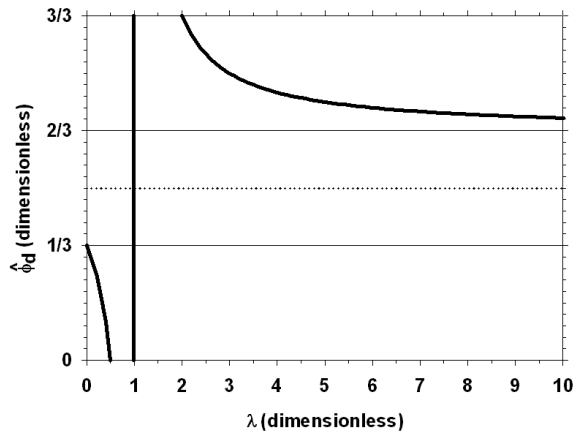

Figure 3. Plot of Equation (17) showing that there is a range from ϕ_d = 1/3 to 2/3 that can't correspond to the inflexion point in P_{eff}. The inflexion point for the Levy model should be placed in ϕ_d = 1/2.

In Figure 4 the O_2, N_2 and CH_4 permeabilities of the copolyimide BPDA-ODA-PEO(2000) thermally treated at 250 ºC as a function of the volume fraction of PEO (ϕ_d) are depicted. The same features as seen in Figure 2 are now observed and in this case only the predictions of the EMA model are shown.

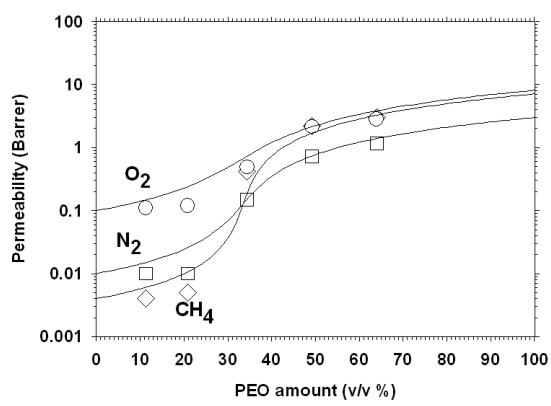

Figure 4. Effective permeability of: O_2, N_2 and CH_4 for a thermally segregated polyimide. The lines correspond to the EMA model.

In Figure 5 the permeability for O_2 of the copolyimide BPDA-ODA-PEO(2000) thermally treated at 250 ºC is shown as a function of the volume fraction of PEO (ϕ_d) along with the predictions of the models given by Equations: (3) (Brugeman) ; (4) (Bötcher); (5) (de Loor); (6) and (7) (Lewis-Nielsen) and by Equation (8) (Pal). It seems clear that all these models diverge or at least do not approximate to the pure PEO permeability for $\phi_d = 1$. The Lewis-Nielsen (with A= 2) and Pal (with d=3) models have been taken with $\overline{\phi}_d = 0.64$ as should correspond to the maximum packing of spherical inclusions. It seems clear that none of them adequately fits the experimental results.

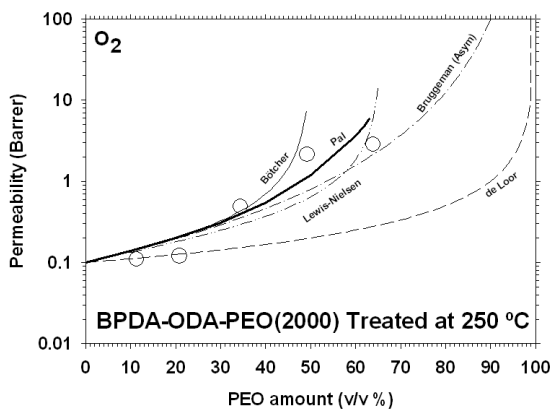

Figure 5. Effective permeability of O_2 and predictions of some models for low content of a dispersed phase. The Lewis-Nielsen (with A=2) and the Pal (with d=3) models have been shown for $\overline{\phi}_d$ =0,64.

In Figure 6 the values of $\overline{\phi}_d$ for the Pal model (that seems to be the most acceptable among the models shown in Figure 5) are changed in order to compare its predictions with the data for the N_2 permeability (again for the BPDA-ODA-PEO(2000) copolyimide thermally treated at 250 ºC) as a function of the volume fraction of PEO (ϕ_d). It appears clear that the Pal model cannot account for the real dependence of permeability for any value of $\overline{\phi}_d$.

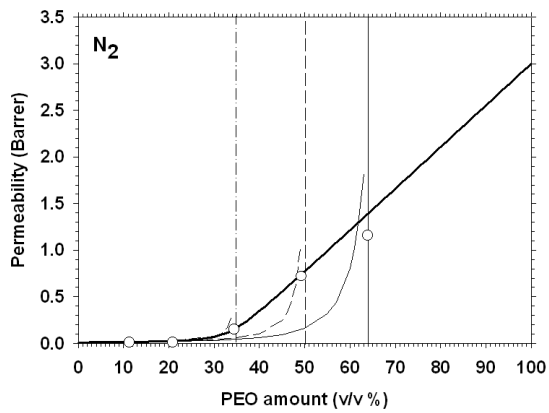

Figure 6. Effective permeability of N_2 and predictions of the Pal model (with d = 3) for three different Effective permeability of N_2 and predictions of the Pal model (with d = 3) for three different $\overline{\phi}_d$.

The predictions of the percolation model of Zhang (Equation (22)) clearly do not fit the experimental results for low volume fractions of PEO as shown for the CH_4 permeability (for the BPDA-ODA-PEO(2000) copolyimide thermally treated at 250 ºC) in Figure 7. In this Figure, the two discontinuous lines correspond to fixed and fitted values for ϕ_t and P_t. Clearly they do not show significant differences. The values obtained for N are also quite similar. It may be noted that the percolation based model proposed by Zhang *et al.* predicts that a percolation threshold would appear only if the ratio of the permeability of the filler to the polymer permeability was larger than 10^5, which in the present case is not satisfied [59]. This requirement is clear in Figure 7 where it is seen that the assumption of a percolation threshold would lead to a predicted permeability of CH_4 for the continuous phase that would be 10^{-5} barrer for a PEO permeability of the order of unity.

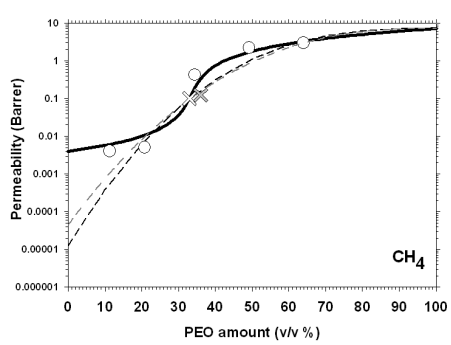

Figure 7. Effective permeability of CH_4 and predictions of the percolation model of Zhang. The white cross corresponds to a fixed pair ϕ_t and P_t while the gray one corresponds to values obtained for ϕ_t and P_t after fitting.

The values of N, 2.55 and 2.83, are somehow out of the range that could be expected for electrical or thermal conductivity and for permeability as far as it is well known that N = 2 in a three-dimensional percolation (with an aspect ratio, $\delta = 1$) [60], with $\delta = L/D$, L and D being the length and the diameter of the inclusions.

In Figure 8 the EMA model is applied to the CO_2 permeability of the copolyimides: BPDA-ODA-PEO(2000), BKDA-ODA-PEO(2000) and PMDA-ODA-PEO(2000). The figure shows that a change in the dianhydride has little effect in the dependence of permeability and the point of maximal increase in the effective permeability is quite similar and very close to a volume fraction of PEO $\hat{\phi}_d \approx 1/3$. This could be predicted from Equations (24) an (25) because λ goes from $2.8 \cdot 10^{-3}$ to $17.4 \cdot 10^{-3}$ which corresponds to values of $\hat{\phi}_d$ going from 32.7 % to 33.2 %.

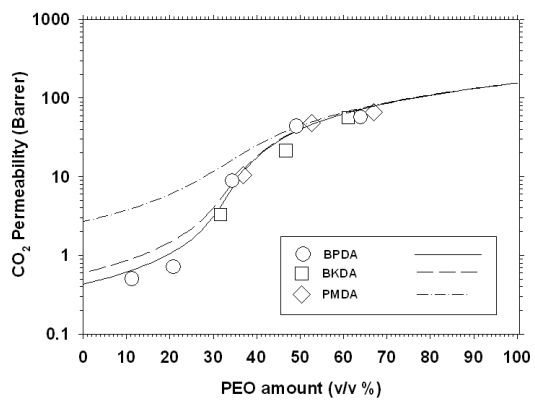

Figure 8. Effective permeability of CO_2 for thermally segregated polyimides with different dianhydrides. The lines correspond to the EMA model.

Figure 9 and 10 correspond to a three phase system BKDA-ODA-PEO(6000) constituted by the pure BKDA-ODA, the amorphous PEO(6000) and the crystalline one. In Figure 9 the white symbols correspond to the total volume proportion of PEO(6000). The EMA model fits the results only when the actual amorphous volume proportion of PEO(6000) is taken into account after subtraction of the crystalline volume as obtained by DSC, [16], and the system is taken as a bi-phase system.

In Figure 10 the three phase system has been fitted to Equation (10), for three phases:

$$\left.\begin{aligned} \sum_{i=1}^{3} \phi_i \frac{P_i - P_{eff}}{P_i + 2P_{eff}} = 0 \\ \sum_{i=1}^{3} \phi_i = 1 \end{aligned}\right\} \tag{26}$$

assuming that the permeability of the crystalline PEO is zero. It is clear that as shown in Figure 10, the EMA model can predict also the permeability across three phase composite segregated copolyimides. In Figure 10 the data for the semicrystalline PEO with 29 % crystallinity has been taken from Lin and Freeman [61] (see Figure 2 of this reference).

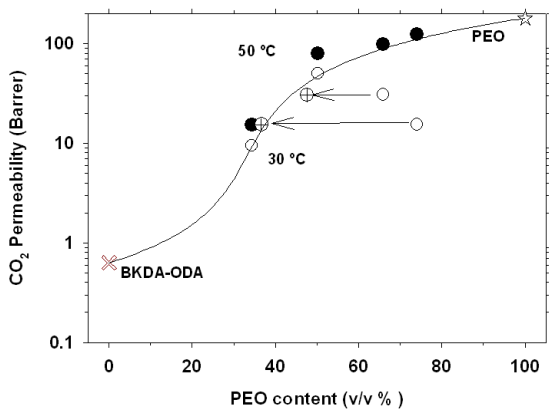

Figure 9. Effective permeability of CO_2 for a partially crystalline PEO within a BKDA-ODA matrix at 30 ºC (○). When the fractions of real amorphous PEO (⊕) are taken into account EMA predictions reproduce the experimental results. The line corresponds to the EMA model. At 50 º C (●) there is no crystallinity and the EMA predictions are again quite good.

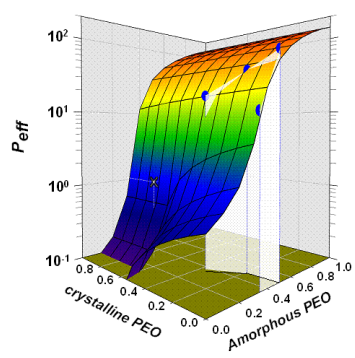

Figure 10. Effective permeabillity of CO_2 for a three-phase system of crystalline and amorphous PEO in a BKDA-ODA matrix and the predicitions of EMA.

11.5 Conclusions

A series of aliphatic aromatic copoly(etherimide)s has been synthesized. Cast films of these copolymers have been thermally treated to ensure the phase segregation of the linear PEO chains from the aromatic moiety of the copoly(etherimide)s. The permeability of O_2, N_2, CO_2 and CH_4 of the resulting membranes have been compared with the predictions of the main usable models adapted to the gas permeability.

The model based on the Effective Medium Approximation (EMA) succeeded to predict the main features of the experimental results. Specifically, it was able to calculate the volume fraction for the maximum increase of permeability, a common feature for all the studied segregated copolymer membranes. The model was even able to predict the permeabilities of a three phase system consisting in the aromatic (BKDA-ODA) rich phase plus the amorphous PEO(6000) and the crystalline PEO(6000) phases.

As discussed, the EMA calculations are especially applicable to composites and polycrystals in which the various components are randomly and symmetrically distributed, so that none of the components is identifiable as a host in which the others are preferentially embedded. The size and orientation of each phase are continuously changing with their proportion; this is the case with the segregated copoly(ether)imides studied here. On the other hand, there is not a constant size network to be filled and the permeabilities of the phases involved are relatively close to each other as to make percolation impossible. Nevertheless they are different enough to have a certain percolation-like sudden step in the effective permeability which is well integrated in the EMA model.

The model has the advantage of being able to be adapted for three phase (or multiphase) composites where the structure of each phase in the mixture is effectively random in nature. This fact has the added advantage of making unnecessary any consideration on the detailed phase-to-phase morphology.

11.6 Acknowledgements

The authors thank the Ministerio de Educación y Ciencia (Plan Nacional de I+D+i) through projects MAT2011-25513 and CTQ2012-31076, Junta de Castilla y León (project VA-324A11-2) and also Acciona Agua for partial funding of this research. We are indebted also to

Ministerio de Economía y Competitividad through project MAT2010-20668. A. Tena thanks CSIC for a predoctoral JAE fellowship.

11.7 References

1. R.W. Baker, Future directions of membrane gas separation technology, Industrial & Engineering Chemistry Research, 41 (2002) 1393-1411.
2. R. Bounaceur, N. Lape, D. Roizard, C. Vallieres, E. Favre, Membrane processes for post-combustion carbon dioxide capture: A parametric study, Energy, 31 (2006) 2556-2570.
3. E. Favre, Carbon dioxide recovery from post-combustion processes: Can gas permeation membranes compete with absorption?, Journal of Membrane Science, 294 (2007) 50-59.
4. I. Bessonov, W.W. Wright, Polyimides: thermally stable polymers, Consultants Bureau, 1987.
5. M.K. Ghosh, K.L. Mittal, Polyimides: Fundamentals and Applications, Marcel Dekker Incorporated, 1996.
6. K.L. Mittal, Polyimides and Other High-temperature Polymers: Synthesis, Characterization, and Applications. Volume 5, VSP, 2009.
7. K. Tanaka, H. Kita, M. Okano, K.-i. Okamoto, Permeability and permselectivity of gases in fluorinated and non-fluorinated polyimides, Polymer, 33 (1992) 585-592.
8. D. Ayala, A. Lozano, J. De Abajo, C. Garcıa-Perez, J. De la Campa, K.-V. Peinemann, B. Freeman, R. Prabhakar, Gas separation properties of aromatic polyimides, Journal of Membrane Science, 215 (2003) 61-73.
9. K. Tanaka, H. Kita, K. Okamoto, A. Nakamura, Y. Kusuki, Gas permeability and permselectivity in polyimides based on 3, 3', 4, 4'-biphenyltetracarboxylic dianhydride, Journal of Membrane Science, 47 (1989) 203-215.
10. T. Barbari, W. Koros, D. Paul, Gas transport in polymers based on bisphenol-A, Journal of Polymer Science Part B: Polymer Physics, 26 (1988) 709-727.
11. Y. Li, M. Ding, J. Xu, Gas separation properties of aromatic polyetherimides from 1, 4-bis (3, 4-dicarboxyphenoxy) benzene dianhydride and 3, 5-diaminobenzic acid or its esters, Journal of applied polymer science, 63 (1997) 1-7.
12. A. Tena, A. Marcos-Fernández, A.E. Lozano, J.G. de la Campa, J. de Abajo, L. Palacio, P. Prádanos, A. Hernández, Thermally treated copoly (ether-imide) s made from bpda and alifatic plus aromatic diamines. Gas separation properties with different aromatic diamimes, Journal of Membrane Science, 387 (2012) 54-65.

13. A. Marcos-Fernández, A. Tena, A.E. Lozano, J.G. de la Campa, J. de Abajo, L. Palacio, P. Prádanos, A. Hernández, Physical properties of films made of copoly (ether-imide) s with long poly (ethylene oxide) segments, European Polymer Journal, 46 (2010) 2352-2364.
14. A. Gil, A. Tena, A. Marcos-Fernández, M.R. De La Viuda, A.E. Lozano, P. Prádanos, Block copolymers for gas separation: Looking for the ideal structure, in: Elsevier (Ed.) Third International Symposium: Frontiers in Polymer Science, Sitges (Spain), 2013.
15. A. Tena, A. Marcos-Fernández, L. Palacio, P. Cuadrado, P. Prádanos, J. de Abajo, A.E. Lozano, A. Hernández, Phase Segregation and Gas Separation Properties of Thermally Treated Copoly (ether-imide) from an Aromatic Dianhydride, an Aromatic Diamine, and Various Aliphatic Diamines, Industrial & Engineering Chemistry Research, 51 (2012) 3766-3775.
16. A. Tena, A. Lozano, L. Palacio, A. Marcos-Fernández, P. Prádanos, J. de Abajo, A. Hernández, Gas separation properties of systems with different amounts of long poly (ethylene oxide) segments for mixtures including carbon dioxide, International Journal of Greenhouse Gas Control, 12 (2013) 146-154.
17. A. Tena, A. Marcos-Fernandez, A.E. Lozano, J.G. De La Campa, J. De Abajo, L. Palacio, P. Pradanos, A. Hernandez, Thermally Segregated Copolymers with PPO Blocks for Nitrogen Removal from Natural Gas, Industrial & Engineering Chemistry Research, (2013).
18. A. Tena, A. Marcos-Fernández, L. Palacio, P. Prádanos, A.E. Lozano, J.d. Abajo, A. Hernández, On the influence of the proportion of PEO in thermally controlled phase segregation of copoly (ether-imide) s for gas separation, Journal of Membrane Science, (2013).
19. H. Chen, Y. Xiao, T.-S. Chung, Synthesis and characterization of poly (ethylene oxide) containing copolyimides for hydrogen purification, Polymer, 51 (2010) 4077-4086.
20. A. Dufresne, J.-Y. Cavaille, Clustering and percolation effects in microcrystalline starch-reinforced thermoplastic, Journal of Polymer Science Part B Polymer Physics, 36 (1998) 2211-2224.
21. O. Levy, D. Stroud, Maxwell Garnett theory for mixtures of anisotropic inclusions: Application to conducting polymers, Physical Review B, 56 (1997) 8035.
22. M. Zimmer, X. Fan, J. Bao, R. Liang, B. Wang, C. Zhang, J. Brooks, Through-Thickness Thermal Conductivity Prediction Study on Nanocomposites and Multiscale Composites, Materials Sciences and Applications, 3 (2012) 131-138.
23. B. Shimekit, H. Mukhtar, Gas permeation models in mixed matrix membranes, in: National Postgraduate Conference (NPC), 2011, IEEE, 2011, pp. 1-5.

24. J.M. Garnett, Colours in metal glasses, in metallic films, and in metallic solutions. II, Philosophical Transactions of the Royal Society of London. Series A, Containing Papers of a Mathematical or Physical Character, (1906) 237-288.
25. A. Eucken, Allgemeine gesetzmabigkeiten fur das warmeleitvermogen verschiedener stoffarten and aggregatzustande, Forschung Gabiete Ingenieur, 11 (1940) 6–20.
26. D.J. Bergman, D. Stroud, Physical properties of macroscopically inhomogeneous media, Solid State Physics, 46 (1992) 147-269.
27. J.C. Garland, D.B. Tanner, O.S. University, U.S.E. Research, D. Administration, N.S. Foundation, Electrical transport and optical properties of inhomogeneous media, Ohio State University, 1977, American Institute of Physics, 1978.
28. D.A.G. Bruggeman, Calculation of various physical constants in heterogeneous substances. I. Dielectric constants and conductivity of composites from isotropic substances, Ann. Phys. (Paris), 24 (1935) 636.
29. M. Haddadi, B. Agoudjil, A. Boudenne, B. Garnier, Analytical and Numerical Investigation on Effective Thermal Conductivity of Polymer Composites Filled with Conductive Hollow Particles, International Journal of Thermophysics, 34 (2013) 101-112.
30. C.J.F. Böttcher, Theory of electric polarisation, Elsevier Pub. Co., 1952.
31. G. DeLoor, Dielectric Proberties of heterogeneous mixtures, in, University of Leiden, Leiden, 1956.
32. H. Ebadi-Dehaghani, M. Nazempour, Thermal Conductivity of Nanoparticles Filled Polymers, in: D.A. Hashim (Ed.) Nanotechnology and Nanomaterials: "Smart Nanoparticles Technology", InTech, 2012.
33. T. Lewis, L. Nielsen, Dynamic mechanical properties of particulate-filled composites, Journal of applied polymer science, 14 (1970) 1449-1471.
34. L.E. Nielsen, Thermal conductivity of particulate filled polymers, Journal of applied polymer science, 17 (1973) 3819-3820.
35. L.E. Nielsen, The thermal and electrical conductivity of two-phase systems, Industrial & Engineering Chemistry Fundamentals, 13 (1974) 17-20.
36. D. Kumlutaş, I.H. Tavman, M. Turhan Çoban, Thermal conductivity of particle filled polyethylene composite materials, Composites Science and Technology, 63 (2003) 113-117.
37. B. Weidenfeller, M. Höfer, F.R. Schilling, Thermal conductivity, thermal diffusivity, and specific heat capacity of particle filled polypropylene, Composites Part A: applied science and manufacturing, 35 (2004) 423-429.

38. D. Kumlutaş, I.H. Tavman, A numerical and experimental study on thermal conductivity of particle filled polymer composites, Journal of Thermoplastic Composite Materials, 19 (2006) 441-455.
39. R. Pal, On the Lewis–Nielsen model for thermal/electrical conductivity of composites, Composites Part A: applied science and manufacturing, 39 (2008) 718-726.
40. H. Davis, L. Valencourt, C. Johnson, Transport processes in composite media, Journal of the American Ceramic Society, 58 (1975) 446-452.
41. R. Landauer, The electrical resistance of binary metallic mixtures, Journal of Applied Physics, 23 (1952) 779-784.
42. P. Karayacoubian, Effective thermal conductivity of composite fluidic thermal interface materials, in: Applied Science In Mechanical Engineering, Univ. Waterloo, Ontario, Canada 2006.
43. D.L. Johnson, P.N. Sen, Physics and chemistry of porous media, American Institute of Physics, 1984.
44. F. Levy, A modified Maxwell-Eucken equation for calculating the thermal conductivity of two-component solutions or mixtures, International Journal of Refrigeration, 4 (1981) 223-225.
45. J. Wang, J.K. Carson, M.F. North, D.J. Cleland, A new approach to modelling the effective thermal conductivity of heterogeneous materials, International Journal of Heat and Mass Transfer, 49 (2006) 3075-3083.
46. T.-S. Chung, L.Y. Jiang, Y. Li, S. Kulprathipanja, Mixed matrix membranes (MMMs) comprising organic polymers with dispersed inorganic fillers for gas separation, Progress in Polymer Science, 32 (2007) 483-507.
47. R. Mahajan, W.J. Koros, Mixed matrix membrane materials with glassy polymers. Part 1, Polymer Engineering & Science, 42 (2002) 1420-1431.
48. T.T. Moore, R. Mahajan, D.Q. Vu, W.J. Koros, Hybrid membrane materials comprising organic polymers with rigid dispersed phases, AIChE journal, 50 (2004) 311-321.
49. J. Felske, Effective thermal conductivity of composite spheres in a continuous medium with contact resistance, International Journal of Heat and Mass Transfer, 47 (2004) 3453-3461.
50. B. Shimekit, H. Mukhtar, T. Murugesan, Prediction of the relative permeability of gases in mixed matrix membranes, Journal of Membrane Science, 373 (2011) 152-159.
51. S.R. Broadbent, J.M. Hammersley, Percolation processes I. Crystals and mazes, in: Proc. Cambridge Philos. Soc, 1957, pp. 629-641.
52. G. Grimmet, Percolation, Springer, 1999.

53. D. Bigg, The effect of compounding on the conductive properties of EMI shielding compounds, Advances in Polymer Technology, 4 (1984) 255-266.
54. J. Clerc, G. Giraud, J. Laugier, J. Luck, The electrical conductivity of binary disordered systems, percolation clusters, fractals and related models, Advances in Physics, 39 (1990) 191-309.
55. Y.P. Mamunya, V. Davydenko, P. Pissis, E. Lebedev, Electrical and thermal conductivity of polymers filled with metal powders, European Polymer Journal, 38 (2002) 1887-1897.
56. W. Tian, R. Yang, Phonon transport and thermal conductivity percolation in random nanoparticle composites, Computer modeling in engineering and sciences, 24 (2008) 123.
57. I.U.K. Godovskiĭ, V.P. Privalko, Thermal and electrical conductivity of polymer materials, Springer, 1995.
58. G. Zhang, Y. Xia, H. Wang, Y. Tao, G. Tao, S. Tu, H. Wu, A percolation model of thermal conductivity for filled polymer composites, Journal of composite materials, 44 (2010) 963-970.
59. M. Kole, D. Tripathi, T.K. Dey, Percolation based enhancement in effective thermal conductivity of HDPE/LBSMO composites, Bulletin of Materials Science, 35 (2012) 601-609.
60. D. Stauffer, A. Aharony, Introduction to Percolation Theory, Taylor & Francis Group, 1992.
61. H. Lin, B.D. Freeman, Gas solubility, diffusivity and permeability in poly (ethylene oxide), Journal of Membrane Science, 239 (2004) 105-117.

CONCLUSIONS

The work described in this thesis is aimed at developing polymeric membrane materials for the separation of CO_2 from light gases. In general, this research has been focused on the development of membrane materials with a high CO_2 permeability rather than a high CO_2/N_2 selectivity. Block copolymers, specifically copoly(ether-imide)s, composed of an aromatic polyimide (hard segment), which provide good mechanical properties to the films, and an aliphatic polyether (soft segments, mainly ethylene oxide chains) which have excellent CO_2 separation properties. The copolymers were thoroughly characterized to evaluate the influence of the structure and composition on the properties. From this study, a number of conclusions in relation to the physico-chemical properties of the copolymers, and as a consequence, the permselectivity properties could be derived.

In this sense, in relation with the physico-chemical properties, the following conclusions can be addressed:

- Complete imidization was achieved at relatively low temperatures (120-160 ºC depending on the PEO content). This is an evident processing advantage when compared with fully aromatic polyimides, that need very high temperatures, generally above 300 ºC, to achieve almost complete imidization. The process was easily followed an confirmed by using FTIR.

- These copolymers were able to experiment phase segregation. The phase-separated morphology improved with the increase in the rigidity of the structure. This behavior was confirmed by SAXS, TMA and DSC. By DSC and TMA, the existence of well defined thermal transitions for the polyether phase and the polyimide phase, was an indirect prove of the existence of a phase-segregated morphology. By SAXS, the phase segregation could be directly proved.

  It was demonstrated that thermal treatment improved the phase separation of the blocks. The transition temperature for the hard domains increased, and the Tg of the soft segment decreased and/or its crystallinity increased. SAXS experiments confirmed the improvement of the phase separated structure by the increase in the relative invariant with the increase in the treatment temperature.

- As expected, the mechanical properties of the copolymers improved when the amount of soft segments decreased.

- It was possible to eliminate, selectively, the aliphatic part of the copolymers by controlled thermal treatment.

Concerning the second mentioned criterion on the relation between the physico-chemical properties and the permeation properties of copolymers:

- There is a direct relationship between permeability and phase segregation. Therefore, the copolymers with higher ability for segregation, or in other words, more rigid structures, showed better CO_2 permeability. This behavior was confirmed by using diverse aromatic diamines and dianhydrides (with different rigidity).

- The thermal treatment increases segregation and favors permeability without any effect on the selectivity. This has been confirmed for different thermal treatments and for different pairs of gases.

- When different polyether diamines different chemical structure were used, in terms of the permselectivity , the gas performances when the gases had different polar natures followed the sequence of polarities of the aliphatic part of the copolymers.

- Analyzing the influence of the length of PEO in permselective properties, it was observed that the ability of PEO to crystallize is a crucial factor. Thus, when the temperature of measurement for the permeability is sufficiently high (for example, at 50 ºC the main part of the polyethylene glycol of a MW of 6000 g/L is in the amorphous state), the permeability increases with the length of the polyether.

- In general, the permeability increases with increasing the PEO percentage on the copolymer, without any substantial effect on the selectivity. For the samples with the longer PEO (PEO-6000) a decrease in permeability was observed due to its partial crystallization, but this effect wasn't detected at higher measurement temperatures.

- For PEO contents below 50%, the more rigid aromatic monomers produce better segregation, and in turn higher permeability values. For PEO proportions over 50%, the permeability obtained were similar regardless of what aromatic monomer was used. In this case, the permeability only depends on the percentage of PEO in the copolymer.

- The model based on the Effective Medium Approximation (EMA) succeeded to predict the main features of the experimental results. Specifically, it was able to calculate the volume fraction for the maximum increase of permeability, a common feature for all the studied segregated copolymer membranes. The model has the advantage of being able to be adapted for three phase (or multiphase) composites where the structure of each phase in the mixture is effectively random in nature. This fact has the added advantage of making unnecessary any consideration on the detailed phase-to-phase morphology.

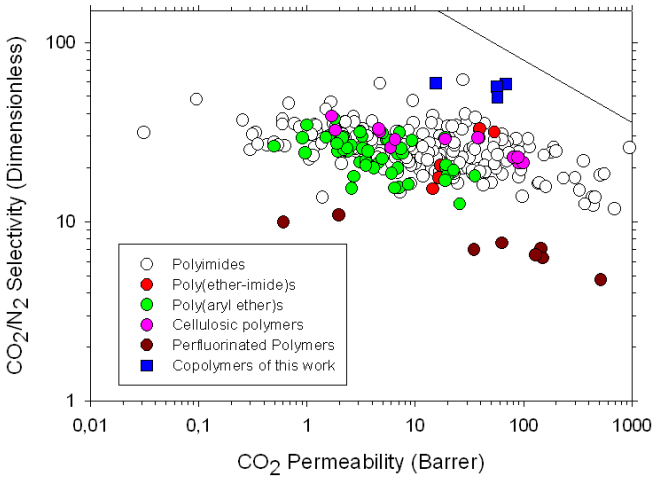

Robeson's plot for the pair CO_2/N_2 for different polymer from the bibliography and some of the copolymers obtained in this work.

As main conclusion, it seems clear that these copolymers are suitable for separations where CO_2 or other condensable gases are involved along with (or mixed with) non-condensable gases , especially for the separation CO_2/N_2. These separations have a great importance in the remediation of greenhouse effects and make these membranes good candidates for their application at an industrial level.

FUTURE DIRECTIONS

In view of the results obtained in this work, the following steps could be interesting and merit uterior research in order take profit of the potentialities of this type of copolymers:

- To try to obtain as high as possible polyether contents with acceptable mechanical properties.
- To use a very high permeable polyether (i.e. PDMS) with the ability to produce phase segregation.
- To develop a method to obtain a polyether with very high molecular weight and a low or null crystallinity.
- To explore new experimental processes to decrease the crystallinity without affecting permeability properties (i.e. “soft crosslinkkage”).
- To find a good method to eliminate in a selective way the polyether from the copolymer structure in order to create a pseudo carbon molecular sieve (CMS) structures with controlled sieve ability.
- To evaluate the applicability of the EMA model for other more complex and promising copolymers or to partially pirolized copolymers.

SUMMARY

The work described in this thesis aimed at the development of polymeric membrane materials for the separation of CO_2 from light gases. The augment of carbon dioxide concentration in the atmosphere due to the use of fossil fuels has caused a global warming that, because of its potential dangerous effects, requires energic actions. 60 % of total CO_2 emissions are produced by power generation facilities and industrial factories. Of course research should focus on the optimization of clean energy sources and on the more efficient use of energy. However, it is also necessary to reduce CO_2 levels, so carbon capture and storage (CCS) must be considered as an urgent issue. CO_2 can be captured by a variety of methods, which can be classified as post-combustion, pre-combustion and oxy-combustion ones. Among these methods, post-combustion appears as one of the most attractive alternatives. This process can be applied to different sources: power, steel, cement or petrochemical plants etc. In this process the flue gas after the combustion step must be concentrated and purified to meet the transport and storage specifications.

The role of polymeric membranes applied to gas separation is increasingly gaining importance. Currently they are presented as a good alternative for this type of processes when compared with the processes that have been used up to now.

The amount of CO_2 in the flue gas ranges from low (4%) to high (30 %) concentrations and therefore the applied technology should consider these differences. Other compounds in the flue gas are O_2, H_2, CO, NO_x or SO_x, although the most frequent is N_2, which appears in the coal power plants, where CO_2 concentrations are typically around 15%.

Polymers to be applied for this type of separation should have an adequate balance of permeability and selectivity. But, it is also necessary to have a high gas flow and good mechanical and thermal resistance. Glassy polymers and in particular polyimides are well known for their excellent thermal oxidative stability, good organic solvent resistance and exceptional mechanical properties, along with an extraordinary ability to separate complex mixtures of gases in diverse applications.

Typically these materials have a high selectivity but they sometimes do not exhibit sufficiently high permeability. In order to increase the selectivity to CO_2, it is convenient to increase the affinity of the material for this gas. One of the most common approaches to meet these requirements is the use of block-copolymers having moieties able to interact with a certain gas.

Block-copolymers can combine hard and soft blocks. The hard blocks consist in a polymer with well-packed rigid structure; while the soft segments usually contain more flexible chains. The hard

segments are glassy while the soft segments behave as rubbery polymers with relatively high free volume fractions. In this way the glassy polymer segments will provide the mechanical resistance. The rubbery segments generally form continuous nanodomains with high gas permeability.

It is widely known that CO_2 is highly soluble in polyethylene oxide (PEO) and thus it has been used to separate carbon dioxide from other light gases. In view of this, the use of block-copolymers combining aromatic diamines with aliphatic ones based on PEO (Jeffamines), appears to be a promising route. These compounds have good permselectivity for the couple CO_2/N_2, which was attributed mainly to the high solubility-selectivity due to the existence of strong interactions between the hydrophilic and rubbery domains of the oxyethylene groups in PEO and CO_2. The role of the interaction between CO_2 and ethylene oxide (EO) groups in CO_2 selectivity has been discussed and used for the development of new promising membranes.

In addition, it is necessary to reach a good balance between the hard and soft block segments in order to provide good gas separation balance without loss of permeability. For this reason, this research has been focused on the development of membrane materials with a high CO_2 permeability rather than a high CO_2/N_2 selectivity. Block copolymers, specifically copoly(ether-imide)s, composed of an aromatic polyimide hard segment, which provide good mechanical properties to the films, and aliphatic ethylene oxide chains as soft segments, which have excellent CO_2 separation properties, were prepared. A complete analysis of the influence of the structure and composition of the synthesized copolymers was performed.

The copolymers were synthesized by combination of a dianhydride (BPDA, BKDA or PMDA) with an aromatic amine (ODA, BNZ or PPD), and an aliphatic amine (PEO-900, PEO-2000, PEO-6000, PPO-2000, PPO-4000, RT-1000, pTHF-350 or pTHF-1700). Besides the structure of the monomers, the content of the aliphatic diamines was varied.

In the synthesis of the copolymers, first, the aliphatic diamine (x mmol), and the aromatic diamine (y mmol), were mixed in different weight ratios from 1:4 to 6:1 (w/w), dissolved in anhydrous NMP (5 mmol (x+y)/10 mL) in a 100 mL three-necked flask blanketed with nitrogen. Then, the reaction mixture was cooled down to 0 ºC, and under mechanical stirring, a stoichiometric amount of aromatic dianhydride (x+y mmol) was added and the mixture was stirred overnight at room temperature. During this time the dianhydride completely dissolved and the solution reached high viscosity.

The resultant viscous copolyamic acid solution was diluted with NMP to the appropriate viscosity for casting, filtered through a nominal #1 fritted glass funnel, degassed, and cast onto leveled a glass plate. The resulting film was covered with a conical funnel to avoid fast evaporation of the solvent, dried at 80 ºC overnight, and finally thermally treated under inert atmosphere at different temperatures. In this way all the films prepared in this work were obtained, and eventually characterized.

By FTIR-ATR the imidization process was followed. A complete imidization was achieved at relatively low temperatures (120-160 ºC depending on the PEO content). This is an evident processing advantage respect to fully aromatic polyimides, for which very high temperatures, generally above 300 ºC, are necessary to achieve almost complete imidization.

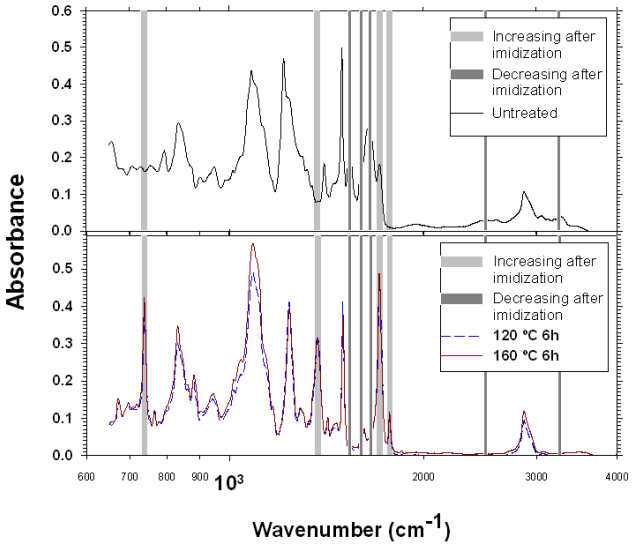

Figure 1. Typical FTIR spectra showing the difference between imidized and not imidized BPDA-PEO2000-ODA 2:1.

The TGA technique allowed the analysis of the thermal stability of the samples. It was observed that it was possible to eliminate in a selective way the aliphatic part of the copolymers by controlled thermal treatment. In this way, it could be possible to create partial pyrolyzed membranes (PPM) with properties comparable to that of the carbon membranes but with the stability of the pure aromatic polyimides.

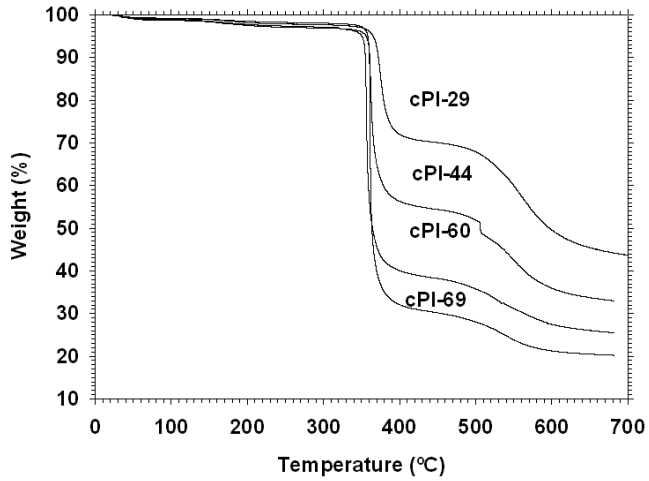

Figure 2. TGA curves in dynamic conditions for PEO based copolymers.

From SAXS, the phase segregation was analyzed, and the improvement on the phase separation with the increase in the treatment temperature demonstrated. Two parameters can be calculated from these scattering curves: the relative invariant, Q′, as the integral below the curve Iq^2 vs q, which is related to the extent of the phase separation; and the maximum on the scattering curve, q_{max}, related to the size scale of the separated phases, calculated also from the curve Iq^2 vs q. Following the changes of Q' and q_{max} at real time, it was possible to analyze the evolution of the segregation as a function of the structure and composition, and the thermal treatment.

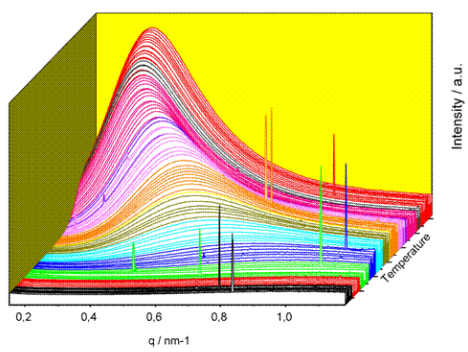

Figure 3. Evolution of the Iq^2-q curves with temperature for copolymer BPDA 2/1.

DSC was employed in order to determine the T_g and T_m of the aliphatic part of the sample and to determine the percentage of crystalline PEO in the sample. Besides, it was possible to analyze the evolution of these parameters with the thermal treatment. No transition for the aromatic polyimide segments could be detected by DSC. However, it was possible to obtain the Tg of the aromatic

block by TMA. The detection of two T_g clearly demonstrated the existence of a phase-segregated morphology in our systems. The values obtained for these parameters gave an idea of the purity of the phases. Thus, a closer value for the glass transition temperature of the aliphatic part to the value for the pure aliphatic monomer, was related to a higher purity exist of this phase, thus, a better phase separation. These results confirmed the results observed by SAXS. This copolymers were able to experiment phase segregation, and it was observed that when the rigidity of the structure was higher the ability of the copolymers to segregate increased.

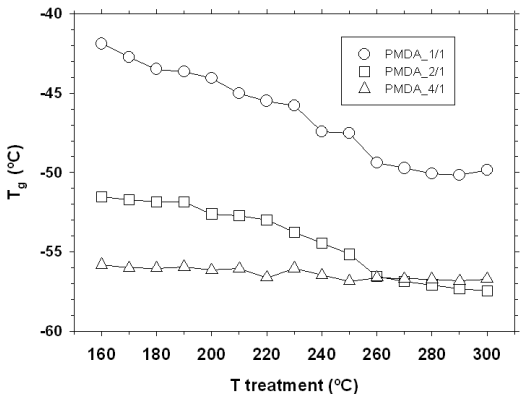

Figure 4.- T_g for PEO in the copolymers of the PMDA series annealed at 160 ºC, 6h, after ‘‘instantaneous” treatment at different temperatures

Tensile tests were performed in order to determinate the mechanical properties of the samples. In general, the mechanical properties were good for all copolymers; as expected, the mechanical properties of copolymers improved when the amount of soft segments decreased.

With respect to the gas permeation properties, interesting relations with the previous properties was found. The thermal treatment increased the purity of the phases, or in other words, increased the phase segregation, and when these results were related with the permeability, it was found that permeability improved with the thermal treatment for all the gases and in all the copolymers synthesized without a significant effect on the selectivity.

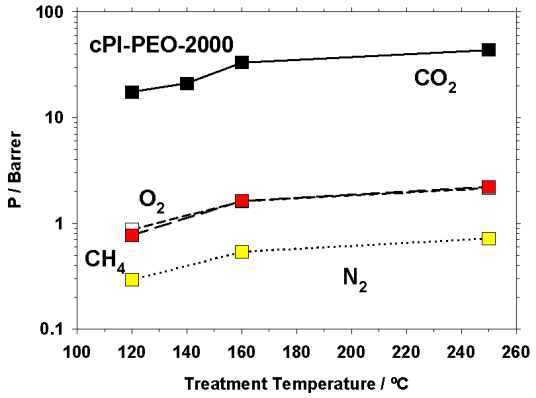

Figure 5. Permeability of the different gases studied as a function of the temperature of treatment for cPI-PEO-2000 copolymer.

There was a direct relationship between permeability and phase segregation, thus, copolymers with higher ability for segregation, that is, with more rigid structures, showed better CO_2 permeability results, with the selectivity remaining constant. This behavior was confirmed using diverse aromatic diamines and dianhydrides (with different rigidity).

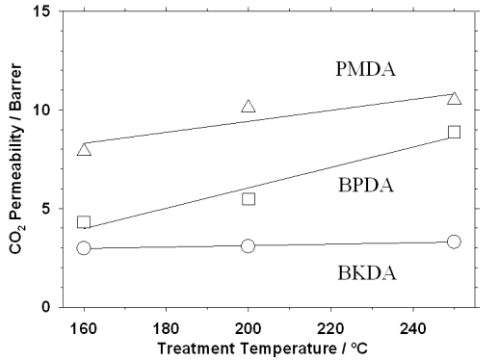

Figure 6. Evolution of the CO_2 permeability as a function of the temperature of annealing for the copolymers with dianhydrides and a weight ratio 1:1 between diamines.

When different polyether diamines were used, in terms of permselectivity, the gas performances when the gases had different polar natures followed the sequence of polarities of the aliphatic part of the copolymers. When the influence of the length of PEO in permselective properties was evaluated, it was observed that the ability of PEO crystallization was a crucial factor. Thus, when the temperature of measurement for the permeability was sufficiently high (at 50 ºC the main part of the polyethylene glycol is in the amorphous state), the permeability increased with the length of the polyether.

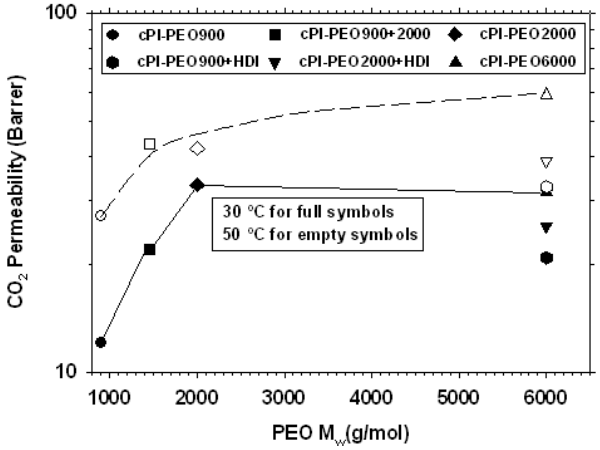

Figure 15. CO_2 permeability as a function of the PEO length, for HDI extended copolymers (treated at 160 ºC) and for the rest of copolymers (treated at 250 ºC).

In general, the permeability increased with increasing the PEO percentage on the copolymer, without effect on the selectivity. For the samples with the longer PEO (PEO-6000) it was observed a decrease due to the higher crystallization ability, but this effect was not detected at higher measurement temperatures.

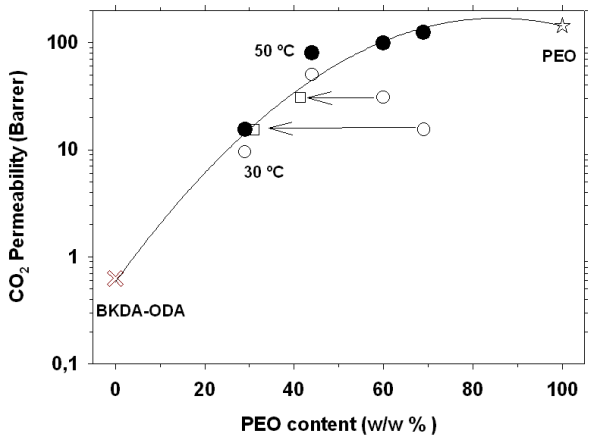

Figure 8. CO_2 permeability for samples treated at 260 ºC containing different percentages of PEO.

For PEO contents below 50%, the more rigid aromatic monomers produced better segregation, and in turn higher permeability values. For PEO proportions over 50%, the permeability obtained was similar regardless of the rigidity of the aromatic monomer. In this case, the permeability only depended on the PEO percentage in the polymer.

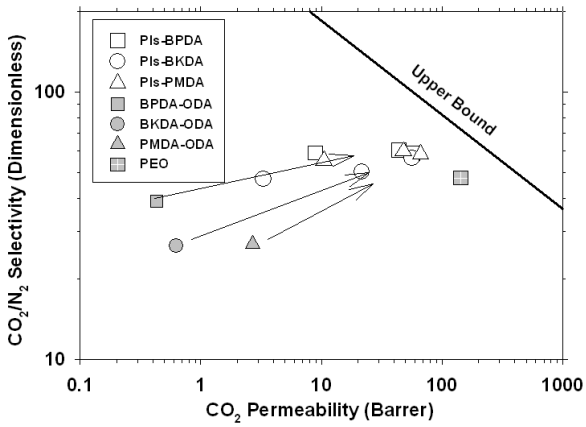

Figure 9. CO_2 permeability vs CO_2/N_2 for the copolymers synthesized from different aromatic dianhydride annealed at 250 ºC, and for the homopolymers (BPDA-ODA, BKDA-ODA, PMDA-ODA and PEO). Arrows correspond to increasing PEO content. PIs refer to the corresponding polyimides.

The model based on the Effective Medium Approximation (EMA) succeeded to predict the main features of the experimental results with much more accuracy than other existing models. Specifically, it was able to calculate the volume fraction for the maximum increase of permeability, a common feature for all the studied segregated copolymer membranes. The model was even able to predict the permeabilities of this kind of copolymers. The model has the advantage of being able to be adapted for three phase (or multiphase) composites where the structure of each phase in the mixture is effectively random in nature. This fact has the added advantage of making unnecessary any consideration on the detailed phase-to-phase morphology.

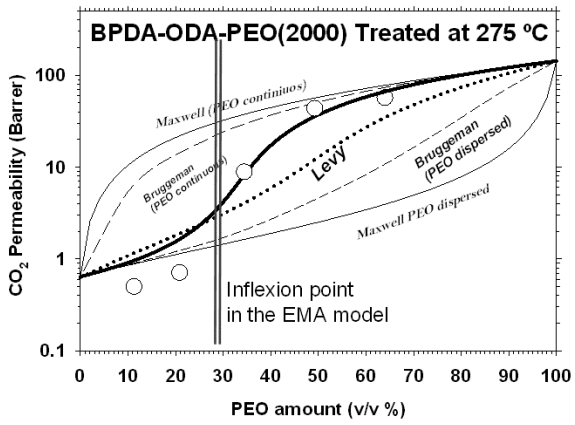

Figure 10. Effective medium approximations or effective medium theory (EMA or EMT).

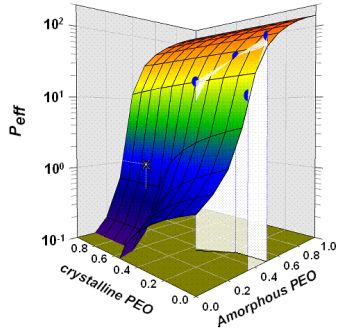

Figure 11. Effective permeabillity of CO_2 for a three-phase system of crystalline and amorphous PEO in a BKDA-ODA matrix and the predicitions of EMA.

There are many bibliographic data permeation properties for different kind of polymers. If we represent some of the existing data in the literature for different families of polymers and the results obtained for the copolymers prepared in this work, it is possible to observe with greater clarity the goodness of the results for these copolymers.

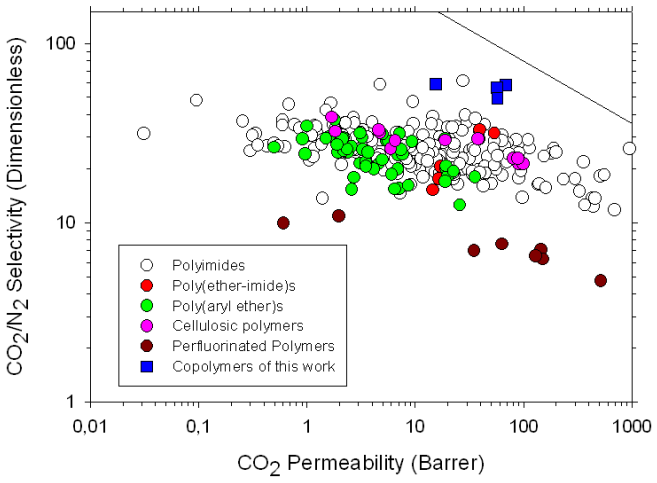

Figure 12. Robeson's plot for the pair CO_2/N_2 for different polymer from the bibliography and some of the copolymers obtained in this work.

As main conclusion, it seems clear that these copolymers are suitable for separations where CO_2 is involved and non-condensable gases are involved, especially for the separation CO_2/N_2. These separations have a great importance in the remediation of greenhouse effect and the results presented in this work make these membranes good candidates for their application at industrial level.

RESUMEN

El trabajo descrito en esta tesis tiene como finalidad el desarrollo de nuevos materiales poliméricos para la fabricación de membranas de separación de gases, en concreto, separación de CO_2 de gases ligeros. El aumento de la concentración de dióxido de carbono en la atmósfera, debido al uso de combustibles fósiles es una de las causas del calentamiento global lo cual, por sus efectos potencialmente peligrosos, requiere acciones enérgicas. El 60 % de las emisiones totales de CO_2 se producen en las instalaciones de producción de energía y en las fábricas industriales.Por supuesto, la investigación debe centrarse en la optimización de las fuentes de energía limpia y en el uso más eficiente de la energía. Sin embargo, también es necesario reducir los niveles de CO_2, por lo que la captura y almacenamiento de carbono (en su acrónimo inglés, CCS) debe ser considerado como un tema urgente. El CO_2 se puede capturar con varios métodos, que se pueden clasificar como de post-combustión, pre-combustión y los oxi-combustión. Entre estos métodos, los de post-combustión son una de las alternativas más atractivas. Este proceso se puede aplicar a diferentes fuentes: plantas de energía, acero, cemento o petroquímica, etc. En este proceso el gas de combustión después de la etapa de combustión de debe concentrar y purificar para cumplir con las especificaciones de transporte y de almacenamiento.

El papel de las membranas poliméricas aplicadas a la separación de gas está ganando cada vez más importancia. Actualmente se muestran como una buena alternativa para este tipo de procesos cuando se compara con los procesos que se han utilizado hasta ahora.

La cantidad de CO_2 en los gases de combustión, tiene un rango concentraciones amplio (desde el 4% hasta altas concentraciones en torno al 30%), por lo que la tecnología aplicada debe tener en cuenta estas diferencias. Además hay que tener en cuenta la presencia de otros compuestos en los gases de combustión, como O_2, H_2, CO, NO_x o SO_x, y el más frecuente N_2, que aparece en las centrales térmicas de carbón, donde las concentraciones de CO_2 son típicamente alrededor del 15%.

Los polímeros que se utilicen en este tipo de separación, deben tener un equilibrio adecuado de permeabilidad y selectividad. Pero, también es necesario tener un flujo de gas de alto y una buena resistencia mecánica y térmica. En este sentido los polímeros vítreos y en particular las poliamidas son bien conocidos por su excelente estabilidad térmica oxidativa, buena resistencia a los disolventes orgánicos y con propiedades mecánicas excepcionales, junto con una extraordinaria capacidad para separar mezclas invernadero complejas en diversas aplicaciones.

Típicamente, estos materiales tienen una alta selectividad, pero a veces no presentan una permeabilidad suficientemente alta. Con el fin de aumentar la selectividad al CO_2, es conveniente aumentar la afinidad del material para este gas. Uno de los métodos más comunes para satisfacer estos requisitos es el uso de copolímeros en bloques que tienen fracciones capaces de interaccionar con ciertos gases.

Los copolímeros en bloque pueden combinar segmentos duros y blandos. Los bloques duros consisten en un polímero con estructura rígida bien empaquetada; mientras que los segmentos blandos, por lo general, contienen cadenas más flexibles. Los segmentos duros son vítreos mientras que los segmentos blandos se comportan como polímeros gomosos con fracciones de volumen libre relativamente altas. De esta manera, los segmentos de polímero cristalinos proporcionarán la resistencia mecánica. Los segmentos de blandos generalmente forman nanodominios continuos con alta permeabilidad al gas.

Se sabe que el CO_2 es altamente soluble en óxido de polietileno (PEO) y por lo tanto se ha utilizado para separar dióxido de carbono de otros gases ligeros. En vista de esto, el uso de copolímeros en bloque que combinan diaminas aromáticas con los alifáticos basados PEO (Jefaminas), parece ser una ruta prometedora. Estos compuestos tienen buena permeabilidad selectiva para la pareja CO_2/N_2, que se atribuyó principalmente a la alta solubilidad selectividad debido a la existencia de fuertes interacciones entre los dominios hidrófilos y elásticos de los grupos oxietileno en PEO y CO_2. El papel de la interacción entre el CO_2 y los grupos de óxido de etileno (EO) en la selectividad de CO_2 ha sido discutido y utilizado para el desarrollo de nuevas membranas prometedoras.

Además, es necesario llegar a un buen equilibrio entre los segmentos de bloques duros y blandos con el fin de proporcionar un buen equilibrio en la separación de gas sin pérdida de permeabilidad. Por esta razón, esta investigación se ha centrado en el desarrollo de materiales de membrana con una alta permeabilidad al CO_2 más que en una alta selectividad CO_2/N_2. Se prepararon copolímeros en bloque, específicamente copoli (éter-imida) s, compuestos por una poliimida aromática (segmento duro), que proporcionan buenas propiedades mecánicas de las películas, y las cadenas de óxido de etileno alifáticos (segmentos blandos), que tienen excelentes propiedades de separación de CO_2. Y se realizó un análisis completo de la influencia de la estructura y la composición de los copolímeros sintetizados.

Los copolímeros fueron sintetizados por combinación de un dianhídrido (BPDA, BKDA o PMDA) con una amina aromática (ODA, BNZ o PPD), y una amina alifática (PEO-900, PEO-2000, PEO-

6000, PPO-2000, PPO -4000, RT-1000, pTHF-350 o pTHF-1700). Además en la estructura de los monómeros, se varió el contenido de las diaminas alifáticas.

En la síntesis de los copolímeros, primero, la diamina alifática (x mmol), y la diamina aromática (y mmol), se mezclaron en diferentes proporciones en peso, desde 1:4 a 6:1 (w/w), se disolvió en NMP anhidro (5 mmoles (x+y)/10 mL) en un matraz de 100 mL de tres bocas con nitrógeno. A continuación, la mezcla de reacción se enfrió a 0 º C, y bajo agitación mecánica, se añadió una cantidad estequiométrica de dianhídrido aromático (x + y mmol) y la mezcla se agitó durante la noche a temperatura ambiente. Durante este tiempo el dianhídrido se disolvión completamente y la solución alcanzó una alta viscosidad.

La solución viscosa de ácido copoliámico resultante se diluyó con NMP hasta alcanzar la viscosidad apropiada para su expensión, filtrándose a través de un embudo de vidrio # 1, desgasificándose, y finalmente depositada sobre una placa de vidrio nivelada. La película resultante se cubre con un embudo cónico para evitar la evaporación rápida del disolvente, se seca a 80 º C durante la noche, y finalmente se trata térmicamente en atmósfera inerte, a diferentes temperaturas. De esta manera se obtuvieron todas las películas preparadas en este trabajo, las cuales fueron caracterizadas.

El proceso de imidación fue seguido por FTIR-ATR. La imidización completa se logró a temperaturas relativamente bajas (120-160 º C dependiendo del contenido de PEO). Ésta es una ventaja evidente respecto al procesamiento de las poliimidas totalmente aromáticas, para las que son necesarias para lograr una imidización casi completa, temperaturas muy altas, generalmente por encima de 300 º C.

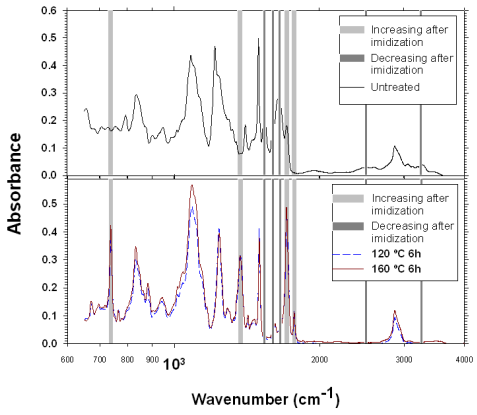

Figura 1. Típico espectro de FTIRdonde se muestra la diferencia entre una BPDA-PEO2000-ODA 2:1 imidada y una no imidada.

La técnica TGA permitió el análisis de la estabilidad térmica de las muestras. Se observó que era posible eliminar de manera selectiva la parte alifática de los copolímeros por tratamiento térmico controlado. De esta manera, podría ser posible crear membranas pirolizadas parcialmente (PPM) con propiedades comparables a las de las membranas de carbono pero con la estabilidad de las poliimidas aromáticas puras.

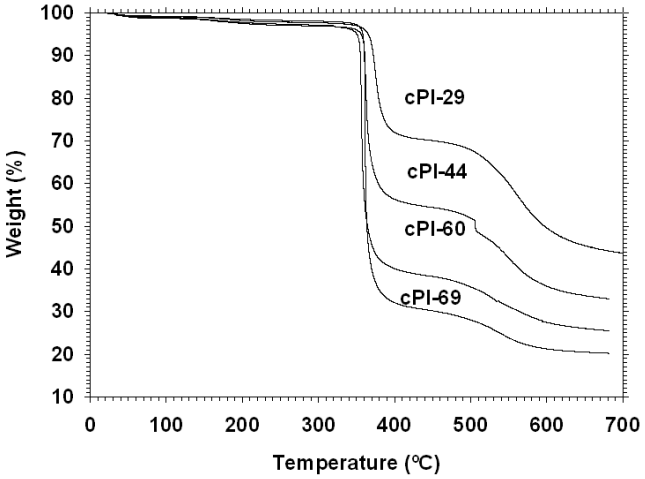

Figura 2. Curvas de TGA en condiciones dinámicas para copolímeros con PEO.

A partir de la información obtenida mediante SAXS, la segregación de fases fue analizada, y de este modo se observo una clara tendencia de mejora en la segregación de fases con el aumento de la temperatura de tratamiento. Dos parámetros pueden ser calculados a partir de estas curvas: la invariante relativa, Q ', como la integral por debajo de la curva de IQ^2 vs q, que está relacionada con la extensión de la segregación de fases, y el máximo en la curva, Q_{max}, relacionado con el tamaño de las fases segregadas, calculado también a partir de la curva IQ^2 vs q. Siguiendo los cambios de Q 'y Q_{max} en tiempo real, fue posible analizar la evolución de la segregación en función de la estructura, la composición y el tratamiento térmico.

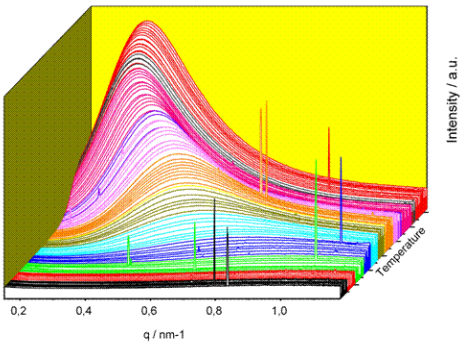

Figura 3. La evolución de las curvas de IQ^2-q con la temperatura para el copolímero BPDA 2/1.

La DSC se empleó con el fin de determinar la Tg y Tm de la parte alifática de los copolimeros y al mismo tiempo determinar el porcentaje de PEO cristalino. Además, fue posible analizar la evolución de estos parámetros con el tratamiento térmico. La transición vítrea de los segmentos de poliimida aromática no pudo ser detectada mediante DSC. Sin embargo, fue posible obtener la Tg del bloque aromático mediante TMA. La detección de dos Tg demostró claramente la existencia de una morfología de fases segregadas en nuestros sistemas. Los valores obtenidos para estos parámetros dieron una idea de la pureza de las fases. Por lo tanto, un valor más cercano a la temperatura de transición vítrea de la parte alifática, indica un que la parte alifática se encuentra más aislada, más pura, esto está relacionado con una mayor pureza de esta fase, por lo tanto, una mejor segregación. Estos resultados confirman los resultados observados por SAXS. Estos copolímeros fueron capaces de experimentar segregación de fases, y se observó que cuando la rigidez de la estructura fue mayor, la capacidad de segregación de los copolímeros aumenta.

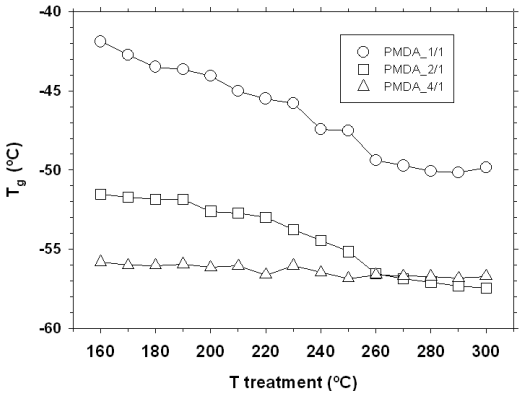

Figura 4 -. Tg de PEO en los copolímeros de la serie PMDA tratadas a 160 º C, 6 h, después de tratamiento" instantánea "a diferentes temperaturas.

En general, las propiedades mecánicas fueron aceptables para todos los copolímeros; como era de esperar, las propiedades mecánicas de los copolímeros mejoraron cuando la cantidad de parte alifática disminuyó.

Las propiedades anteriores han sido correspondidas con su comportamiento en separación de fases. El tratamiento térmico aumenta la pureza de las fases, o en otras palabras, el aumento de la segregación de fases, y cuando estos resultados fueron relacionados con la permeabilidad, se encontró que la permeabilidad mejoraba con el tratamiento térmico para todos los gases y en todos los copolímeros sintetizados sin efecto significativo en la selectividad.

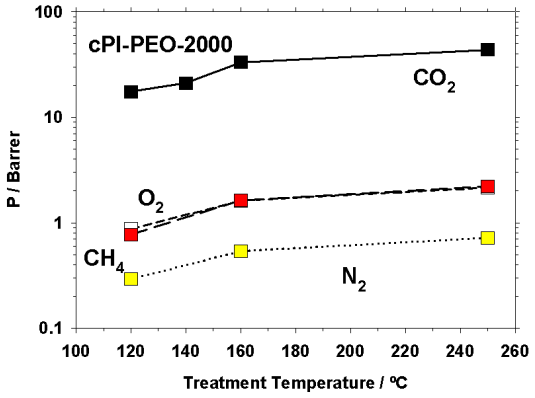

Figura 5. La permeabilidad de los diferentes gases en función de la temperatura de tratamiento para el copolímero de CPI-PEO-2000.

Fue encontrada una relación directa entre la permeabilidad y la segregación de fases, por lo tanto, copolímeros con mayor capacidad de segregación, es decir, con estructuras más rígidas, mostraron mejores resultados de permeabilidad para el CO_2, mientras que la selectividad permanece constante. Este comportamiento se confirmó mediante la síntesis de diferentes diaminas aromáticas y dianhıdridos (con diferente rigidez).

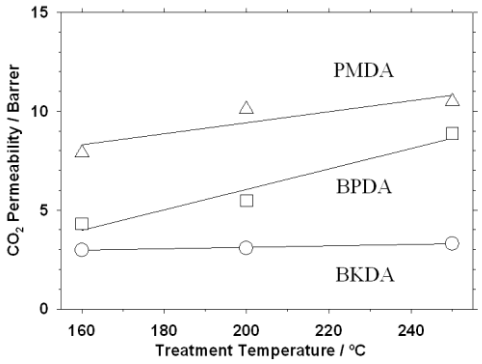

La Figura 6. Evolución de la permeabilidad al CO_2 en función de la temperatura de tratamiento para los copolímeros con distintos dianhídridos y una relación en peso de 1:1 entre diaminas.

Cuando se usan diferentes polieter diaminas, en terminos de permselectividad, el comportamiento a los diferentes gases cuando los gases tenían diferentes naturalezas polares siguió la secuencia de polaridades de la parte alifática de los copolímeros. Cuando se evaluó la influencia de la longitud de PEO en las propiedades de permeabilidad, se observó que la capacidad de cristalización de PEO fue un factor crucial. Por lo tanto, cuando la temperatura de medida de permeabilidad era suficientemente alta (a 50 º C la parte principal del polietilenglicol se encuentra en el estado amorfo), la permeabilidad aumentó con la longitud del poliéter.

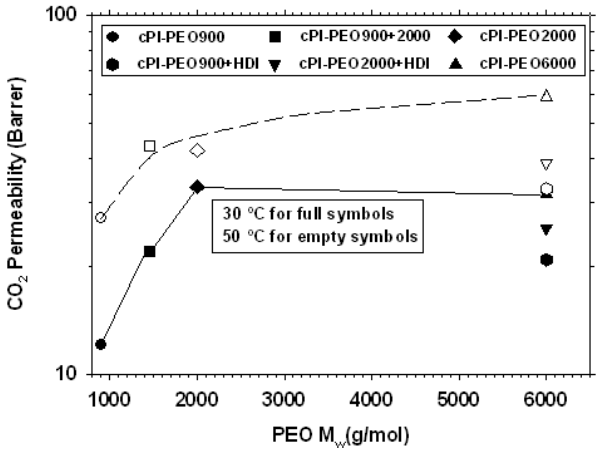

Figura 7. Permeabilidad al CO_2 en función de la longitud de PEO, para los copolímeros con extendedor HDI (tratados a 160 º C) y para el resto de los copolímeros (tratados a 250 º C).

En general, la permeabilidad aumentó con el aumento del porcentaje de PEO en el copolímero, sin efecto sobre la selectividad. Para las muestras con el PEO más largo (PEO-6000) se observó una

disminución debido a la capacidad de cristalización más alta, pero este efecto no fue detectado a temperaturas más altas de medida.

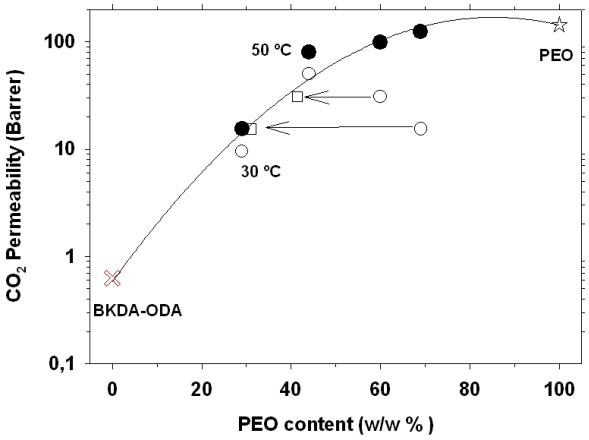

Figura 8. Permeabilidad de CO_2 para las muestras tratadas a 260 º C que contienen diferentes porcentajes de PEO.

Para contenidos de PEO por debajo del 50%, los monómeros aromáticos con mayor rigidez producen una mejor segregación, y a su vez unos valores de permeabilidad más altos. Para proporciones de PEO más de 50%, la permeabilidad obtenida fue similar independientemente de la rigidez del monómero aromatic usado. En este caso, la permeabilidad sólo dependía del porcentaje de PEO en el polímero.

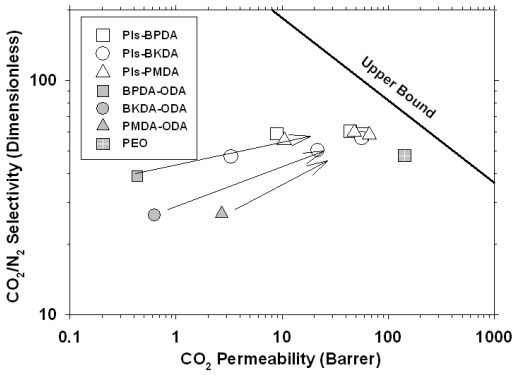

La Figura 9. Permeabilidad al CO_2 frente a las selectividad CO_2/N_2 para los copolímeros sintetizados a partir de diferentes dianhídridos aromáticos tratados a 250 º C, y para los homopolímeros (BPDA-ODA, BKDA-ODA, PMDA-ODA y PEO). Las flechas corresponden al aumento del contenido de PEO.

El modelo basado en la aproximación de campo medio (EMA) predijo de modo bastante preciso las características principales de los resultados experimentales con mucha más precisión que otros

modelos existentes. Específicamente, fue capaz de calcular la fracción de volumen para el aumento máximo de la permeabilidad, una característica común para todas las membranas de los copolímeros estudiados. El modelo fue incluso capaz de predecir la permeabilidad de este tipo de copolímeros. El modelo tiene la ventaja de ser capaz de ser adaptado para un sistema trifásico (o multifase) compuestos en donde la estructura de cada fase en la mezcla es azar. Este hecho tiene la ventaja adicional de no ser necesaria ninguna consideración detallada sobre la morfología de las fases.

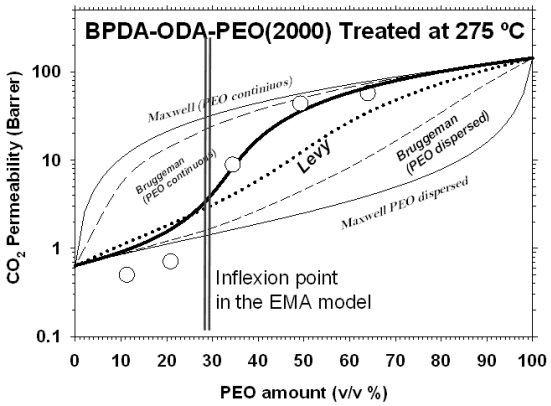

La Figura 10.Modelo de campo medio o la teoría de medio efectivo (EMA o EMT).

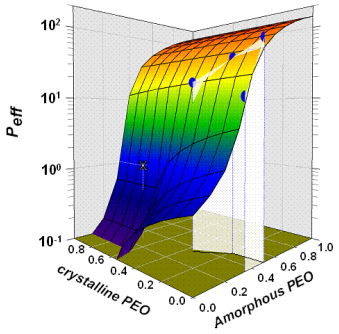

La Figura 11. Permeabilidad efectiva de CO_2 para un sistema trifásico de PEO cristalino y amorfo en una matriz BKDA-ODA y las predicciones de EMA.

Hay muchas propiedades de permeación en la bibliografía para diferentes tipos de polímeros. Si representamos algunos de los datos existentes en la bibliografía para diferentes familias de polímeros y los comparamos con los resultados obtenidos para los copolímeros preparados en este

trabajo, es posible observar con claridad la bondad de los resultados para estos copolímeros.

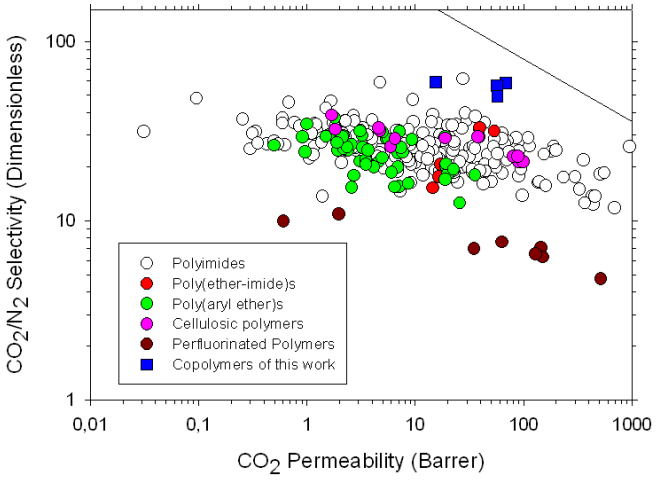

Figure 12. Representacion de Robeson para la pareja de gases CO_2/N_2 donde se representan los resultados de diferentes polímeros de la bibliografía y los datos de algunos de los copolimeros obtenidos en este trabajo

Como principal conclusión, parece claro que estos copolímeros son adecuados para la separación donde el CO_2 y otros gases no condensables están involucrados, sobre todo para la separación CO_2/N_2. Estas separaciones tienen una gran importancia en la mitigación del efecto invernadero y los resultados presentados en este trabajo hacen pensar que estas membranas poliméricas son buenas candidatas para su aplicación a nivel industrial.